Investigations on Ionospheric Electrodynamics over Low Latitudes in Indian Sector

A thesis submitted in partial fulfilment of

the requirements for the degree of

Doctor of Philosophy

by

Pandey Kuldeep Rambabu

(Roll No. 13330004)

Under the guidance of

Prof. R. Sekar & **Dr. D. Chakrabarty**

Space & Atmospheric Sciences Division

Physical Research Laboratory, Ahmedabad, India

Discipline of Physics

Indian Institute of Technology Gandhinagar

2018

to

my parents

Declaration

I declare that this written submission represents my ideas in my own words and where others' ideas or words have been included, I have adequately cited and referenced the original sources. I also declare that I have adhered to all principles of academic honesty and integrity and have not misrepresented or fabricated or falsified any idea/data/fact/source in my submission. I understand that any violation of the above can cause disciplinary action by the Institute and can also evoke penal action from the sources which have thus not been properly cited or from whom proper permission has not been taken when needed.

Pandey Kuldeep Rambabu

(Roll No: 13330004)

Certificate

We feel great pleasure in certifying that the thesis entitled "**Investigations on Ionospheric Electrodynamics over Low Latitudes in Indian Sector**" by **Mr. Pandey Kuldeep Rambabu** has been carried out under our supervisions and this work has not been submitted anywhere else for any degree or diploma.

Prof. R. Sekar
(Thesis supervisor)
Physical Research Laboratory
Ahmedabad-380009, Gujarat, India

Dr. D. Chakrabarty
(Thesis co-supervisor)
Physical Research Laboratory
Ahmedabad-380009, Gujarat, India

Acknowledgements

The journey of my doctoral work at Physical Research Laboratory (PRL), Ahmedabad would not be possible without the help and support of many of you. It is a pleasant opportunity to express my sincere gratitude for all that I have received, though a few pages of acknowledgement can never do justice to all.

First and foremost, I express my sincere gratitude to my supervisor, Prof. R. Sekar for his invaluable guidance, patience, and concerns toward my continuous progress during the tenure of thesis work. His unique way of understanding the scientific processes and criticality encourages me to probe deeper into a scientific problem. His valuable suggestions and comments have helped me to improve the scientific outcomes. I express my sincere gratitude to my co-supervisor, Dr. D. Chakrabarty. He has been a guide, friend, critic, motivator throughout these years. His constant guidance and enthusiasm have immensely helped me to explore the new world of ideas. I am thankful to both of them for providing me with unending support, and freedom of independent thinking. The unique opportunity to constantly interact with both of them, with expertise in different areas of research, has immensely improved my scientific understanding in the field of ionospheric studies. I had the luxury to walk-in to their offices at any time or catch them anywhere and start the conversation. I will be forever indebted to both of them.

I had the fortune to interact with Prof. B. G. Anandarao in early days my Ph.D. tenure and started wonderful collaborative works by suitably making use of the equatorial electrojet model developed earlier by him. I'm grateful to him for providing me the Fortran code of the electrojet model and explaining the insights of it. This granted me an opportunity to employ the model to explore the possible answers to a few scientific problems.

I am thankful to Prof. S. P. Gupta for helping me to understand the insights of in-situ measurements of electron density and plasma irregularities that were obtained using sounding rocket flight experiments conducted from Thumba. His important suggestions have improved research outcomes of this thesis work. I am grateful to him for his scientific discussions and keeping the environment lively.

I am obliged to Prof. D. Pallamraju, the then division chairman, for allowing me to join the Space & Atmospherics Sciences Division as a doctoral student. I would also like to thank him for valuable suggestions for the progress of my scientific research throughout these years and being a member of my Doctoral Students Committee.

I am thankful to Mr. R. Naraynan for teaching me the insights of operating the airglow photometer that was built in-house. I am thankful to Dr. Amitava Guharay for the scientific discussions, his friendly and helping nature.

I express my sincere thanks to all the faculty and staff members of Space & Atmospheric Sciences Division. I am grateful to Prof. S. Ramachandran, chairman of the division and student's committee, for his prompt and cooperative help/suggestions in academic and administrative matters.

I thank Prof. R. Sridharan, Prof. H. Chandra, Dr. Y. B. Acharya, Prof. A. K. Patra (NARL), Dr. Smitha Thampi (SPL) for showing interest in my research work and giving encouraging remarks. I thank Dr. T. K. Pant (SPL) for all the help during collaborative airglow campaigns at VSSC, Trivandrum.

I thank the PRLs Director, Dean, Registrar, Academic Committee for their constant help and support. I thank all the PRL faculties for providing an overall view of research works carried out in PRL. My sincere thanks to Prof. J Banerji for teaching communication skills during the coursework. I express my appreciation to the staff members of PRLs Computer center, Library, Canteen, CMD for continuously providing the necessary facilities to smoothly carry out the research work. My special thanks to Mr. Pradeep Kumar for his help and cooperation. I am grateful to staff members of PRL's Mount Abu guest house (Hill View) for their hospitalities during airglow campaigns.

I am thankful to my present/former laboratory colleagues, Dipti, Debrup, Deepak, Sandeep, Sivakandan, Avik, Subir, Nidhi, Ankit and Sovan for their friendly company. I am grateful to Dipti and Debrup for their help, wonderful company and long discussions on numerous academic and non-academic aspects. I thank Atul who is the person I approach first for any issues related to computer and MATLAB. I thank Mitesh, Aditya, Anil for their wonderful company during field campaigns and helpful nature in the lab. I thank Sneha Nair, Pradeep, Surajeet, Mahipath, and others for their extended help and cooperation.

I would like to thank the Director, Dean, Associate Dean and the academic section of IIT Gandhinagar for their support and help. My special thanks to Dr. Nithin V. George, Dr. Vinod Chandra and Mr. Piyush for their prompt responses and helps on official matters.

My sincere gratitude to the Department of Science & Technology (India) for providing me with the funding supports to present my research works at AOGS-2018 meeting held in Hawaii (USA). I am grateful to the organizers of Heliophysics Summer School-2018 for selecting me to attend this prestigious school. I am thankful to the dean of school, Prof. Amitava Bhattacharjee (Princeton University, USA) for his encouraging words and suggestions for my research works.

I am grateful to Indian Institute of Geomagnetism, Navi Mumbai; Coordinated Data Analysis Web, NASA; World Data Center for Geomagnetism, Kyoto and several others for providing the enormous datasets in open source. I would like to acknowledge MATLAB, Google, TexStudio, Getdata, TableCurve2D etc. to make my work simpler.

I feel lucky to join in the wonderful batch-2013: Rukmani, Satish, Navpreet, Prahlad, Kumar, Rupa, Hemant, Ali, Chandan, Jabir, Yasir. I have really enjoyed their company since I entered PRL which is unforgettable. My special thanks to Rukmani for the long discussions, care and helps during these years. I also thank the seasonal friends Santosh, Chandni, and Ashish.

I am thankful to my wonderful seniors/juniors and friends who made my stay at PRL a pleasant and lively experience. To name a few - Sunil Chandra, Sushant, Amrendra, Gavrav Tomar, Waagesh, Arko, Tanmoy, Priyanka, Manojit, Anjali, Naveen, Arun, Girish Kumar, Ikshu, Bivin, Pankaj, Apurva, Chandana, Naman, Vishnu, Niharika, Ashish, Rahul, Subir, Kaustav, Aarthy, Archita, Richa, Arvind, Varun, Shaifali, Randeep, Harish, Sandeep, Priyank, Abdur, Surendra, Deepali, Nisha, Sushree, Kamlesh, Hirdesh, Lijo, Sneha Yadav, Fazlul, Bighnaraj, Piyush, Renuka, Srinivasa, Hrushikesh, Sana, Vipin, Atif and many more... Thanks for making a cooperative, helpful and cheerful environment at Thaltej hostel.

My sincere gratitude to my teachers Mr. Aanand Kumar (Delhi University), Mr. Nitinkumar Bijewar (Mumbai University), Ms. Jyotsna Gandhi (Bhavan's College, Mumbai), Ms. Madhulika Pathak (Rizvi College, Mumbai), Mr. Sanjay Tiwari (B. L. Ruia High School, Mumbai) and several others for their excellent teachings, helps and encouragements at different stages of my educational carrier.

Thanks to my friends Pawan, Ram Singh, Khalid, Dheeraj and others for their constant support and encouragements.

Most importantly, I express my indebtedness, love, and gratitude to my parents (Rambabu & Kanti) and sisters (Shraddha & Vibha). My parents take care of all the things and provide me the luxury to freely focus on my academic carrier. Howsoever I write, words cannot express my gratitude towards them.

Pandey Kuldeep Rambabu

Abstract

The central theme of the present doctoral thesis work is to understand the occurrence of equatorial counter electrojet (CEJ) or reductions in equatorial electrojet (EEJ) strength under geomagnetically quiet and disturbed conditions. Since variation in the ionospheric zonal electric field is central to any meaningful study on EEJ or CEJ, it is important to know the zonal electric field variations to understand these events. Since systematic measurements of electric fields covering all local times and seasons over the Indian sector are not available, the vertical drifts from the presently available global empirical models [*Scherliess and Fejer*, 1999; *Fejer et al.*, 2008a] are used. Detailed investigations on the applicability of these empirical models over the Indian sector are carried out based on the comparisons with the measured and derived drifts. This investigation revealed that *Fejer et al.* [2008a] model drifts represent the quiet time vertical drifts over the Indian sector fairly well barring early morning hours. Therefore, the drifts obtained from *Fejer et al.* [2008a] model are used in the subsequent investigations, whenever applicable.

Observational studies over the Indian longitudes revealed that the occurrence of quiet time CEJ events is most frequent in afternoon hours during June solstice in solar minimum. An investigation carried out to understand the generation mechanism of these CEJ events showed that these CEJ events are caused by westward Sq electric fields and hence are part of the Sq current system extending from pole to equator. Further, the reversal of EEJ due to disturbance dynamo is investigated and it is found that reductions in the daytime electric field can be significantly large (0.7 ± 0.2 to 1.2 ± 0.3 $m\mathrm{Vm}^{-1}$) during disturbance dynamo events. In order to explain such large westward electric field perturbations, additional role of semi-diurnal tides is indicated. Further, the strength of nighttime equatorial E-region current, used as the base level to determine the EEJ strength, are estimated to be about 0.3 - 0.7 $\mu\mathrm{Am}^{-2}$ based on three methods. The corresponding strength of the horizontal component of magnetic field induced at ground is found to be within 6 nT.

Keywords: Low latitude ionosphere, Sq electric field, plasma drifts, equatorial electrojet (EEJ), equatorial counter electrojet (CEJ), disturbance dynamo, D_{dyn}, reversed electrojet, nighttime E-region current.

Contents

Chapter 1

Introduction

1.1 Background

The evolution of secondary atmosphere of the Earth with abundance of neutral species paved way for supporting the existence of life. Terrestrial neutral atmosphere interacts with the incoming solar radiations and protects the high energy radiations from reaching the lower altitudes. The upper atmosphere of Earth hosts plasma medium with sufficient electron density to affect the radio wave propagation passing through it. This region is known as the "Ionosphere of Earth". The altitude distribution of electron-ion pairs depends on production, loss and transport processes. Over low latitudes, electrodynamics and plasma diffusion play important role at lower and higher altitudes of the ionosphere respectively. Low latitude ionosphere hosts a variety of ionospheric processes such as, plasma fountain, equatorial electrojet, convective ionospheric storm (plasma bubble generation), etc. The ionospheric plasma processes crucially depend on the electrodynamics in this region which is driven by the solar quiet (Sq) electric fields as well as by the impulsively and varying perturbation electric fields during disturbed space weather conditions. This provides complexity to the ionospheric processes and the prediction of the state of ionosphere becomes difficult. In order to comprehensively understand the ionospheric electrodynamics and related processes, it is important to understand and quantify the contributions from quiet and disturbed time electric fields.

This chapter provides a brief introduction to the Earth's atmosphere in general and ionosphere, in particular. A brief introduction is also provided to the generation mechanism of solar quiet (Sq) time electric field over low latitudes and the important role the electric field plays in controlling the large scale plasma processes like equatorial electrojet, plasma fountain, plasma irregularities, etc. As the thesis work mainly concentrates on the processes over the Indian longitudes, the availability of Sq electric field measurements over the Indian sector is discussed. In addition, the prompt and delayed perturbations in electric fields during disturbed space weather conditions are briefly discussed.

1.2 Neutral Atmosphere and Ionosphere

The neutral atmosphere is classified into several regions based on physical parameters like temperature profile, mixing ratios of the constituents. Figure 1.1 depicts typical altitude profiles of neutral temperature (black curve) and density (red curve) over low latitudes. The values represent typical neutral atmosphere during quiet time and are obtained using NRLMSISE-00 Atmosphere Model [*Picone et al.*, 2002] run from Community Coordinated Modeling Center of NASA Goddard Space Flight Center (https://ccmc.gsfc.nasa.gov/). Based on the neutral temperature variation with altitude, the atmosphere is divided into **Troposphere** (0 - 15 km), **Stratosphere** (15 - 50 km), **Mesosphere** (50 - 85 km) and **Thermosphere** (85 - 100 km).

The neutral number density decays exponentially with increasing altitude. The atmospheric constituents below 100 km are mixed homogeneously in composition due to turbulence. This region is known as the "**Homosphere**". Above this region, the distribution of atmospheric constituents is dictated by molecular diffusion process and hence, depend on the mass of the species. The region above 100 km altitude is known as "**Heterosphere**". The altitude profiles of major atmospheric constituents in the Heterosphere are depicted in Figure 1.1 with dashed and dotted curves.

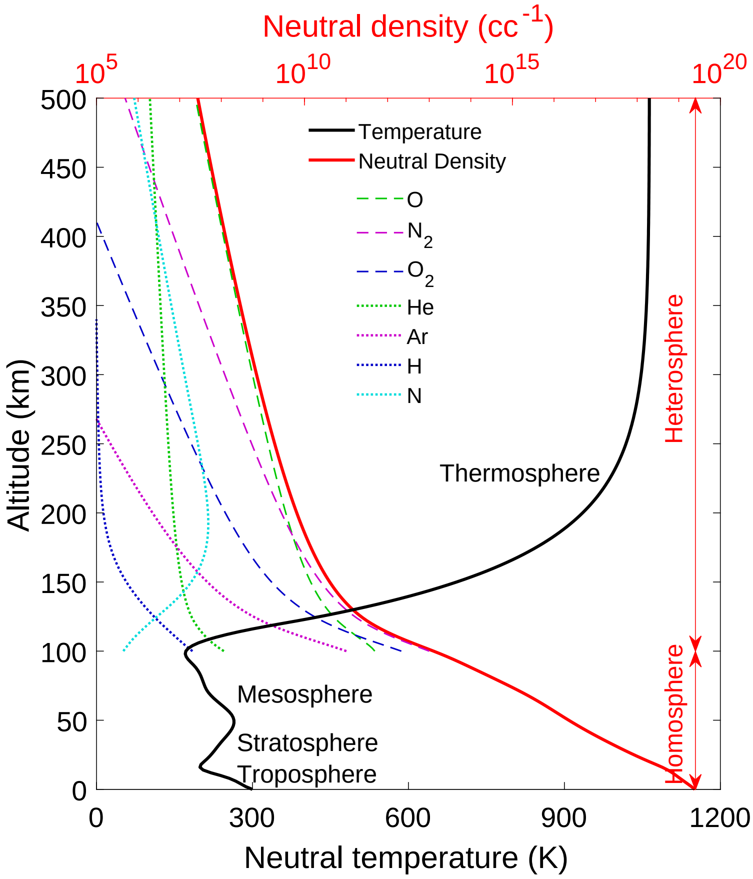

Figure 1.1: Altitude profiles of neutral temperature (red) and number density (black) over equatorial latitudes [based on NRLMSISE-00 model outputs].

The upper atmosphere of the Earth over low latitude region is partially ionized essentially by the electromagnetic radiations emitted from the Sun. This forms a plasma environment around the Earth known as the "**Ionosphere**" that extends from ∼70 km to 1000 km altitudes and it is the region of interest for this thesis work. Figure 1.2 depicts typical altitude profiles of electron density around the magnetic equator. The solid and dashed curves represent the profiles corresponding to noon and midnight hours. The values are generated using IRI-2007 model [*Bilitza and Reinisch*, 2008] runs available from Community Coordinated Modeling Center of NASA Goddard Space Flight Center (https://ccmc.gsfc.nasa.gov/). Different regions of ionosphere, e.g. D (70 - 90 km), E (90 - 150 km) and F (150 - 1000 km) layers are marked in the figure. The E region sustains during nighttime with reduced levels of electron density. Around noon hours, the F-region often splits into two: the lower one being the

F1 region and the higher one, the F2 region. Historically, the name E-region was used for the first layer observed by experiments using radio waves, and subsequently the layers above and below this region were called F and D regions, respectively.

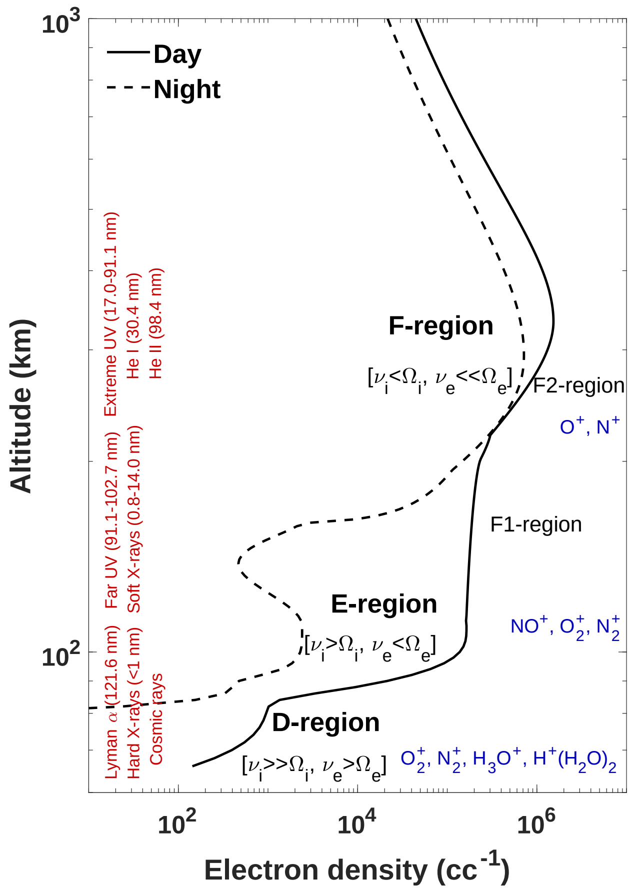

Figure 1.2: Altitude profiles of electron density over equatorial ionosphere during day (solid) and night (dash) times [based on IRI-2007 model outputs].

Over low latitudes, photo-ionization is mainly produced by solar X-ray and wide spectrum of ultra-violet (UV) radiations. The main sources of ionization in D-region are Hydrogen Lyman α line (121.6 nm), hard X-rays ($<$ 1 nm) and to some extent, cosmic X rays [*Nicolet and Aikin*, 1960; *Francey*, 1970]. The ionic species are mainly complex ions like O_2^+, N_2^+, H_3O^+, $H^+(H_2O)_2$. In E-region, also referred to as dynamo region, the main sources of photo-ionization are Far UV radiation (91.1 - 102.7 nm) and soft X-rays (0.8 - 14.0 nm). The dominant ionic species are molecular ions like NO^+ and O_2^+. The NO^+ is a chemical product of interaction between N_2^+, O_2^+ and O^+. During nighttime, the lower levels of plasma density in the E-region are maintained by the Lyman α (121.6 nm) and Lyman β (102.6 nm) radiations [*Strobel et al.*, 1974]. These emissions are from the solar radiation that are resonantly scattered through the geo-corona into the night sector and some contribution is from stellar sources. In F-region, the principle source of photo-ionization is Extreme UV radiation (17.0 - 91.1 nm) along with contributions from HeI (58.4 nm), $HeII$ (30.4 nm) lines at lower F-region. At the lower F-region, the predominant ions are NO^+ and O_2^+ and a gradual transition takes place around 200 km altitude, beyond which O^+ becomes the dominant ion. The substantial difference in ion composition with altitude is also due to the fact that recombination rate of molecular ions with electrons is much higher compared to that of atomic ions. The peak plasma density in F region attains a value as large as 10^6 cc^{-1} around noon hours. Near the peak F-region almost all the ions are O$^+$.

Both electrons (e) and ions (i) tend to gyrate along the geomagnetic field lines with gyro-frequencies Ω_e and Ω_i respectively. In addition, the plasma constituents undergo continuous collisions with the neural atmosphere. As the neutral number density exponentially decreases with altitude, the neutral-collision frequency (ν) decreases rapidly with height whereas, the gyro-frequency does not vary that rapidly with altitude. Therefore, both electrons and ions are controlled by neutral atmosphere ($\Omega_e < \nu_e$, $\Omega_i << \nu_i$) at D-region heights. Medium frequency radio waves get attenuated in the D-region as the energy provided to electrons dissipates into neutral atmosphere due to high electron-neutral collision frequency. The radio wave absorption in D-region is quite significant and is very important for the calculation of the lower usable frequency. In F-region, both electrons and ions are magnetized ($\Omega_e >> \nu_e$, $\Omega_i > \nu_i$) and their motions are governed by the geomagnetic field. In E-region, due to differential behaviour of electron and ion motions in repose to winds, motions of electrons and ions are controlled differently ($\Omega_e > \nu_e$ and $\Omega_i < \nu_i$). The motions of electrons are governed by geomagnetic field, while the motions of ions are controlled by neutral winds. This differential response of ions and electrons to the neutral winds is responsible for the generation of Sq electric field in the E-region.

1.3 Generation of Sq electric field

The differential solar heating (of the atmosphere) and differential gravitational acceleration of lunar origin produce tidal forces in the atmosphere with periods of fractions of the solar and lunar days. These forces set up standing waves in the atmosphere which result in primarily horizontal motions of air. This, in turn, follows the generation of ionospheric Sq current system that flows from pole to equator. These currents are, in general, counter-clockwise in northern hemisphere and clockwise in southern hemisphere during daytime. The centre of these current vortices is called Sq focus. The Sq currents are essentially driven by an electromotive force (*emf*) that is generated by the motion of air, carrying ions with it, and current across the geomagnetic field lines. Owing to anisotropic nature of ionospheric conductivities, this current cannot flow freely along all the directions and polarization charges are thereby set up, modifying the flow of current. As a result, the Solar quiet (Sq) electric field [*Rishbeth and Garriott*, 1969] gets generated. This process is known as the "**E-region dynamo**". The large-scale (scale size greater than a few kilometres) feature of zonal Sq electric field at low latitude E-region gets mapped to the equatorial F-region through equipotential geomagnetic field lines. This zonal electric field drifts the plasma along vertical direction in the F-region.

At F-region, the zonal winds flowing across the geomagnetic field lines produce vertical ion current, which is quite small compared to E-region currents. In order to make the current divergenceless, polarization electric field gets developed along the vertical direction. The strength of this electric field increases till the net current along vertical direction reduces to zero. This is known as the "**F-region dynamo**" [*Rishbeth*, 1981]. The vertical F-region electric field maps to E-region along north-south direction and drifts the electrons along the zonal direction. During daytime, as the E-region conductivities are large, the F-region vertical electric fields gets shorted out. Whereas, after F-region sunset and during nighttime this shorting effect is reduced due to the fact that magnetic field line-integrated E-region conductivity gets reduced considerably because of the reduction in electron densities in E-region owing to fast recombination. The F-region dynamo contributes mainly to vertical electric field during nighttime and partially to the zonal electric field at the sunset terminator in order to maintain the curl-free electric field.

Typical diurnal variations of F-region plasma drifts along zonal and vertical directions are depicted in top and bottom panels of Figure 1.3. These values are based on measurements obtained using incoherent scatter radar over Jicamarca (Peru) in equinoctial months. The red, blue and black curves in the top panel depict the average zonal drifts under low, moderate and high solar flux levels. The zonal drifts are westward during daytime and eastward at night. The amplitudes of zonal drifts are larger in nighttime as compared to daytime. The red, blue and black curves in the bottom panel depict the average vertical drifts corresponding to low, moderate and high solar flux levels. The vertical drifts are upward in daytime and downward at night.

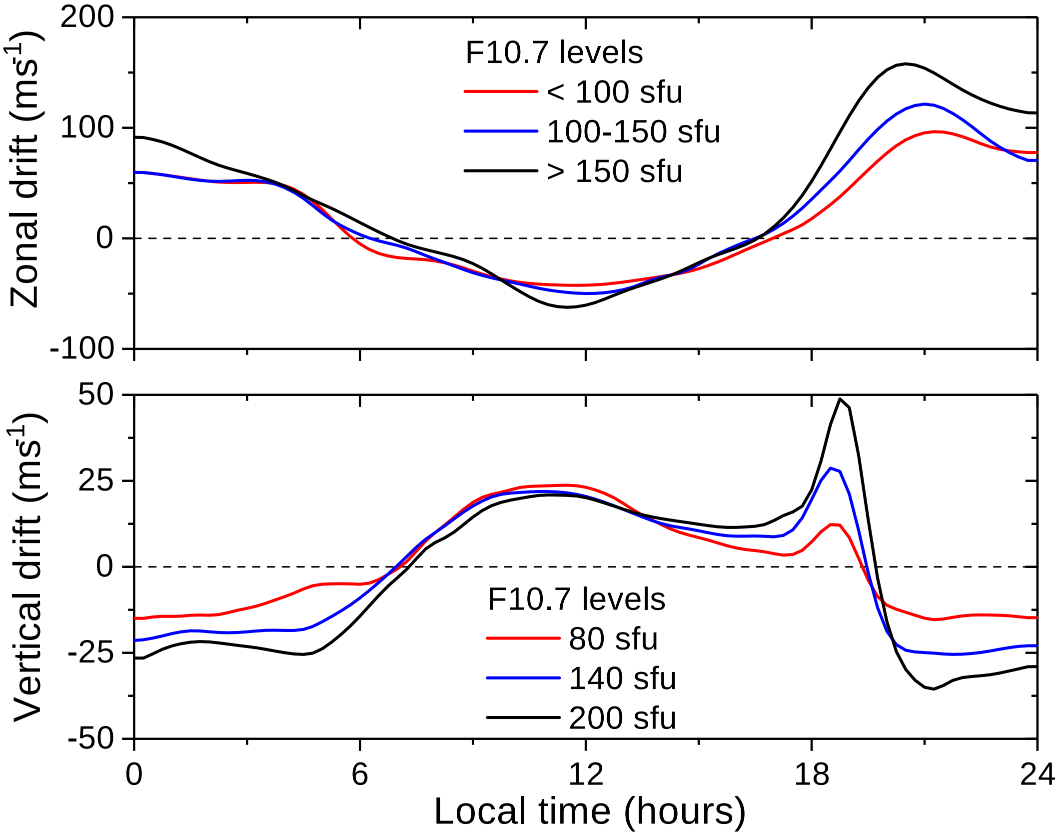

Figure 1.3: Diurnal variation of F-region plasma drifts along zonal [from *Fejer et al.*, 1991] and vertical [from *Scherliess and Fejer*, 1999] directions over Jicamarca in equinoctial months under different solar flux levels.

It is to be noted that, around sunset hours, the vertical drifts deviate from their decreasing trend and reach higher values before finally turning downwards. This is known as the "**pre-reversal enhancement (PRE)**" of vertical drifts. The PRE is generated due to coupled effects of E and F region dynamos. During sunset hours, sharp conductivity gradient exists along zonal direction. This inhibits the flow of hall current, along zonal direction, driven by the north-south electric field at off-equatorial E-region that is mapped from equatorial F-region vertical electric field. As a result, an additional polarization electric field gets developed along the zonal direction that drifts the F-region plasma with stronger amplitude. A recent review [*Eccles et al.*, 2015] on different mechanisms for the generation of PRE is available in the literature.

In the presence of geomagnetic field ($\mathbf{B}$), electric field ($\mathbf{E}$) drifts the plasma with velocity ($\mathbf{V}$) given by,

$$\mathbf{V} = \mathbf{E} \times \mathbf{B}/B^2 \tag{1.1}$$

Therefore, the information of zonal and vertical drifts can provide the ionospheric electric fields along vertical and zonal directions respectively. It is to be noted that the altitude gradient in vertical drifts is negligibly small except during PRE hours [*Pingree and Fejer*, 1987; *Fejer et al.*, 2014]. The resultant difference in vertical drifts at equatorial E-region and peak F-region is less than 2 ms^{-1} in general that is smaller than the resolution of vertical drifts measured by most of the experimental techniques.

1.4 Important roles of Sq electric field on different ionospheric processes

In earlier years, the main emphasis in the ionospheric studies was on the processes related to plasma production and loss, ion chemistry, geomagnetic field variations, and airglow emissions. With the development of radar and space-borne techniques, systematic measurements of electric fields have become available for scientific studies. These techniques have immensely helped to understand the ionosphere in greater detail and the fundamental role played by electric fields has been addressed with unprecedented detail. However, in the absence of an ISR over the Indian sector the electric field variations over this longitude sector couldn't be studied systematically. In view of the availability of electric field information over Indian longitudes using satellite measurements in recent times, detailed investigation over Indian sector is needed. The present thesis work deals with the variations in zonal electric field under geomagnetically quiet and disturbed conditions over the Indian sector. This, in turn, has helped to resolve some of the outstanding scientific problems on low latitude ionosphere. The ensuing subsections briefly describe some of these processes that occur over low latitude ionosphere and the important role of electric field.

1.4.1 Equatorial Electrojet and Counter Electrojet

In daytime, an enhanced eastward current flows overhead in a narrow latitudinal belt centred at the magnetic equator referred to as "**Equatorial Electrojet (EEJ)**" [*Chapman*, 1951]. The generation of EEJ can be understood by a thin-shell model depicted in Figure 1.4.

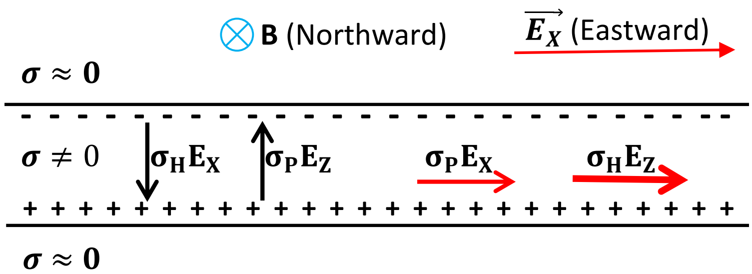

Figure 1.4: Equatorial electrojet in a thin slab geometry.

The daytime eastward Sq electric field causes drift of the E-region electrons in the upward direction whereas, the collisionally bound ions remain at lower altitude. The vertical flow of electrons is inhibited by sharp reduction in the conductivity. This results in an upward electric field (E_z) during daytime that stops the further flow of electrons. This implies the net vertical current to be zero and this can be mathematically represented as follows,

$$J_Z = -\sigma_H E_X + \sigma_P E_Z = 0 \tag{1.2}$$

The vertical electric field maximizes around 105 km altitude with amplitude of about 30 times the zonal electric field. This vertical electric field causes drift of the electrons along westward direction like a jet stream. The results is enhancement in net eastward current given by,

$$J_X = \sigma_H E_Z + \sigma_P E_X = \sigma_C E_X \qquad (1.3)$$

where, $\sigma_C = (J_H^2 + J_P^2)/\sigma_P$

Strength of this current maximizes at the dip-equator due to horizontal nature of geomagnetic field and reduces with increasing latitude. In-situ measurements of E-region current density were obtained [e.g., *Davis et al.*, 1967; *Sastry*, 1970; *Sampath and Sastry*, 1979] based on magnetometer experiments on-board sounding rocket flights. These experiments revealed that the EEJ strength peaks around 105 km altitude. The magnetic field induced at ground by EEJ can be obtained continuously using the measurements by ground based magnetometers.

Several models are available in the literature to explain the observed features of EEJ. A brief description of these models is presented below. *Baker and Martyn* [1953] obtained the ionospheric electric fields under the assumption that the vertical currents are zero and the dynamo region is a thin sheet. Later on, *Sugiura and Cain* [1966] developed a thin-shell numerical model derived from the equation of *Baker and Martyn* [1953] and for the first time brought out the observed longitudinal differences in electrojet. The model was developed based on the assumptions that vertical flow of currents is inhibited and north-south electric fields are negligible. The model by *Baker and Martyn* [1953] is not self-consistent [*Untiedt*, 1967] as it gives rise to strongly divergent current system, whereas the ionospheric currents are non-divergent. *Untiedt* [1967] put forth a two-dimensional model in which allowance was made for meridional currents and a north-south electric field at the magnetic equator. Inclusion of these meridional currents (which become vertical in the vicinity of magnetic equator) doubled the magnetic variations obtained by the thin-shell model [*Sugiura and Cain*, 1966]. This doubling effect relaxed the need for very large wind speed required to produce east-west polarization field [*Tarpley*, 1970] to generate the Sq current system. *Untiedt* [1967] considered a dipole geomagnetic field and computed the electrojet currents by solving a partial differential equation. *Sugiura and Poros* [1969] considered the spherical harmonic expansion to represent the geomagnetic field and solved for two-dimensional current system. The authors [*Sugiura and Poros*, 1969] succeeded in reproducing the inequalities in electrojet current strength at different longitudes, though negative current densities are obtained at about 7° - 8° on either sides of the dip-equator. This feature of negative current density is not obtained in later models [*Richmond*, 1973; *Anandarao*, 1976; *Forbes and Lindzen*, 1976]. *Anandarao* [1976] showed that those negative currents were obtained because of larger grid size in solving the equations numerically. *Anandarao* [1976] improved the grid resolutions used in *Sugiura and Poros* [1969] to obtain the strength of electrojet. In addition, electric fields induced by neutral winds were incorporated in the model to investigate the effects in electrojet current imposed by the neutral winds and shears in it. The important results obtained from this model can be found in earlier works [*Anandarao*, 1976, 1977; *Anandarao and Raghavarao*, 1987; *Raghavarao and Anandarao*, 1987]. In the present thesis work, this model is used without invoking the wind effects. A brief introduction to the model is provided in Chapter 2.

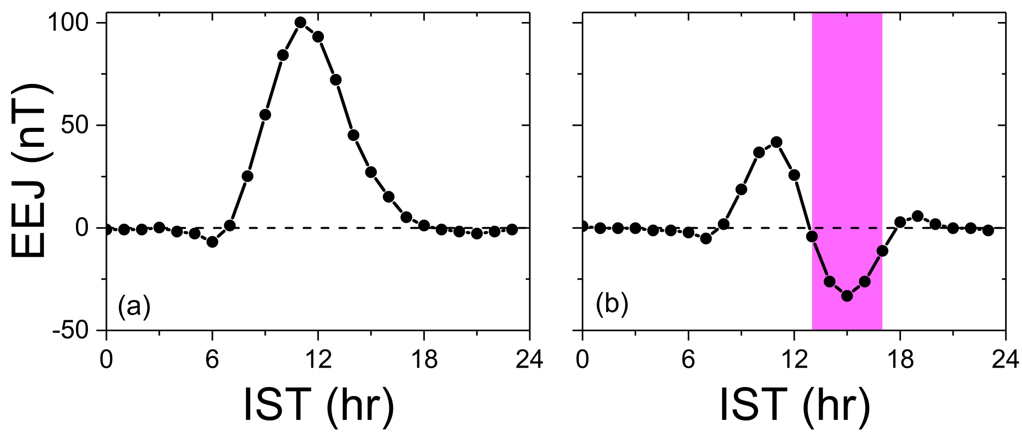

Figure 1.5: Magnetic signatures of (a) normal and (b) counter electrojet.

As stated earlier, in general, the flow of electrojet current is eastward during daytime. However, on many occasions, flow of this current reverses to westward direction that is known [*Gouin*, 1962; *Gouin and Mayaud*, 1967] as "**Counter Electrojet (CEJ)**". The magnetic signature of CEJ is opposite to that of normal electrojet. Figure 1.5 depicts the magnetic signatures of a normal and counter (pink coloured shaded region in Figure 1.5b) electrojet events. Many mechanisms have been proposed to explain the generation of CEJ events on geomagnetically quiet [*Hutton and Oyinloye*, 1970; *Rastogi*, 1974; *Raghavarao and Anandarao*, 1980; *Stening*, 1989a, 1992; *Sridharan et al.*, 2009] and disturbed [*Blanc and Richmond*, 1980; *Kobea et al.*, 2000; *Kikuchi et al.*, 2003] conditions. However, whether the geomagnetically quiet CEJ events are generated locally or part of Sq current system extending from pole to equator, still remains an unresolved issue. It is clear from above that, information on ionospheric zonal electric field is central to any meaningful study on EEJ or CEJ. Some efforts to understand the generation of CEJ events over the Indian sector has been carried out in this thesis work and is discussed in Chapter 4.

1.4.2 Equatorial E-region irregularities

The equatorial E-region hosts plasma irregularities like Two-stream and Gradient-drift waves. Excellent review on these plasma irregularities is provided by *Fejer and Kelley* [1980]. A tutorial on the equatorial E-region and its plasma instabilities is presented by *Farley* [2009].

The "**Two-stream waves or Type 1 irregularities**" are generated when electrons drift through the background ions at a speed exceeding the ion acoustic velocity of the medium. Mathematically this condition is as follows,

$$V_D > (1 + \Psi_0)C_S \tag{1.4}$$

here C_S is the sound speed of the medium and

$$\Psi_0 = \frac{\nu_e \nu_i}{\Omega_e \Omega_i} \tag{1.5}$$

where ν and Ω represent the collision and gyro frequencies respectively.

The basic characteristics of Two-stream waves were obtained using radar based measurements at Peru [e.g., *Bowles et al.*, 1960; *Cohen and Bowles*, 1967] and also using rocket borne probes by pioneering efforts of Indian group [e.g., *Prakash et al.*, 1972; *Gupta*, 2000]. The Two-stream waves appear at altitudes between 103 km and 107 km with a narrow spectrum. These plasma waves are generated over a wide range of zenith angle. The scale sizes of Two-stream waves are about 10 - 1 meters [*Balsley and Farley*, 1971]. The maximum linear growth rate occurs for wavelengths of the order of 3 m [*Farley*, 1963]. These plasma waves are observed during both day and nighttimes. Many features of Two-stream waves can be explained by a modified Two-stream instability theory developed by *Buneman* [1963] and *Farley* [1963]. It is shown [*Sekar et al.*, 2013] that these waves are very sensitive to the location of dip-equator.

The "**Gradient-drift waves or Type 2 irregularities**" are generated if the gradient in electron density is parallel to the direction of background electric field. The average phase velocity of Gradient-drift waves is smaller than the ion acoustic velocity of the medium and is approximately proportional to the cosine of the radar elevation angle [*Balsley*, 1969]. The spectral width is much broader than that due to Two-stream waves and is often much greater than the mean Doppler shift. Studies based on linear growth can explain generation of these waves with scale sizes ranging from a few hundreds to a few tens of meters. Large scale irregularities can transfer their energy and non-linearly cascade down to Gradient-drift waves with scale sizes of a few meters or more [*Sudan et al.*, 1973]. Therefore, Gradient-drift waves can be observed in wide range of wavelengths from ∼300 m to 3 m. These waves are present irrespective of the presence or absence of Two-stream waves. During day and nighttimes the Gradient-drift waves are generated in presence of eastward and westward Sq electric field respectively in regions of positive and negative gradients in electron density. In daytime, these irregularities are not observed during CEJ events. These waves occur between ∼90 km and 120 km altitude range. Investigations by *Sekar et al.* [2014] revealed that the altitude initiation of Gradient-drift waves depends on the square of strength of geomagnetic field and hence, over India and Peru these waves are observed at around ∼87 km and ∼93 km beyond. The vertical electric field for the generation of these waves depend on Sq electric field over the dip-equator. In other words, over the dip-equator the vertical electric field is related to zonal electric field by a factor of about 30 around 105 km altitude (to be discussed in detail in Chapter 3). Thus, generation of both these plasma waves depend on Sq electric field.

1.4.3 Equatorial plasma fountain

As the solar flux is more over the equatorial region, it is generally expected that the ionospheric densities are more at the equator compared to low latitudes. However, latitudinal structure in plasma density was found [*Namba and Maeda*, 1939; *Appleton*, 1946] to be anomalous with a ionization trough at the geomagnetic equator and crests near ±15° about the dip-equator. Several review articles [*Hanson and Moffett*, 1966; *Anderson*, 1973; *Rajaram*, 1977; *Raghavarao et al.*, 1988; *Sastri*, 1990; *Balan et al.*, 2018] are available which explain this anomalous behaviour in terms of the so-called "plasma fountain" effect. This effect is driven by daytime eastward Sq electric field which drifts the equatorial plasma upward followed by diffusion of plasma to either side of the dip-equator along geomagnetic field lines under the influence of pressure gradient force and gravity [*Anderson*, 1973]. Therefore, a latitudinal structure in the plasma density is generated by equatorial plasma fountain effect. A schematic of this process is provided in Figure 1.6. A strong correlation between integrated EEJ strength and the development of plasma fountain has been reported [*Rush and Richmond*, 1973; *Raghavarao et al.*, 1978; *Rama Rao et al.*, 2006; *Aggarwal et al.*, 2012]. Thus, the Sq electric field plays important role in redistribution of plasma in low latitude F-region.

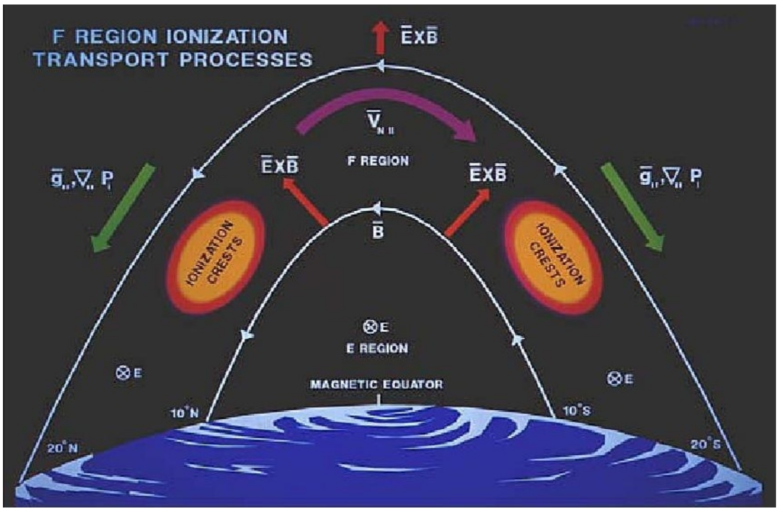

Figure 1.6: Schematic of formation of equatorial plasma fountain [image credit: Air Force Research Laboratory].

1.4.4 Equatorial spread F

After sunset, the ionosonde radar echoes from F-region are spread in the range and/or frequency which is traditionally known as Spread-F. Such events over the equatorial latitudes are known as "**Equatorial spread F (ESF)**". Several experimental [*Woodman and La Hoz*, 1976; *Subbarao and Krishna Murthy*, 1994; *Muralikrishna et al.*, 2003; *Sekar et al.*, 2004; *Reinisch et al.*, 2004; *Muralikrishna*, 2006; *Sekar et al.*, 2012; *Rodrigues et al.*, 2015] and theoretical studies [*Huba et al.*, 1987; *Sekar and Raghavarao*, 1987; *Sekar and Kelley*, 1998; *Sekar and Chakrabarty*, 2008; *Huba and Joyce*, 2007; *Huba et al.*, 2008] have been carried out to explain the generation of irregularities which scatter and spread over various ranges and/or frequencies. A review of ESF observations from Jicamarca and associated theories is provided by *Woodman* [2009]. It is identified that generalized Rayleigh instability involving gravity, electric field and neutral wind are responsible for the growth of these irregularities. The physical mechanism is as follows.

In absence of photoionization after E-region sunset hours, the plasma density in equatorial E-region depletes rapidly due to fast recombination process whereas the ionization in F-region is maintained by slower recombination rate and dynamical processes. Therefore, a steep electron density gradient gets generated at the bottom side F-region during post-sunset hours. Under this condition, a heavier fluid (F-region) is supported by the lighter fluid (bottom side F-region) tends to become unstable under the action of gravity. Under suitable conditions, the plasma density gradient anti-parallel to the gravity results in Rayleigh-Taylor instability. The primary instability is assisted by zonal electric field [*Hanson et al.*, 1986] and neutral winds [*Sekar and Kelley*, 1998]. Under favourable circumstances, the generalized instability grows non-linearly and generate plasma bubbles that sometimes convect to the topside ionosphere.

The scale sizes of plasma irregularities associated with ESF range from several hundreds of kilometres to a few centimetres. Further, as the radar echoes from F layer are spread during ESF events, it is difficult to trace the plasma layer. Under this scenario, it is difficult to obtain the plasma drifts based on radar echoes.

1.5 Sq electric field measurements over India

Continuous measurements on the diurnal variation of plasma drifts driven by Sq electric field [*Woodman*, 1970] are possible by effectively using Incoherent Scatter Radar (ISR) that works on the principle of Thompson scattering [*Gordon*, 1958; *Bowles*, 1958; *Woodman*, 1970]. Several other techniques have also been employed to indirectly obtain the zonal electric fields over different locations. These are ground based experiments (HF/VHF radars, magnetometers) as well as vapour release experiments conducted using sounding rockets. Details of these techniques are briefly presented in Chapter 2. However, the continuous and accurate measurements of vertical drifts over a place are difficult to obtain based on techniques other than ISR. It must be noted that over the dip-equatorial latitudes, the ISR facility is available only at Jicamarca. Therefore, over the longitude sectors other than Jicamarca, systematic measurements on diurnal variations of Sq electric field covering different seasons and solar flux levels are not available.

To some extent, this problem is circumvented based on satellite experiments that can provide vertical drifts along its path around the globe. These measurements can be used to provide the climatological picture of the vertical drifts. Based on such measurements under geomagnetically quiet conditions, *Scherliess and Fejer* [1999] and *Fejer et al.* [2008a] developed global empirical models for quiet time vertical drifts over the dip-equator. In order to increase the statistical significance of model outputs, the measured drift values are averaged over 30° or 15° longitude bins. Details of the inputs to models and criterion employed to develop them are briefly discussed in Chapter 2.

Based on extensive studies using satellite experiments, it is well known that F-region plasma density show longitudinal structures [*Sagawa et al.*, 2005; *Lin et al.*, 2007]. Similar longitudinal structures are observed in EEJ [*Jadhav et al.*, 2002; *Lühr et al.*, 2008; *Lühr and Manoj*, 2013] and equatorial vertical drifts [*Kil et al.*, 2007, 2008, 2009; *Alken and Maus*, 2010]. These observations support the association of longitudinal structure in plasma density with the equatorial vertical drift or Sq electric field. The diurnal non-migrating eastward-propagating tide with zonal wave number 3 (DE-3 tide) is suggested [*Immel et al.*, 2006; *England* *et al.*, 2006; *Hagan et al.*, 2007; *Ren et al.*, 2010] as the driver of longitudinal structure of vertical drift. These variabilities arise from different sources, like tropospheric latent heat release, that modulate the migrating tides excited by the absorption of solar radiation and produce longitudinal variations in the combined tidal strength at E-layer altitudes [*Hagan and Forbes*, 2002].

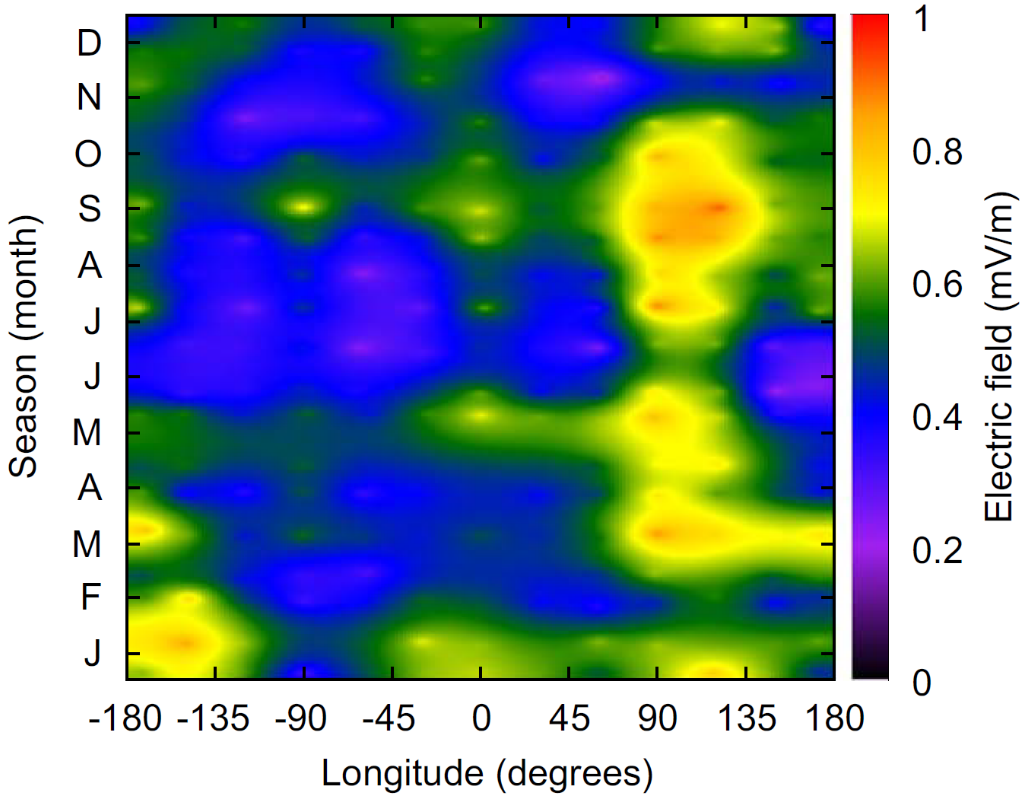

Figure 1.7: Quiet time electric field as a function of longitude and season around 1200 LT [from *Alken and Maus*, 2010].

A typical longitudinal variation of the average zonal electric field at noon as a function of longitudes and months is depicted in Figure 1.7 obtained from [*Alken and Maus*, 2010]. It is clearly visible that the Sq electric field show longitudinal variability. In addition, it has local time dependence [e.g. *Fejer et al.*, 2008a]. Around the Indian sector (80°E longitude), the Sq electric fields show considerable longitudinal variabilities. Therefore, it is important to investigate the applicability of global empirical models [*Scherliess and Fejer*, 1999; *Fejer et al.*, 2008a] over the Indian sector as these models are developed by averaging the vertical drifts over 15° or 30° longitude bins. This problem is dealt in Chapter 3 of this thesis work.

1.6 Electric fields during geomagnetically disturbed periods

The geomagnetic disturbances are primarily driven by our nearest star, the Sun. The sun continuously emits charged particles (∼5 - 20 cc^{-1}) that is known as the solar wind. As the electric conductivity in solar wind is extremely high, the magnetic field is "frozen in" the solar wind plasma. For an observer on Earth, the interplanetary electric field (**IEF**) is given by,

$$\mathbf{IEF} = -\mathbf{V}_{SW} \times \mathbf{B}_{SW} \tag{1.6}$$

here $\mathbf{V}_{SW}$ and $\mathbf{B}_{SW}$ are solar wind velocity and interplanetary magnetic field (IMF) respectively. The southward component of IMF (IMF Bz) is more geoeffective as it favours the reconnection with Earth's dipolar magnetic field which is northward. For a southward IMF Bz, IEF will be along the dawn-dusk direction (IEFy), where X, Y and Z components are based on Geocentric coordinate system like GSM (Geocentric Solar Magnetospheric). After merging on the day side, the magnetic field lines are dragged to night side magnetotail region. Large-scale reconnection process on the night side and subsequent convection of plasma in the earthward direction brings these particles closer to the Earth and these are eventually trapped by the Earth's magnetic field. When these particles encounter closed geomagnetic field lines, electrons and protons drift towards east and west respectively that results in a westward ring current at a distance of 4 - 6 Earth radii. This current induces a southward magnetic field at ground. Therefore, enhancement in the ring current strength indicates the occurrence of a "**geomagnetic storm**" as it results from a series of processes that starts with day side merging of the magnetic field followed by dragging of field lines by solar wind magnetic reconnection and earthward plasma convection. The decrease in horizontal component of Earth's magnetic field strength indicate the severity of a geomagnetic storm.

In general, there are four different phases of a geomagnetic storm: (*i*) sudden storm commencement (SSC), (*ii*) initial phase, (*iii*) main phase, and (*iv*) recovery phase. Different phases of a typical geomagnetic storm are depicted in Figure

1.8. These phases are defined based on the variations of horizontal component of magnetic field and is marked based on Disturbance Storm Time (Dst) index (described in Chapter 2). The red line in Figure 1.8 is drawn at zero Dst level. The SSC is caused due to sudden compression of magnetosphere on the day side by solar wind ram pressure. As a result, the Dst shows step-like enhancement followed by elevated initial phase. These phases are mostly developed during the northward IMF Bz condition. During southward IMF Bz, the ring current enhances that results in Dst enhancement, known as the main phase. When IMF Bz turns northward, the recovery phase of the geomagnetic storm starts because the ring current weakens due to loss of the ring current ions through charge exchange processes and pitch angle scattering. The life time of a typical geomagnetic storm can range from a few hours to a few days.

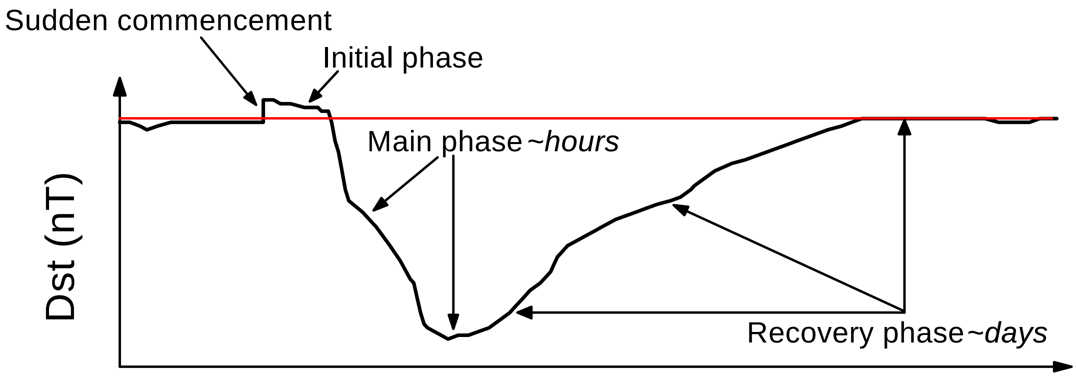

Figure 1.8: Different phases of a typical geomagnetic storm [from *Andriyas and Andriyas*, 2015].

During geomagnetically disturbed conditions, perturbations in the ionospheric electric field over low latitude can arise from the short-lived prompt perturbation electric fields driven by sudden turning of IMF Bz and/or by the relatively longer lasting ionospheric disturbance dynamo effects driven by modified wind conditions due to enhanced energy and momentum deposition into the high latitude ionosphere. In addition, the prompt electric field perturbations can also be driven by the magnetospheric substorm processes. The ensuing subsections provide a brief introduction to the prompt and delayed electric field perturbations over low latitude.

1.6.1 Prompt penetration/over-shielding electric field perturbations

As the dawn-dusk component of Interplanetary Electric Field (IFE_y) field can generate earthward plasma convection from the magnetotail, it is also known as convection electric field. This electric field maps, with varying efficiency, down to high latitude ionosphere through the highly conducting geomagnetic field lines and drives a two-cell convection pattern known as the DP2 (Disturbance-Polar current Type 2). Under suitable conditions, the convection electric field promptly penetrates from high latitude to low latitude ionosphere. This is known as "**prompt penetration (PP) electric field**". The effects of PP electric field have been studied by several researchers [*Pai and Sarabhai*, 1964; *Nishida*, 1968; *Wolf*, 1970; *Vasyliunas*, 1970; *Senior and Blanc*, 1984; *Sastri et al.*, 2000; *Kelley et al.*, 2003; *Huba et al.*, 2005; *Chakrabarty et al.*, 2005, 2015, 2017].

When the convecting plasma from outer magnetosphere reaches closed geomagnetic field lines, it undergoes gradient and curvature drift motions. The drifts of electrons and ions in opposite directions lead to accumulation of positive and negative charges on the dusk and dawn sectors respectively. Therefore, a dusk to dawn electric field builds up at the inner edge of the ring current which eventually shields the inner magnetosphere from further penetration of convection electric field to low-latitude ionosphere.

In order to attain the divergence free current density condition ($\nabla \cdot \mathbf{J} = 0$) at the ring current region, Region 1 (R1) and Region 2 (R2) field-aligned currents (FAC) are generated. A schematic of these currents is depicted in Figure 1.9. R1 FACs are located at higher latitudes ($\sim$67° - 75°), while R2 FACs are located at relatively lower latitudes ($\sim$63° - 68°). The R1 FACs connect outer magnetosphere with the auroral ionosphere and maps the convection electric field to the ionosphere. On the other hand, the R2 FACs close through the highly conducting auroral ionosphere, equatorward to R1 FAC, and shields the effects due to R1 FACs.

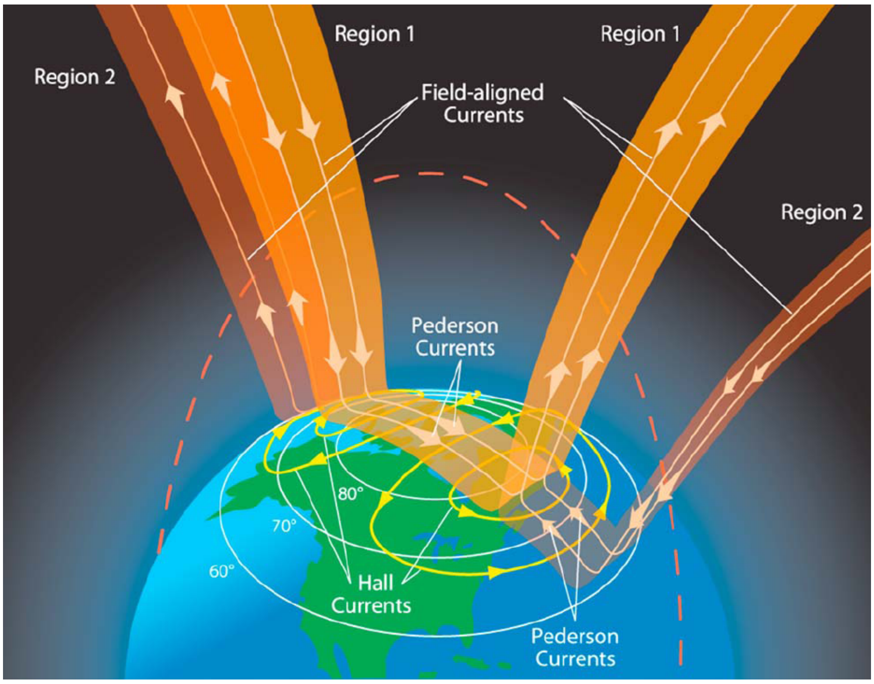

Figure 1.9: Schematic of R1 and R2 FACs and ionospheric current system they connect to [from *Le et al.*, 2010].

The time constant of shielding electric field is ∼20 - 30 min [*Senior and Blanc*, 1984; *Somayajulu et al.*, 1987; *Spiro et al.*, 1988; *Peymirat et al.*, 2000]. Hence, shielding electric field takes time to build. During this time, the effects of PP electric field are experienced over low-latitude ionosphere. On the other hand, if convection electric field is suddenly reduced owing to northward turning of IMF Bz, the fully grown shielding electric field takes time to decay. Under this scenario, the low-latitude ionosphere is over shielded and it experiences the effects of "**over-shielding (OS) electric field**". In general, the polarity of PP electric field perturbations is eastward till 2200 LT and westward in post-midnight hours [*Nopper and Carovillano*, 1978]. The polarity of OS electric field perturbations is opposite to that of PP.

1.6.2 Substorm induced electric field perturbations

The Earth's magnetotail acts like a reservoir for the energy that is generated by interaction between solar wind and Earth's magnetosphere. At some point, this energy must release, and the processes by which it is released is known as "**substorm**". The substorm is one of the most important magnetospheric phenomena and subject of extensive research [*Akasofu and Chapman*, 1961; *McPherron et al.*, 1973; *Kikuchi et al.*, 2003; *Reeves et al.*, 2013]. Initially it was believed that storms are summation of substorms. However, substorms can occur in absence of storm [*Henderson et al.*, 1996] or any apparent triggering mechanism [*Liu et al.*, 2011]. The exact process that triggers substorm is still under debate [*Johnson and Wing*, 2014].

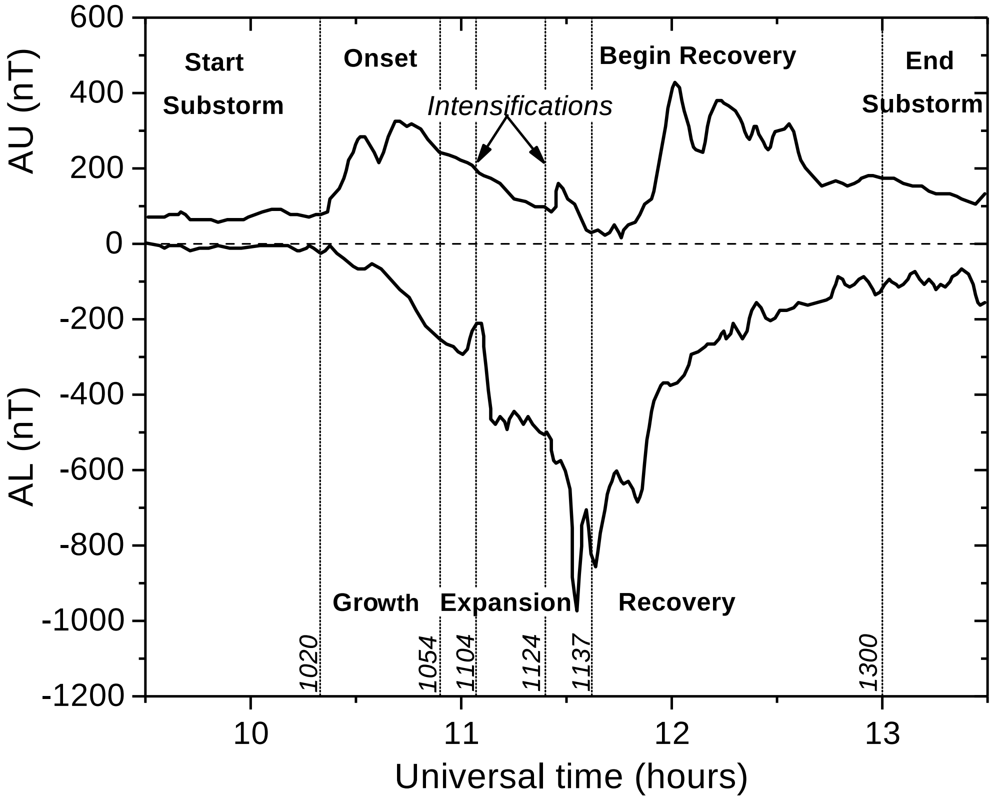

Figure 1.10: Different phases of a typical substorm as seen from AU and AL indices [from *Kivelson and Russell*, 1995].

The lifetime of a substorm is about 2 - 3 hours. During this time, highly structured auroras are seen over auroral regions. There are three phases of a substorm: (*i*) growth, (*ii*) expansion, and (*iii*) recovery phases. A schematic of different phases of substorm are depicted in Figure 1.10. Here, AU and AL are indices for eastward and westward auroral electrojets (details provided in Chapter 2). During the growth phase, magnetic field at the night side becomes stretched. In expansion phase, the sudden dipolarisation of geomagnetic field occurs that results in explosive release of the stored energy, and the auroral activity intensifies over the polar region. In the recovery phase, magnetosphere comes back to its pre-storm condition. The magnitude of AL exceeding 400 nT (i.e. AL < -400 nT) can be used as proxy for the occurrence of substorm [*Janzhura et al.*, 2007]. The most convincing signature of substorm is the dispersionless particle injection (i.e. simultaneous increase in particle fluxes at multiple energy channels) at the geosynchronous orbit that occurs due to the sudden dipolarisation of magnetic field [*Reeves et al.*, 1991].

The fast varying magnetic field induces an electromotive force ($emf = d\phi/dt$, where ϕ is magnetic flux) in the magnetosphere during substorm dipolarisation. The spatial variations in emf produce electric field perturbations in ionosphere. The impact of substorm induced prompt electric field perturbations over the low latitude ionosphere are extensively studied by several researchers [*Kikuchi et al.*, 2003; *Sastri et al.*, 2003; *Huang et al.*, 2004; *Huang*, 2012; *Chakrabarty et al.*, 2008, 2010, 2015]. Recently, it is shown [*Hui et al.*, 2017] that the magnitude of substorm-induced electric fields over low latitudes can be significant and, at times, exceed the magnitude of PP electric field perturbations. Further, it is also shown that substorm induced electric field perturbations can be both additive or subtractive in nature [e.g., *Hui et al.*, 2017].

1.6.3 Disturbance dynamo electric field perturbations

During active phases of geomagnetic storms, the auroral electrojets are intensified that transfer energy to thermosphere via Joule heating. This changes the wind pattern globally. Hadley type of circulation cells are generated at F-region. These winds extend from auroral zones to low latitudes with a small return flow at E-region altitudes around the equator. At mid latitudes, due to Coriolis force action, the equatorward flow turns westward which drives a part of ionized fluid. The westward movement of ionized plasma, in combination with downward component of Earth's magnetic field, produces an equatorward Pedersen current. The result is accumulation of positive charges at the equator (and electrons towards the poles) until a sufficiently strong poleward electric field is established that can restrict the net flow of charges along meridional direction. The poleward electric field gives rise to a large eastward Hall current and a poleward Pedersen current. This physical process is called the "**ionospheric disturbance dynamo**". The first theoretical description of disturbance dynamo (DD) was given by [*Blanc and Richmond*, 1980]. The schematic of that model is depicted in Figure 1.11.

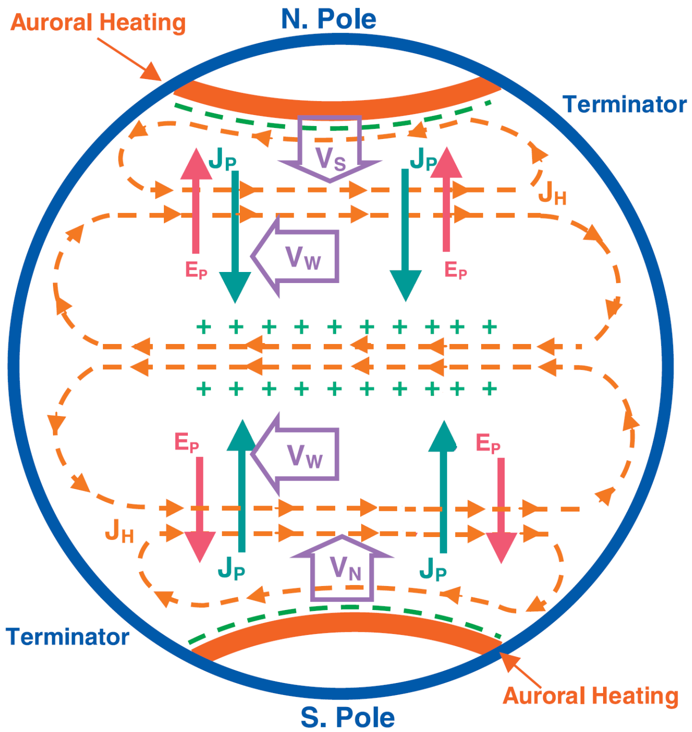

Figure 1.11: Schematic of disturbance dynamo model [from *Abdu et al.*, 2006].

The Hall currents are interrupted at the dawn and dusk terminators owing to large longitudinal gradient in ionospheric conductivities. This sets up polarization charges at the terminators and result in an electric field directed from dusk to dawn. Over low latitudes, the polarity of disturbance dynamo (DD) electric field is opposite to that of the Sq electric field (i.e. westward during daytime and eastward at night). Owing to its association with thermospheric wind circulation, effects of DD are delayed and reach low-latitudes couple of hours after the initiation of main phase of a geomagnetic storm. The effects of DD last from a few hours to a few days [*Huang*, 2013]. For a storm with minimum Dst ~ -95 nT, the effects of DD perturbations is shown [*Yamazaki and Kosch*, 2015] to persist for 24 hrs during the recovery phase.

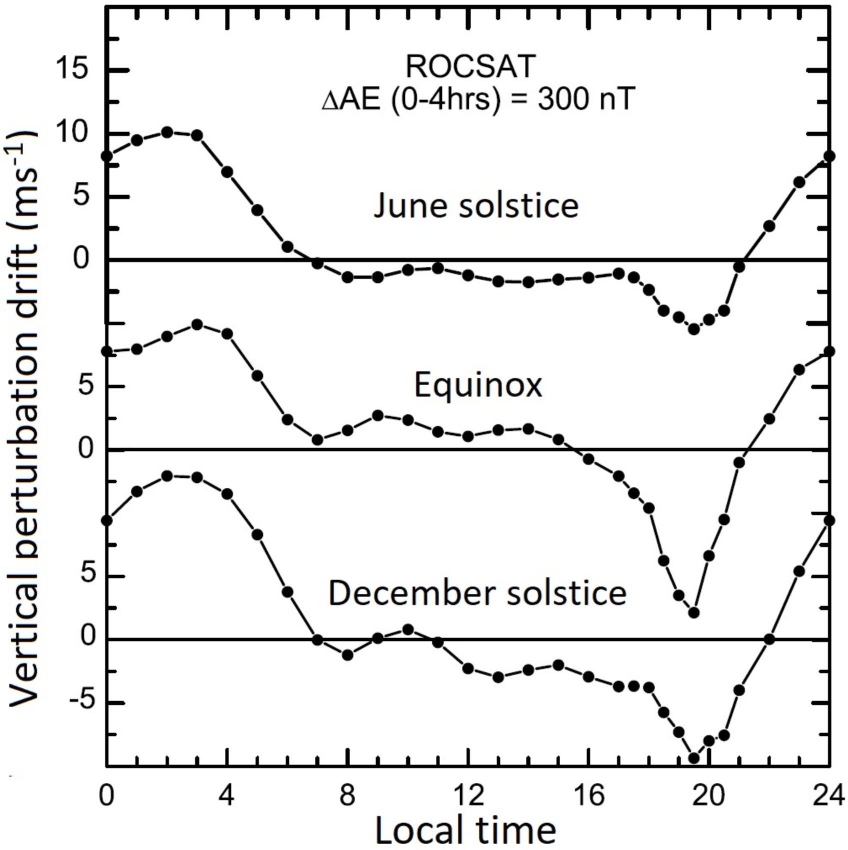

Figure 1.12: Vertical drift perturbations due to disturbance dynamo in different seasons [from *Fejer et al.*, 2008b].

The magnitude of DD electric fields increases with the duration of energy input [*Huang et al.*, 2005]. The DD electric fields are stronger in nighttime compared to daytime [*Scherliess and Fejer*, 1997]. The daytime DD electric fields are smaller due to larger drag force in daytime and shorting out of DD dynamo electric fields by the large E-region conductivities [*Huang and Chen*, 2008]. These features can be seen in the longitudinally averaged values of vertical perturbation drifts of disturbance dynamo origin during June solstice (May - June - July - August), Equinox (March - April, September - October) and December solstice (November - December - January - February) depicted in Figure 1.12 [based on *Fejer et al.*, 2008b]. Modelling study by [*Huang and Chen*, 2008] suggest that in daytime, maximum DD electric field due to strong auroral activity continuing for 24 hours, can reach up to $\sim$0.5 mVm^{-1}. This corresponds to significant increase in the ionospheric electric field as the magnitude of Sq electric field is about 0.5 - 1 mVm^{-1}. The penetration electric fields and/or disturbance dynamo electric fields may dominate during the PRE hours and hence affect the generation of ESF [*Abdu et al.*, 2003; *Abdu*, 2012]. *Yamazaki and Kosch* [2015] carried out a detailed study of disturbance time perturbations in EEJ over Peruvian and Indian sectors. The work by *Yamazaki and Kosch* [2015] showed that reduction in EEJ strength over the Indian sector maximizes near noon, whereas the variations in EEJ strength over Peruvian sector is characterized by a semidiurnal variation with the current disturbances being westward in the morning and eastward in the afternoon. The longitudinal, seasonal, and solar cycle variations of the disturbance dynamo effects are also shown by *Huang* [2013]. Direct observational evidence for disturbance dynamo on daytime ionosphere are shown by *Thampi et al.* [2016]. The observations showed suppression of equatorial plasma fountain due to westward electric field perturbations of disturbance dynamo origin.

The general characteristics of DD electric field have been addressed earlier based on many theoretical [e.g., *Blanc and Richmond*, 1980; *Spiro et al.*, 1988; *Richmond et al.*, 2003] and empirical [e.g., *Scherliess and Fejer*, 1997; *Fejer et al.*, 2008b] models. A recent review on DD perturbations over low latitudes is provided by *Fejer et al.* [2017]. It is to be noted that for the modelling studies of DD an idealized step like increase in auroral region is considered, which need not be the case in reality.

1.7 Aim and overview of the thesis

Primary focus of the present doctoral thesis work is to understand the occurrence of CEJ or reductions in EEJ strength under geomagnetically quiet and disturbed conditions over the Indian sector. As the variation in ionospheric zonal electric field is central to any meaningful study on EEJ or CEJ, it is important to know the zonal electric field variations to understand these events. Since systematic measurements of electric fields covering all local times and seasons over the Indian sector are not available, the vertical drifts from the presently available global empirical models are used after investigating their applicability over the Indian sector.

In this thesis work, a method is evolved to derive the zonal electric fields during daytime from the EEJ strength and the electrojet model [*Anandarao*, 1976]. The models and datasets used for this thesis along with methodology to obtain daytime electric fields are discussed in *Chapter 2*.

In *Chapter 3*, a detailed investigation is carried out to test the applicability of global empirical models of vertical drifts [*Scherliess and Fejer*, 1999; *Fejer et al.*, 2008a] over the Indian sector using the scattered measurements and the electric field deduced from magnetic field measurements from India. In addition, the threshold values and polarity of vertical drifts, inferred based on earlier observations of Two-stream and Gradient-drift waves, are also utilized.

It is noticed that over the Indian sector, occurrence of afternoon CEJ events on geomagnetically quiet days is most frequent during June solstice in solar minimum epoch. A detailed investigation is carried out on whether these CEJ events are part of the Sq current system extending from pole to equator or generated locally. The results obtained and the supporting evidences from the variety of earlier measurements are discussed in *Chapter 4*.

It is difficult to quantify the changes in EEJ due to disturbance dynamo as these changes are mostly coupled with the PP/OS and/or substorm events. This is even more challenging during daytime owing to absence of continuous measurements of the daytime electric fields over different longitude sectors. In the present thesis work, based on 16 years' of EEJ observations, the cases of disturbance dynamo are identified which are free from PP/OS and/or substorm events. The perturbation electric field on these events are estimated and the results obtained are presented in *Chapter 5*.

Night time magnetic field variations are taken as base level to obtain the EEJ strength. Despite that only a few attempts have been made to estimate the nighttime base level. In this thesis work, the strength of night time E-region current is estimated based on three methods. The magnetic field induced at ground by this current is also estimated. The results obtained are presented in *Chapter 6*.

The future scope based on this thesis work is briefly discussed in *Chapter 7*.

Chapter 2

Models and dataset used

The comprehensive understanding of ionospheric processes requires measurements of different parameters and modelling efforts. This thesis work makes use of the plasma drift models developed earlier and datasets obtained from a variety of experiments. The details of the models, methodologies and datasets employed are briefly discussed in this chapter.

An equatorial electrojet model developed by *Anandarao* [1976] is used in this work to compute the strength of equatorial E-region current densities and magnetic fields induced at ground. For the sake of completeness, a brief introduction to this model is given in section 2.1. The sensitivity studies are carried out and the results obtained are provided in section 2.1.3. Further, a methodology is evolved to compute the zonal electric field from the observations of electrojet strength deduced using ground based magnetometers. This method is described in section 2.2. In addition, the datasets and criteria used to develop the global empirical models of vertical drifts [*Scherliess and Fejer*, 1999; *Fejer et al.*, 2008a] are discussed for the sake of completeness.

In the later part of this chapter, a brief introduction is provided to different solar and geomagnetic indices that are used in this work. Measurement techniques employed to obtain the magnetic field variations at ground, in-situ profiles of E-region electron density and irregularities, vertical plasma drifts are briefly discussed. These measurements span from 1957 to 2015 and are utilized during the course of this thesis work. Sources of the datasets utilized are also provided.

2.1 Theoretical model of EEJ

A physics based model for equatorial electrojet was developed by *Anandarao* [1976] using basic equation of generalized Ohm's law

$$\mathbf{J} = \sigma_0 \mathbf{E}_{\parallel} + \sigma_P \mathbf{E}_{\perp} + \sigma_H \frac{\mathbf{B} \times \mathbf{E}_{\perp}}{B} \tag{2.1}$$

with conditions of current conservation

$$\nabla \cdot \mathbf{J} = 0 \tag{2.2}$$

and curl-free electric field

$$\nabla \times \mathbf{E} = 0 \tag{2.3}$$

Here $\mathbf{J}$ is current density, $\mathbf{E}_{\parallel}$ and $\mathbf{E}_{\perp}$ are electric fields parallel and perpendicular to magnetic field of the Earth ($\mathbf{B}$), and σ_0, σ_P, σ_H represent direct, Pedersen, Hall conductivities respectively. These conductivities can be expressed [*Rishbeth and Garriott*, 1969] mathematically as follows,

$$\begin{aligned}
\sigma_0 &= \frac{N_e}{B}\left[\frac{\omega_e}{\nu_e} + \frac{\omega_i}{\nu_i}\right] \\
\sigma_P &= \frac{N_e}{B}\left[\frac{\nu_e\ \omega_e}{\nu_e^2 + \omega_e^2} + \frac{\nu_i\ \omega_i}{\nu_i^2 + \omega_i^2}\right] \\
\sigma_H &= \frac{N_e}{B}\left[\frac{\omega_e^2}{\nu_e^2 + \omega_e^2} - \frac{\omega_i^2}{\nu_i^2 + \omega_i^2}\right]
\end{aligned} \tag{2.4}$$

where N_e is electron density and ω, ν are gyro-frequency and neutral collision frequency. Subscripts e and i corresponds to electron and ion respectively.

Equations (2.1), (2.2) and (2.3) are solved numerically in geocentric coordinate system (r, θ, ϕ) where r is radial distance from the centre of the Earth, θ is the magnetic co-latitude and ϕ is the longitude. The variation of ionospheric parameters involved in the model calculations with respect to ϕ is assumed to be negligible. *Richmond* [1973] estimated the error due to this assumption to be about 14% in the electrojet current, if the fields and conductivities vary in ϕ direction with typical scale lengths of 6490 km (or 1 radian in ϕ). This assumption can be taken to be valid even in the presence of slowly varying electric field with longitude as reported in recent observations [e.g., *Fejer et al.*, 2008a]

Equation (2.2) implies that the current density $\mathbf{J}$ can be expressed in terms of vector potential $\mathbf{A}$ as follows,

$$\mathbf{J} = \nabla \times \mathbf{A} \tag{2.5}$$

Let A_ϕ be the longitudinal component of vector potential $\mathbf{A}$ and a be the radius of Earth. The above equation in component form is written as,

$$\begin{aligned} J_r &= -\frac{a}{r^2 \sin\theta} \frac{\partial \psi}{\partial \theta} \\ J_\theta &= \frac{a}{r \sin\theta} \frac{\partial \psi}{\partial r} \end{aligned} \tag{2.6}$$

here ψ is current function defined as,

$$\psi = -r \sin\theta A_\phi \tag{2.7}$$

From equation (2.3) we have,

$$\begin{aligned} \frac{\partial}{\partial \theta}(E_\phi \sin\theta) &= 0 \\ \frac{\partial}{\partial r}(r E_\phi) &= 0 \\ \frac{\partial}{\partial r}(r E_\theta) - \frac{\partial}{\partial \theta} E_r &= 0 \end{aligned} \tag{2.8}$$

It is clear from the first two equations of (2.7) that E_ϕ can be represented by,

$$E_\phi = \frac{a}{r} \frac{E_{\phi 0}}{\sin\theta} \tag{2.9}$$

here $E_{\phi 0}$ is a constant and it is the primary zonal electric field that needs to be furnished as input to calculate the current function.

The components $\mathbf{J}$ from equation (2.1) in r, θ, ϕ directions are,

$$\begin{aligned} J_r &= (\sigma_0 S^2 + \sigma_P C^2) E_r + (\sigma_0 - \sigma_P) E_\theta S C - \sigma_H E_\phi C \\ J_\theta &= (\sigma_0 - \sigma_P) E_r S C + (\sigma_0 C^2 + \sigma_P S^2) E_\theta - \sigma_H E_\phi S \\ J_\phi &= \sigma_H E_r C - \sigma_H E_\theta S + \sigma_P E_\phi \end{aligned} \tag{2.10}$$

From these the following equations of E_r and E_θ can be obtained,

$$\begin{aligned} E_r &= \frac{\sigma_H}{\sigma_P} C E_\phi + J_r(\rho_0 C^2 - \rho_P S^2) - J_\theta(\rho_0 - \rho_P) S C \\ E_\theta &= -\frac{\sigma_H}{\sigma_P} S E_\phi - J_r(\rho_P - \rho_0) S C + J_\theta(\rho_P S^2 - \rho_0 C^2) \end{aligned} \tag{2.11}$$

here S and C denote $\sin I$ and $\cos I$ with 'I' representing the dip-angle, and $\rho_0 = 1/\sigma_0$, $\rho_P = 1/\sigma_P$. Substituting equations (2.6) and (2.11) in the equation (2.8) we get the following second order elliptic partial differential equation,

$$f_1 \frac{\partial^2 \psi}{\partial r^2} \; + \; 2f_2 \frac{\partial^2 \psi}{\partial r \partial \theta} \; + \; f_3 \frac{\partial^2 \psi}{\partial^2 \theta} \; + \; f_4 \frac{\partial \psi}{\partial r} \; + \; f_5 \frac{\partial \psi}{\partial \theta} \; + \; f_6 = 0 \tag{2.12}$$

The coefficients f_1 to f_6 are functions of ionospheric conductivities and the zonal electric fields [*Sugiura and Poros*, 1969; *Anandarao*, 1977]. These are given by,

$$\begin{aligned}
f_1 &= \rho_P S^2 + \rho_0 C^2 \\
f_2 &= \frac{1}{r}(\rho_P - \rho_0) SC \\
f_3 &= \frac{1}{r^2}(\rho_P C^2 + \rho_0 S^2) \\
f_4 &= \frac{\partial}{\partial r}(\rho_P S^2 + \rho_0 C^2) - \frac{1}{r}\cot\theta(\rho_P - \rho_0)SC + \frac{1}{r}\frac{\partial}{\partial \theta}(\rho_P - \rho_0)SC \\
f_5 &= \frac{1}{r}\frac{\partial}{\partial r}(\rho_P - \rho_0)SC - \frac{1}{r^2}(\rho_P - \rho_0)SC - (\frac{\cot\theta}{r^2})(\rho_P C^2 + \rho_0 S^2) + \frac{1}{r^2}\frac{\partial}{\partial \theta}(\rho_P C^2 + \rho_0 S^2) \\
f_6 &= -E_{\phi 0}\left[\frac{1}{r}\frac{\partial}{\partial \theta}(\frac{\sigma_H C}{\sigma_P}) - \frac{1}{r}\frac{\sigma_H}{\sigma_P} C \cot\theta + \frac{\partial}{\partial r}(\frac{\sigma_H S}{\sigma_P})\right]
\end{aligned} \tag{2.13}$$

The equation (2.12) is solved for ψ numerically using the method of successive over-relaxation in two dimensions: along the vertical (80 - 200 km) and co-latitudinal (75° to 105°) directions. The grid sizes of $\Delta r = 1$ km and $\Delta\theta = 0.25°$ are employed for the present thesis work. $\psi = 0$ at all the boundaries (i.e. $\psi_{\text{at 80 km, 200 km, 75°, 105°}} = 0$).

After obtaining $\psi(r, \theta)$, the components of current density J_r and J_θ are obtained using equation (2.6). Subsequently, J_r and J_θ are used to compute E_r and E_θ based on first two equations of (2.10). Finally, J_ϕ (equatorial electrojet current density) is computed using these values in the last equation of (2.10). Further details of this model can be found in the doctoral thesis of *Anandarao* [1977] and works of *Anandarao* [1976]; *Raghavarao and Anandarao* [1980]; *Anandarao and Raghavarao* [1987].

2.1.1 Inputs to the model

Inputs to the electrojet model are zonal Sq electric field (as $E_{\phi 0}$), altitude profiles of E-region electron density, atmospheric neutral density and temperature, and three dimensional geomagnetic field.

As discussed in Chapter 1, the systematic ground based measurements of Sq electric field over India covering all local times and seasons are not available because of absence of an incoherent scatter radar. Based on the scattered data that were available, the author showed (Chapter 3) that the vertical drifts reported by *Fejer et al.* [2008a] model corresponding to 60°E longitude (with ±15° longitude) represent the vertical drifts over the Indian sector fairly well at different local times of the day barring early morning hours [*Pandey et al.*, 2017]. Therefore, the *Fejer et al.* [2008a] model drifts are used as input to EEJ model in Chapters 4 and 6. Details of the *Fejer et al.* [2008a] model are discussed in second part of this chapter.

The input of E region electron densities is based on the in-situ measurements [*Subbaraya et al.*, 1983; *Gupta*, 2000] that have been obtained using high frequency Langmuir probe [*Prakash and Subbaraya*, 1967] measurements on-board sounding rocket experiments from India. These experiments were conducted from Trivandrum at different local times between 1968 and 1982. Further details on it are presented in section 2.6. The altitude profiles of neutral density and temperature corresponding to different latitudes are obtained from NRLMSISE-00 [*Picone et al.*, 2002] model outputs. The geomagnetic fields at different altitudes and latitudes are taken from IGRF-12 [*Thébault et al.*, 2015] model.

2.1.2 On the temporal variation of the model outputs

It is to be noted here that the temporally advanced solutions from the model are obtained using piecewise method and not by solving the continuity equation. The model solutions are obtained in E-region which is governed by photo-chemical equilibrium. Thus, the usage of temporally advanced (later in time) electron densities and electric fields as inputs into the model fairly represents time advanced (later in time) solution.

2.1.3 Calculation of magnetic field induced at ground by EEJ

In order to estimate the magnetic field induced at ground by ionospheric current, a method described by *Anandarao* [1977] is adopted. In this method, the magnetic field potential (V) induced by an infinitely long line of current is defined based on Biot-Savart's law as,

$$V = \frac{\mu_0 C}{2\pi} \tan^{-1}\left(\frac{\cos\theta}{(r/a) - \sin\theta}\right) \tag{2.14}$$

where μ_0 and C are the permeability of free space and line current (in Amperes) respectively. The line current C is obtained from current density J_x using

$$C = \int_r \int_\theta J_\phi \, dr \, d\theta \tag{2.15}$$

here the symbols a and r denote the radius of Earth and distance of the line current from the centre of Earth respectively. Further, the horizontal (magnetic-northward) component of magnetic field (H) induced due to ionospheric current is given by,

$$H = -\frac{1}{r}\frac{\partial V}{\partial \theta} = \frac{\mu_0 C}{2\pi r} \frac{(r/a)\sin\theta - 1}{(r/a)^2 + 1 - 2(r/a)\sin\theta} \tag{2.16}$$

The numerical simulation plane is divided into 1° (in θ) $\times$ 4 km (in r) blocks and induced H is calculated. Subsequently, the H values of each block are added up to get the net induced values at ground.

2.1.4 Sensitivity study of the model outputs

A sensitivity study of the model outputs is performed by changing each input individually (keeping other inputs constant) and the corresponding changes in peak output values are noted. A zonal electric field of 1 mVm^{-1} is used as reference. Noontime average electron density as depicted in Figure 2.2(c) is used. The neutral density and temperature are taken from Figure 1.1. Table 2.1 lists the changes in maximum values of output vertical electric field, zonal current density and horizontal component of magnetic field induced at ground corresponding to the changes in individual inputs, namely zonal electric field, electron density, neutral density and temperature. It is found that the changes in vertical electric field are linearly dependent on changes in input electric field and independent of electron density, as expected. The changes in vertical electric field are not found to vary significantly with neutral density and temperature. Further, the changes in zonal current density depend linearly on changes in input electric field and electron density. However, the changes in zonal current density are non-linear and not very significantly dependent on neutral density and temperature. The sensitivity of horizontal magnetic field induced at ground on the individual inputs is similar to that of zonal current density.

Input	Change in input (%)	Change in output (%)		
		Vertical electric field	Zonal current density	Horizontal magnetic field induced at ground
Zonal electric field	-10	-10	-10	-10
	-5	-5	-5	-5
	+5	+5	+5	+5
	+10	+10	+10	+10
Electron density	-5	0	-5	-5
	-2	0	-2	-2
	+2	0	+2	+2
	+5	0	+5	+5
Neutral density	-8	+1.5	-4.2	-5.3
	-4	+0.7	-2.1	-2.6
	+4	-0.1	+2.0	+2.6
	+8	-0.2	+3.8	+5.1
Neutral temperature	-8	+2.3	+1.0	+0.7
	-4	+1.1	+0.5	+0.3
	+4	-0.9	-0.5	-0.3
	+8	-1.8	-0.9	-0.6

Table 2.1: Electrojet model outputs vis-a-vis individual input parameters.

2.1.5 Maximum uncertainties in the model outputs

In order to estimate the maximum uncertainty in the electrojet model outputs, the uncertainties involved in the input parameters are analysed. The resolution of drift measurements (or corresponding electric field) is 10% [*Fejer et al.*, 2008a], and the accuracy of electron density measurements is 2% at daytime and 5% at night [*Subbaraya et al.*, 1983]. Further, the standard deviations in neutral parameters is about 4% [*Marcos et al.*, 2006]. Therefore, changes in the maximum values of output parameters are noted by changing each input parameter with respective uncertainty/standard deviation in different combinations. The results obtained for daytime conditions are shown in Table 2.2.

It is found that the maximum uncertainty in the computed vertical electric field, zonal current density and horizontal magnetic field induced at ground are about 14%, 18% and 19%, respectively, at daytime. For nighttime conditions, when uncertainty in electron density is more, the uncertainties in the computed zonal current density and horizontal magnetic field induced at ground increase to about 21% and 22%.

Uncertainty/standard deviation in input (%)				Maximum change in output (%)		
Zonal electric field	Electron density	Neutral density	Neutral temperature	Vertical electric field	Zonal current density	Horizontal magnetic field induced at ground
-10	-2	-8	-8	-6.6	-14.4	-15.9
			+8	-10.5	-16.4	-17.0
		+8	-8	-8.3	-7.4	-6.7
			+8	-11.9	-9.3	-7.9
+10	+2	-8	-8	+14.1	+8.9	+7.0
			+8	+9.3	+6.3	+5.6
		+8	-8	+12.0	+17.8	+18.7
			+8	+7.6	+15.3	+17.1

Table 2.2: Maximum change in electrojet model outputs corresponding to maximum uncertainty/standard deviation in input parameters.

2.2 A method to estimate daytime zonal electric fields

As stated in the Chapter 1, in the absence of ISR over the Indian sector, it is difficult to obtain the daytime Sq electric fields. In order to overcome this issue, a methodology is devised to obtain the daytime electric field from the EEJ strength deduced using magnetometer observations of horizontal magnetic field induced at ground by the equatorial electrojet current using the EEJ model.

By assuming a reasonable input electric field ($E_{\phi 0}$), the values of zonal current density (J_ϕ) and magnetic field (H) induced by it are computed for the particular time, season and solar epoch. The computed H value is compared to the value of the EEJ strength deduced using magnetometer observations and the difference between the two is noted. Based on the polarity and amplitude of this difference the input $E_{\phi 0}$ is altered step-by-step till the difference between H and deduced EEJ strength reduces to 0.1 nT, which is equivalent to the accuracy of magnetometer measurements.

The uncertainty in the estimated zonal electric field arises essentially due to the uncertainty/standard deviation in the input electron density and neutral parameters as the error due to uncertainty in magnetic field measurement is insignificant. The average electron density profiles, having day-to-day variations within 20% (discussed in detail in section 2.9), are utilized as input for the computation of zonal electric fields. Therefore, the uncertainty in the computed zonal electric field would be less than 25%.

2.3 Global empirical models of quiet time vertical drifts over the dip-equator

The measurements of vertical drifts in the vicinity of the dip-equator around the globe have been carried out with Ion Drift Meter (IDM) on board satellites [e.g., *Hanson and Heelis*, 1975]. The instrument is oriented in direction of motion of satellite that moves with supersonic velocity. This makes the ion beam collimated at the entrance aperture of IDM. The angle of arrival of ions at the detector are determined to derive the two orthogonal components (with respect to satellite motion) of drifts. This information is used to calculate the ion drift in the ionosphere. Based on vertical drifts measured using satellite experiments, *Scherliess and Fejer* [1999] and *Fejer et al.* [2008a] developed the empirical models of the seasonally averaged diurnal variations of the dip-equatorial vertical drifts under geomagnetically quiet condition (Kp $\leq$ 3) corresponding to different longitude sectors. The details of datasets and methodology used to develop these empirical models are discussed in ensuing paragraphs.

In *Scherliess and Fejer* [1999] model, the vertical drifts measured around the globe with IDM on board Atmospheric Explorer-E (AE-E) satellite from 1977 to 1979 are used. In addition, the vertical drifts measured by an Incoherent Scatter Radar (ISR) over Peru during 1968 - 1992 are utilized. The vertical drifts measured over $\pm 7.5°$ dip-latitude and $\pm 30°$ longitude are averaged. Further, the local time and longitudinal dependence of vertical drifts are obtained by products of universal normalized cubic-B splines of order four. These vertical drifts are constrained to satisfy the curl-free nature of electric field ($\oint \mathbf{E} \cdot d\mathbf{l} = 0$) by employing different statistical weights to vertical drifts around the globe. Based on these criteria, *Scherliess and Fejer* [1999] reported the vertical drifts for different sectors centred at 60° E and other longitudes. These drifts are presented for F10.7 levels of 90 sfu and 180 sfu corresponding to solar minimum and maximum conditions respectively.

Fejer et al. [2008a] model utilized the vertical drifts measured using Ionospheric Plasma and Electrodynamics Probe Instrument (IPEI) on board Republic of China Satellite-1 (ROCSAT-1) during 1999 - 2004. The vertical drifts measured over $\pm 5°$ dip-latitude and $\pm 15°$ longitude are averaged to develop the model. The vertical drifts for different sectors separated by 60° longitudes are present for F10.7 levels of 130 sfu and 200 sfu.

In Chapter 3, the applicability of vertical drifts presented by both these empirical models over the Indian sector is investigated. In Chapters 4 and 6, the *Fejer et al.* [2008a] model, which is found to represent the vertical drifts over Indian sector better than *Scherliess and Fejer* [1999] model, is utilized to provide the corresponding Sq electric field input to the equatorial electrojet model. It should be noted that both the empirical models use the IDM measurements that are reliable if the background plasma density is more than 10^3 cc^{-1}. As a consequence, uncertainties in the model plasma drifts can be expected to be higher during late night-sunrise period, especially for low solar flux values, when the plasma densities reduce substantially.

2.4 Solar and geomagnetic indices

The solar radio flux at 10.7 cm wavelength originates from upper chromosphere and lower corona of the solar atmosphere. These are traditionally termed as F10.7 index and reported in solar flux units (sfu, 1 sfu = 10^{22} Wm^{-2}Hz^{-1}). The F10.7 correlates well with the sunspot number and visible solar irradiance records. In addition, the Extreme Ultra-violet (EUV) emissions that impact the thermosphere-ionosphere system match well with the F10.7 index. Further, measurements of F10.7 can be made reliably and accurately from the ground in all weather conditions. Therefore, it is a very robust data set and can be utilized as a proxy for solar activity.

The F10.7 index is provided as one of the inputs to neutral atmosphere model [NRLMSISE-00, *Picone et al.*, 2002] that is made as a part of a subroutine in the EEJ model [*Anandarao*, 1976]. The F10.7 values are obtained from Laboratory for Atmospheric and Space Physics website (http://lasp.colourado.edu/lisird/tss/noaa_radio_flux.html). The annually averaged F10.7 index values are depicted from 1950 in Figure 2.1. Based on these values, it is identified whether the ionospheric measurements of a given year belong to low or high solar epoch.

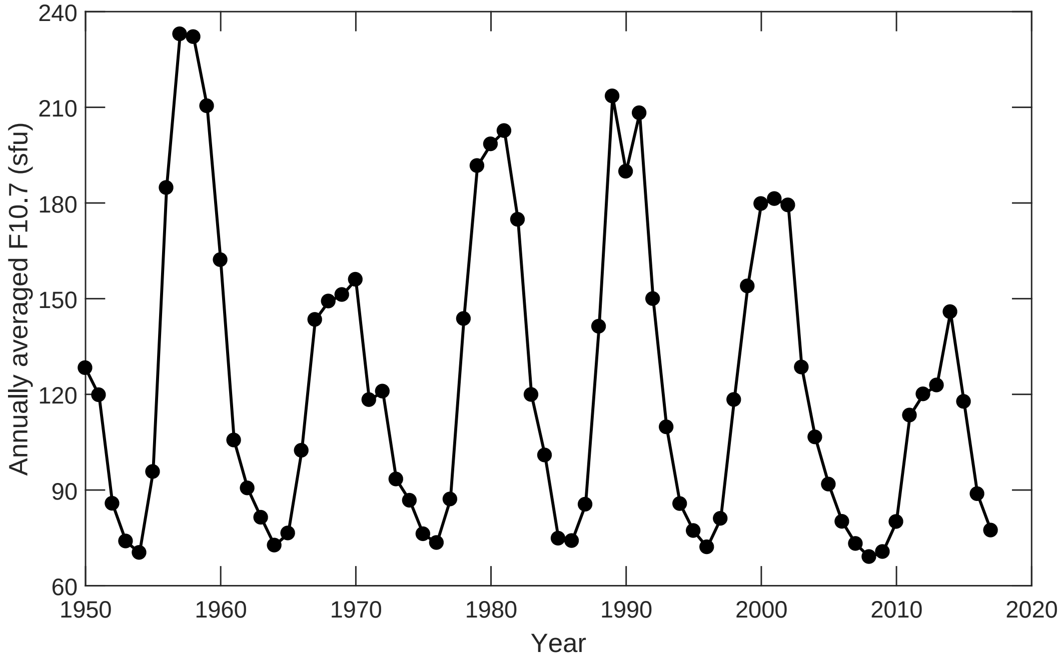

Figure 2.1: Annually averaged solar F10.7 index from 1950 onwards.

In this thesis work, solar wind parameters are obtained based on the observations at L1 point (first Lagrangian point of the Sun-Earth system). Measurements of interplanetary magnetic field (IMF) are obtained by Advanced Composition Explorer (ACE), WIND satellites situated at L1 point. The north-south component of IMF (IMF Bz), time shifted to the nose of the Earth's bow shock, are obtained from Coordinated Data Analysis Web (CDAWeb, https://cdaweb.sci.gsfc.nasa.gov/index.html/) of NASA.

The Dst (Disturbance storm time) index is used to characterize the severity of a geomagnetic storm. It is based on average of hourly horizontal geomagnetic fields measured at four observatories, namely Hermanus (34.4° S, 19.2° E), Kakioka (36.2° N, 140.2° E), Honolulu (21.3° N, 158.1° W) and SanJuan (18.4° N, 66.1° W). These observatories are located at distances sufficiently away from the auroral and equatorial electrojets and they are distributed in longitudes as evenly as possible. The Dst index provides the strength of magnetic field induced at ground by the ring current, which increases during geomagnetic storms. In the case of a classic geomagnetic storm, the Dst index shows a sudden rise, corresponding to the storm sudden commencement, and then decreases sharply as the ring current intensifies. In the present thesis, the Dst index is utilized to categorize days with and without history of geomagnetic storm. The values of index are obtained from the World Data Center, Kyoto (WDC Kyoto, http://wdc.kugi.kyoto-u.ac.jp/).

The AE indices were devised by *Davis and Sugiura* [1966] as a measure of electrojet activity over the auroral zone. The index is derived from horizontal component of geomagnetic fields measurements at 10 - 13 observatories in northern auroral zone (60° - 70° N). For all these stations, the variations above quiet time level (average of five geomagnetically quiet days) corresponding to the same UT are superposed. The upper and lower envelopes of this superposition define the AU (amplitude upper) and the AL (amplitude lower) indices, respectively. The difference between two envelopes determines the Auroral Electrojet, AE (AU−AL) index. Enhancement in the westward electrojet makes the AL index decrease (intensify in magnitude) and enhancement in eastward electrojet causes the AU index increase. In this thesis work, the AL index is utilized (Chapter 5) to infer [*Janzhura et al.*, 2007] the possible occurrence or absence of substorm. The datasets of AE indices are obtained from NASA CDAWeb (https://cdaweb.sci.gsfc.nasa.gov/index.html/).

2.5 Ground based magnetometers to observe EEJ strength

The ground based magnetometers have been extensively used to measure the overhead currents after suitably taking care of the various components of the Earth's internal magnetic field. A large number of magnetic field observatories around the globe continuously measure the geomagnetic fields.

Over the Indian longitudes, the observatories with fluxgate magnetometers cover a wide range of latitudes extending from the dip equator up to the focus of the Sq current system. This provides a unique opportunity to study the phenomena of ionospheric Sq current system as well as the equatorial electrojet. The geomagnetic equator passes through the southern peninsular region of India. The geomagnetic field observatories like Trivandrum (TRD: 8.5°N, 76.9°E) and

Tirunelveli (TIR: 8.7°N, 77.8°E) are situated in the vicinity of the geomagnetic equator. The Trivandrum observatory was operational from 1957 to 1999 and observations from Tirunelveli are available from 1999 onwards. The off-equatorial geomagnetic field observatory Alibag (ABG: 18.6°N, 72.9°E) was established in 1904 as the substitute for nearby Colaba Observatory that continuously recorded the magnetic field data since 1846. These observatories are continuously operated by the Indian Institute of Geomagnetism, Mumbai and provide the hourly variations of geomagnetic fields to the word data centres. The present thesis work utilized the hourly values of horizontal component of geomagnetic field observations during 1985 - 1995 from TRD and ABG as well as observations from TIR and ABG during 2000 - 2015. These datasets are obtained from World Data Centre for Geomagnetism, Navi Mumbai (http://iigm.res.in) and WDC, Kyoto (http://wdc.kugi.kyoto-u.ac.jp/). In the present work, these datasets are utilized to deduce the strength of magnetic field induced at ground by the electrojet current. Details of this method are described in the ensuing paragraphs.

The observations of horizontal component of geomagnetic field (H) from an equatorial (eq) and off-equatorial (off-eq) stations are conventionally [*Cohen and Bowles*, 1963; *Rastogi*, 1974; *Rastogi and Patel*, 1975] used to deduce the strength of equatorial electrojet as follows,

$$\text{EEJ strength} = \Delta H_{\text{eq}} - \Delta H_{\text{off-eq}} \tag{2.17}$$

here ΔH is obtained by subtracting averaged nighttime value (average of H values from 23 LT of previous day to 03 LT) from instantaneous H values. This removes the contribution from Earth's crustal magnetic field with the assumption that during nighttime the ionospheric currents are negligible. However, studies on estimate of nighttime current density over the equatorial E region are sparse and in Chapter 6 of this thesis, its' estimates are presented using three methods. Further, the ΔH variations of the off-equatorial station (outside electrojet belt) are subtracted from the ΔH variations of the equatorial station to remove the magnetic effects of current system flowing at large distances (e.g., ring current) and can be considered to induce magnetic fields of same strengths at both the stations.

Therefore, LHS of equation (2.17) captures the strength of equatorial electrojet current. Further, it is noticed [*Rastogi and Patil*, 1986] that magnetometer observed EEJ strength show excellent correlations with Doppler shifts of the VHF radar echoes from E region irregularities during geomagnetically quiet as well as disturbed days. The generation of these E region irregularities depends on the amplitude and/or polarity of the zonal electric field. Therefore, the observed variations in EEJ strength are extensively utilized [e.g., *Raghavarao et al.*, 1978; *Sridharan et al.*, 1999; *Anderson et al.*, 2004; *Rout et al.*, 2017] as proxy for the variations in ionospheric zonal electric fields at time scales in which the ionospheric conductivities remain nearly same.

2.6 E-region electron density profiles

In order to estimate the ionospheric current densities using EEJ model, the electron density profiles in the altitude region of 80 - 200 km are needed. These electron density profiles are mainly taken from the in-situ measurements made from Thumba using Langmuir probes. *Mott-Smith and Langmuir* [1926] developed Langmuir probe technique to study the properties of plasma in a laboratory gas discharge. In this technique, a probe electrode is inserted in the plasma medium under study, with electric potential varying from a convenient negative value through zero to positive value and the probe current is measured continuously. The resulting current-voltage (I-V) curve is used to determine the plasma parameters such as electron and ion density, electron temperature, etc.

The Langmuir probe technique was employed for the ionospheric studies in 1946 by Spencer and his colleagues in USA. Many groups [e.g., *Spencer et al.*, 1962; *Smith*, 1964; *Prakash and Subbaraya*, 1967] from different parts of the world developed various versions of the basic technique and a large amount of data has been collected using these systems on board sounding rockets. In rocket borne Langmuir probe system, the probing electrode is well insulated from the reference electrode which is the rocket body itself or an insulated portion of it.

A modified version of the basic technique was developed at Physical Research Laboratory, India by *Prakash and Subbaraya* [1967]. In this system a guard electrode was incorporated that greatly reduced the leakage current and enhanced the frequency response of the system. Additional modifications were done by *Prakash et al.* [1972] to study the small scale plasma irregularities with scale size down to 0.5 m [*Gupta et al.*, 2004] and amplitude resolution of 0.1% of the ambient density.

The modified Langmuir probe with high frequency response probe was launched on a large number of sounding rocket flight experiments conducted from Thumba Equatorial Rocket Launching Station (TERLS), Trivandrum. These experiments [e.g. *Subbaraya et al.*, 1983, 1985; *Prakash et al.*, 1971a; *Prakash and Pal*, 1985; *Gupta*, 2000] were conducted at different times of the day covering all the seasons under high and low solar epochs to measure the equatorial E-region electron density profiles along with the amplitudes of Two-stream and Gradient-drift wave structures. In the present thesis work, the in-situ measurements of electron density profiles obtained between 1967 and 1982 are utilized. The measurements made at night are used to estimate the equatorial E-region current density during nighttime (Chapter 6). The daytime measurements are utilized to investigate the possible cause of frequent counter electrojet observed in afternoon hours over India during June solstice in solar minimum years (Chapter 4).

Figures 2.2a and 2.2c depict the altitude profiles of electron densities measured [*Subbaraya et al.*, 1983; *Prakash and Pal*, 1985] around noon hours (1000 - 1400 LT) during years with annually averaged F10.7 $\leq$ 120 sfu and F10.7 $>$ 120 sfu. The black coloured solid line depicts the averaged electron density profile. In addition, the percentage change in electron densities from the averaged profile at different local times is depicted in Figures 2.2c and 2.2d with the same colours as used in the Figures 2.2a and 2.2b. It is noticed that electron density profiles over the electrojet altitudes (100 - 110 km) do not reveal significant temporal variation (greater than 20%) during 1000 - 1400 LT. Therefore, the averaged electron density profiles corresponding to low (figures 2.2a) and high (figure 2.2c) solar flux levels are used as reference noon time electron density profiles since in-situ measurements of electron density profiles are not available at all local times. Therefore, the empirical relationship between the electron density and solar zenith angle (χ) through $\cos^{1.31/2}(\chi)$ [IRI-90, *Bilitza*, 1990] factor is used along with the measured average noontime density profile to generate electron density profiles during 0730 - 1730 LT.

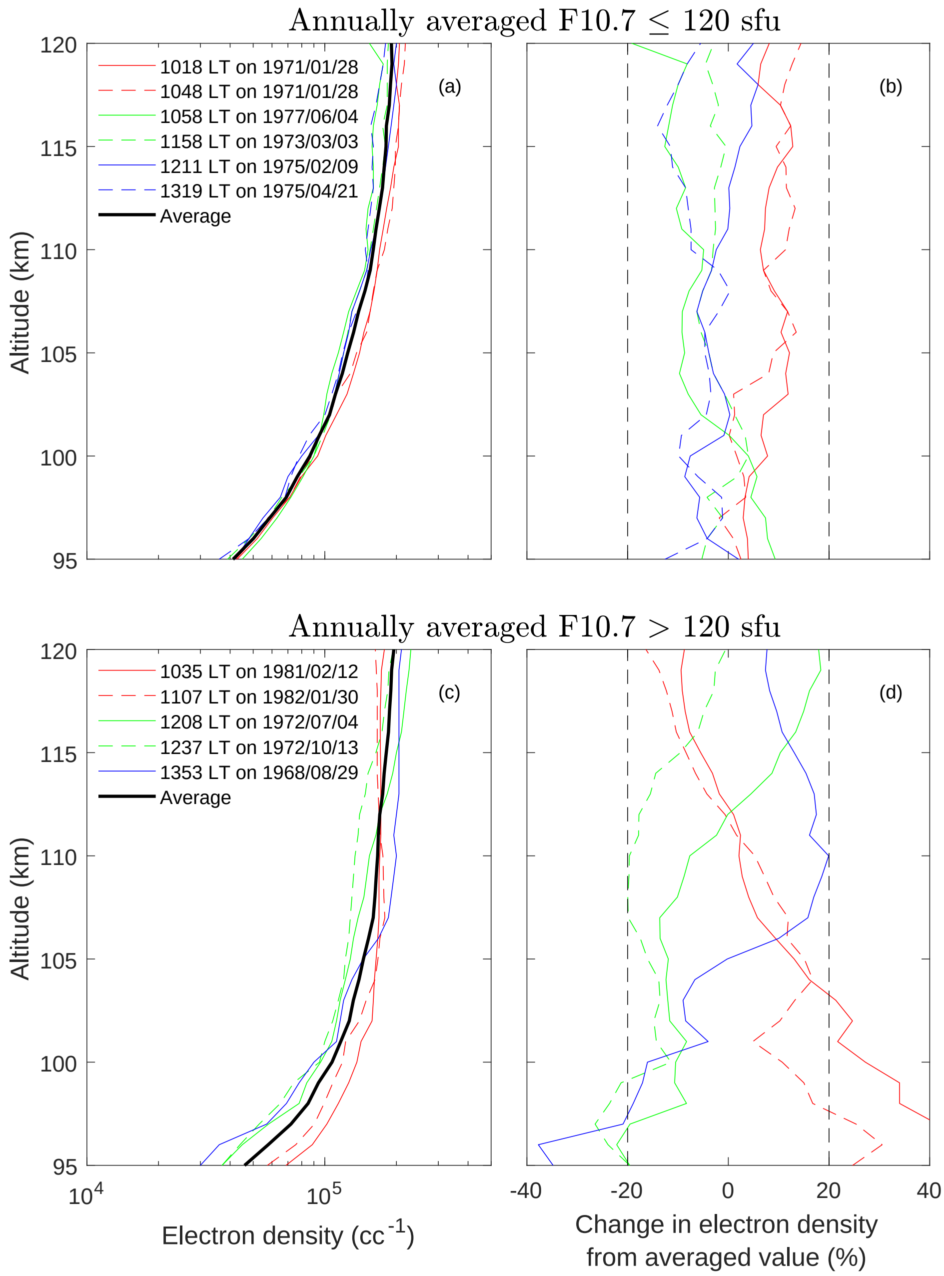

Figure 2.2: Altitude profiles of electron densities measured during 1000 - 1400 LT years with annually averaged (a) F10.7 $\leq$ 120 sfu (c) and F10.7 $>$ 120 sfu with averaged profiles. Change in individual electron densities from the averaged values are depicted on the right panels (b) and (d).

2.7 Vertical plasma drift measurements by various methods

It is well known that over the dip-equatorial regions, electric field (E) cause electrodynamic drifts of the plasma, $\mathbf{V} = \frac{\mathbf{E}\times\mathbf{B}}{B^2}$ where $\mathbf{B}$ is Earth's magnetic field. Therefore, the measurements of vertical plasma drifts can provide information on the zonal electric field. The plasma drifts are obtained using various techniques and can be inferred indirectly from other observations also. In the ensuing subsections, these methods are described briefly.

2.7.1 F-layer movement

The vertical movement of bottom-side F-layer over the equatorial ionosphere is a result of the effects of production (photo-ionization), loss (chemical recombination) and transport (electrodynamic drift). During daytime all three processes occur simultaneously and makes it difficult to obtain the vertical drift based on F-layer movement. However, in absence or negligible production of plasma during nighttime, the temporal movement of ionospheric layers after subtracting the contribution due to recombination losses, can be used to compute the vertical plasma drifts. Since recombination process always causes an apparent upward drift velocity of the F-layer, it is easier to make corrections using established methods [e.g., *Subbarao and Krishna Murthy*, 1994]. The vertical movement due to chemical recombination can be computed using the loss rate and scale height of the ionosphere. Further, if the movement of F-layer is above 300 km altitude, the contribution due to recombination losses is shown [*Bittencourt and Abdu*, 1981] to be negligible. Therefore, this technique is extensively used around the globe to obtain the F-layer vertical drifts. The temporal movement of plasma layers is derived using the measurements from Ionosonde, phase path sounder and HF Doppler radar.

In an Ionosonde, High Frequency (HF) radio waves in range of 1 - 30 MHz are transmitted. The transmitter continuously sweeps in this frequency range, transmitting short pulses. These pulses are reflected at various layers of the ionosphere, where the transmitted frequency matches with the plasma frequency. The reflected echoes are received by the receiver and analysed by the control system. Based on time taken by the radio signal from transmission to reception, the height of plasma layer is estimated. The result is displayed in the form of an ionogram - a graph of virtual reflection height versus carrier frequency. In this thesis work, the measurements obtained from Trivandrum [*Subbarao and Krishna Murthy*, 1994; *Krishna Murthy and Hari*, 1996; *Madhav Haridas et al.*, 2015] and Kodaikanal [*Sastri*, 1984] are utilized.

The HF pulsed phase path sounder at a particular frequency measures the temporal changes in phase path of the reflected echoes. One such sounder was operated from Kodaikanal [*Ramesh and Sastri*, 1995; *Sastri*, 1996] to obtain the F-layer movements. Similarly, a HF Doppler radar was used to measure the Doppler shift in frequency of the received reflected echo with respect to the transmitted frequency. One such radar was operated from Trivandrum [*Nair et al.*, 1993] to deduce the apparent vertical drifts. These results are used to build up a consolidated picture of vertical drifts over India.

The published results of F-region vertical drifts, spanning over five decades (1957 - 2008), are utilized in Chapter 3 to investigate the temporal variations of vertical drifts over the Indian sector corresponding to different seasons and solar epochs.

2.7.2 Doppler shifts of plasma irregularities at 150 km

The radar observations made at Jicamarca [*Balsley*, 1964] exhibited a narrow (140 - 170 km), stratified echoing regions during daytime. The generation of these echoes is possibly [*Oppenheim and Dimant*, 2016] due to electron waves driven by photoelectrons, though the recent observations [*Patra et al.*, 2017] on occurrence and intensity of the echoes suggest departures from this mechanism. Therefore, clear understanding of the processes responsible for the generation of these irregularities is still illusive. *Kudeki and Fawcett* [1993], nearly 30 years after *Balsley's* observation, noticed that the vertical Doppler velocities of these irregularities represent the vertical drift velocities. It has also been shown [*Chau* *and Woodman*, 2004] that the vertical Doppler shift of the 150 km echoes could be reliably used as vertical plasma drifts during daytime. In the recent years, it has become routine to monitor the vertical plasma drifts by measuring the Doppler shifts of 150 echoes [*Alken*, 2009; *Hui and Fejer*, 2015]. Over the Indian sector, such measurements for a limited period were made using MST radar at Gadanki (13.5°N, 79.2°E) [*Patra and Rao*, 2006; *Patra et al.*, 2012, 2014; *Pavan Chaitanya et al.*, 2014]. The measurements made during June solstice in solar minimum years are used to understand the frequent occurrence of afternoon CEJ events over India in this season (Chapter 4).

2.7.3 Vapour cloud release

Based on motion of artificial ion clouds in the upper atmosphere, different ionospheric parameters can be obtained [*Haerendel et al.*, 1967]. These experiments provide in-situ measurements of plasma drifts during twilight time. Barium vapour release experiments were conducted over Trivandrum [*Anandarao et al.*, 1977; *Anandarao*, 1977] and Sriharikota (13.7°N, 80.2°E) [*Raghavarao et al.*, 1987; *Sekar*, 1990] to obtain the twilight time plasma drifts. The technique involves Barium-Strontium (Ba-Sr) puff releases at designated altitudes using sounding rockets. The Ba cloud gets ionized by solar UV radiations above 150 km while Sr cloud remains neutral. These vapour clouds resonantly scatter solar radiations and thus can be photographed from the ground stations wherein the nighttime condition prevails. By triangulation, the position of the cloud at a particular time can be obtained. Temporal sequence of photographs are then used to derive the drift of the ion clouds. In the present thesis work, the twilight time vertical drifts reported by *Anandarao et al.* [1977], *Anandarao* [1977], *Raghavarao et al.* [1987], and *Sekar* [1990] are utilized (Chapter 3).

2.7.4 Equatorial E-region irregularities

As discussed in Chapter 1, the equatorial E-region hosts plasma irregularities known as Two-stream waves (Type I) and Gradient-drift waves (Type II). These plasma waves are observed using high frequency response Langmuir probe on board rocket flight experiments conducted from Trivandrum. Based on these experiments, the simultaneous measurements of electron density profiles, and Two-stream and Gradient-drift waves were reported by earlier workers [e.g., *Prakash et al.*, 1969, 1970, 1974; *Prakash and Pal*, 1985; *Gupta and Prakash*, 1979; *Gupta*, 1986, 1997].

The presence or absence of Two-stream plasma waves can also be observed using the VHF backscatter radar experiments. These radars probe the velocity of plasma waves with scale size equal to half the radar wavelength. Based on such backscatter radars over Trivandrum, presence of Two-stream waves were reported by earlier workers [e.g., *Prakash and Muralikrishna*, 1976; *Tiwari et al.*, 2003].

The present thesis work makes use of the information on Two-stream and Gradient-drifts waves reported using sounding rocket flight and back scatter radar experiments conducted during during 1967 - 1999. As the generation of Two-stream and Gradient-drift waves depend on the strength and/or polarity of Sq electric fields, these informations are utilized to deduce the direction and threshold limits of vertical drifts (Chapter 3).

Chapter 3

Comparison of model and measured plasma drifts during quiet times

Excerpt

As discussed in the Chapter 1, systematic measurements of vertical drifts over India covering all local times of the day, season and solar epoch are not available due to absence of the Incoherent Scatter Radar over this region. However, satellite experiments have been used to develop a few global empirical models [e.g., *Scherliess and Fejer*, 1999; *Fejer et al.*, 2008a] of vertical drifts with certain bin sizes. Applicability of these models over Indian sector is investigated by utilizing the vertical drifts inferred or measured from the earlier (1957 - 2008) experiments conducted over this sector. Threshold vertical plasma drifts and their direction (upward/downward) are inferred from E-region irregularities reported earlier using different experiments conducted from India during geomagnetically quiet times. In addition, hourly variations of magnetometer data sets are used in conjunction with an equatorial electrojet model [*Anandarao*, 1976] to deduce the vertical drifts during 07:30 - 17:30 LT. These results are then compared with the vertical drifts presented by empirical models [*Scherliess and Fejer*, 1999; *Fejer et al.*, 2008a] corresponding to the 60°E longitude sector. In general, the vertical drifts presented by empirical models are consistent with those inferred from snapshot measurements of E-region irregularities at different local times of the day except around sunrise hours. Further, the vertical drifts presented by *Fejer et al.* [2008a] model match fairly well with seasonally averaged vertical drifts deduced (within 1σ variation) using magnetometer data. A time difference is noticed between occurrence of pre-reversal enhancement in the measured vertical drifts over India reported earlier using different techniques and *Scherliess and Fejer* [1999] model output. Probable reason for the time difference is discussed. The occurrence characteristic of afternoon equatorial counter electrojet in June solstice during low solar epoch (discussed in detail in Chapter 4) is consistent with the drifts obtained from *Fejer et al.* [2008a] model. Seasonally averaged vertical drifts during nighttime reported earlier using ionosonde/HF radar experiments are not consistent with the presence of Two-stream plasma waves on a few occasions. Further, the measured nocturnal vertical drifts are found to be systematically less than the model outputs and probable reason for this is discussed.

3.1 Introduction

The generation of Sq electric field and its' important role in several ionospheric processes (like equatorial electrojet, plasma fountain, Two-stream and Gradient-drift waves, plasma bubble) over low latitudes are discussed in Chapter 1. Hence, in order to address the low latitude ionospheric processes in a comprehensive manner, it is important to know the variations in Sq electric field in different seasons and solar cycles. Measurements of vertical drifts (V_z) are used to obtain the zonal electric field, $E_x = V_z \times B$ where B is the strength of geomagnetic field. The vertical drifts are known [*Fejer*, 1981] to be upward during daytime and downward in nocturnal hours under geomagnetically quiet periods. The diurnal variations of vertical drifts in different seasons over the Peruvian sector had been presented [e.g., *Woodman*, 1970] in the past using highly accurate (better than 2 ms^{-1}) measurements of vertical drifts obtained with Incoherent Scatter Radar (ISR) at Jicamarca.

The vertical drifts or zonal electric fields over Indian sector had been traditionally deduced (refer Chapter 2) based on ionosonde, phase path sounder and HF Doppler radar measurements. Magnetometer measurements are used as a proxy to obtain the electric field variations [e.g., *Rastogi and Patil*, 1986] during daytime. Considering the fact that each of these techniques come with their own limitations and uncertainties (discussed later), it is important to evaluate the consistency of the vertical drifts derived from different techniques with those obtained from global empirical models that are already available. This will help not only to understand the merits and demerits of individual techniques in a better way but also to evaluate the applicability of global models of vertical drifts to accurately capture the ionospheric processes over the Indian sector.

As already stated, each technique used to derive the vertical drift comes with its own limitation(s). For example, in an ionosonde experiment the recorded movement of ionospheric F-layer along the vertical direction can be due to production by photo-ionization and/or loss by chemical recombination and/or by electrodynamic processes. Presence of all the three processes during daytime makes it difficult to compute the vertical drifts from the recorded layer movements. However, during nighttime, when plasma production is negligible in the absence of solar ionizing radiation, vertical drifts can be deduced from the temporal movement of F-layer (apparent drift) after correcting for the layer movement due to chemical loss [*Bittencourt and Abdu*, 1981; *Krishna Murthy et al.*, 1990].

The measurements of V_z during twilight time and their nocturnal variations have been reported earlier (refer section 3.2) using several experiments conducted from Trivandrum (TRD: 8.5°N, 76.9°E). In addition, the threshold value and direction (upward/downward) of vertical drift can be deduced from the presence/absence of E-region irregularities (Two-stream and Gradient-drift waves) reported earlier (refer section 3.2) at different local times of the day using sounding rocket flight and VHF radar experiments over TRD.

A number of works reported in the past provided snap-shot as well as seasonally averaged vertical drifts. In the present work, an attempt is made to consolidate the measurements of vertical drifts made by a few techniques from the Indian dip-equatorial stations and compare those with the drifts presented by global empirical models of *Scherliess and Fejer* [1999] and *Fejer et al.* [2008a] (henceforth Scherliess-99 and Fejer-08), to investigate their degree of applicability over the Indian sector. Further, considering the fact that in empirical models, the vertical drifts have been averaged over at least ±5° dip-latitude, the vertical drifts presented earlier using ionosonde and HF radar technique over Kodaikanal (KDK: 10.3°N, 77.5°E), whose geomagnetic-latitude is less than 1.5°, are also used for comparison. In addition, the daytime vertical drifts estimated from seasonally averaged EEJ variations, based on method described in Chapter 2, are compared.

3.2 Details of the dataset

In the present investigation, the average F-region vertical drifts measured during nighttime from ionosonde [*Sastri*, 1984; *Subbarao and Krishna Murthy*, 1994; *Krishna Murthy and Hari*, 1996; *Madhav Haridas et al.*, 2015], phase path sounder [*Ramesh and Sastri*, 1995; *Sastri*, 1996] and HF Doppler radar [*Nair et al.*, 1993] experiments are used. Further, the electric fields deduced from E-region irregularities during day and night are also utilized. As the equatorial vertical drifts are sensitive to geomagnetic conditions [*Fejer et al.*, 2008b], the present work pertains to only the quiet time conditions with three hourly Kp ≤ 3. The available observational data sets span over five decades (1957 - 2008), the annually averaged F10.7 values during this period are depicted in Figure 2.1 of Chapter 2. Therefore, these datasets spanned over several solar cycles wherein the solar flux levels varied between values as low as ∼70 sfu and as high as ∼230 sfu. In the present investigation, the solar flux levels of $F_{10.7} < 130$ sfu and $F_{10.7} > 160$ sfu are respectively used to represent the low and high solar epochs considering the solar flux levels used into empirical models and available datasets.

The observations with different time axes are converted into a single time format corresponding to the local time (LT) at TRD (longitude 76.9°E). The observations are classified into three seasons, namely, December solstice (November - December - January - February), equinox (March - April, September - October) and June solstice (May - June - July - August) similar to the seasonal classifications followed in Scherliess-99 and Fejer-08.

The ionosonde observations of F layer movement reported by *Subbarao and Krishna Murthy* [1994] are converted into vertical plasma drift after correcting for chemical recombination effects based on their work. Further, apparent drifts reported by *Sastri* [1984] using ionosonde observations over KDK during 1957 - 1959 can be treated as electrodynamic drifts since the layer heights are well above 300 km during solar maximum.

The vertical drifts have been reported using phase path sounder over KDK [*Ramesh and Sastri*, 1995; *Sastri*, 1996] and Doppler radar over TRD [*Nair et al.*, 1993] operated at 4 MHz and 5.5 MHz respectively. As the altitudes of reflecting layers, corresponding to these high operative frequencies, were considered to be well above 300 km during pre-midnight hours, no explicit corrections for the recombination losses were made to those drifts.

The presence of Two-stream and Gradient-drift waves was reported using back scatter radars operated from TRD in HF (18 MHz) [*Tiwari et al.*, 2003] and VHF (54.95 MHz) [*Prakash and Muralikrishna*, 1976] frequencies. The limiting values of plasma drifts using threshold condition of Two-stream waves (refer section 3.3) and their polarities from Doppler shift are deduced. The Doppler shifts from the E-region Gradient-drift waves [e.g., *Reddy et al.*, 1987; *Viswanathan et al.*, 1987] are not considered in the present work, as the calibration factors for converting these to ambient plasma drifts are not available. Based on Canadian Doppler ionosonde [*MacDougall et al.*, 1995] experiments over Tirunelveli, *Sripathi et al.* [2016] reported the monthly averaged quiet time vertical drifts. Though variations in these vertical drifts are similar to those obtained using digisonde [*Bibl and Reinisch*, 1978] and from *Scherliess and Fejer* [1999] model, the magnitudes are much larger. This is possibly due to lack of proper calibration factor. Therefore, these vertical drifts are not used in this thesis work.

The in-situ measurements [e.g., *Prakash et al.*, 1971a; *Gupta*, 2000] of electron density profiles and structures in them had been obtained using high frequency Langmuir probes [*Prakash and Subbaraya*, 1967; *Subbaraya et al.*, 1983, 1985] on board rocket flight experiments. Those experiments were conducted over TRD at different local times of the day covering different seasons under high and low solar epochs. As the generation electron density structures depend on the ambient electric fields, the limiting plasma drifts are deduced from the presence of Two-stream waves. The limiting values (explained later) of vertical drift for the presence of Two-stream waves ($> +12$ ms^{-1} during daytime, < -12 ms^{-1} during nighttime) while the inverse conditions are taken for their absence. Further, for the time interval when Two-stream waves have been detected on some days and found absent on some other days within a same season the vertical drift are taken to be $\sim \pm 12$ ms^{-1}. These observations of Two-stream waves spanned from 1967 to 1999 when the dip-angle over TRD was between $-0.9°$ and $+1.2°$ [IGRF-12, *Thébault et al.*, 2015]. Hence, the existence of Two-stream waves is consistent with the conclusion arrived by *Sekar et al.* [2013] that the Two-stream waves over Thumba during magnetically quiet periods at noontime exist when the dip angle is lesser than 1.5°. In addition, the observed gradient in the altitude profile of electron densities and the presence/absence of Gradient-drift waves are used to deduce the polarity of vertical electric field from which the direction of zonal electric field is inferred, as these two components are related over the dip-equator.

Barium vapour cloud release experiments provide in-situ measurements of plasma drifts associated with ambient electric field. Vertical drifts around twilight time measured with these experiments over TRD [e.g., *Anandarao et al.*, 1977; *Anandarao*, 1977] and Sriharikota (13.7°N, 80.2°E, a station close to the dip-equator) [e.g., *Raghavarao et al.*, 1987; *Sekar*, 1990] are used in the present work.

The methodology described in Chapter 2 (section 2.2) is adopted to derive the daytime vertical drift from observed electrojet strength under geomagnetically quiet conditions. The hourly magnetometer measurements from a dip-equatorial station Trivandrum (TRD: 8.5°N, 76.9°E, geom.-lat. 1°S) and an off-equatorial station Alibag (ABG: 18.6°N, 72.9°E, geom.-lat. 10°N) during 1985 - 1995 are used to obtain the electrojet strength ($\Delta H_{\text{equator}} - \Delta H_{\text{off-equator}}$) on geomagnetically quiet days (Kp ≤ 3 and Dst ≥ -20, on the selected day and also on the previous day). Figure 3.1 depicts the observed values of $\Delta H_{\text{TRD}} - \Delta H_{\text{ABG}}$ on individual quiet days (grey) and their seasonally averaged (black) values along with standard deviation (1σ value in vertical bars). The values corresponding to high and low flux epochs are depicted in the left and right panels. Based on these seasonally averaged values of $\Delta H_{\mathrm{TRD}} - \Delta H_{\mathrm{ABG}}$, the vertical drifts corresponding to zonal electric fields are obtained during ~07:30 - 17:30 LT.

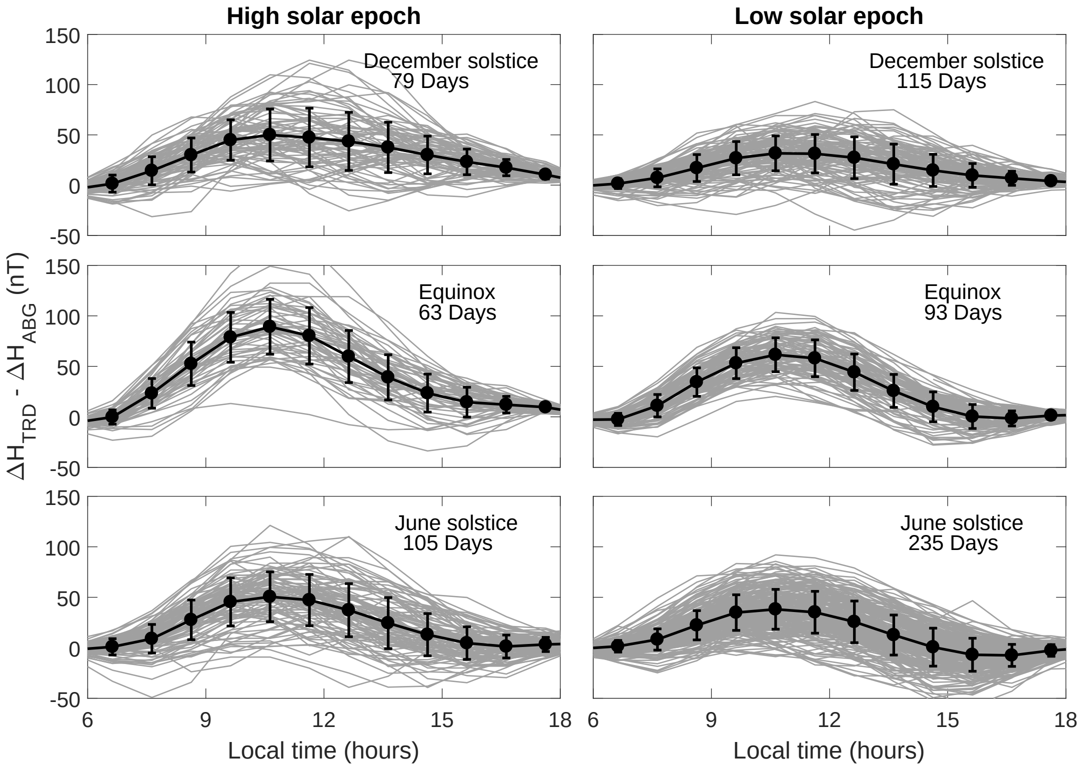

Figure 3.1: Hourly variations of individual quiet days (grey) and seasonally averaged (black) $\Delta H_{\mathbf{TRD}} - \Delta H_{\mathbf{ABG}}$ values along with standard deviation (1σ value in vertical bars). The variation during high and low solar epochs are depicted in left and right panels. From top to bottom are variations corresponding to December solstice, equinox and June solstice. The number of days used for seasonal average are also listed in each panel.

As stated earlier, the empirical models (Scherliess-99 and Fejer-08) provide the dip-equatorial vertical plasma drifts at different local times and seasons during geomagnetically quiet periods. In order to compare with the vertical drifts derived based on measurements by different techniques mentioned earlier, the model drifts corresponding to 60°E longitude which is closest to Indian sector are reproduced from Figure 8 of Scherliess-99 and Figure 7 of Fejer-08.

3.3 Results

Figure 3.2 depicts the diurnal variations of vertical drift (black coloured solid curves) presented by Scherliess-99 model for high solar epoch. Figures 3.2(a), 3.2(b) and 3.2(c) show the vertical drifts in December solstice, equinox and June solstice, respectively.

In figure 3.2(a), the blue and green coloured (solid, dash and dash-dot) curves portray the average nocturnal variations of V_z obtained using ionosonde/radar experiments from TRD and KDK, respectively. The blue coloured dashed curve represents V_z computed using the average nocturnal variations of $h'F$ presented by *Subbarao and Krishna Murthy* [1994]; and blue coloured dash-dot curve portrays the average V_z variation during nighttime presented by *Madhav Haridas et al.* [2015]. The green coloured dashed and solid curves depict the average vertical drifts during dusk-midnight hours presented by *Sastri* [1984] and *Ramesh and Sastri* [1995] respectively. The 1σ variation in vertical drift at prereversal enhancement (PRE) time, as provided by *Ramesh and Sastri* [1995], is reproduced with green coloured solid vertical bar on the top right corner of figure 3.2(a) as well as in figures 3.2(b - c). It must be noted that information on the 1σ variation for the earlier results will be mentioned whenever available.

The twilight time in-situ measurements of vertical drifts reported by *Anandarao et al.* [1977] and *Sekar* [1990] are shown with magenta coloured dots at the particular LT of the experiments. The average nocturnal variation of vertical drifts corresponding to the zonal electric fields presented by *Krishna Murthy and Hari* [1996] is shown with the dark magenta coloured solid curve. In addition, average variation of vertical drift during daytime deduced from magnetometer records is portrayed with the maroon coloured solid curve. The standard deviation (1σ) of these deduced vertical drifts, estimated based on the variations in $\triangle H_{\mathrm{TRD}} - \triangle H_{\mathrm{ABG}}$, is shown as vertical bars on the curve.

The vertical arrows (at the bottom of figure) are drawn at the particular LT corresponding to drifts derived from the sounding rocket experiments in which the Two-stream waves were observed. Similarly, the solid horizontal lines (at the bottom of figure) are drawn for the particular time interval during which the

Two-stream waves were observed using VHF radar experiments. The presence or absence of Two-stream waves is respectively portrayed with teal or red colours. It is to be noted that teal and red coloured horizontal lines are simultaneously used for certain durations when presence of Two-stream waves were detected on some days and found absent on some other days during the same season.

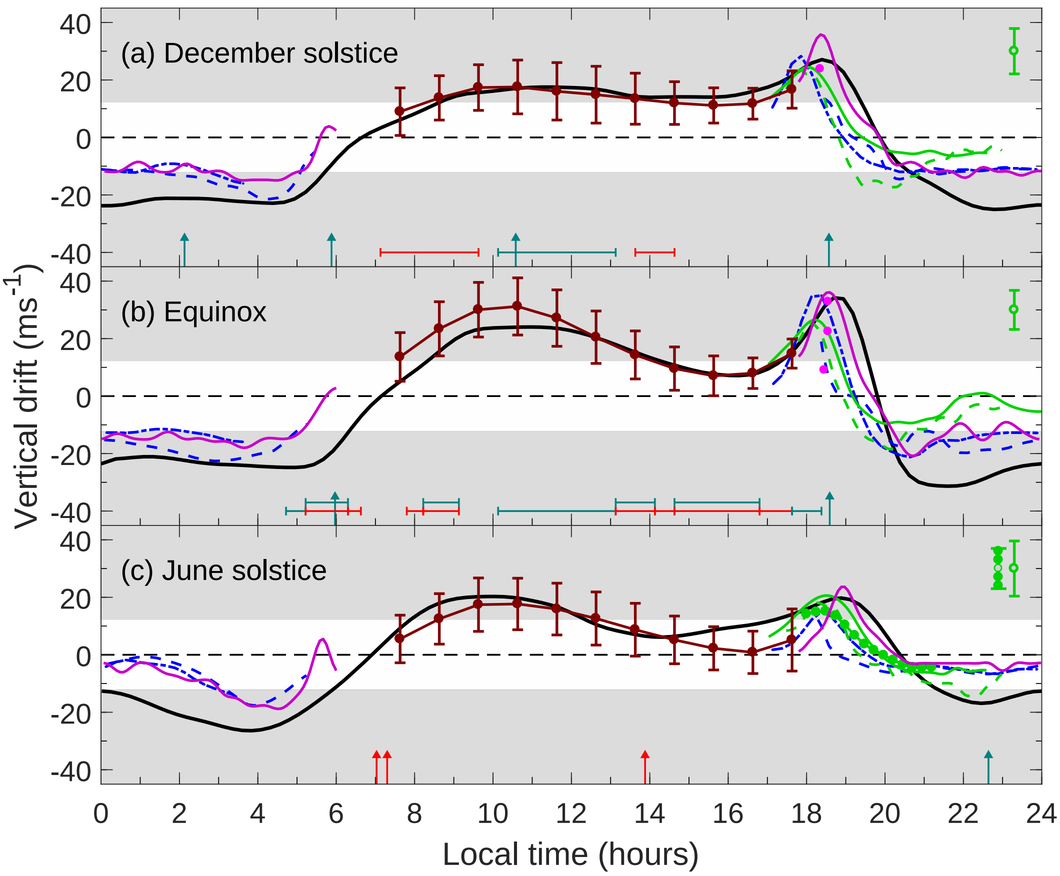

Figure 3.2: Vertical drift variations during high solar epoch over the Indian sector provided by *Scherliess and Fejer* [1999] model (black) and experiments conducted from TRD and KDK (blue, dark magenta and green coloured curves, respectively) are depicted along with the 1σ variation in those (wherever available) on the top right corner. Vertical drifts measured using vapour release experiments (magenta coloured dots) and those deduced from magnetometer records (maroon coloured curves) are also shown. The presence or absence of Two-stream waves observed using sounding rocket flights (vertical arrows) and VHF Doppler radars (horizontal lines) are portrayed with teal or red colours, respectively. The durations when Two-stream waves were detected on some days and found absent on some other days within a same season are depicted with simultaneous horizontal lines in teal and red colours.

In figures 3.2(b) and 3.2(c) the same notations which have been used in figure 3.2(a) are followed to present the vertical drifts corresponding to equinox and June solstice, respectively. An additional green coloured dotted curve in figure 3.2(c) depicts the vertical drift presented by *Sastri* [1996]. The 1σ variation in vertical drifts at PRE time, as provided by *Sastri* [1996], is reproduced with green coloured dotted vertical bar on top right corner in figure 3.2(c).

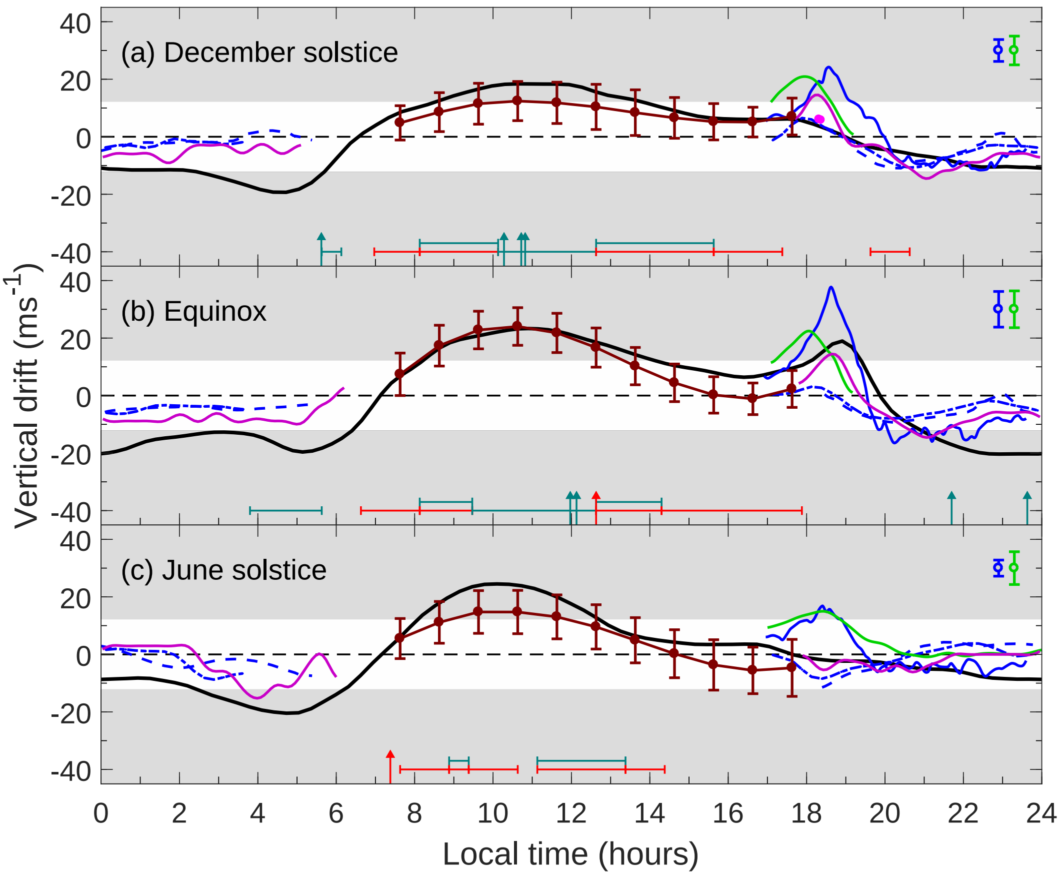

Figure 3.3: Same as Figure 3.2 but corresponds to low solar epoch.

Figure 3.3 depicts the diurnal variations of vertical drift (black solid curves) presented by Scherliess-99 model corresponding to different seasons under low solar epoch. The values of V_z obtained using experiments conducted from TRD, KDK, SHK and magnetometer records are overlaid in respective figures with same notations as in Figure 3.2. Note that, if the ionosonde/radar derived average nocturnal vertical drifts are not available from the same works that are used to construct Figure 3.2, the respective colour codes and types of the legends are not utilized in Figure 3.3 to maintain uniformity and avoid ambiguity. The additional blue coloured solid curves in Figure 3.3 portray the average nocturnal V_z variations presented by *Nair et al.* [1993]. The nighttime averaged 1σ variation in vertical drifts, as provided by *Nair et al.* [1993], is reproduced with blue coloured solid vertical bars in respective panels of Figures 3.3.

Figures 3.4 and 3.5 depict the diurnal variations of vertical drifts (black curves) presented by Fejer-08 model corresponding to different seasons under high and low solar epochs, respectively. The vertical drifts obtained using experiments conducted over TRD, KDK, SHK and magnetometer records under high and low solar epochs are overlaid in Figures 3.4 and 3.5 with same notations and colour codes as in Figures 3.2 and 3.3, respectively.

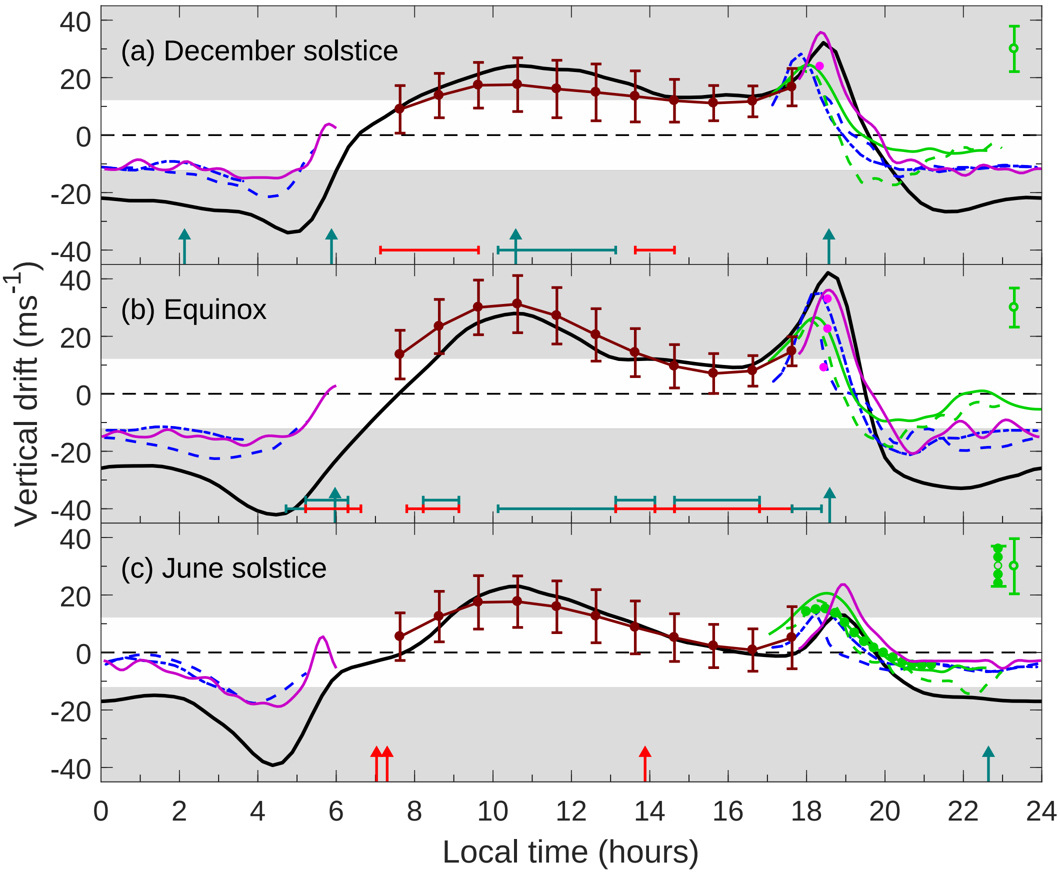

Figure 3.4: Same as Figure 3.2 but comparison is with the *Fejer et al.* [2008a] model drifts.

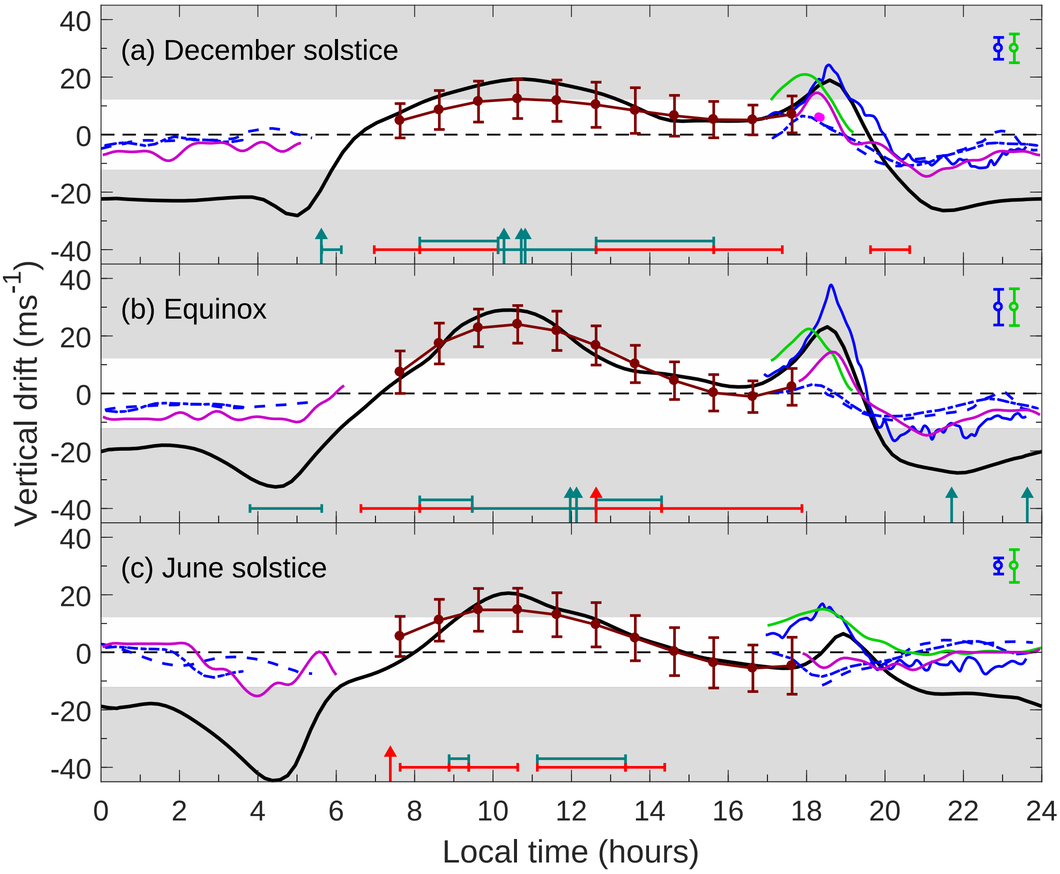

Figure 3.5: Same as Figure 3.3 but corresponds to low solar epoch.

Grey coloured horizontally shaded region in each figure marks the range of vertical drift values in which presence of Two-stream waves can be expected. The reasoning for this demarcation is as follows. Generation of Two-stream waves is known [*Farley*, 2009] to get triggered whenever magnitude of zonal drift (V_x) of electrons exceeds the ion-acoustic speed of the medium, which is about 370 ms^{-1} at ∼105 km altitude over the Indian sector. Plasma drifts along the zonal (V_x) and vertical (V_z) directions are known [*Anandarao et al.*, 1977; *Sekar et al.*, 2013] to be related over the dip-equator by $V_x = RV_z$, where $R = \frac{\sigma_H}{\sigma_P}$. The value of R is shown [*Pandey et al.*, 2016] to remain nearly same, irrespective of local time of day and solar epoch, with a value of about 30 at ∼105 km altitude. Hence, whenever the Two-stream waves are present the magnitude of vertical drift must be greater than 12 ms^{-1}. Above inference of limiting plasma drift of $\sim \pm 12$ ms^{-1} gets the support from the occurrence of Two-stream waves on some days and absence on some other days within a same season (see figures 3.2b, 3.3a-c, 3.4b, 3.5a-c). It is expected that the vertical drifts would lie within or outside this grey coloured shaded region whenever the Two-stream waves are present (teal coloured vertical arrows/horizontal lines) or absent (red coloured vertical arrows/horizontal lines).

Tables 3.1 and 3.2 summarize the results from sounding rocket flights and VHF radar experiments. Vertical drift necessary for the observed presence (>+12 ms^{-1} or <−12 ms^{-1}), absence (≤+12 ms^{-1} or ≥−12 ms^{-1}) or some days presence and some days absence (∼±12 ms^{-1}) of Two-stream waves is provided in the respective entries of these tables. In addition, vertical drifts obtained from Scherliess-99 and Fejer-08 models at respective LT, season and solar epoch of the rocket flights are also given. Further, vertical drifts obtained from both the empirical models corresponding to the starting time of the respective VHF radar experiments are also provided. Note that, if the magnitude of vertical drift obtained from empirical model deviates from the criterion of deduced $|V_z|$ given above, the value is highlighted with red colour. Further, if the direction of vertical drift differs from that deduced from observation, the cell is highlighted with grey background. This notation is not followed for cases wherein deduced $|V_z|$ ∼12 ms^{-1}.

Season	Experiment	Date	Time/ Duration	Vertical drift (ms^{-1}) Deduced	Scherliess-99	Fejer-08	Literature
December solstice	Rocket	21-12-1978	02:08	< −12	−21.2	−24.4	*Gupta* [2000]
		21-12-1978	05:53	< −12	−09.5	−15.8	*Gupta* [2000]
		12-02-1981	10:35	> +12	+17.4	+24.0	*Prakash and Pal* [1985]
		02-02-1968	18:34	> +12	+26.8	+30.5	*Prakash et al.* [1969]; *Gupta and Prakash* [1979]
	Radar	03-02-1999	07:08 - 09:38	≤ +12	+03.3	+05.4	*Tiwari et al.* [2003]
		03-02-1999	10:08 - 13:08	> +12	+16.3	+23.2	*Tiwari et al.* [2003]
		03-02-1999	13:38 - 14:38	≤ +12	+14.3	+17.1	*Tiwari et al.* [2003]
Equinox	Rocket	28-04-1980	05:58	> +12	−18.3	−23.1	*Gupta* [2000]
		12-03-1967	18:35	> +12	+32.9	+41.5	*Gupta* [2001]
	Radar	19-03-1991	04:43 - 05:13	< −12	−24.8	−41.5	*Ravindran and Krishna Murthy* [1997a]
		15-03-1991	06:18 - 06:38	≥ −12	−06.5	−13.0	*Ravindran and Krishna Murthy* [1997a]

Table contd.

Equinox	Radar	15-03-1991	07:48 - 08:13	$\leq +12$	+07.2	+02.7	*Ravindran and Krishna Murthy* [1997a]
		20-03-1979, 15-03-1991, 17-03-1991	07:53 - 09:08	$\sim +12$	+12.3	+08.0	*Viswanathan et al.* [1987]; *Ravindran and Krishna Murthy* [1997a]
		20-03-1979, 21-03-1979, 21-09-1979	10:08 - 13:38	$> +12$	+23.8	+27.0	*Viswanathan et al.* [1987]; *Ravindran and Krishna Murthy* [1997b]
		20-03-1979, 21-03-1979	13:38 - 14:08	$\sim +12$	+15.3	+12.0	*Viswanathan et al.* [1987]
		21-03-1979	14:08 - 14:38	$\leq +12$	+12.8	+12.0	*Viswanathan et al.* [1987]
		15-03-1979, 21-03-1979	14:38 - 16:48	$\sim +12$	+10.8	+11.4	*Viswanathan et al.* [1987]; *Ravindran and Krishna Murthy* [1997a]
		15-03-1979, 16-03-1979, 21-03-1979	16:48 - 17:38	$\leq +12$	+07.7	+10.2	*Viswanathan et al.* [1987]; *Ravindran and Krishna Murthy* [1997a]
		15-03-1979, 16-03-1979	17:38 - 18:23	$> +12$	+15.6	+21.5	*Ravindran and Krishna Murthy* [1997a]
June solstice	Rocket	13-08-1982	07:02	$\leq +12$	+01.6	−02.9	*Gupta* [2001]
		12-08-1982	07:18	$\leq +12$	+05.1	−02.0	*Gupta* [2001]
		29-08-1968	13:53	$\leq +12$	+06.5	+08.7	*Gupta* [2001]
		29-08-1968	22:38	< -12	−16.6	−16.2	*Prakash et al.* [1970]; *Gupta and Prakash* [1979]

Table 3.1: Comparison of vertical plasma drifts in high solar epoch deduced from experimental observations (rocket/radar) with global empirical model (Scherliess-99 and Fejer-08) drifts. Positive and negative values indicate upward and downward drifts, respectively. The red coloured entries denote the instances when the magnitudes of model drifts are different from the threshold drifts deduced from E-region irregularity observations, whereas the yellow boxes identify the instances when the polarity of the model drifts are not in accordance with the inferred polarities.

Season	Experiment	Date	Time/ Duration	Vertical drift (ms^{-1})			Literature
				Deduced	Scherliess-99	Fejer-08	
December solstice	Rocket	09-02-1975	05:37	< -12	-13.1	-18.8	*Gupta* [1986]
		28-01-1971	10:18	$> +12$	$+18.2$	$+18.9$	*Prakash et al.* [1971a]
		19-02-1975	10:43	$> +12$	$+18.4$	$+19.1$	*Gupta* [1997]
		28-01-1971	10:48	$> +12$	$+18.4$	$+19.3$	*Prakash et al.* [1971a]
	Radar	18-01-1974	05:38 - 06:08	< -12	-13.0	-24.6	*Prakash and Muralikrishna* [1976]
		18-01-1974, 23-11-1983	06:58 - 08:08	$\leq +12$	$+03.7$	$+03.6$	*Prakash and Muralikrishna* [1976]; *Viswanathan et al.* [1987]
		23-11-1983, 25-11-1983, 05-01-1993	08:08 - 10:08	$\sim +12$	$+10.4$	$+10.9$	*Viswanathan et al.* [1987]; *Ravindran and Krishna Murthy* [1997b]
		23-11-1983, 25-11-1983, 26-11-1983, 05-01-1993	10:08 - 12:38	$> +12$	$+17.9$	$+18.5$	*Viswanathan et al.* [1987]; *Ravindran and Krishna Murthy* [1997b]
		23-11-1983 to 26-11-1983, 05-01-1993	12:38 - 15:38	$\sim +12$	$+15.6$	$+14.7$	*Viswanathan et al.* [1987]; *Ravindran and Krishna Murthy* [1997b]
		23-11-1983, 26-11-1983	15:38 - 17:23	$\leq +12$	$+06.5$	$+04.8$	*Viswanathan et al.* [1987]
		06-12-1973	19:38 - 20:38	$\leq +12$	-03.6	-01.3	*Prakash and Muralikrishna* [1976]
Equinox	Rocket	03-03-1973	11:58	$> +12$	$+21.2$	$+19.5$	*Gupta* [2001]
		07-04-1972	12:08	$> +12$	$+20.6$	$+17.9$	*Gupta and Prakash* [1979]
		13-10-1972	12:38	$\leq +12$	$+18.6$	$+13.6$	*Gupta* [2001]
		15-03-1975	21:42	< -12	-16.9	-27.5	*Gupta* [1997]

Table contd.

Equinox	Radar	06-09-1994	03:53 - 05:38	< -12	-13.7	-30.0	*Krishna Murthy et al.* [1998]
		10-03-1972, 05-09-1994	06:38 - 08:38	$\leq +12$	-08.9	-06.0	*Prakash et al.* [1974]; *Krishna Murthy et al.* [1998]
		10-03-1972, 12-10-1983	08:38 - 09:38	$\sim +12$	$+16.5$	$+15.9$	*Prakash et al.* [1974]; *Sastri et al.* [1991]
		10-03-1972, 12-10-1983, 05-09-1994	09:38 - 13:08	$> +12$	$+20.8$	$+26.7$	*Prakash et al.* [1974]; *Viswanathan et al.* [1987]; *Krishna Murthy et al.* [1998]
		10-10-1983, 12-10-1983, 05-09-1994	13:08 - 14:38	$\sim +12$	$+16.6$	$+09.7$	*Viswanathan et al.* [1987]; *Krishna Murthy et al.* [1998]
		10-03-1972, 11-10-1983, 12-10-1983, 05-09-1994	14:38 - 17:53	$\leq +12$	$+10.4$	$+06.3$	*Prakash et al.* [1974]; *Viswanathan et al.* [1987]; *Krishna Murthy et al.* [1998]
June solstice	Rocket	12-08-1972	07:23	$\leq +12$	$+02.8$	-04.9	*Gupta and Prakash* [1979]
	Radar	20-06-1983, 24-06-1983	07:53 - 08:53	$\leq +12$	$+09.6$	-01.1	*Viswanathan et al.* [1987]
		21-06-1983, 24-06-1983	08:53 - 09:23	$\sim +12$	$+20.0$	$+09.6$	*Viswanathan et al.* [1987]
		23-06-1983, 24-06-1983	09:23 - 10:23	$\leq +12$	$+23.1$	$+14.8$	*Viswanathan et al.* [1987]
		20-06-1983 to 23-06-1983	11:23 - 13:23	$\sim +12$	$+21.4$	$+16.3$	*Viswanathan et al.* [1987]
		20-06-1983, 23-06-1983	13:23 - 13:53	$\leq +12$	$+07.5$	$+06.8$	*Viswanathan et al.* [1987]

Table 3.2: Same as Table 3.1 but for low solar epoch.

On comparing the vertical drifts given in Tables 3.1 and 3.2, it is observed that, in general, vertical drifts presented by both the empirical models are consistent with the criterion for presence or absence of Two-stream waves, though some deviations are also observed.

The amplitudes of vertical drifts obtained from Scherliess-99 and Fejer-08 models are found to deviate from the deduced threshold values of $|V_z|$ on six and five occasions, respectively (see the red coloured entries in Tables 3.1 and 3.2). The deviations in V_z with respect to Fejer-08 model drifts are within the uncertainly limits of measurements (about 10%) for Fejer-08 model, barring two durations 13:38 - 14:38 LT in December solstice under high solar epoch and 09:23 - 10:23 LT in June solstice under low solar epoch. However, in case of Scherliess-99 model, except for an occasion during 14:08 - 14:38 LT in equinox under high solar epoch, all the deviations in V_z are beyond the uncertainty limits of measurements (relative precision of about 2 ms^{-1}). Even in the cases when Two-stream waves are present on some days and absent on some other days within a same season (implying amplitude of vertical drifts closer to 12 ms^{-1}), the Fejer-08 model drifts seem to be more consistent with deduced vertical drifts than Scherliess-99 model drifts. This is clearly visible during 08:00 - 10:00 LT and 13:00 - 16:00 LT. Hence, Fejer-08 model is found to represent the vertical drifts over the Indian sector better compared to Scherliess-99 model. However, it is observed that both the empirical models fail to capture the polarity of vertical drift during early morning hours (around 6 LT), see yellow coloured cells in Tables 3.1 and 3.2, though in June solstice the Scherliess-99 model seems to predict better compared to Fejer-08 model. The probable reasons for deviations in amplitude and polarity of the vertical drifts presented by empirical models from the deduced V_z on a few occasions are discussed in section 3.4.

In high solar epoch, the average variations of daytime vertical drifts deduced from magnetometer records match (within 1σ variation) with the corresponding variations presented by both Scherliess-99 and Fejer-08 models in all three seasons (see maroon and black coloured solid curves in Figures 3.2 and 3.4). However, the daytime vertical drift deduced during low solar epoch match (within 1σ variation) with the corresponding variations presented by Fejer-08 model better compared to Scherliess-99 model, particularly in equinox and June solstice (see Figures 3.3 and 3.5). In December solstice the deduced values of vertical drifts match (within 1σ variation) with the corresponding variations presented by both the empirical models irrespective of solar epoch. In general, the average values of deduced vertical drift match fairly well with both the empirical models during high solar epoch while these values match well with Fejer-08 model during low solar epoch. This is probably due to better longitudinal resolution used in Fejer-08 model compare to Scherliess-99 model (refer section 3.4). Further, the values of vertical drifts deduced from magnetometer data are observed to capture the presence or absence of Two-stream waves. Interestingly, the deduced vertical drifts are $\sim$12 ms^{-1} during the time intervals wherein Two-stream waves were detected on some days and found absent on some other days within a same season.

During nighttime, the zonal electric fields corresponding to the average values of vertical drifts obtained using ionosonde/radar experiments are not sufficient for the generation of Two-stream waves in low solar epoch (see Figures 3.3 and 3.5) on a few occasions. On the other hand, in high solar epoch, the pre-midnight vertical drifts in both the solstices are, in general, sufficient to account for the presence of Two-stream waves (see figures 3.2a, 3.4a and 3.2c, 3.4c). However, during post-midnight hours, these vertical drifts are sufficient to account for the presence of Two-stream waves on some occasions (see figures 3.4a and 3.4c). During equinox in high solar epoch, some of the average vertical drifts are consistent with the presence of Two-stream waves. Further, it is observed that the ionosonde/radar deduced vertical drifts are always smaller than those presented by empirical models in different seasons (e.g., see figures 3.4a-c) and solar flux levels (e.g., see figures 3.4a and 3.5a). In general, the differences are about 10 ms^{-1} or greater with the maximum deviation occurring in equinoctial months (e.g., notice the difference in V_z of middle panel compared to top or bottom panel in any figure). It is to be noted that considering typical height resolution of 3 km [*Patra et al.*, 2005] and the temporal resolution of 15 min in ionosonde experiments [*Sastri*, 1984; *Krishna Murthy and Hari*, 1996; *Madhav Haridas et al.*, 2015], the typical uncertainty in vertical drift is ∼5 ms^{-1}. The uncertainty in the vertical drifts deduced using HF phase path sounder or Doppler radars is less than 1 ms^{-1} [*Prabhakaran Nayar and Sreehari*, 2004]. Therefore, the observed differences between the measured vertical drifts (derived using ionosonde/Phase path sounder/Doppler radar) and the model drifts are larger than the typical uncertainties of the measurements involved. The probable reasons for significant difference are discussed in section 3.4. In addition, it is observed that during nighttime Scherliess-99 model values of V_z are smaller compared to Fejer-08 model. The probable reasons for this are also discussed in section 3.4.

During PRE hours, the peak amplitude of vertical drift over Indian sector is known to vary day-to-day [*Balan et al.*, 1992] and also dependent on the solar flux level [*Ramesh and Sastri*, 1995; *Sastri*, 1996]. However, the time of PRE over the Indian sector have been shown [*Namboothiri et al.*, 1989; *Nair et al.*, 1993] to be same within a solar epoch and hence the occurrence times of PRE are compared. Incidentally, it is found that the vertical drifts presented using ionosonde/radar experiments maximize around the time of Barium vapour cloud experiments (the solid blue, green and magenta coloured curves in Figures 3.4(a), 3.4(b) and 3.5(a) peak around the time of magenta coloured solid circles). It is also to be noted that the time of PRE observed in vertical drift presented by Scherliess-99 model is later in LT compared to these times (e.g., see Figure 3.2). A probable reason for this difference in time is discussed in section 3.4.

3.4 Discussion

As stated in section 3.3, Fejer-08 model is found to be more consistent with the reported presence or absence of Two-stream waves than Scherliess-99 model. Further, the vertical drift provided by Fejer-08 model also seem to represent the measured drifts better during low solar epoch as far as the PRE and daytime deduced drifts are concerned. To investigate the probable reasons for Fejer-08 model being more consistent than Scherliess-99 model, the data sets and methodology used to develop these empirical models are looked into.

It is to be noted that empirical models were developed based on the in situ observations of plasma drifts at the altitude of satellite. The techniques employed to measure the plasma drifts are different from the experimental techniques adopted to get these observations over the Indian sector. In Scherliess-99 model, the input for vertical drifts were obtained from Ion Drift Meter (IDM, on board AE-E satellite) measurements over $\pm 7.5°$ dip-latitude ranges around the globe during 1977 - 1979 and Jicamarca ISR measurements from 1968 to 1992. On the other hand, in Fejer-08 model the input for vertical drifts were obtained from Ionospheric Plasma and Electrodynamics Probe Instrument (IPEI, on board ROCSAT-1 satellite) measured vertical drifts over $\pm 5°$ dip-latitude ranges around the globe from 1999 to 2004. These vertical drifts were binned over 60° and 30° longitudes in Scherliess-99 and Fejer-08 models, respectively. Further, different methodologies were adopted to develop both the empirical models. In Scherliess-99 model, the V_z values around the globe were constrained with different statistical weights to make electric field curl-free ($\oint \mathbf{E} \cdot d\mathbf{l} = 0$). However, in Fejer-08 model, the vertical drifts were not constrained to satisfy for irrotational electric field, though, this condition was used to estimate the accuracy of this model. As mentioned in *Scherliess and Fejer* [1999], satellite measurements of V_z during nighttime (that have more uncertainty compared to daytime) were given less statistical weight compared to daytime measurements and whenever the highly accurate daytime vertical drifts were available from Jicamarca ISR, those data sets were given even higher statistical weight (about 75%). Under this scenario, the V_z values provided by Scherliess-99 model over the Indian sector, which is nearly at antipodal point of the Peruvian sector, could become uncertain.

The occurrence of afternoon equatorial counter electrojet (CEJ) had been shown [*Rastogi et al.*, 2014] to be highest during June solstice under low solar epoch. Interestingly, the Fejer-08 model drift values reveal downward drifts in the afternoon hours which is consistent with the observations of *Rastogi et al.* [2014]. The presence of downward drift in June solstice during solar minimum years also gets credence from the works of *Gurubaran* [2002] and *Bhattacharyya and Okpala* [2015]. It was shown that equatorial CEJ under similar conditions was due to additional contribution from global current system that gets superimposed on the *Sq* current system. Further, the small afternoon upward drifts in this season given by Scherliess-99 model are also favorable for the generation of CEJ with a little help from additional external agency. Therefore, both the models support the morphological feature of occurrence of CEJ during this season. A detailed investigation is carried out on the occurrence of these afternoon CEJ events which is presented in Chapter 4. As far as the high solar epoch is concerned, negligible vertical plasma drift obtained from Fejer-08 model in the afternoon hours during the June solstice is consistent with the occurrence characteristics of partial CEJ at this local time reported by *Rastogi et al.* [2014]. This feature is not efficiently captured by Scherliess-99 model. In view of these outcomes, in the forthcoming discussion on vertical drifts during different times of the day, barring evening hours, vertical drifts presented by experimental observations are compared with Fejer-08 model only. During PRE time, a discussion based on both the models is presented.

3.4.1 Vertical drifts in morning hours

The vertical drifts presented using ionosonde/radar experiments are insufficient for the generation of Two-stream waves observed around 6 LT. Their presence is supported by Fejer-08 model, although the polarity of vertical drifts presented by this model is not consistent with the respective observation on a few occasions during 06:00 - 08:00 LT, as mentioned in section 3.3. To investigate the probable reasons for this inconsistency with the empirical model, the diurnal variations of vertical drifts over the dip-equatorial longitudes presented by Fejer-08 become important. Figure 3.6 depicts the contours of iso-vertical drifts with local time at different longitudes. These values correspond to relatively high solar flux levels of 150 sfu for which deviations are noticed in equinox and June solstice (see yellow coloured cells in Table 3.1). Therefore, the plots of these two seasons only are depicted in Figure 3.6.

The iso-vertical drifts during 06 - 08 LT over $60^{\circ} \pm 15^{\circ}$E longitude (around Indian sector) are highlighted with red coloured rectangular boxes in both equinox, and June solstice figures. It is observed that, though the vertical drifts are small during 06 - 08 LT around the Indian sector, they show variation in polarity with longitude even for a particular LT. The similar pattern is also observed in the contours of iso-vertical drifts with local time (resolution 1 hr) at different longitudes (resolution 10°) reported by *Kil et al.* [2008] based on ROCSAT-1 experiments. Therefore, the longitudinal averaging of vertical drifts used in Fejer-08 model (given above) could result in loss of polarity information. Therefore, it is rather difficult to bring out the clear picture of vertical drifts during morning hours.

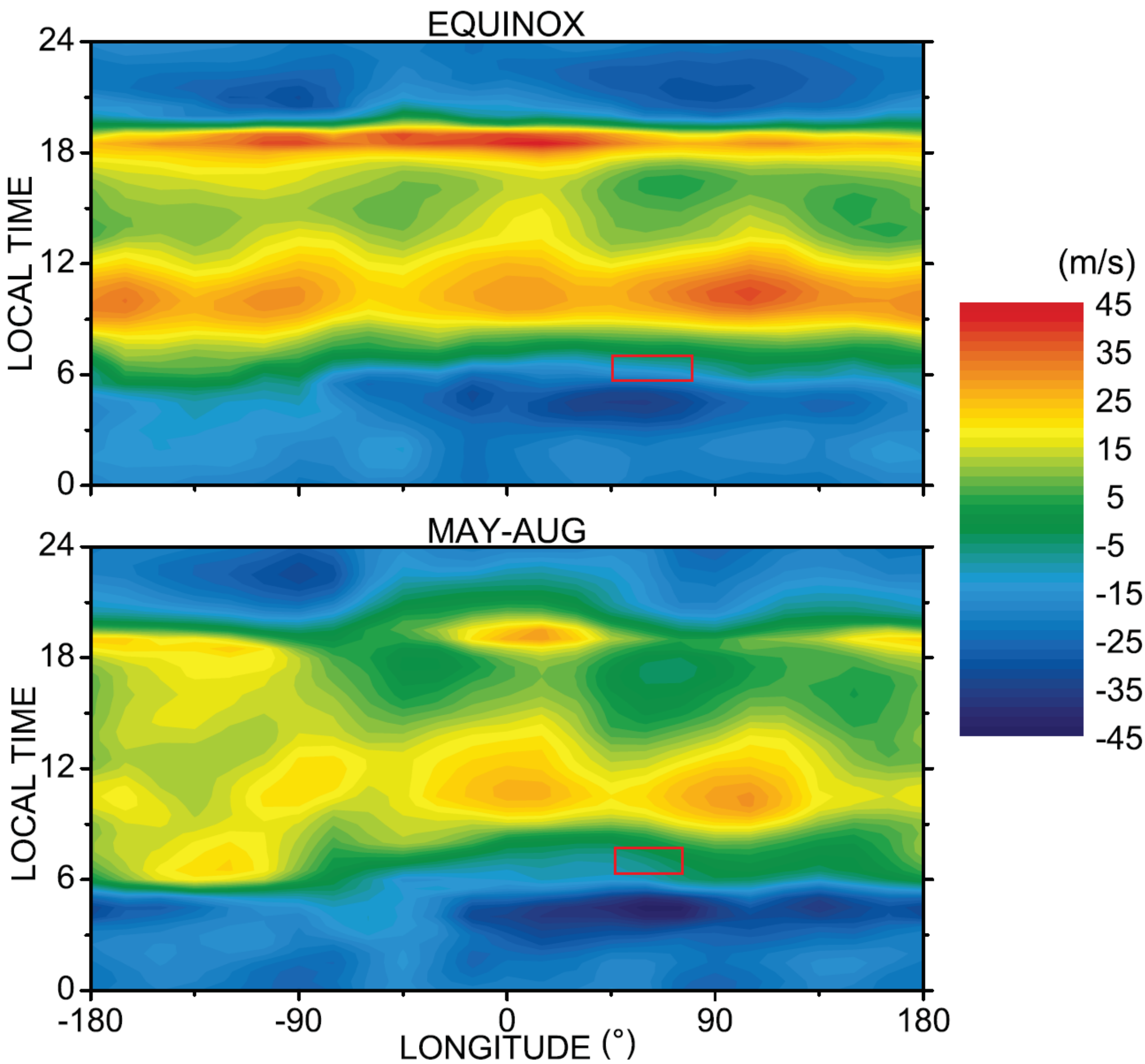

Figure 3.6: Contours of iso-vertical drift with local time at different longitudes corresponding to equinox and June solstice for sfu level of 150 [after *Fejer et al.*, 2008a]. The vertical drifts during ∼06 - 08 LT over 60 ± 15°E longitude are highlighted with red coloured rectangular box.

3.4.2 Vertical drifts during daytime

In general, daytime vertical drifts presented by Fejer-08 model and those deduced using magnetometer data sets during ∼07:30 - 17:30 LT match within 1σ variation. In general, the magnetometer deduced V_z capture the presence or absence of Two-stream waves, suggesting that the magnetometer data can be effectively used to gauge the vertical drift/zonal electric field variations in daytime.

3.4.3 Vertical drifts in evening hours

It is noticed that the time of occurrence of PRE, as predicted by Scherliess-99 model, is slightly later than the corresponding times observed by most of the ionosonde/HF radar experiments during high solar epoch. In this regard, Fejer-08 model is closer to the Indian observations. This may be partly due to the better longitudinal resolution of the Fejer-08 model as compared to the Scherliess-99 model. More importantly, the Indian stations are located east of 60°E longitude and the model drifts have been presented corresponding to 60°E with finite longitudinal averaging. As the local sunset will occur over the Indian sector earlier than that over 60°E, the model drifts can occur at a later time with respect to the Indian observations. During low solar epoch, the PRE feature itself is more conspicuous in Fejer-08 model (particularly during solstices) than in Scherliess-99 model. The time of occurrence of PRE in the Indian observations are reasonably consistent with the Fejer-08 model outputs in all the seasons except in June solstice.

It is interesting to note here that in June solstice under low solar epoch, PRE was found to be present [e.g., *Ramesh and Sastri*, 1995] or absent (e.g., Scherliess-99) on occasions and also reversed [e.g., *Subbarao and Krishna Murthy*, 1994; *Chakrabarty et al.*, 2014] on a few occasions. Therefore, the occurrence of PRE in June solstice under low solar epoch is ambiguous. The suppression of PRE in June solstice under low solar epoch was also reported over Peruvian [*Scherliess and Fejer*, 1999] and African [*Oyekola*, 2006] sectors. Further, the occurrence of reverse PRE is also noticed in the vertical drifts over African sector that was presented in Figure 1(a) of *Oyekola et al.* [2007] corresponding to June solstice in low solar epoch. In general, the occurrence of reverse PRE is found in June solstice when solar flux level is low. Modelling studies of reverse PRE are not found, though simulation results for suppressed PRE are available [*Fesen et al.*, 2000; *Millward et al.*, 2001]. The observed variability on the occurrence of PRE during June solstice in low solar epoch needs to be investigated in detail to arrive at a bigger picture. There are differences, of course, between the magnitude of V_z during PRE time given by Indian observations and the model values on some occasions. It is known that the peak values of V_z during PRE hours depend on solar flux level [*Fejer et al.*, 1996; *Sastri*, 1996] and change on a day-to-day basis [*Woodman*, 1970; *Balan et al.*, 1992]. In the absence of significant recombination effect (as the layer height is generally more than 300 km) during PRE time and unlikely occurrence of Equatorial Spread-F before PRE, ionosonde/HF radar measurements can be used to infer V_z on a day-to-day basis.

3.4.4 Vertical drifts during nighttime

The vertical drifts presented by Fejer-08 model capture the observed presence/ absence of Two-stream waves during nighttime. However, the vertical drifts presented using ionosonde/HF radar experiments are not sufficient, on most of the occasions, to capture the observed presence of Two-stream waves and differ from vertical drifts presented by Fejer-08 model by 10 ms^{-1} or more, in general. The sources of these deviations could be improper correction of chemical loss, gradients in vertical drifts, instrumental bias and/or inaccurate determination of height of plasma layer, etc. To delineate the probable causes of these large differences, the contributions that can arise from these factors are looked into.

As the vertical drifts (used in the present work) are, in general, obtained only for the duration when altitude of plasma layers remains above 300 km, the contribution due to chemical recombination would be negligible [*Krishna Murthy et al.*, 1990]. Even otherwise, it is shown [*Kakad et al.*, 2012; *Subbarao and Krishna Murthy*, 1994] that contribution due to recombination process can be about 2 ms^{-1} or 4 ms^{-1} corresponding to the movement of plasma layer above or below 300 km, respectively.

The altitude variation of vertical drifts over the Indian sector around PRE hours have been reported earlier [*Raghavarao et al.*, 1987; *Sastri et al.*, 1995; *Prabhakaran Nayar and Sreehari*, 2004]. However, the altitude gradient in vertical drifts during nighttime over the Indian sector are not known. Based on ISR experiments over another dip-equatorial station (Jicamarca), *Pingree and Fejer* [1987] reported the altitude gradient in the vertical drift over the dip-equator. The temporal variation of these values are depicted Figure 3.7. The altitude averaged gradient in nocturnal V_z is around 0.005 ms^{-1} km^{-1} (averaged nighttime value). These values are taken as a representative value of altitude gradient in vertical drifts during nighttime. As the altitudes probed by the ionosonde/radar experiments (bottom side of F-layer, i.e. around 300 km) and the ROCSAT-1 satellite (used in Fejer-08 model) are separated by about 300 km, V_z values could differ by about 2 ms^{-1}. Further, if the altitude gradient in vertical drifts are assumed to follow the opposite pattern above and below F-layer peak as observed by *Fejer et al.* [2014] and simulated by models [*Klimenko et al.*, 2012; *Qian et al.*, 2015], the difference in V_z is expected to be even less than 2 ms^{-1}.

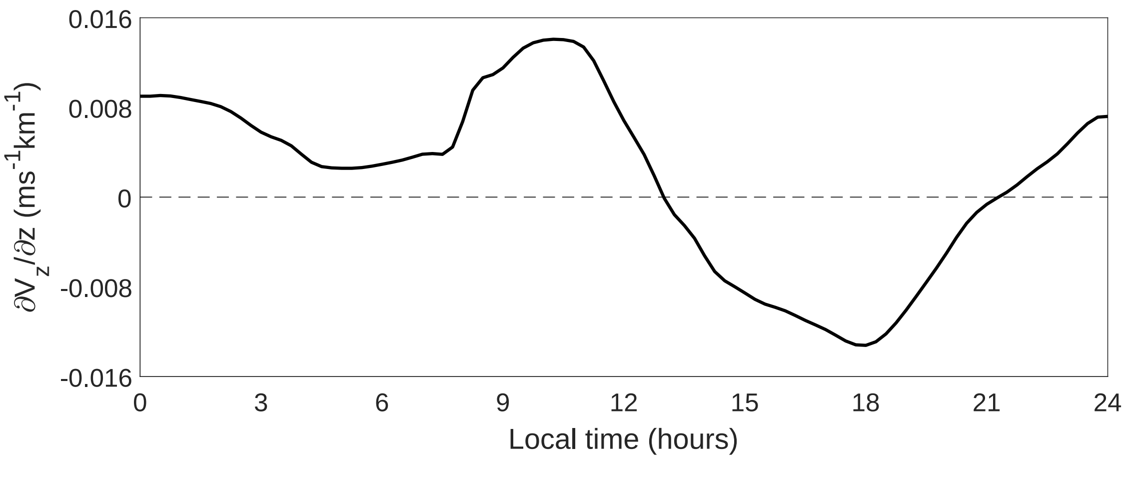

Figure 3.7: Temporal variation of altitude gradient in vertical drifts [after *Pingree and Fejer*, 1987].

Finally, the accuracy of vertical drifts deduced using ionosonde/radar experiments depends (to the first order) on how accurately the altitude of plasma layer is determined. This is particularly difficult during Equatorial Spread-F (ESF) events. Therefore, to investigate a possible relationship, if any, between the percentage occurrence of ESF [*Subbarao and Krishna Murthy*, 1994] over TRD and difference between V_z, obtained using ionosonde/radars experiments and Fejer-08 model, the two parameters are looked together. In general, the differences in V_z are found to follow the percentage of occurrence of ESF. For e.g., under high solar epoch, the occurrence of ESF was higher [*Subbarao and Krishna Murthy*, 1994] during pre-midnight than post mid-night hours in all the seasons; and the corresponding differences in vertical drifts are observed to follow the similar pattern (see Figure 3.4). Under low solar epoch, the ESF occurrence in June solstice is higher during post-midnight than pre-midnight hours; and corresponding differences in vertical drifts are observed to follow this pattern (see figure 3.5b). Further, under high solar epoch the occurrence of ESF during pre-midnight hours is maximum in equinox; and the differences in vertical drifts are also maximum during pre-midnight hours in equinox (see figure 3.4b). Under low solar epoch, the occurrence of ESF during post-midnight is maximum in June solstice; and the difference in vertical drifts during post-midnight is also maximum in June solstice (see figure 3.5c).

From the above discussion, it appears that the seasonal V_z presented using ionosonde/radar experiments might have suffered from an uncertainty arising out of the inaccurate determination of ionospheric height parameter in the presence of ESF events. It is important to note that the plasma irregularities associated with ESF move upward and thus can result in systematic underestimation of the downward drifts, which is seen in Figures 3.2 - 3.5. Therefore, presence of ESF is probably the most important reason for the underestimation of ionosonde/HF radar derived vertical drifts. Further, with appropriate (without ESF traces) choice of ionograms and proper correction for recombination loss, the ionosonde/HF radar experiments can be used to deduce the vertical drifts during nighttime. Another interesting feature in vertical drifts during June solstice under low solar epoch was reported by *Chakrabarty et al.* [2014]. They had shown that the vertical drifts increase and become upward during midnight hours, which is not observed in vertical drifts presented by the empirical models but confirmed by C/NOFS observations.

3.5 Summary

The vertical plasma drifts obtained or deduced with several techniques over the Indian sector are compared with those presented by the global empirical models [*Scherliess and Fejer*, 1999; *Fejer et al.*, 2008a]. The salient points that have emerged from this study are as follows:

1. In general, the vertical drifts presented by *Fejer et al.* [2008a] model represent vertical drifts over the Indian sector better than *Scherliess and Fejer* [1999] model and other average nocturnal vertical drifts deduced using ionosonde/radar experiments.

2. The empirical models fail to capture the direction of vertical drifts in morning hours (around 6 LT). This is probably due to longitudinal averaging that results in loss of polarity information.

3. The vertical drifts (corresponding to zonal electric fields) deduced during daytime ($\sim$07:30 - 17:30 LT) from magnetometer records match well with vertical drifts presented by *Fejer et al.* [2008a] model and found to be sufficient for the presence/absence of Two-stream waves in general.

4. For distinctive drift features like PRE, the time of PRE reported by the empirical models and the ground-based observations is found to differ on some occasions and this can be due to the different longitudinal averaging schemes used in the models.

5. The seasonally averaged nocturnal vertical drifts deduced using ionosonde/HF radar experiments are not sufficient, on most of the occasions, to capture the observed presence of Two-stream waves. The deviations of vertical drifts obtained using ionosonde/HF radar experiments from the *Fejer et al.* [2008a] model drift values closely follow the percentage occurrence of ESF indicating inaccuracy in the determination of vertical drifts based on ionospheric height variations in the presence of ESF.

6. Both the empirical models *Scherliess and Fejer* [1999] and *Fejer et al.* [2008a] support the occurrence characteristic of afternoon equatorial CEJ in June solstice under low solar epoch.

Chapter 4

Afternoon CEJ over India during June solstice in solar minimum

Excerpt

In the previous chapter, it has been shown that the *Fejer et al.* [2008a] model drifts corresponding to 60°E longitude represent the vertical drifts over the Indian sector well during daytime barring early morning hours. In this chapter, these drifts are utilized to investigate the possible reason for the afternoon equatorial counter electrojet (CEJ) which is defined in the Chapter 1. Observational studies over the Indian longitudes [*Patil et al.*, 1990a; *Rastogi et al.*, 2014] revealed that the occurrence of CEJ events in afternoon hours is more frequent during June solstice (May - June - July - August) in solar minimum than in other periods. In general, the June solstice solar minimum CEJ events occur between 1500 LT and 1800 LT with peak strength of about -10 nT at around 1600 LT. In order to understand the frequent occurrence of these CEJ events, an investigation is carried out using an equatorial electrojet model [*Anandarao*, 1976] and the empirical vertical drift model by *Fejer et al.* [2008a]. The strength, duration, peak value and the occurrence time of CEJ obtained using electrojet model match remarkably well with the corresponding observations of average geomagnetic field variations. The occurrence of CEJ is found to be due to solar quiet (Sq) electric field in the westward direction which is manifested as downward drift in *Fejer* *et al.* [2008a] model output during 1500 - 1800 LT. Further, the occurrence of afternoon reversal of Sq electric field in this season is shown to be consistent with earlier studies from Indian sector. Therefore, this investigation provides explicit evidence for the role of westward Sq electric field on the generation of afternoon CEJ during June solstice in solar minimum periods over the Indian sector indicating that the CEJ current system is a part of Sq current system extending from pole to equator. Thus, the requirement of a separate return current becomes superfluous.

4.1 Introduction

A strong eastward current is driven in the E-region over the magnetic dip-equator owing to the orthogonal orientation of the Solar-quiet (Sq) electric field and the horizontal component of geomagnetic field. This current flows within ±3° dip-latitude at around 105 km and is well known as equatorial electrojet (EEJ). In order to characterize the EEJ, a large number of studies were extensively conducted using ground-based [*Egedal*, 1947; *Rastogi and Patil*, 1986; *Venkatesh et al.*, 2015], rocket-borne [*Davis et al.*, 1967; *Sastry*, 1970] and satellite-based magnetometers [*Cain and Sweeney*, 1973; *Onwumechili and Agu*, 1981; *Jadhav et al.*, 2002; *Lühr et al.*, 2004]. Modelling efforts were also carried out to simulate different characteristics of EEJ [*Sugiura and Poros*, 1969; *Richmond*, 1973; *Anandarao*, 1976; *Forbes and Lindzen*, 1976; *Stening*, 1985]. Excellent reviews on this topic are available in the literature [*Forbes*, 1981; *Raghavarao and Anandarao*, 1987; *Reddy*, 1989; *Stening*, 1992; *Yamazaki and Maute*, 2017]. The electrojet region is also known to host different types of plasma irregularities as reported comprehensively by earlier workers [*Prakash et al.*, 1971a; *Fejer and Kelley*, 1980; *Gupta*, 2000; *Kelley*, 2009]. Further, the geomagnetic field variations due to electrojet current can be taken as a proxy for electric field variations [*Rastogi and Patel*, 1975] on a time scale shorter than the time scale associated with ionospheric conductivity variation. As mentioned earlier in the Chapter 1, these electric fields during magnetically quiet times are referred to as solar quiet (Sq) electric field generated essentially by a dynamo action driven by tidal winds and hence, associated with Sq current system extending from pole to equator. The dip-equatorial vertical plasma drifts driven by Sq electric fields are measured directly using radar [e.g., *Woodman*, 1970; *Fejer*, 1981], Barium vapor cloud [e.g., *Haerendel et al.*, 1967] and Ion-Drift-Meter [e.g., *Hanson and Heelis*, 1975] techniques. A few methodologies were described in literature [e.g., *Anderson et al.*, 2004; *Pandey et al.*, 2017] to derive the zonal Sq electric field from geomagnetic field observations.

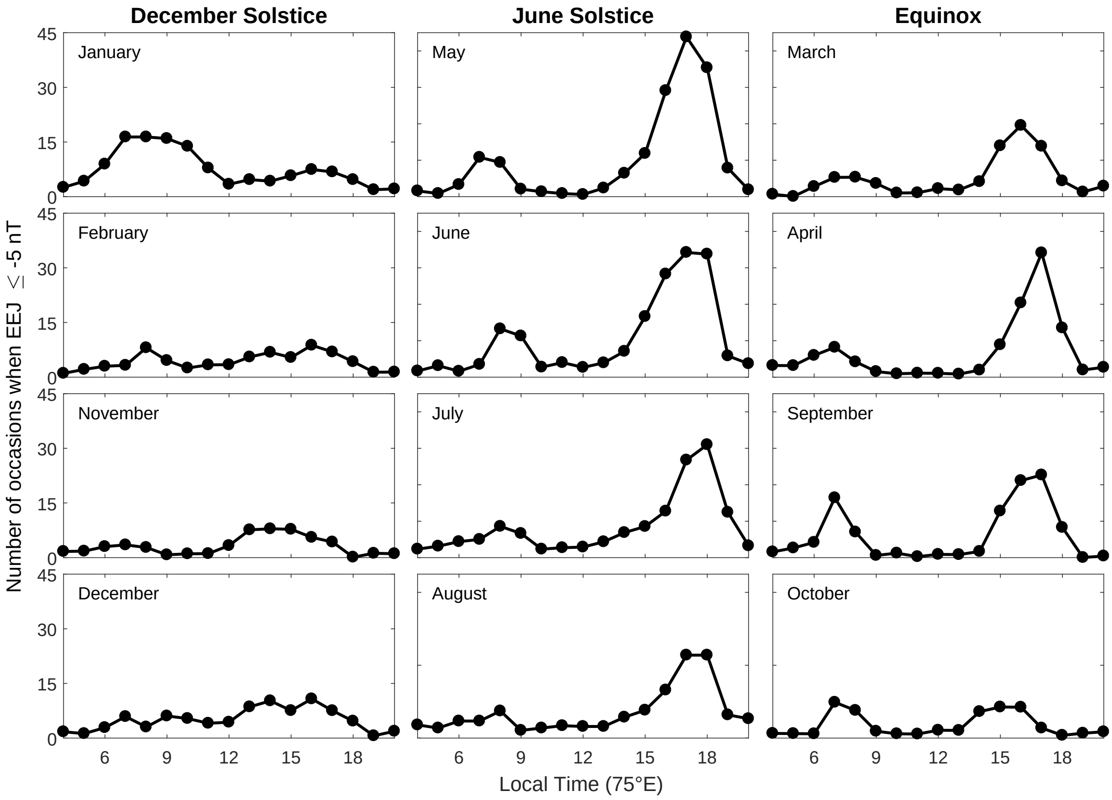

Figure 4.1: Number of CEJ events at different local times of the day during different months in solar minimum period 1964 - 1965 [after *Patil et al.*, 1990a].

In general, as mentioned earlier, the EEJ is eastward during daytime. On many occasions, however, the flow is observed to be westward during the afternoon periods [*Gouin and Mayaud*, 1967]. This is generally referred to as the equatorial counter electrojet (CEJ). A number of studies [*Bhargava and Sastri*, 1979; *Patil et al.*, 1990a,b; *Vichare and Rajaram*, 2011; *Rabiu et al.*, 2017] reported the occurrence of CEJ events around the globe and their characteristics were established. Figure 4.1 [based on *Patil et al.*, 1990a] depicts temporal variation of total number of CEJ events per month during solar minimum periods 1964 - 1965. The criterion for choosing CEJ events was based on the EEJ strength $\leq$-5 nT. The left and middle panels represent the number of CEJ events during December (November - December - January - February) and June (May - June - July - August) solstices while the right panel represent the number of CEJ events during equinox (March - April, September - October). It is clearly evident from this figure that the maximum number of CEJ events during afternoon hours occur in June solstice period.

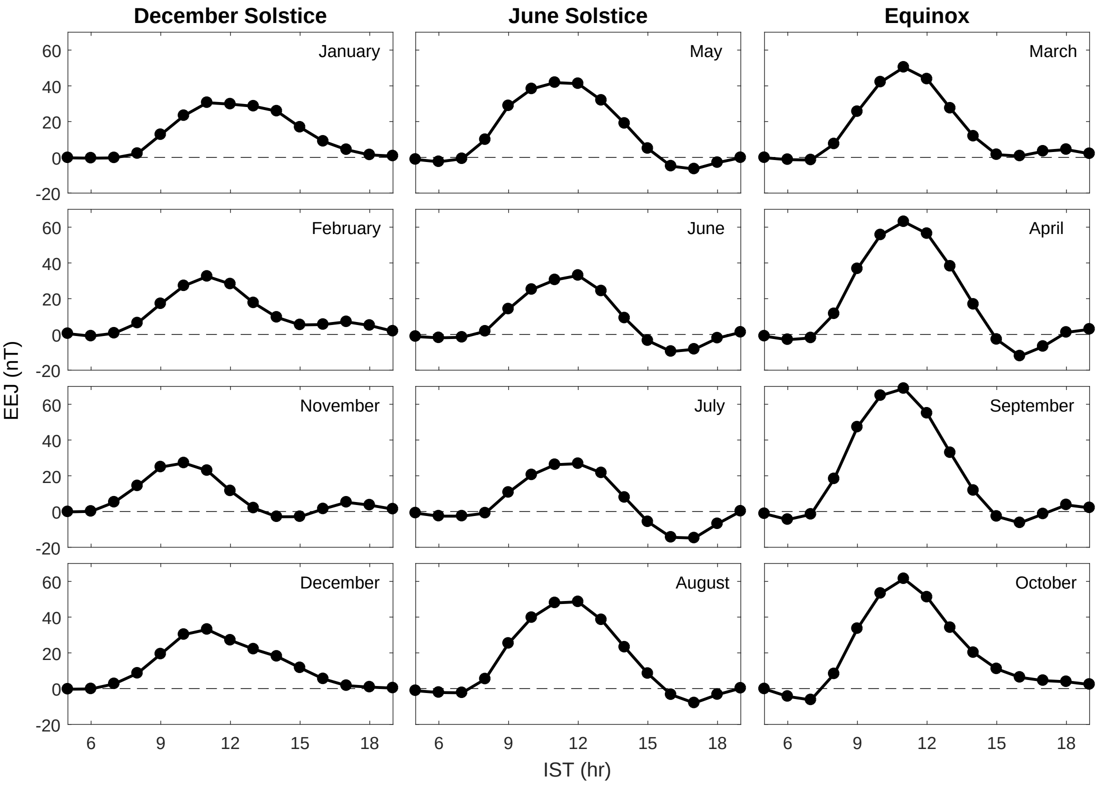

Figure 4.2: Temporal variation of monthly averaged values of strength of EEJ during 1976 [after *Rastogi et al.*, 2014].

Similar conclusion can be arrived based on the work of *Rastogi et al.* [2014]. Figure 4.2 [based on *Rastogi et al.*, 2014] depicts the temporal variation of monthly averaged strength of EEJ during 1976. This figure also reveals that the occurrence of CEJ events is more in June solstice than other seasons. Based on 40 years of magnetic field observations from the Indian longitudes, *Rastogi et al.* [2014] reported a similar feature in every solar cycle. Thus, the frequent occurrence of afternoon CEJ is not unique to any particular solar cycle which can be seen from the observations presented at a later time in this chapter. Further, the day-to-day variations in EEJ strength for the month of July 1976 [see Figure 4.3, based on *Rastogi et al.*, 2014] revealed that the afternoon CEJ events occurred on 25 days in this month.

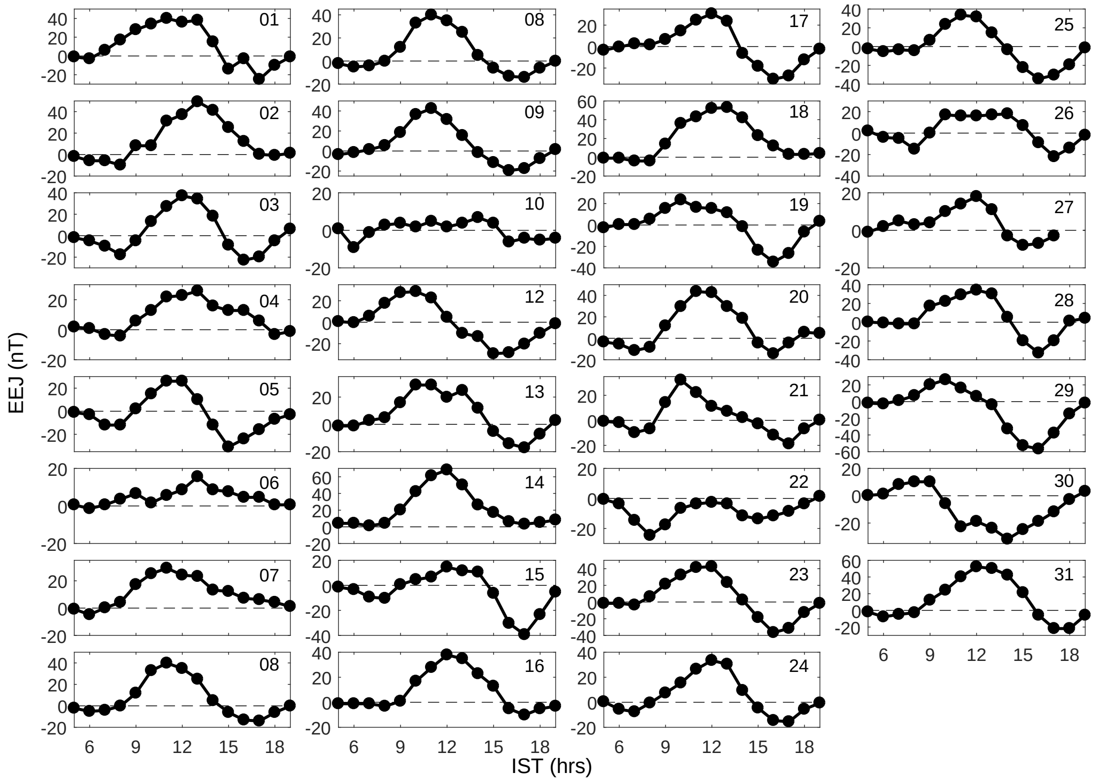

Figure 4.3: Variations of EEJ strength on individual days of July 1976 [after *Rastogi et al.*, 2014].

All the earlier morphological studies [*Patil et al.*, 1990a,b; *Rastogi et al.*, 2014] strengthen the characteristics of frequent occurrence of afternoon CEJ events during June solstice in solar minimum years. However, those studies do not take care of the geomagnetic conditions during the time period of investigation. Recently, based on vector magnetometer data obtained from CHAMP satellite on geomagnetically quiet days (Kp $\leq$ 3) during 2001 - 2010, *Singh et al.* [2018] reported the frequent occurrence of afternoon CEJ events during June solstice over the Indian sector. In order to ascertain that this feature holds good during magnetically quiet periods also, an exercise is carried out. Figure 4.4 depicts the percentage of CEJ events that occurred during 15 - 18 LT on geomagnetically quiet days of each month. The numbers are based on EEJ strength deduced using magnetic field observations during descending (1985 - 1987) and ascending (1993 - 1995) phases of solar cycle 22. In addition, percentage of these CEJ events out of the total geomagnetically quiet days in each month are also depicted in Figure 4.4. It is to be noted that, seasonally the occurrence of afternoon CEJ are maximum in June solstice. Therefore, all these investigations strengthen the fact that occurrence of afternoon CEJ over the Indian longitudes are maximum during June solstice in solar minimum years.

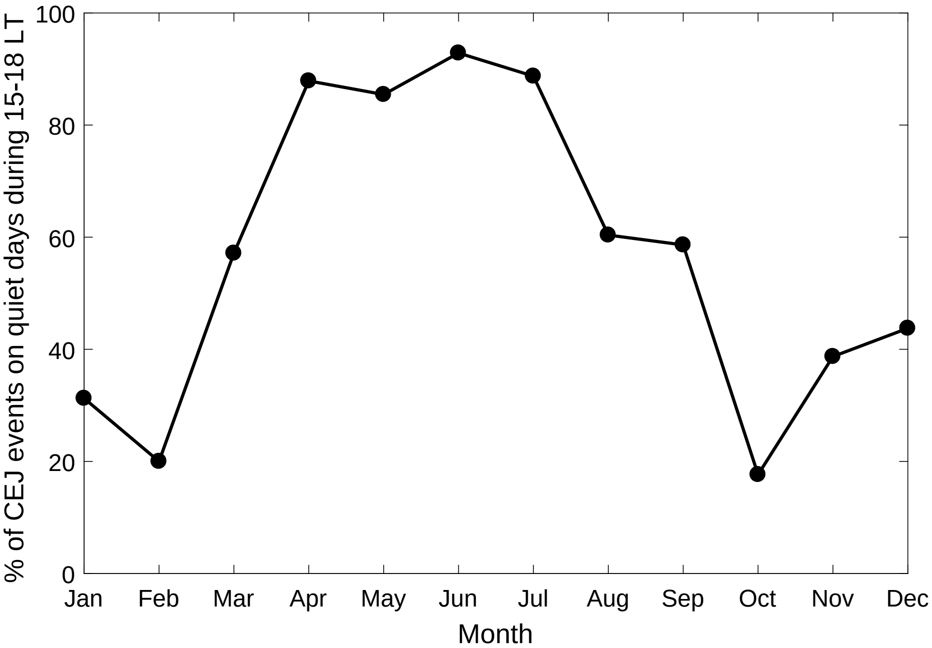

Figure 4.4: Percentage of CEJ events that occurred during 15 - 18 LT on quiet days of each month based on magnetic field observations spanned over six low solar flux years (F10.7 $\leq$ 120 sfu) of solar cycle 22.

Many mechanisms were proposed to explain the occurrence of CEJ events. *Gouin and Mayaud* [1967] suggested a possible scenario wherein there exists two counter streaming current systems at two different altitudes and depending on their relative strengths, the EEJ or CEJ can be generated. However, the experimental support for this hypothesis in the form of a vertical profile of current density is not available in the literature. The effects of lunar phase variation on the occurrence of CEJ are extensively studied [*Hutton and Oyinloye*, 1970; *Rastogi*, 1974; *Stening*, 1989a]. However, as described earlier (Figure 4.3) occurrence of afternoon CEJ on 25 days in a month of July during solar minimum over the Indian sector [*Rastogi et al.*, 2014] cannot be accounted for by the lunar phase variation. *Raghavarao and Anandarao* [1980] showed that large vertical winds ($\sim$20 ms^{-1}) of gravity wave origin can generate CEJ. However, sustenance of such winds on daily basis lasting for $\sim$3 hrs could be difficult [*Stening*, 1992]. Further, the effects of zonal wind and its vertical shears were shown to be mostly ineffective in altering the polarity of zonal current over the dip-equator [*Richmond*, 1973; *Anandarao and Raghavarao*, 1987]. It is also known that the polarity of the Sq electric field can be altered [e.g., *Chau et al.*, 2009, 2012; *Fejer et al.*, 2010] by the winds associated with the significant rise in temperature (known as Sudden Stratospheric Warming or SSW) in the polar stratosphere in the winter hemisphere [*Schoeberl*, 1978] owing to disruption of polar vortex of westerly winds. This can lead to occurrence of CEJ during SSW events [*Sridharan et al.*, 2009]. However, the effects of SSW are pronounced in local winter [*Schoeberl*, 1978] and hence, frequent occurrence of CEJ in June solstice is not likely to be of SSW origin. Therefore, these mechanisms cannot successfully account for the characteristics of CEJ events in June solstice over the Indian sector. Though space weather events like disturbance dynamo [*Blanc and Richmond*, 1980; *Pandey et al.*, 2018], overshielding [*Kobea et al.*, 2000] and substorm [*Kikuchi et al.*, 2003] also produce CEJ, however, the present study is focused on the occurrence of CEJ during geomagnetically quiet conditions. The abnormal depressions in horizontal magnetic field over the dip equatorial stations, similar to the magnetic field signatures of CEJ events, were correlated with foF2 variation by *Onwumechili and Akasofu* [1972]. Although those observations were in another season (December solstice) and might have a common driver, these authors did not explicitly discuss the possible role of Sq electric field. In addition, these authors [*Onwumechili and Akasofu*, 1972] did not remove off-equatorial magnetic field in their work, which was shown in later years [*Rastogi*, 1975] to be essential to ascertain CEJ events. In another investigation, the possibility of CEJ being part of Sq current system was discussed by *Gurubaran* [2002]. However, in the investigation of *Gurubaran* [2002], the alteration of Sq electric fields was not explicitly discussed.

Taking into account of the facts that the Sq electric field pattern changes with season (as seen in Chapter 3) and the occurrence of CEJ events maximize over the Indian sector during June solstice in solar minimum years, an investigation is carried out to establish the connection between polarity change in the temporal variation of Sq electric field and the occurrence of these CEJ events. This is done by computing the E-region current densities and the corresponding horizontal magnetic field induced at ground using electrojet model by *Anandarao* [1976] (described in Chapter 2) and providing inputs corresponding to June Solstice in solar minimum years.

4.2 Datasets used

The datasets utilized to compute magnetic field based on equatorial electrojet model and the observations used to compare these outputs are described below.

As described in Chapter 2, the E-region current densities along the zonal direction (J_ϕ) and the corresponding horizontal component of the magnetic field induced at ground by this current for local times between 0930 and 1730 hrs are computed using electrojet-model and inputs corresponding to June solstice in solar minimum conditions. The model requires zonal Sq electric field, altitude profiles of E region electron density, neutral atmospheric density and temperature, in addition to the three dimensional geomagnetic field. The electron density profile at noon is obtained based on sounding rocket flight experiments [*Subbaraya et al.*, 1983] conducted over Thumba and at other local times of the day with the empirical relationship between the electron density and solar zenith angle (χ) through $\cos^{1.31/2}(\chi)$ [IRI-90, *Bilitza*, 1990] (for details see Chapter 2). The input Sq electric fields are obtained from *Fejer et al.* [2008a] model drifts over 60°E longitude corresponding to June solstice in low solar flux levels. It is shown in Chapter 3 that the zonal electric fields corresponding to *Fejer et al.* [2008a] model drifts represent well the Sq electric fields over the Indian sector barring early morning hours. These input electron density profiles and Sq electric fields at different local times are depicted in Figure 4.5. The other inputs namely neutral atmospheric density and temperature are obtained from NRLMSISE-00 [*Picone et al.*, 2002] model and the geomagnetic field is taken from IGRF-12 [*Thébault et al.*, 2015] model.

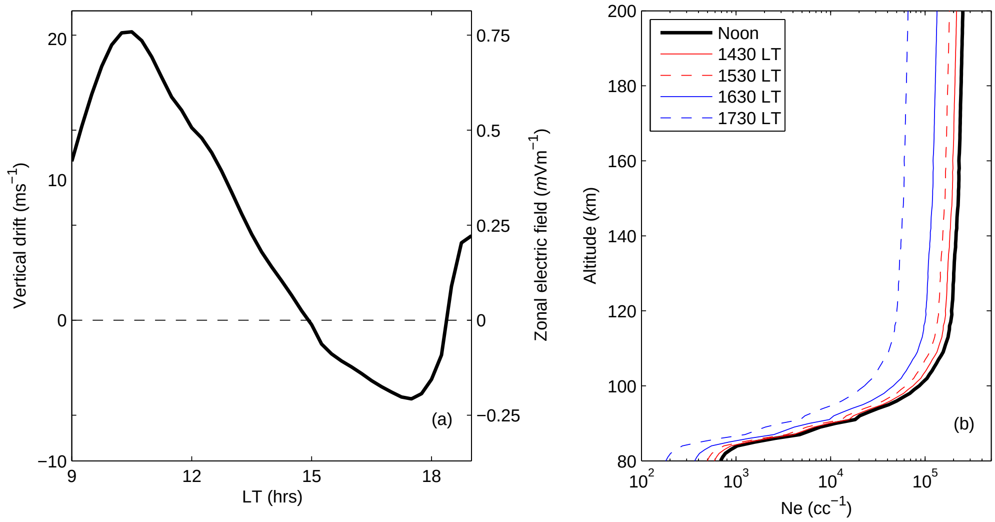

Figure 4.5: Inputs to the electrojet model (a) Vertical drifts (left Y-axis) over 60°E longitude from *Fejer et al.* [2008a] and the corresponding zonal electric field (right Y-axis); (b) altitude profiles of electron density at different local times in low solar activity periods [$\langle F10.7\rangle \leq$120 sfu].

In order to compare the computed magnetic field with the observations of electrojet strength, the EEJ variations obtained using magnetometer observations are utilized. The hourly EEJ strengths on geomagnetically quiet days during low solar flux years [$\langle F10.7\rangle \leq 120$ sfu] of solar cycle 22 are considered. The criterion for a quiet day is that the Kp $\leq$ 3 and DST ≥ -20, with similar geomagnetic conditions on previous day to avoid the effects of disturbance dynamo. These cover 235 days of EEJ observations that are spread over ascending (1985 - 1987) and descending (1993 - 1995) phases of solar cycle 22.

4.3 Results

The model-generated contours of iso-current densities along the zonal direction in altitude-dip latitude plane are depicted in Figure 4.6 at various local times. The strength of zonal current density (J_ϕ in units of μAm^{-2}) is also shown on each contour with the maximum value marked at the center.

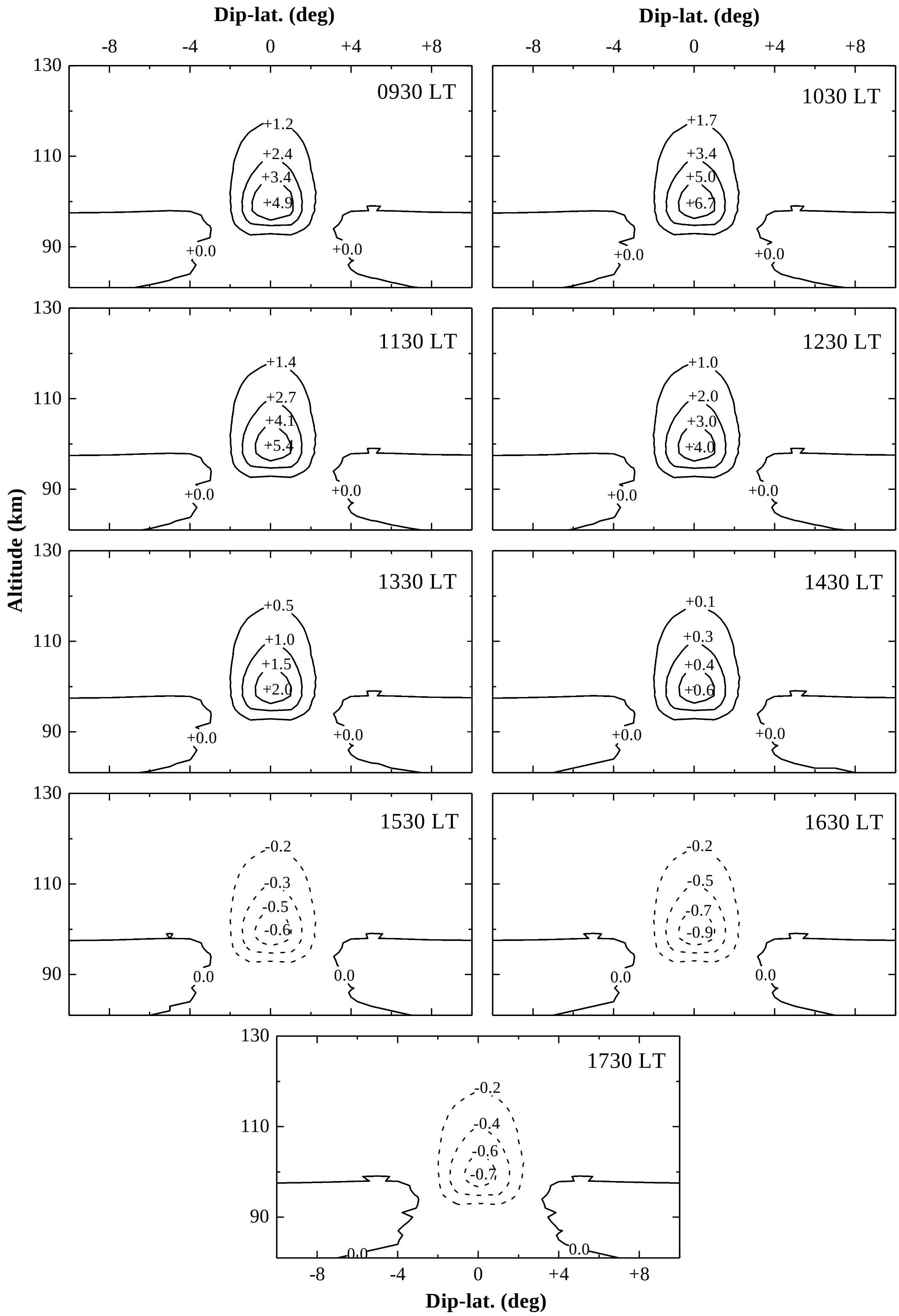

Figure 4.6: The contours of iso-current densities (in μAm^{-2}) in the zonal direction, obtained from electrojet model in altitude-dip-latitude plane corresponding to inputs at different local times.

The sensitivity studies carried out with various model inputs were reported in Chapter 2. Based on this, the uncertainty in current density was found to be less than 18% [*Pandey et al.*, 2016]. The contours of current density plotted with solid and dashed lines correspond to the positive (eastward) and negative (westward) values of current density, respectively. It is to be noted that eastward electrojet peaks around 1030 LT. The flow of current becomes westward between 1430 LT and 1530 LT and it remains so till 1730 LT. The peak of westward current density, in general, is found to be $\sim -1\ \mu\text{Am}^{-2}$ between 1530 LT and 1630 LT.

The horizontal components of magnetic field induced at ground by the electrojet currents are computed based on equation (2.16) of Chapter 2. The computation is carried out for every 15 min interval from 0930 LT and 1730 LT. Figure 4.7 depicts the computed variations of magnetic field (red curve with dots). The observed hourly variations of $\Delta H_{\text{TRD}} - \Delta H_{\text{ABG}}$ for 235 quiet days during June solstice in solar minimum periods are also shown in this Figure 4.7 as the blue and grey coloured curves corresponding to normal EEJ and afternoon CEJ days, respectively. Out of these 235 quiet days of observations, CEJ occurred during 1500 - 1800 LT on 194 days. In order to generate a quiet time average variation of $\Delta H_{\text{TRD}} - \Delta H_{\text{ABG}}$, all the 235 quiet days (including both normal EEJ and afternoon CEJ days) are considered. This average curve is depicted in black with dots indicating hourly intervals. In addition, the 1σ variation for each point is indicated with vertical bars.

It is evident from the Figure 4.7 that, the model-computed and mean of observed magnetic fields match well (within 1σ variation) between 0930 LT and 1730 LT. The peak magnetic field values corresponding to eastward electrojet occur ~1030 LT in both computed and observed values. On an average, CEJ events occur between 1500 LT and 1800 LT with peak (~ -10 nT) occurring around 1600 LT. In spite of using averaged inputs from different sets of data (refer section 4.2), remarkable similarities are observed between the computed and mean observed values of magnetic field during CEJ hours (~1500 - 1730 LT). The time of commencement and the duration of CEJ obtained from the model computations closely follow the respective observations. Further, the strength of peak CEJ and its time of occurrence obtained from model computations are almost the same as those from observations. The implications of these results are discussed in the following section.

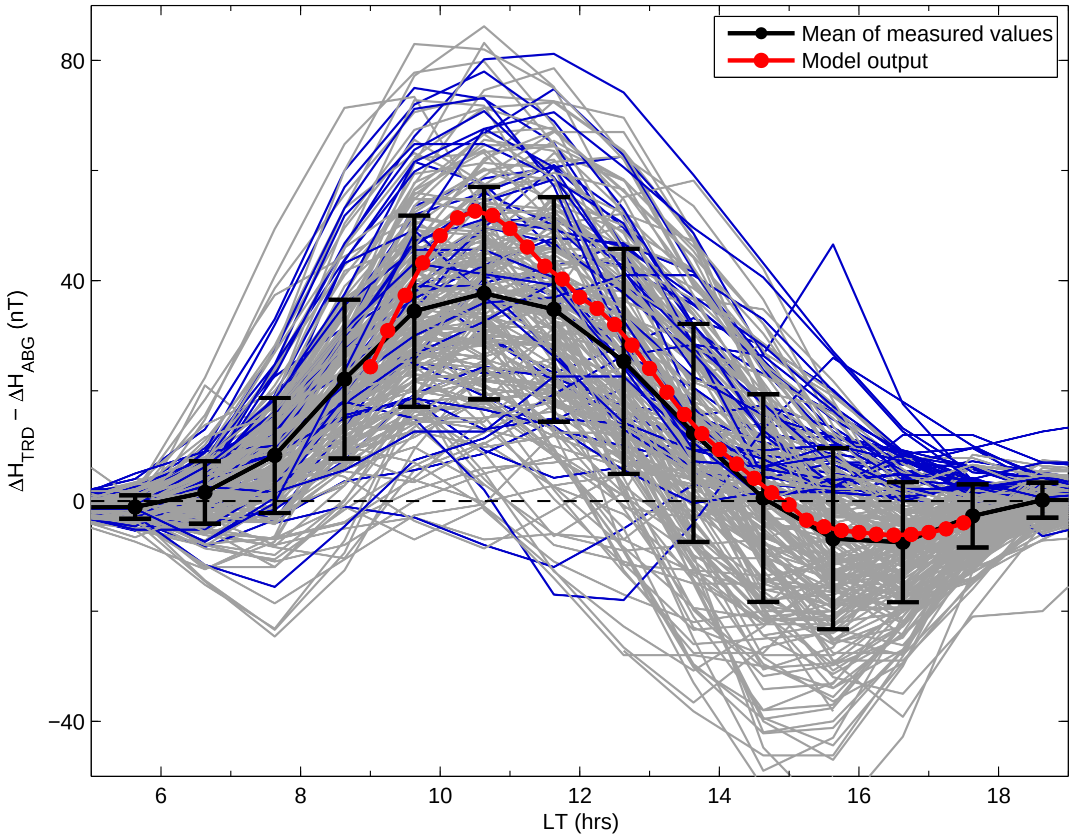

Figure 4.7: The EEJ strength deduced using magnetometer data corresponding to individual geomagnetic quiet days with normal (blue) and afternoon counter (gray) electrojet during June solstice in solar minimum years of solar cycle 22. It consists of 235 quiet days of observations whose mean values are depicted by black curve. The 1σ variation for each point is also indicated with vertical bars. The red coloured curve corresponds to the magnetic field strength computed using EEJ model.

4.4 Discussion

From Figures 4.5a and 4.7 it is clear that the reversal in electrojet current takes place when the Sq electric field becomes westward. It is to be noted that the peak of the current density (see Figure 4.6) and the magnetic fields (see Figure 4.7) corresponding to normal electrojet are found to be at the same time (∼1030

LT) when the zonal Sq electric field from empirical model [*Fejer et al.*, 2008a] maximizes (see Figure 4.5a). Incidentally, the local time corresponding to the monthly mean of Sq focii over the Indian sector during June solstice in solar minimum period was found to be around 1030 LT [*Vichare et al.*, 2017]. However, in afternoon hours, local time corresponding to the peak of counter electrojet current (~1630 hrs) does not coincide with the time when westward Sq electric field maximizes (~1730 hrs). This is due to considerable amount of decrease in electron density with χ variation after 1630 LT (see Figure 4.5b) that results in a reduction of CEJ strength after ~1630 LT. Hence, the time of peak westward current is determined from optimum values of zonal Sq electric field and electron density.

The average characteristics of CEJ events (strength, duration, peak value and its time of occurrence) reported by earlier studies [*Patil et al.*, 1990a; *Rastogi et al.*, 2014] pertain to different solar cycles and are similar to the observations presented in Figure 4.7. Further, the results obtained in the present work using electrojet model have exceptional similarities with these observations. However, on some occasions, the amplitude of CEJ is observed to be substantially larger than 1σ compared to averaged CEJ strength and commencement of some CEJ events are at earlier local times ($<$ 1500 LT). These aspects are discussed later. It is clear from Figure 4.6, that depending on the polarity of the zonal Sq electric field being eastward or westward, the normal or counter electrojet appears. Thus, it is important to know the polarity of the zonal Sq electric field in afternoon hours. *Fejer et al.* [2008a] model, employed in the present investigation, reveals westward Sq electric field during 1500 - 1800 LT in June solstice in solar minimum over Indian longitudes. Considering the smaller values of westward Sq electric field after ~1500 LT and the uncertainties (less than 10% particularly during daytime) associated with the *Fejer et al.* [2008a] model, additional clues for the westward Sq electric fields during afternoon hours in this season over the Indian region are gleaned from the earlier works.

4.4.1 Earlier observations that indirectly support westward Sq electric field during afternoon hours

Various earlier measurements that indicate to a westward Sq electric field in afternoon hours over the Indian sector during June solstice in solar minimum periods are described in the ensuing paragraphs.

The vertical Doppler drifts from the radar echoes due to the presence of plasma irregularities at 150 km region act as a proxy to zonal Sq electric field [*Kudeki and Fawcett*, 1993; *Chau and Woodman*, 2004]. These measurements have been extensively used over the Peruvian sector [*Hui and Fejer*, 2015]. Over the Indian sector, such measurements of the vertical drifts over Gadanki (13.5°N, 79.2°E, dip-lat. 6.5°N) are reported by *Pavan Chaitanya et al.* [2014] and *Patra et al.* [2014]. *Patra et al.* [2014] reported the vertical drifts for four days during July-August, 2009. The blue coloured curves in Figure 4.8 represent the vertical drifts measured by *Patra et al.* [2014] while the red coloured dots correspond to vertical drifts obtained using Ion Drift Meter (IDM) on board C/NOFS satellite. In addition, the black coloured curves are overlaid in Figure 4.8 which represent the hourly variations of EEJ strength on those days. Note that the vertical drifts on these days indicate downward trend at ∼1500 LT. As the radar observational time was limited to ∼1500 LT, the westward Sq electric field could not be ascertained on most of the cases beyond this local time. However, on one occasion (31 July 2009), simultaneous measurements of vertical drifts based on 150 km echo and in-situ measurements by C/NOFS revealed westward electric field at ∼1400 LT. On this day, continuous operation of radar revealed westward electric field till the end of observation (∼1530 LT). On other two days (with exception of 23 July 2009), the vertical drifts during afternoon hours decreased continuously followed up by the occurrence of afternoon CEJ events. Some of the earlier reversals seen in Figure 4.7 can be accounted by earlier reversals of electric fields similar to the observation on 31 July 2009. Further, *Pavan Chaitanya et al.* [2014] reported observations of 150 km echoes during five months in 2009 for a few consecutive days in each month. It is noticed from their observations that, on an average, the vertical drifts are close to zero or negative ∼1500 LT in June and July months and show decreasing trend around this time. Note that, the decreasing trend in afternoon hours in months other than June solstice (e.g., December month) was not observed by both *Pavan Chaitanya et al.* [2014] and *Patra et al.* [2014]. Thus, these case studies give credence to the presence of westward Sq electric fields in afternoon hours during June solstice in solar minimum period.

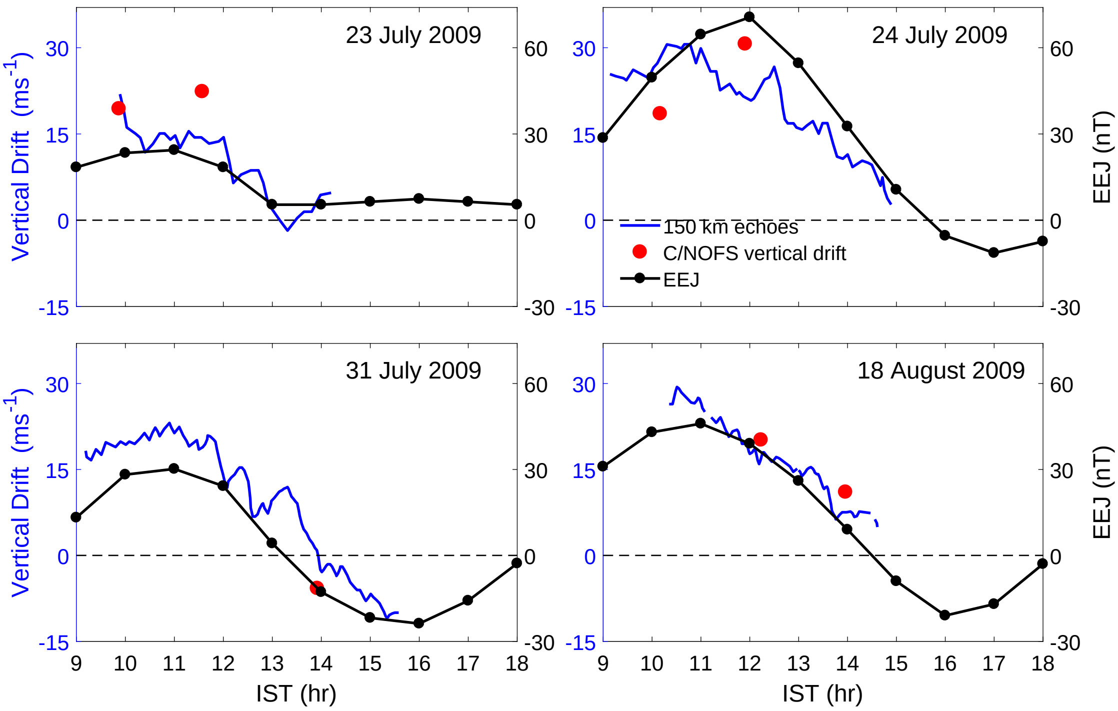

Figure 4.8: The vertical drifts measured using ion drift meter on board C/NOFS (red dots) and temporal variation of vertical drifts measured using 150 km radar echoes (blue curves) [from *Patra et al.*, 2014]. The hourly variations of EEJ strength are overlaid with black colour.

The polarity of Sq electric field can also be inferred from the measurements of E-region electron density profiles and structures in them [*Pandey et al.*, 2017]. Recently, *Pandey et al.* [2017] have shown that the polarity of zonal Sq electric field and the limiting values of the drift deduced from such measurements match well with the empirical model of vertical drift of *Fejer et al.* [2008a]. A rocket flight experiment was conducted [*Prakash et al.*, 1976] at 1532 IST on 17 August, 1972 from Trivandrum to measure the E-region electron density profile and structures in them. Figure 4.9a depicts the profiles of electron density and amplitude of irregularities measured by *Prakash et al.* [1976]. In addition, the EEJ variations

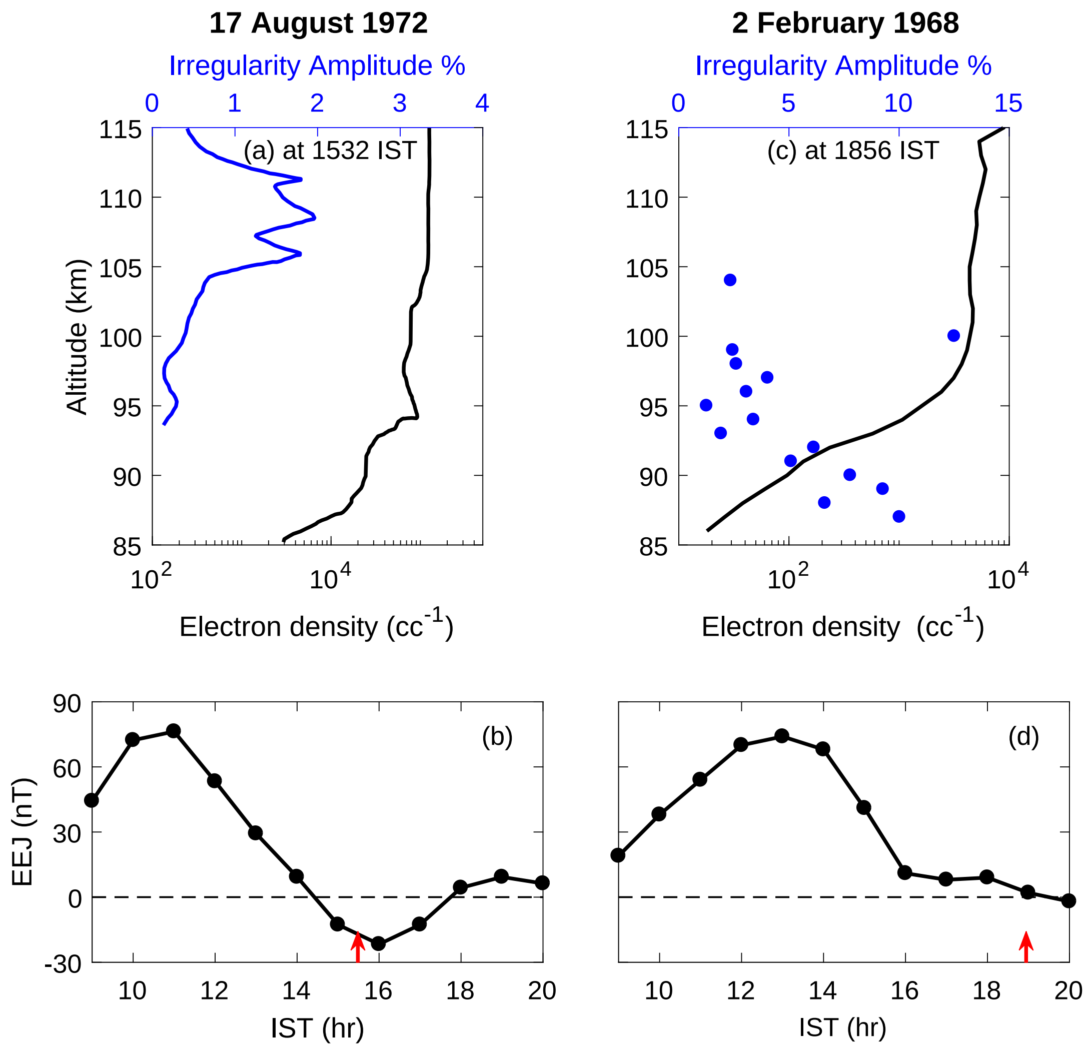

Figure 4.9: (a) Altitude profiles of electron density (black) and irregularity percentage (blue) measured by rocket flight experiment conducted at 1532 IST on 17 August 1972 [from *Prakash et al.*, 1976]. (b) The EEJ variations on this day along with an arrow mark at the time of rocket flight.

on this day are also depicted in Figure 4.9b. The time of rocket flight experiment is indicated by the red arrow and at that time CEJ was present. Further, the Two-stream waves are observed around 105-110 km. The presence of irregularities around 95 km (region of negative gradient in electron density) is noticed. The amplitude of irregularities at altitudes below 94 km are of the order of non-geophysical noise level and thus considered by *Prakash et al.* [1976] as absence of irregularities. In general, the Gradient-drift waves over the Indian sector are observed above 87 km. This can be seen from the altitude profiles of irregularity amplitude and electron density depicted in Figure 4.9c corresponding to a normal electrojet day (2 February 1968) that are reported by *Prakash et al.* [1971b, 1972]. The time of rocket flight experiment is indicated by the red arrow and at that time normal electrojet was present. It is to be noted that the altitude of initiation of Gradient-drift waves is shown [*Sekar et al.*, 2014] to depend on the strength of geomagnetic field. As a result, the Gradient-drift waves over Indian and Peruvian sector are observed from 87 km and 93 km onwards. Further, around these altitudes electrojet current is negligible due to low value of R (ratio of Hall to Pedersen conductivities) [*Pandey et al.*, 2016]. Thus, the absence of Gradient-drift waves in the positive gradient region at very low altitudes ($\sim$90 km) and the presence of Gradient-drift waves in the negative gradient region indicate toward the westward Sq electric field on that day. Further, the presence of Two-stream waves above 105 km altitude indicates that the downward drift corresponding to zonal Sq electric field was more than the limiting value of 12 ms^{-1} [*Pandey et al.*, 2017]. Thus the Sq electric field can be westward and with large amplitude on some occasions during afternoon in June solstice under solar minimum periods. This can account for large deviations (more than 1σ) in the amplitude of CEJ as observed on some occasions compared to the averaged CEJ strength depicted in Figure 4.7. Thus, the above set of observations provide another evidence for the presence of westward Sq electric field during daytime on a CEJ day.

The strength of Sq electric field can also be gauged from the morphology of the latitudinal location of the peak of ionization. The latitudinal distribution of ionization in low latitude F-region is controlled by plasma fountain effect. The equatorial plasma fountain is due to eastward Sq electric field pumping up the plasma from equatorial region vertically upward which subsequently diffuses along the geomagnetic field with the modulation due to meridional wind to form ionization crests region over low latitudes [*Hanson and Moffett*, 1966]. However, the location of the crest region of equatorial plasma fountain depends on the strength of zonal electric field [*Anderson*, 1973]. The stronger eastward electric field shifts the crest of plasma fountain further away from the dip-equator. Several works reported strong correlation between integrated EEJ strength and the development of plasma fountain [*Rush and Richmond*, 1973; *Raghavarao et al.*, 1978; *Rama*

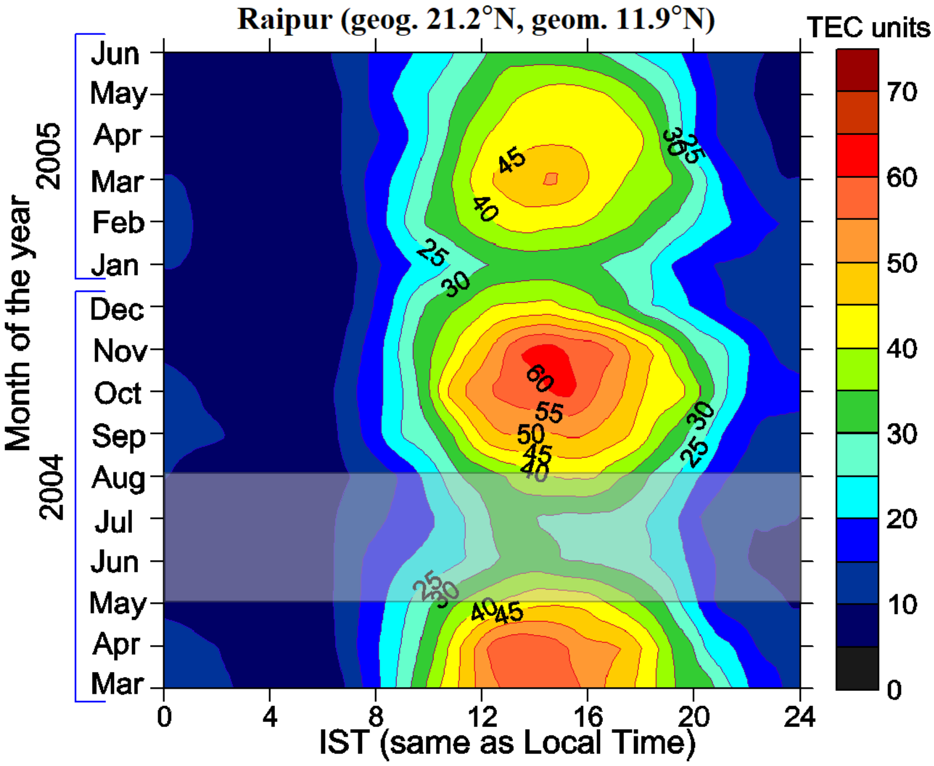

Figure 4.10: Temporal variations of TEC over Raipur (mag-lat 11.9°N) during low solar flux years 2004-2005 [from *Rama Rao et al.*, 2006].

Rao et al., 2006; *Aggarwal et al.*, 2012]. This correlation was also observed in Total Electron Content (TEC) variations reported by earlier workers [e.g., *Iyer et al.*, 1976], though seasonal dependence of TEC under different solar epochs are sparse [*Rama Rao et al.*, 2006; *Yadav et al.*, 2013]. In one such work by *Rama Rao et al.* [2006], the monthly mean values of TEC at different latitudes over India are reported. The crest location of TEC during 2004, which is in the descending phase of solar cycle 23 [$\langle F10.7 \rangle \leq 110$ sfu], is at ~12°N dip-latitude. It is of interest to note the temporal variation of TEC at this crest location. Therefore, the temporal contours of iso-TEC values during different months in 2004 - 2005 over Raipur (geog-lat 21.2°N, geom-lat 11.9°N) are reproduced in Figure 4.10 from the work of *Rama Rao et al.* [2006]. Note that the TEC values peaked for a short interval of time around noon and fall off sharply afterwards during June-July compared to other months. The noontime peak in TEC indicates that zonal Sq electric field peaks around 1000 - 1030 LT as it takes about 2 hrs [*Sanatani*, 1966] to diffuse to the location of 12°N dip-latitude. In addition, sharp reduction

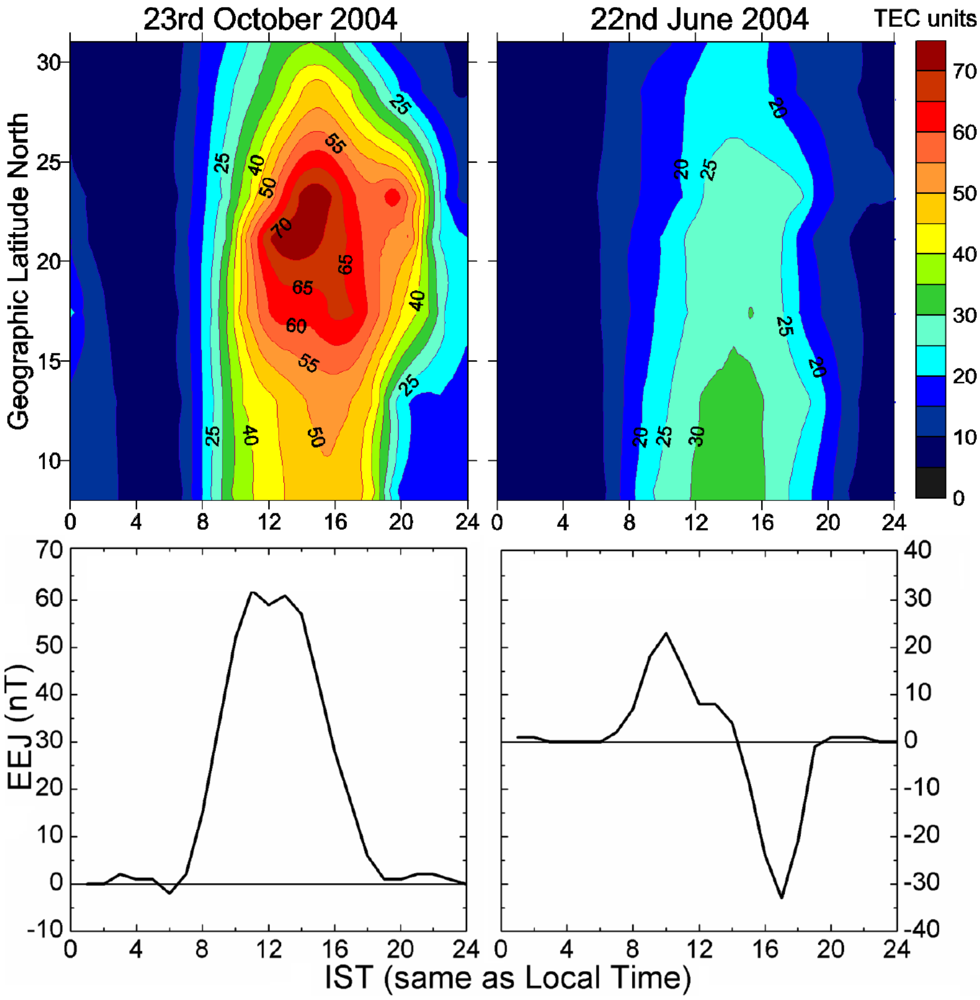

Figure 4.11: Temporal variation of TEC with latitude on a normal (23 October 2004) and counter (22 June 2004) electrojet days along with EEJ strength on those days [after *Rama Rao et al.*, 2006].

in TEC after noon indicates sharp decrease in zonal electric field. Further, the location of peak TEC was shown not to exceed beyond 6°N dip-latitude during an afternoon day in June solstice, indicating that the zonal Sq electric field was relatively weak. The TEC variations and EEJ strength on this afternoon CEJ day and on a normal electrojet day are reproduced in Figure 4.11. Thus, the morphological variations of TEC over India indicate the decreasing trend of Sq electric field in the afternoon hours during June solstice in solar minimum periods. Since the latitudinal extent of EEJ is limited (±3°), the correlation between EEJ and plasma fountain obtained by previous workers indicate the common role of Sq electric field in controlling both the phenomena.

An indirect inference of earlier (afternoon) reversal of Sq electric field can be obtained from the magnetic field observations at the focii of Sq current system. Based on geomagnetic field observations using chain of magnetometers during low solar activity [$\langle F10.7 \rangle < 90$ sfu] years 2006 - 2010, *Vichare et al.* [2017] reported the monthly mean local time corresponding to the focii of Sq current system over the Indian sector. Figure 4.12 which is reproduced from *Vichare et al.* [2017] represents those variations. It is to be noted that the local time corresponding to monthly mean of focii of Sq current system over the Indian sector during June solstice occurs earlier (∼1030 LT) compared to other seasons. Interestingly, the time of maximum eastward electric field corresponding to vertical drifts over Indian sector reported by *Fejer et al.* [2008a] model is also earlier (∼1030 LT) in June solstice compared to other seasons. These observations are consistent with morphological variations of TEC observations discussed earlier. As the maximum of Sq current is observed earlier, it is expected that the descending phase of diurnal tide starts early during this season. Under these conditions, the contributions from components other than diurnal tides can govern the Sq current system and hence the zonal electric field depending upon the relative magnitudes and phases of diurnal and higher order tidal components. These aspects can result in small or opposite polarity of zonal Sq electric field in afternoon hours during June solstice compared to other seasons.

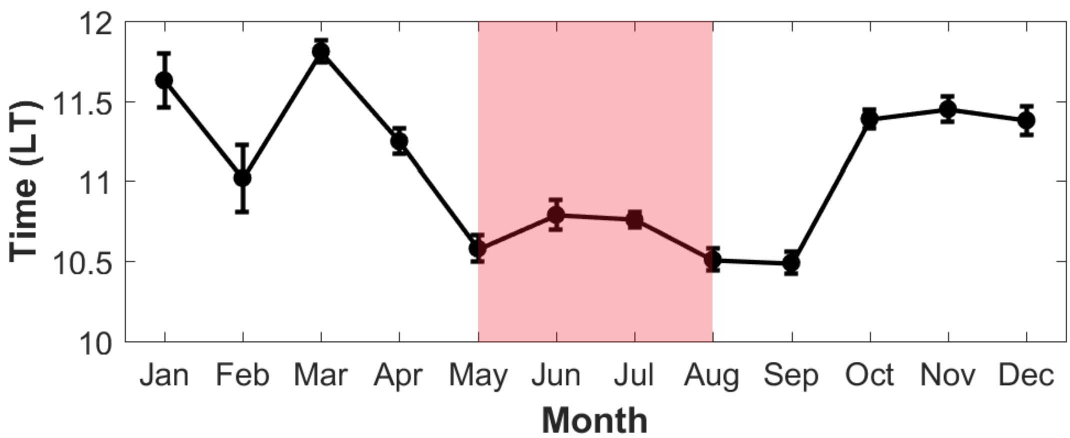

Figure 4.12: Monthly variation of the monthly mean local time corresponding to the focii of Sq current during 2006 - 2010 [from *Vichare et al.*, 2017].

A chain of magnetic field observations can also provide a clue to the polarity of the Sq electric field. Based on the principal component analysis of geomagnetic field variations measured using a chain of magnetometers over Indian region during June - July 1995, *Gurubaran* [2002] reported that the second harmonic plays a crucial role in the occurrence of CEJ in afternoon hours. The outputs of first and 2 - 5 components corresponding to a afternoon CEJ day (26 July 1995) are reproduced from the work of *Gurubaran* [2002] in top panels of Figure 4.13. It is to be noted that, a clockwise current system (located ∼20 dip-lat in afternoon hours) owing to higher harmonics is superposed on the normal counter-clockwise Sq current vortex (located ∼30 dip-lat at noon) due to primary component. The author wondered whether CEJ is a part of Sq current system.

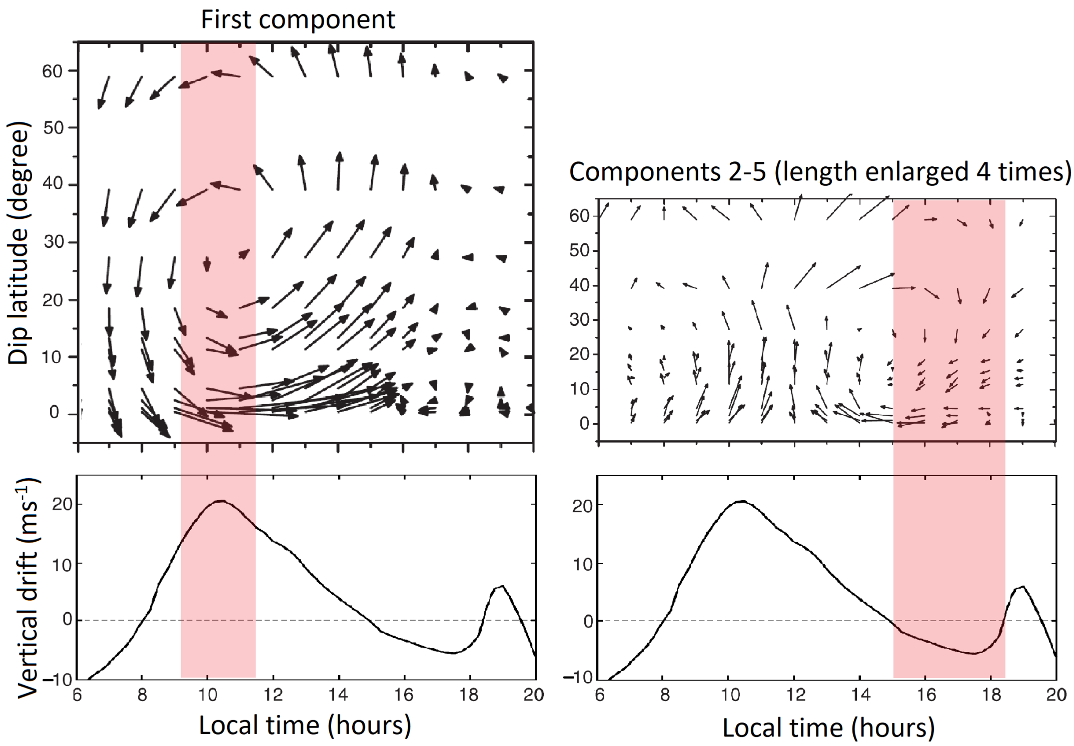

Figure 4.13: Top panel: strength of harmonic components obtained based on Sq current system over the Indian sector on 26 July 1995 [after *Gurubaran*, 2002]. Bottom panel: vertical plasma drifts over the Indian sector reported by *Fejer et al.* [2008a] model.

In bottom panels of Figure 4.13, the vertical drifts from *Fejer et al.* [2008a] drift model are juxtaposed. It is to be noted that the time of peak vertical drift occurs at the time of focus of the first component (see red coloured shaded area on left panel). Further, during the time interval of downward vertical drifts (15 - 18 LT) the components 2 - 5 are in opposite direction to the first component and these 2 - 5 components are stronger than first component (see red coloured shaded region on right panel). *Bhattacharyya and Okpala* [2015] applied a similar analysis to quiet time geomagnetic field variations between 1999 and 2012 and reported that second and third harmonics contribute to the occurrence of CEJ events. In recent investigation, *Bhardwaj and Subba Rao* [2017] showed that the higher harmonics are associated with clockwise current system in afternoon. Therefore, the studies by *Bhattacharyya and Okpala* [2015] can also be taken to produce clockwise current cell in the afternoon. Thus, the results obtained from these systematic magnetic field variations measured using a chain of magnetometers over Indian region indicate towards formation of a counter-clockwise current cell in morning and clockwise current cell during afternoon hours on CEJ days in addition to normal counter-clockwise current cell. This can be taken as a support for eastward Sq electric field in morning hours and westward Sq electric field during afternoon hours at least during the periods of June solstice in solar minimum.

4.4.2 Possible reason for westward Sq electric field in afternoon hours

The subsection 4.4.1 provides alternate evidences for westward Sq electric field around 1500 - 1800 LT during June solstice in solar minimum periods that are consistent with the results of *Fejer et al.* [2008a] for the Indian sector. Possible reason for this westward Sq electric field is discussed below.

Simultaneous long term (1993 - 2011) observations of mesospheric winds by MF radar at Tirunelveli (8.7°N, 77.8°E), a station close to the dip-equator over India, and the strength of EEJ using geomagnetic field observations revealed that the second principal component acts as proxy for the occurrence of CEJ with enhanced tidal activities during solar minimum year when the occurrence of CEJ is more [*Gurubaran et al.*, 2016]. However, the role of relative strengths of diurnal and semidiurnal tides particularly during June solstice in solar minimum periods for the generation of CEJ is not clear from this work. Month-to-month variations of tidal amplitudes of mesospheric winds over Trivandrum obtained using a meteor radar from June 2004 to May 2005 (descending phase of solar cycle 23, $\langle F10.7 \rangle \leq 110$ sfu) are reported by *Deepa et al.* [2006]. The diurnal and semidiurnal tidal amplitudes for the meridional wind component are reproduced in Figure 4.14 from the work of *Deepa et al.* [2006]. It is observed that during June solstice months, the semidiurnal amplitudes are larger than corresponding diurnal amplitude in meridional direction over the altitude region 94 - 98 km. The phase difference between meridional diurnal and semidiurnal was found to be around 12 hrs in the altitude region 94 - 98 km in this solstice barring the month of June.

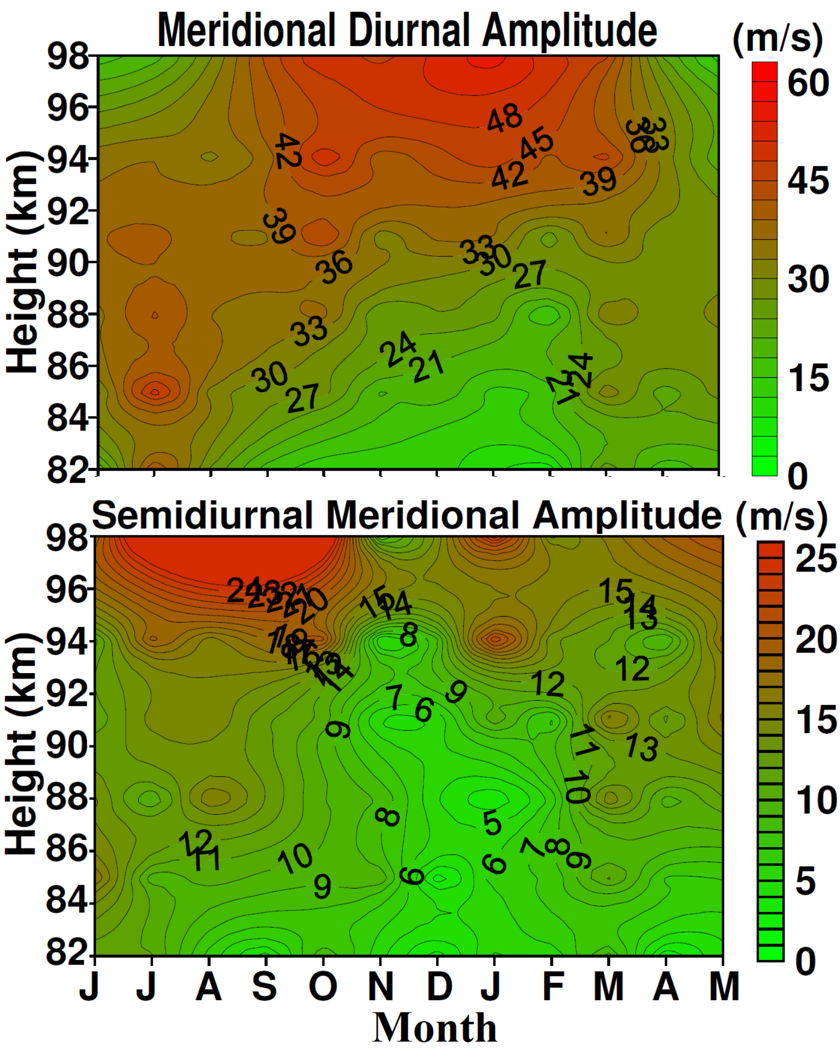

Figure 4.14: Mesospheric meridional diurnal and semidiurnal amplitudes over Indian sector in different months during 2004 - 2005 [after *Deepa et al.*, 2006].

Possible role of semidiurnal tides on equatorial quiet time vertical ion drifts measured by C/NOFS satellite was indicated by *Stoneback et al.* [2011] based on measurements over the Indian sector during deep solar minimum period (2008 - 2010) of solar cycle-23. Further, when semidiurnal tide is effective and contributes to the generation of afternoon CEJ, it is expected to cause eastward electric field influence during midnight hours. This aspect is confirmed by the pre-midnight ascent of F-layer and upward ion-drift observed by C/NOFS over the Indian sector during June solstice in deep solar minimum years 2008 - 2009 [*Chakrabarty et al.*, 2014]. These aspects are in support of role played by the semidiurnal tides during June solstice.

The theoretical studies [*Forbes and Lindzen*, 1976; *Marriott et al.*, 1979; *Hanuise et al.*, 1983] with assumptions of concentric geomagnetic and geographic equator and reduced amplitude of diurnal components, the features of CEJ are modeled by combination of symmetric semidiurnal tides. The observational support for the second assumption was provided by *Sridharan et al.* [2002] wherein a reduction in the diurnal tidal component and/or enhancement in semidiurnal amplitude was reported on afternoon CEJ days during June-July months in 1995 observed over Tirunelveli using MF radar and chain of magnetometers simultaneously. On the other hand, *Stening* [1989b] reproduced many features of CEJ by introducing antisymmetric semidiurnal tidal components. Numerical simulation of simultaneous Sq current and CEJ using different combinations of semidiurnal and diurnal tidal components is beyond the scope of this thesis. However, based on earlier simulation works discussed above and the observational support on tidal winds from recent times, it appears that the semidiurnal tides play a crucial role in altering Sq electric field which is shown by the present investigation to be essential to cause CEJ during June solstice in solar minimum periods over India.

Finally, the present investigation brings out the important consequence of the westward Sq electric fields, that were obtained by *Fejer et al.* [2008a] empirical model over Indian longitudes during June solstice in solar minimum, in the generation of CEJ. Though the process appears to be obvious, the present work reproduces all the observed CEJ characteristics remarkably well. *Onwumechili* *and Akasofu* [1972] raised the issue of return current that is needed if the reverse jet is assumed to be locally generated. In response to this, *Stening* [1977] could not find an unambiguous answer and inferred that reverse jet seems to be associated with the additional imposition of a current system generated by a semidiurnal tidal mode. Further, a few global models [e.g., *Hanuise et al.*, 1983] require CEJ to be a part of a bigger current system in order to simulate it using semidiurnal tides. The inference made in the present investigation that Sq electric field is responsible for the generation of CEJ is not constrained by the requirement of a separate return current. If the Sq electric field is responsible for the generation of CEJ, the requirement of a separate return current becomes superfluous. Therefore, the present investigation suggests that these CEJ events are part of a global current system. As the present work is not exhaustive covering all the seasons and solar epochs, the other suggested mechanisms discussed in the introduction section are not precluded.

4.5 Summary

An investigation was carried out using an equatorial electrojet model and the inputs based on measurements and empirical model of vertical drift to understand frequent occurrence of counter electrojet events in afternoon hours over the Indian sector during June solstice in solar minimum period. The occurrence of CEJ is shown to be due to the westward Sq electric field between 1500 LT and 1800 LT. The westward Sq electric field, as reported in the *Fejer et al.* [2008a] model, is substantiated by various earlier observations from India. The magnetic field derived from the electrojet model is compared with the corresponding magnetic observations from India. The comparison revealed that the strength, duration, peak value and the occurrence time of CEJ computed by the model match well with the observation, suggesting the explicit role of westward Sq electric field in the generation of these CEJ events. Therefore, the present investigation suggests that afternoon CEJ events over the Indian sector during June solstice in solar minimum periods are part of the Sq current system.

Chapter 5

Daytime effects of disturbance dynamo on EEJ

Excerpt

Based on careful analysis of 16 years of hourly variations of the strength of equatorial electrojet (EEJ) derived using the ground-based magnetometers over the Indian sector, the role played by disturbance dynamo electric field on equatorial ionosphere is identified. It is found that most prominent cases of the effects of disturbance dynamo occurred during equinoctial months in high solar activity period. In three extreme cases, the reduction in EEJ strength from quiet time average values of the respective month is more than twice the standard deviations for at least 3 hours. Based on the methodology described in Chapter 2, it is found that the westward electric field perturbations are as large as 0.7 ± 0.2 to 1.2 ± 0.3 mVm^{-1} around noon hours for these three cases. In contrast to the expectation of disturbance dynamo electric field perturbations over equatorial latitudes from the earlier models, these values during daytime are significantly larger and caused counter electrojet events on two occasions. A possible additional source to augment the reduction in the electric field is indicated.

5.1 Introduction

The general characteristics of electric fields over low-latitude ionosphere under geomagnetically quiet conditions have been studied at different longitude sectors [*Woodman*, 1970; *Fejer*, 1981; *Pandey et al.*, 2017] in the past and global empirical models [*Scherliess and Fejer*, 1999; *Fejer et al.*, 2008a] have been constructed. During geomagnetically disturbed conditions, additional electric field perturbations modulate the ionospheric electric field. These electric field disturbances can occur instantaneously or after some delay.

The instantaneous changes in electric field over mid and low latitudes are directly driven by prompt penetration (PP) or over-shielding (OS) of interplanetary electric field owing to imbalance between Region 1 and Region 2 Field Aligned Currents [*Kikuchi et al.*, 1996]. In general, the lifetime of PP/OS electric field perturbations is less than an hour [*Peymirat et al.*, 2000]. Further, due to the Joule heating that occurs in the high latitude ionosphere during geomagnetic storms and/or substorms, the thermospheric circulation changes globally. The meridional circulation modulated by Coriolis force generates the disturbance dynamo effect [*Blanc and Richmond*, 1980]. Owing to the physical movement of neutrals with finite velocity, effects of disturbance dynamo are delayed in nature. After the onset, the effects of Disturbance Dynamo Electric Field (DDEF) can persist for several hours [*Scherliess and Fejer*, 1997]. It is observed [*Yamazaki and Kosch*, 2015] that for an average storm with minimum Disturbance storm time (Dst) index ~ -95 nT, DDEF perturbations persist for approximately 24 hrs during the recovery phase of the storm.

Theoretical [e.g., *Blanc and Richmond*, 1980; *Spiro et al.*, 1988; *Richmond et al.*, 2003; *Huang and Chen*, 2008] and empirical [e.g, *Fejer and Scherliess*, 1995; *Scherliess and Fejer*, 1997; *Fejer et al.*, 2008b] models have been developed to address the general characteristics of DDEF. A recent review paper by [*Fejer et al.*, 2017] provides an excellent overview of physics of the disturbance dynamo and its important characteristics. In theoretical models, DDEF perturbations over low latitudes are computed corresponding to step like increase in the polar cap potential followed by its' sustenance for varying durations. Similarly, in the empirical models, the DDEF perturbations are obtained corresponding to different time delays after the step like increase in Auroral Electrojet (AE) followed by sustenance for varying duration. Based on Digisondes/ionosonde, an HF Doppler radar and magnetometers operated over Brazil and India, *Abdu et al.* [1997] showed that the disturbance dynamo drives opposite changes at the same UT on day and night sides. The eastward electric field of disturbance dynamo origin at night are shown [*Fejer and Scherliess*, 1995; *Abdu et al.*, 1996] to maximize during post-midnight hour. It is also shown that the daytime DDEF may significantly reduce the strength of EEJ [e.g., *Sastri*, 1988] and may even cause Counter Electrojet (CEJ) [e.g., *Rastogi and Chandra*, 2012; *Chandra et al.*, 2016]. Though these CEJ events occurred during the recovery phases of the geomagnetic storm, the effects due to possible over-shielding [*Simi et al.*, 2012] and/or substrom [*Kikuchi et al.*, 2003] are not considered in their works [*Rastogi and Chandra*, 2012; *Chandra et al.*, 2016]. Based on these studies, a few important aspects regarding DDEF emerged out. First, the polarity of DDEF is opposite to the quiet time polarity of the ionospheric electric field [*Abdu et al.*, 1997]. Second, DDEF is stronger in night than during daytime and third, the magnitude of DDEF is less than 0.5 $\mathrm{mVm^{-1}}$ [*Huang*, 2013] during daytime. Further, it is important to rule out other processes for the estimation of effects due to DDEF alone.

During the recovery phase of a geomagnetic storm, PP/OS and substorm induced prompt electric field perturbations may co-exist with DDEF perturbations. Hence, isolating the contribution of DDEF in the electric field perturbations over the equatorial ionosphere remains a challenging job till date. This is an important issue as it can introduce uncertainty in the derived amplitude of DDEF over equatorial latitudes. In order to circumvent this problem, the hourly averaged values of electric fields are generally considered for the development of empirical models of disturbance dynamo. This is based on the assumption that the transient electric field perturbations due to PP/OS electric fields are averaged out owing to their relatively shorter lifetimes. However, on many occasions, the PP electric field perturbations are observed to persist for a much longer duration [*Huang* *et al.*, 2005; *Wei et al.*, 2008]. Under such conditions, the estimation of DDEF can be biased significantly. Therefore, in order to estimate the contributions of disturbance dynamo electric field over equatorial ionosphere, it is important to identify distinct cases of disturbance dynamo effects. In the present investigation, a few distinct cases of DDEF perturbations on day side are identified by utilising the hourly variation of the strength of equatorial electrojet (EEJ) derived based on the ground-based magnetometer observations over the Indian sector during 2000 - 2015. Based on the changes in EEJ, the electric field perturbations are estimated following the method described in Chapter 2.

5.2 Dataset and criteria for selection of events

In the present investigation, the hourly values of ring current index Dst are used to identify different phases of geomagnetic storm. The Dst index reaches minimum well before the occurrence of DD events and it remains in the recovery phase of the geomagnetic storm during the DD. Further, the three-hourly Kp indices are utilised to categorize the geomagnetically quiet and disturbed days. The values of Dst and Kp indices are obtained from the WDC, Kyoto.

The hourly values of IMF Bz, time shifted to the terrestrial bow shock nose, are obtained from NASA CDAWeb. In addition, the hourly values of eastward (AU) and westward (AL) auroral electrojet indices are also obtained from the NASA CDAWeb. IMF Bz > 0 (northward IMF Bz) on the event day is taken as marker for the absence of prompt perturbations driven by interplanetary electric field. Based on earlier study [*Janzhura et al.*, 2007], AL >-400 nT (insignificant westward auroral electrojet activity) on the event day is chosen to be a marker for the absence of magnetospheric substorm. As a consequence, it follows that prompt electric field perturbations can be considered to be absent if these criteria are fulfilled during the time periods when DDEFs are evaluated.

The hourly variations of the horizontal component of geomagnetic field during 2000 - 2015 at Tirunelveli (TIR: 8.7°N, 77.8°E, Geom. Lat 0.4°S) and Alibag (ABG: 18.6°N, 72.9°E, Geom. Lat. 9.9°N), obtained from IIG, Mumbai, are used to determine the strength of EEJ ($= \Delta H_{TIR} - \Delta H_{ABG}$) during this period following the methodology discussed in Chapter 2. The EEJ values on geomagnetically quiet days of each month are averaged to obtain the quiet time EEJ strength of the month along with the standard deviation (1σ). In choosing the quiet days, it is ascertained that Kp ≤ 3 not only on the reference quiet day but also on the previous day. This is to ascertain that the reference quiet days are truly "quiet".

The events are selected based on three criteria: (1) the event occurred during the recovery phase of geomagnetic storm with Dst <-50 nT, (2) the event sustained for at least 3 hours with the reduction in EEJ strength on the event day being more than the standard deviations of the quiet time variations of the respective month, (3) throughout the event day (06 - 18 IST), IMF Bz > 0 and AL >-400 nT. On applying these stringent criteria on hourly EEJ variations during 2000 - 2015, three cases are identified in which the DD effects are found to be very significant (the reduction in EEJ strength is more than the 2σ level). These three events occurred on 03 September 2000, 18 September 2000 and 23 October 2003, and will be discussed in detail. The reduction in the EEJ strengths is between 1σ and 2σ levels for the other 10 cases.

In order to study the effect of DDEF on plasma distribution, the global maps of Total Electron Content (TEC) on the event days are compared with the mean quiet time TEC maps for the respective months. These TEC values are obtained from NASA CDAWeb. Further, the solar EUV flux levels are also evaluated to examine the possible contribution of changes in EUV flux levels. The daily averaged values of solar EUV flux are obtained based on the Solar EUV Monitor (26 - 34 nm) on board SOHO satellite (https://dornsifecms.usc.edu/space-sciences-center/).

5.3 Results

As stated earlier, three events with significant variations in EEJ under the influence of DDEF are presented in this work. Henceforth, for convenience, the DD events on 03 September 2000, 18 September 2000 and 23 October 2003 are referred to as events 1, 2, 3 respectively. These events are described in sequence (Figures 5.1 - 5.3) in the following paragraphs. In order to know the history of the event, figures provide the relevant informations not only on the event day but also on the previous day. In Figures 5.1 - 5.3, the hourly variations in IMF Bz, Dst, AE/AU/AL and EEJ (on the day of event and on the previous day) are plotted sequentially from top to the bottom. The black, orange and dark green coloured solid lines with dots are used to mark respective variations in IMF Bz, Dst and AE indices. The AU and AL variations are marked by filled areas above and below the zero level respectively with the light green colour. The quiet time average EEJ strength of the month and the 1σ variation for each point are shown with blue colour shades in the bottom panel of Figures 5.1 - 5.3. Both UT and IST are given in all the figures.

5.3.1 Event-1 (03 September, 2000)

The DD event on 03 September, 2000 is depicted in Figure 5.1. It may be noted that, IMF Bz turned southward in the early morning hours of the previous day (02 September, 2000) and remained so until midnight. During this time, main phase of a geomagnetic storm is observed with Dst index intensifying up to ~ -55 nT at 2100 IST on 02 September, 2000 which is followed by recovery phase of the geomagnetic storm. Further, the variations in AU and AL are $\sim$200 nT and ~ -400 nT since morning till midnight on 03 September, 2000. The EEJ strength on this day is mostly closer to the quiet time values (within 1σ variations) except for some time when the EEJ strength decreased below the 1σ level.

Event 1 occurred on the next day during the recovery phase of the geomagnetic storm. From dawn to dusk hours on this day (03 September), IMF Bz is continuously northward, and activities in auroral electrojets are negligible (magnitudes of AU/AL and AE are within 100 nT). However, significant reduction in the EEJ strength is observed compared to the monthly average quiet time level. The peak value of EEJ remained closer to 35 nT which is almost one-third of the quiet time peak EEJ level of 105 nT for this month. Interestingly, reduction in EEJ strength from quiet time level is even beyond the 2σ variations variation during 0900 - 1300 IST (highlighted with yellow coloured rectangular box in Figure 5.1).

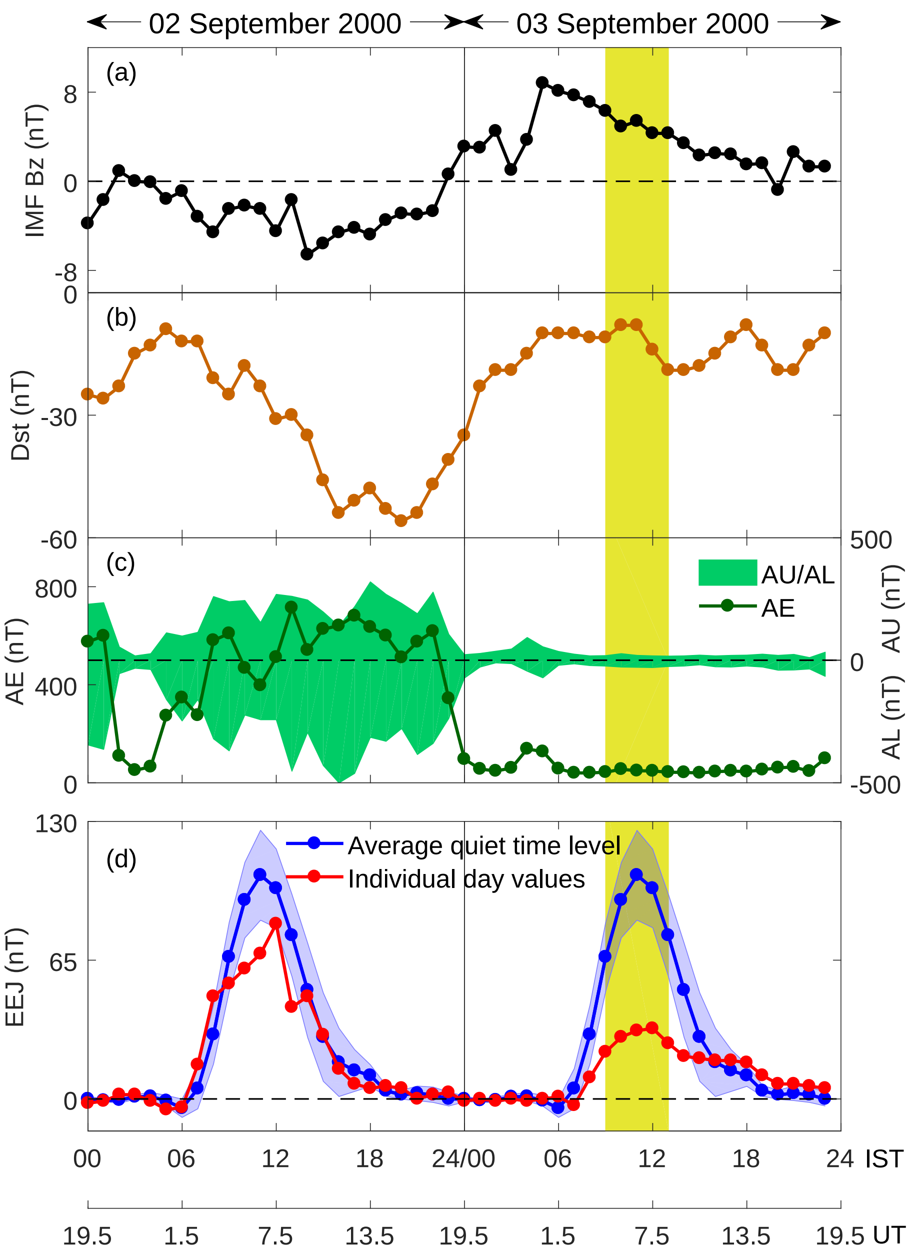

Figure 5.1: The geophysical conditions for event 1 (03 September 2000, on right) and a day prior to it (02 September 2000, on left). From the top to bottom are: (a) hourly values of IMF Bz, (b) Dst, (c) AL & AU, and (d) EEJ along with average quiet time EEJ values of the month with standard deviations (blue coloured shaded area). The time interval during which reduction in EEJ on the event day is more than 2σ is marked with yellow rectangular box.

5.3.2 Event-2 (18 September, 2000)

Figure 5.2 depicts the variations of IMF Bz, Dst, AE/AU/AL and EEJ during Event 2 and on the previous day (17 September). In this case, IMF Bz turned southward during 0200 - 0500 IST on 17 September and remained closer to zero afterwards. During 0200 - 0500 IST on 17 September, auroral electrojet activity also got enhanced. The EEJ strength on this day exceeded the 1σ variation of the quiet time level during noon time.

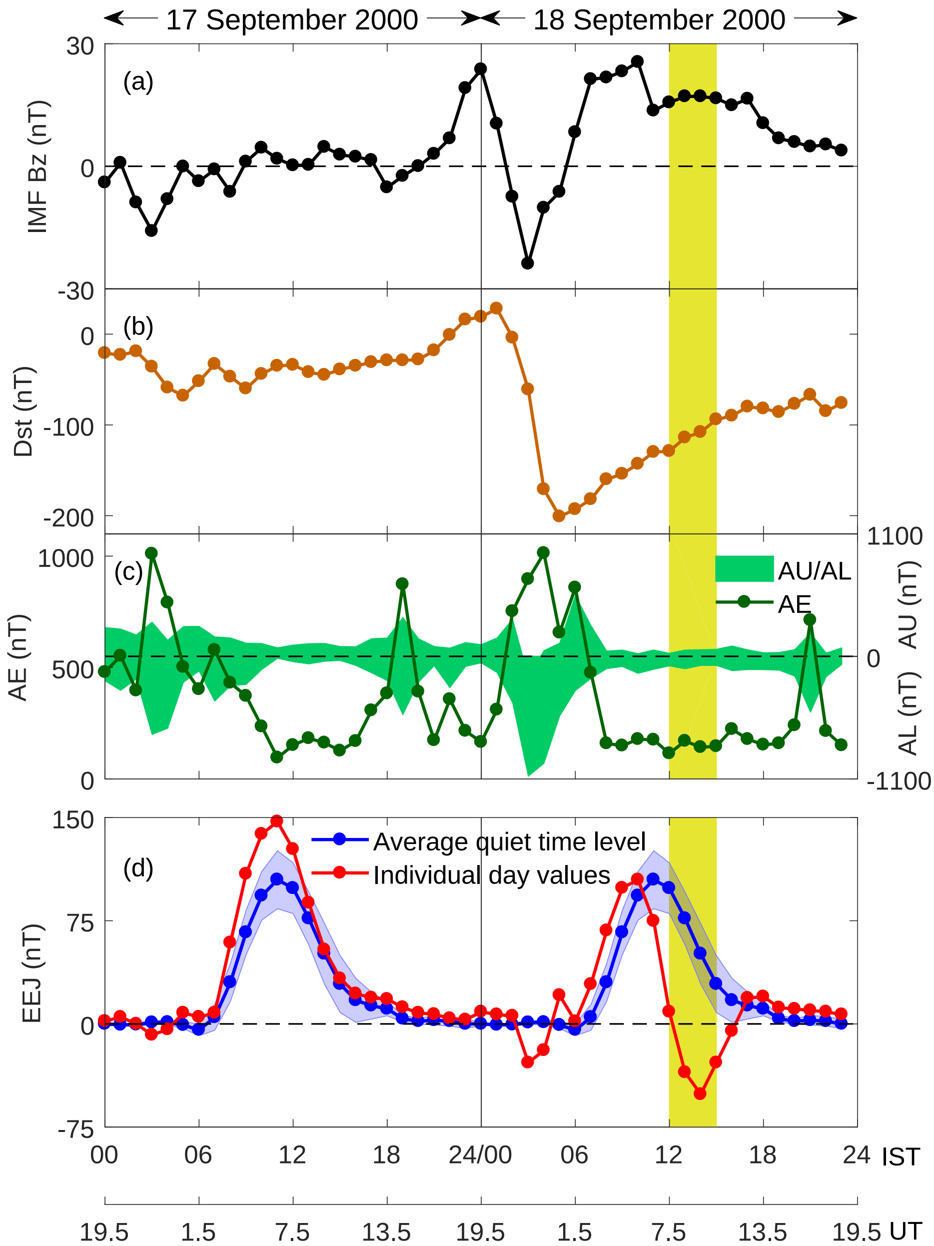

Figure 5.2: Same as Figure 5.1 but for event 2 (18 September 2000, right panel) and a day prior to it (17 September 2000, left panel).

On the event day (i.e. 18 September), IMF Bz turned significantly southward (~ -25 nT) at 0300 IST. This is accompanied by the main phase of a strong geomagnetic storm as indicated by the Dst index that got enhanced up to ~ -200 nT at 0500 IST. The variation of the Dst index after this time indicates the onset of the recovery phase. Importantly, the main phase of the geomagnetic storm was also accompanied with strong intensification of auroral electrojet activity. During 0200 - 0600 IST, the strengths of AU and AL increased to about 550 nT and -1100 nT. During 0600 - 1800 IST on the event day, IMF Bz was northward, and AL did not exceed ~ -300 nT. However, the strength of EEJ decreased drastically during 1200 - 1500 IST (yellow coloured rectangular box in Figure 5.2) and went even below the 2σ variations of the quiet time level. As a consequence, the direction of electrojet current got reversed during 1300 - 1500 IST giving rise to a CEJ event. The CEJ in this case was significantly strong and its peak value reached as high as ~ -50 nT.

5.3.3 Event-3 (23 October, 2003)

On the previous day (i.e. on 22 October, 2003) of the Event 3, IMF Bz was southward on a number of occasions and during those intervals, IMF Bz was ~ -4 nT. In addition, auroral electrojet activities were significant (AU ~ 200 nT and AL~ -500 nT) throughout this day. A geomagnetic storm was already in progress as indicated by the Dst index and the recovery phase of this storm started after mid-day. The EEJ strength on this day is mostly closer to the quiet time level (within 1σ variation) except for some time during the afternoon hours.

The DD event (Event 3) occurred on the next day (23 October) when IMF Bz was northward and the auroral electrojet activities were minimal (AU/AL magnitudes below 100 nT). However, the EEJ strength decreased even below the 2σ variation from the quiet time level of the month during 1000 - 1500 IST (yellow coloured rectangular box in Figure 5.3) and similar to Event 2, a CEJ occurred during afternoon hours with its peak strength ~ -20 nT.

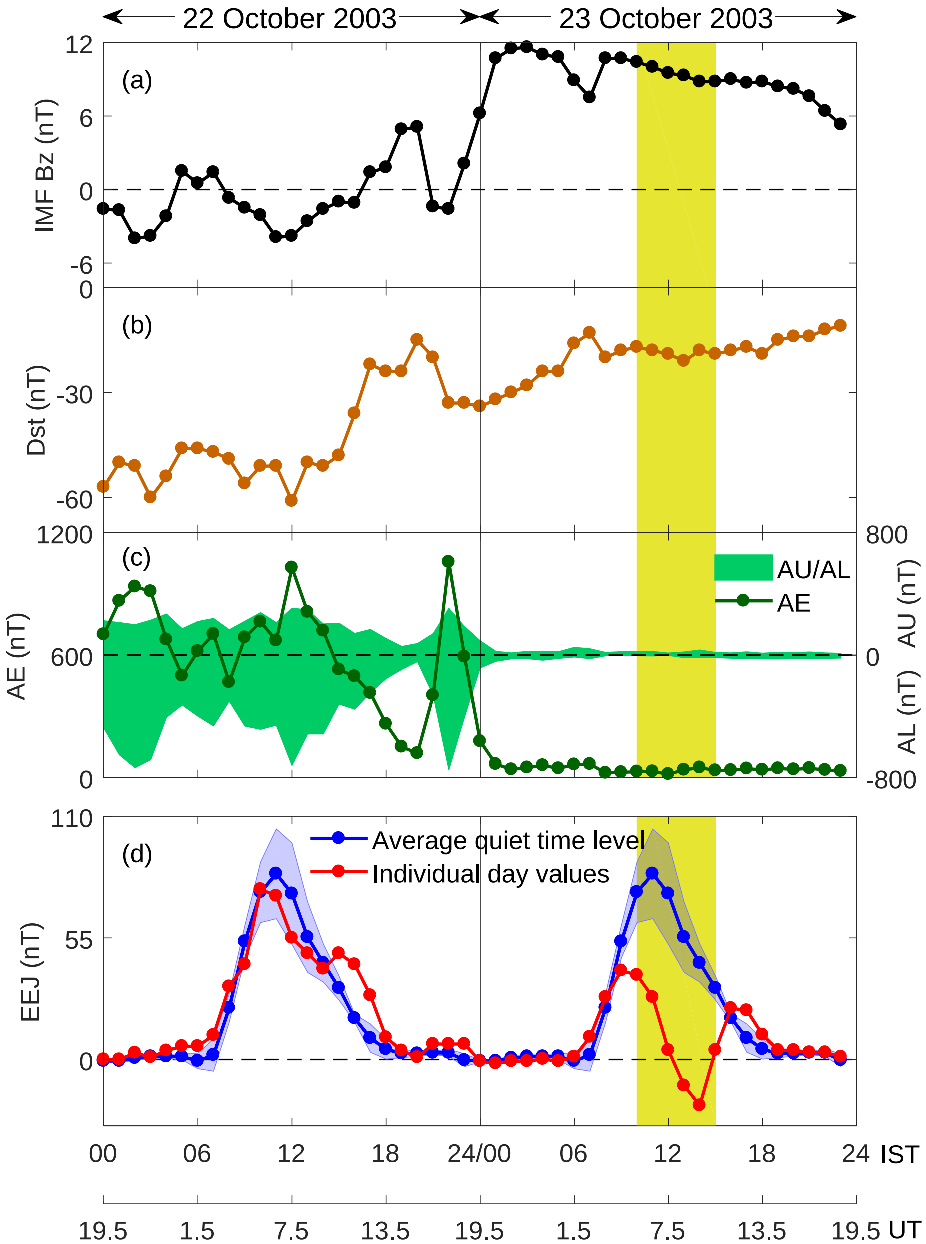

Figure 5.3: Same as Figure 5.1 but for event 3 (23 October 2003, right panel) and a day prior to it (22 October 2003, left panel).

The temporal changes in the EEJ strengths for events 1 - 3 from the respective quiet time levels of the month are obtained. It is to be noted that the present work focuses on reductions in EEJ strength due to disturbance dynamo. In order to remove the possible contributions of day-to-day variations from the reductions in EEJ strength, the lower envelope (-1σ level) of quiet time variations (marked in Figures 5.1 - 5.3) is taken as reference level for calculating the changes in EEJ. Thus, changes in EEJ, $\Delta EEJ(t) = EEJ_{Eventday}(t) - [EEJ_{Avg.quiet}(t) - 1\sigma(t)]$.

Temporal changes in the ΔEEJ for events 1 - 3 are depicted in Figure 5.4(a - c). For events 1 - 3 the maximum strength of ΔEEJ are about -52 nT, -93 nT and -56 nT at 1100 IST, 1300 IST and 1400 IST, respectively.

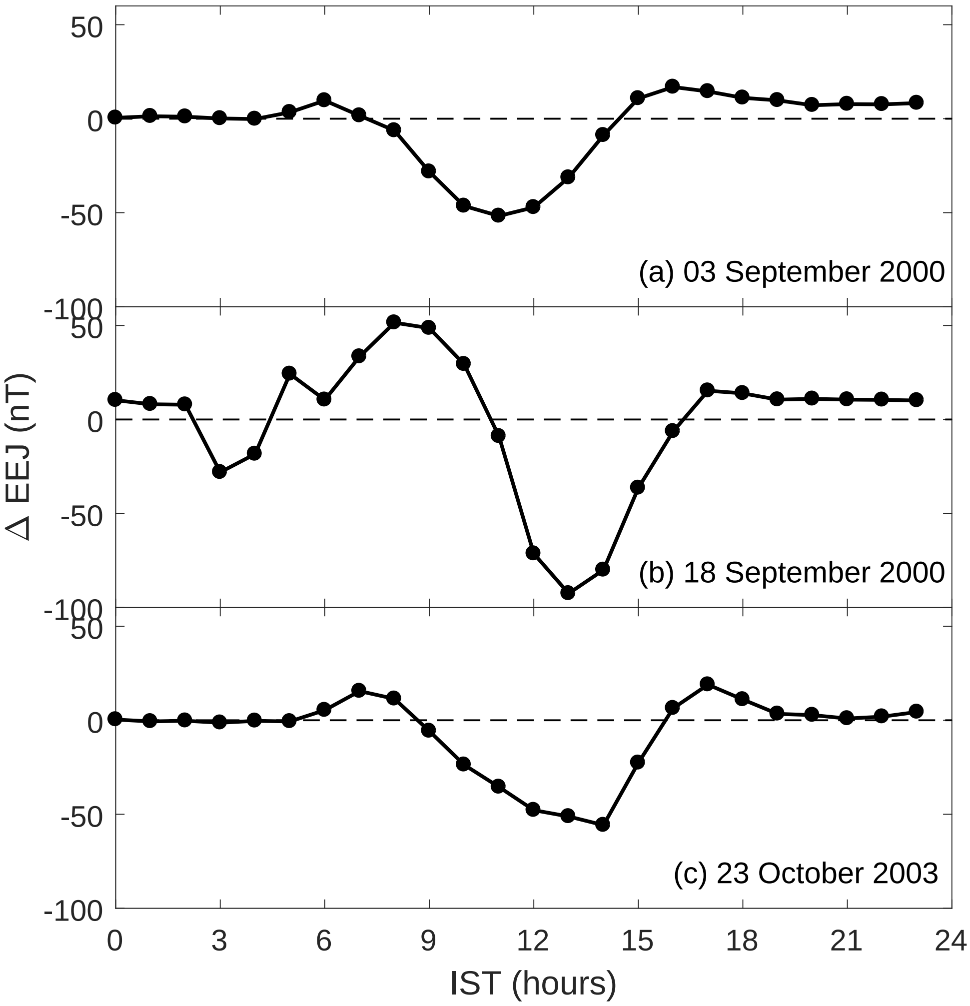

Figure 5.4: Temporal variation of change in EEJ, $\Delta EEJ(t) = EEJ_{Eventday}(t) - [EEJ_{Avg.quiet}(t) - 1\sigma(t)]$ for Events 1, 2 and 3 are depicted in (a), (b) and (c) respectively.

Yamazaki and Kosch [2015] considered about 1300 geomagnetic storm events and provided the average values of changes in EEJ strength from quiet time level over Indian sector. In their study, the reductions in EEJ after about 4 - 5 hrs (treated predominately due to disturbance dynamo) are found to be within -30 nT. The reductions in EEJ observed on events 1 - 3 are significantly larger. Thus, these studies indicate that the occurrence of such events is small in number. It may be noted that as the quiet time reference variations changes with local time, the maximum ΔEEJ occur at slightly different local times compared to the time of minimum in actual EEJ variations depicted in Figures 5.1 - 5.3.

In order to compare with the model estimations of disturbance dynamo electric field, it is important to know the magnitude of the westward electric field perturbations for the three events under consideration. Based on the method described in Chapter 2, the reductions in the electric fields are estimated for Events 1 - 3 corresponding to the maximum strengths of ΔEEJ. The estimates of zonal electric field perturbations for events 1, 2 and 3 are -0.7 ± 0.2, -1.2 ± 0.3 and -0.8 ± 0.2 mVm^{-1} respectively. It is to be noted that the solar EUV flux on all three cases remained on the same level (within 5%) as on the quiet days of the respective months. Therefore, the changes in EEJ are driven by the changes in electric fields only.

The electric field changes over the dip-equator due to DD are expected to suppress the plasma fountain affect over low latitudes. In order to verify this aspect, the global TEC maps are generated corresponding to the time that is $\sim$2 hrs after the maximum reduction in ΔEEJ for the events 1 - 3. This is to account for the time associated with plasma diffusion processes [*Sanatani*, 1966] described earlier in Chapter 4. For comparison with the event days, the mean quiet time TEC maps for the respective months are also generated for the same local time as that of the event day. Figure 5.5 depicts the global TEC maps on the event day (right panel) and mean quiet time level of the respective months (left panel). Locations of the dip-equator along with $\pm10°$ and $\pm20°$ dip-latitudes are drawn with the black colored solid, dashed and dotted curves, respectively. It can be noticed that the crests of the plasma fountain are well separated during quiet periods. However, on the event days, the crests are not well separated indicating the weakening of plasma fountain effect under the influence of westward DDEF. This indicates towards the weakening of the plasma fountain effect under the influence of significant DDEF.

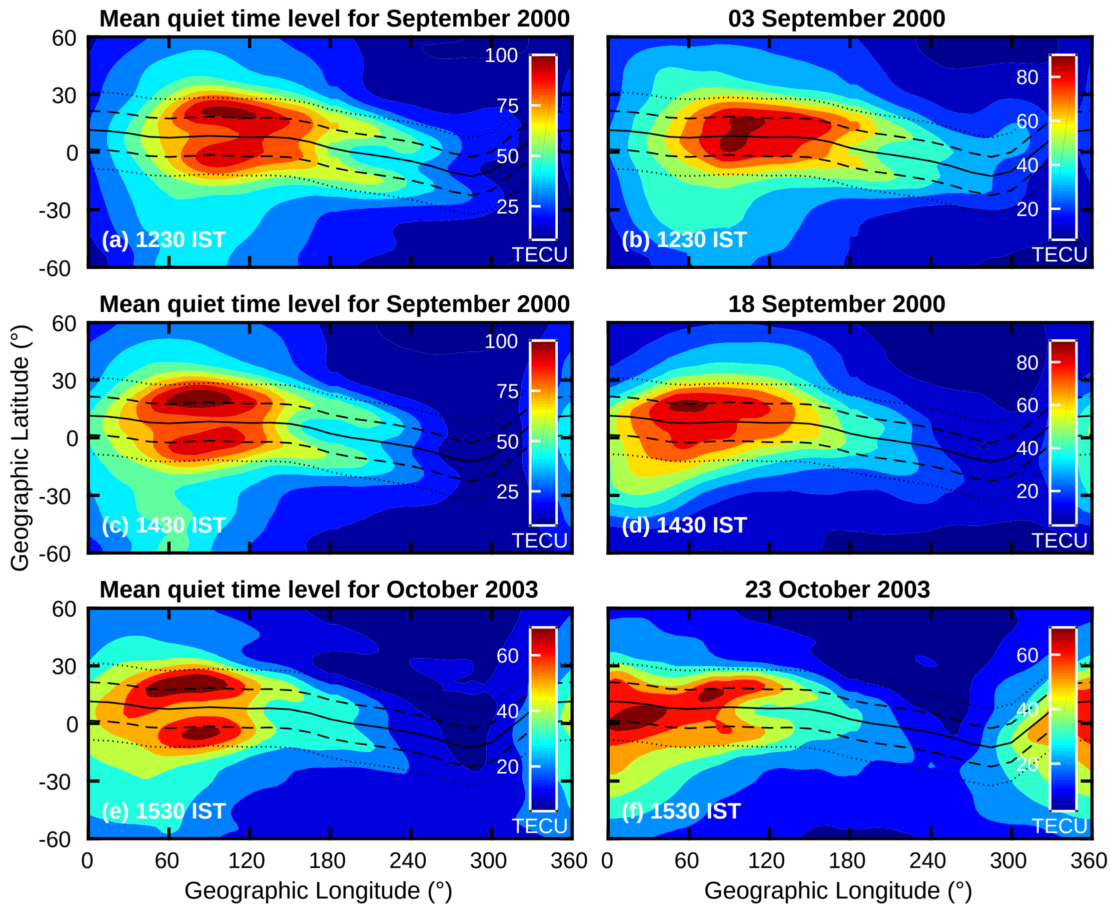

Figure 5.5: Global TEC maps on event day (right) and mean quiet time level for the respective months (left). The TEC maps corresponding the time that is about 2 hrs after the maximum changes in ΔEEJ for events 1 - 3 are depicted from top to the bottom. Locations of the dip-equator along with $\pm10^{\circ}$ and $\pm20^{\circ}$ dip-latitudes are drawn with the black colored solid, dashed and dotted curves, respectively. The TEC values are in units of TECU, wherein 1 TECU = 10^{16} electrons m^{-2}.

5.3.4 Other cases

The three cases presented so far pertain to the equinoctial months and high solar activity period. By relaxing the selection criterion in which reduction in EEJ is more than 2σ to a criterion in which reduction in EEJ is between 1σ and 2σ and keeping the rest of the criteria intact, 10 more cases are identified. These cases are tabulated in Table 5.1 in which the dates, time interval (IST) during which reduction in EEJ is between 1σ and 2σ, and the maximum zonal electric field corresponding to maximum strength of ΔEEJ are shown.

It can be seen from Table 5.1 that out of 10 cases, 9 cases pertain to the high solar activity period and 6 cases pertain to the equinoctial months. Therefore, it is clear that the effects of DD on equatorial ionosphere are more prominent during equinoctial months in high solar epoch. These cases are not discussed further as the focus of the present investigation is to address the significant (more than 2σ) reductions in EEJ strength under the influence of DD. The maximum changes in electric fields, corresponding to the changes in EEJ, are also listed in Table 5.1. It is to be noted that, on most of the events, solar EUV flux remained at the same level (within 5%) as on the quiet days of the respective months barring 24 September 2001, 20 January 2005 and 08 March 2012. Therefore, the changes in EEJ, on most of the events, are driven by the changes in electric fields only.

Date	Time-interval (IST) during which reduction in EEJ is between 1σ and 2σ	Maximum change in zonal electric field (mVm^{-1})
13 August 2000	10 - 12	-0.24
25 January 2001	13 - 16	-0.29
14 September 2001	09 - 13	-0.38
24 September 2001	13 - 15	-0.15
25 March 2002	10 - 12	-0.25
05 November 2003	14 - 16	-0.44
20 January 2005	12 - 15	-0.17
08 March 2012	11 - 15	-0.39
18 March 2013	11 - 13	-0.21
31 October 2013	11 - 14	-0.10

Table 5.1: Details of the events in which reduction in EEJ is between 1σ and 2σ. The maximum change in electric field is estimated (with 25% uncertainty) corresponding to maximum strength of ΔEEJ.

5.4 Discussion

Three examples are presented in this investigation revealing significant reduction in the strength of EEJ (occurrence of CEJ in two cases) in the recovery phase of a geomagnetic storm without any prompt electric field perturbations. Subsequent to the disturbances in the auroral electrojet at an earlier time, these reductions in EEJ occurred with varying time delays. This suggests the influence of westward electric field perturbations on the equatorial ionosphere due to DD effect. Westward electric field influences on the equatorial ionosphere during daytime can also arise due to overshielding condition [e.g., *Wolf et al.*, 2007; *Simi et al.*, 2012] wherein IMF Bz suddenly turns northward after being stably southward for some time. This is not the case here. As there were minimal AE/AU/AL activities on all the three event days, the role of substorms [*Kikuchi et al.*, 2003] in causing the reduction in EEJs can also be ruled out.

Recently, it is shown [*Rout et al.*, 2018] that even in absence of a typical geomagnetic disturbances (i.e., Dst > 0 and AL > -400 nT), significant changes can occur in EEJ and low latitude electric fields. These perturbations are shown [*Rout et al.*, 2018] to be driven by Prompt penetration/Overshielding electric fields due to the passage of the sheath region of Interplanetary Coronal Mass Ejection (ICME) when the IMF Bz flip-flops between the positive and negative values in quick successions. In order to rule out this possibility, the IMF Bz values with 1 minute temporal resolution are looked into. It is found that, during events 1 - 3, the IMF Bz values with even 1 minute resolution are continuously northward (except being about -2 nT for two minutes at $\sim$0930 IST for event 1). Therefore, the role of fast fluctuating IMF Bz to cause electric field changes over low latitudes in these cases can be ruled out.

It is known that the sudden stratospheric warming (SSW) events can drive perturbations in the ionospheric electric field [*Fejer et al.*, 2010] and current [*Sridharan et al.*, 2009]. The list of major SSW events during 1958 - 2013 is provided by *Butler et al.* [2017]. It is verified that neither events 1 - 3 nor those listed in Table 5.1 occurred during the period of SSW events. Therefore, the role of SSW in causing electric field changes in these cases can be ruled out.

Sr no.	Station	Geog. Lat.	Geog. Lon.	Geom. Lat.
1	Novosibirsk	55.0°N	82.9°E	45.2°N
2	Alam Ata	43.3°N	76.9°E	33.9°N
3	Kashi	39.5°N	76.0°E	30.3°N
4	Golmud	36.4°N	94.9°E	26.0°N
5	Silchar	24.9°N	92.8°E	14.7°N
6	Ujjain	23.2°N	75.8°E	14.1°N
7	Nagpur	21.2°N	79.1°E	11.9°N
8	Alibag	18.6°N	72.9°E	9.9°N
9	Visakhapatnam	17.7°N	83.3°E	8.1°N
10	Pondicherry	11.9°N	79.9°E	2.6°N
11	Tirunelveli	8.7°N	77.8°E	0.4°S
12	Tuntungan	3.5°N	98.6°E	6.8°S
13	Martin De Vivies	37.8°S	77.6°E	46.4°S
14	Port Aux Francais	49.4°S	70.3°E	56.9°S
15	Mawson	67.6°S	62.9°E	73.1°S

Table 5.2: Magnetometer stations used to obtain latitudinal variations in D_{dyn}.

In order to ascertain that ΔEEJ during events 1 - 3 are associated with DD caused by global scale disturbed winds, the reductions in the horizontal component of geomagnetic field from the average quiet time levels at different latitudes are investigated. As the present investigation pertains to DD effects over the Indian sector, the changes in horizontal component of magnetic field [$D_{dyn} = \Delta H - S_R - Dst \times cos(L)$] are obtained for stations situated along the Indian geographic meridian (Geog. Lon. 80° ± 20°E). This method is same as that used by *Le Huy and Amory-Mazaudier* [2005], *Zaka et al.* [2009] and *Amory-Mazaudier et al.* [2017] except for the fact that the construction of quiet time reference curve consists of a number of quiet days instead of a single quiet day. Following this method, D_{dyn} is calculated for the magnetometer stations from geomagnetically high to low latitudes. These stations are listed in Table

5.2 with geographic coordinates and geomagnetic latitudes. The data for these stations are obtained from WDC, Kyoto and IIG, Mumbai.

The variations in D_{dyn} for the events 1 - 3 with geomagnetic latitude are depicted in Figure 5.6 with blue, red and black colours respectively. These latitudinal profiles correspond to the times when magnitude of ΔEEJ is maximum (at 1100 IST, 1300 IST and 1400 IST for events 1, 2, and 3 respectively) for each event. It is to be noted that the positive D_{dyn} corresponds to southward deviation in geomagnetic field compared to the quiet level. On all three events, the latitudinal variations are similar to those obtained by *Zaka et al.* [2009]. The reductions in D_{dyn} are maximum over geomagnetic equator (Tirunelveli) and have opposite polarity compared to those for higher magnetic latitudes. This confirms the flow of an “anti-Sq” current system driven by the disturbance dynamo.

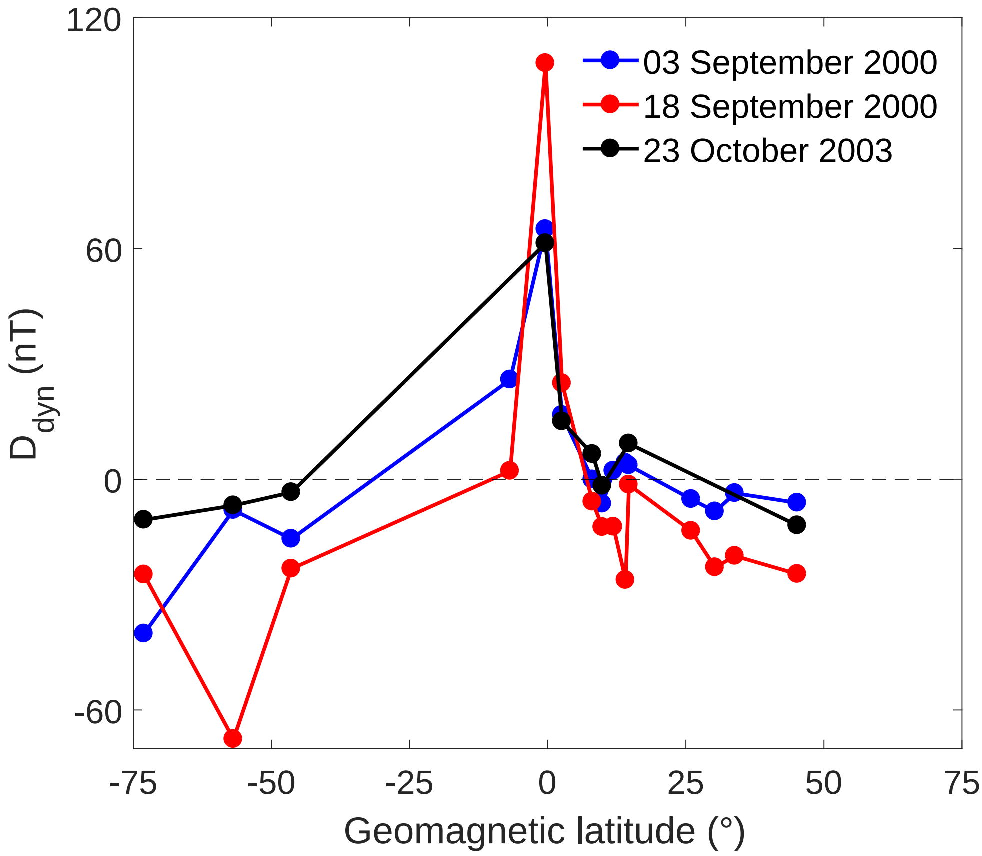

Figure 5.6: Latitudinal variations of the reduction in magnetic field (D_{dyn}) for Events 1 (blue), 2 (red) and 3 (black). The values correspond to the time at which the strength of ΔEEJ is maximum for Events 1 (1100 IST), 2 (1300 IST) and 3 (1400 IST).

In order to compare the estimates of electric fields with earlier modeling studies on DDEFs, it is worthwhile to discuss the results obtained by the earlier workers [e.g., *Blanc and Richmond*, 1980; *Fejer et al.*, 2008b]. Based on the empirical models of DD [*Fejer and Scherliess*, 1995; *Scherliess and Fejer*, 1997; *Fejer et al.*, 2008b], the maximum perturbations in vertical drift were reported to be stronger during night time (∼20 ms^{-1}) and weaker in daytime (∼−10 ms^{-1}). These values correspond to electric field perturbations of ∼0.5 mVm^{-1} during nighttime and ∼−0.25 mVm^{-1} in daytime. On the other hand, the investigations based on the theoretical models of DD [*Blanc and Richmond*, 1980; *Richmond et al.*, 2003; *Huang et al.*, 2005; *Huang*, 2013] revealed that the DDEF perturbations in daytime are below −0.5 mVm^{-1}. *Huang and Chen* [2008], based on numerical simulation, obtained the maximum DDEF perturbation to be within −0.5 mVm^{-1} during daytime over the geomagnetic equator. As discussed in earlier studies [e.g., *Blanc and Richmond*, 1980; *Fuller-Rowell et al.*, 2002; *Richmond et al.*, 2003; *Huang et al.*, 2005], DDEF is generated by the westward and equatorward wind systems in both the hemispheres due to the Joule heating over the auroral regions subsequent to geomagnetic disturbances. The altered circulation patterns in each hemisphere generate an anti-Sq current system over the low latitude region that positively charges the low latitude ionosphere especially around the local midnight hours. Therefore, the DDEF effects are usually expected to be maximum during local midnight hours [*Fuller-Rowell et al.*, 2002]. During daytime, these positive charges that are built up due to the Pedersen and Hall currents associated with westward and equatorward circulation, get mostly shorted out by large E-region conductivities [*Huang*, 2013]. Further, as the disturbance winds over both the hemispheres will experience comparable drag forces during equinox, competing hemispherical effects will be minimum during equinoctial months. Hence the DDEF effects are expected to be more in equinoctial months [*Huang*, 2013]. During solstices, the DDEF effects may get reduced over the dip equatorial region depending on the strength of the trans-hemispherical winds. Further, the disturbance DDEF generation is dependent on solar epoch, with higher magnitude during high solar epoch [*Scherliess and Fejer*, 1997]. The impact of DD is expected to affect the equatorial ionosphere 6 - 15 hrs after the onset of AE activity [*Fejer and Scherliess*, 1995; *Huang and Chen*, 2008].

In the present investigation, events 1 - 3 occurred in equinoctial months during high solar epoch. In addition to these events, 6 out of 10 events listed in Table 5.1 occurred in equinoctial months and 9 occurred in high solar epoch. Therefore, the present observations are consistent with the prevalent understanding as far as the season, solar epoch and the polarity of disturbance dynamo perturbations are concerned. The magnitude of reduction in electric field for events listed in Table 5.1 are below 0.5 mVm^{-1}. However, for events 1 - 3, the magnitudes of reduction in electric field are 0.7 ± 0.2, 1.2 ± 0.3 and 0.8 ± 0.2 mVm^{-1}. Therefore, the values obtained on events 1 - 3 are unusually large compared to the earlier estimates of daytime DDEF based on theoretical and empirical models. This suggests towards a possible additional contribution for the reduction of electric field. In order to investigate this possibility, Figure 5.7 is presented.

Figure 5.7 depicts hourly variations of the strength of EEJ on 147 geomagnetically quiet days during September-October months under solar maximum condition. Figure 5.7 does not contain events 1 - 3 and the cases presented in Table 5.1. In Figure 5.7, the EEJ variations on individual quiet days are depicted by gray and multi coloured curves. The mean EEJ strength and 1σ variation are depicted by black coloured curve and vertical bars, respectively. The observations on most of the days follow the average quiet time pattern of generally rising from 0700 IST onwards and reaching peak value of 80 ± 30 nT at 1100 IST before gradually falling to zero level around 1900 IST. However, on quite a few days, the EEJ values during afternoon hours are substantially reduced below 1σ variations and become closer to zero or negative. These are selectively marked with multicoloured lines in Figure 5.7. It is important to note that the peak EEJ strength on these days are also less than the 1σ variations and occurred earlier in local time. This essentially indicates towards the influence of semi-diurnal tides in generating the quiet time dynamo electric field. Under these circumstances, the quiet time reference curve may not be truly representative of the processes occurring on these days and this may bias the estimation of DDEF.

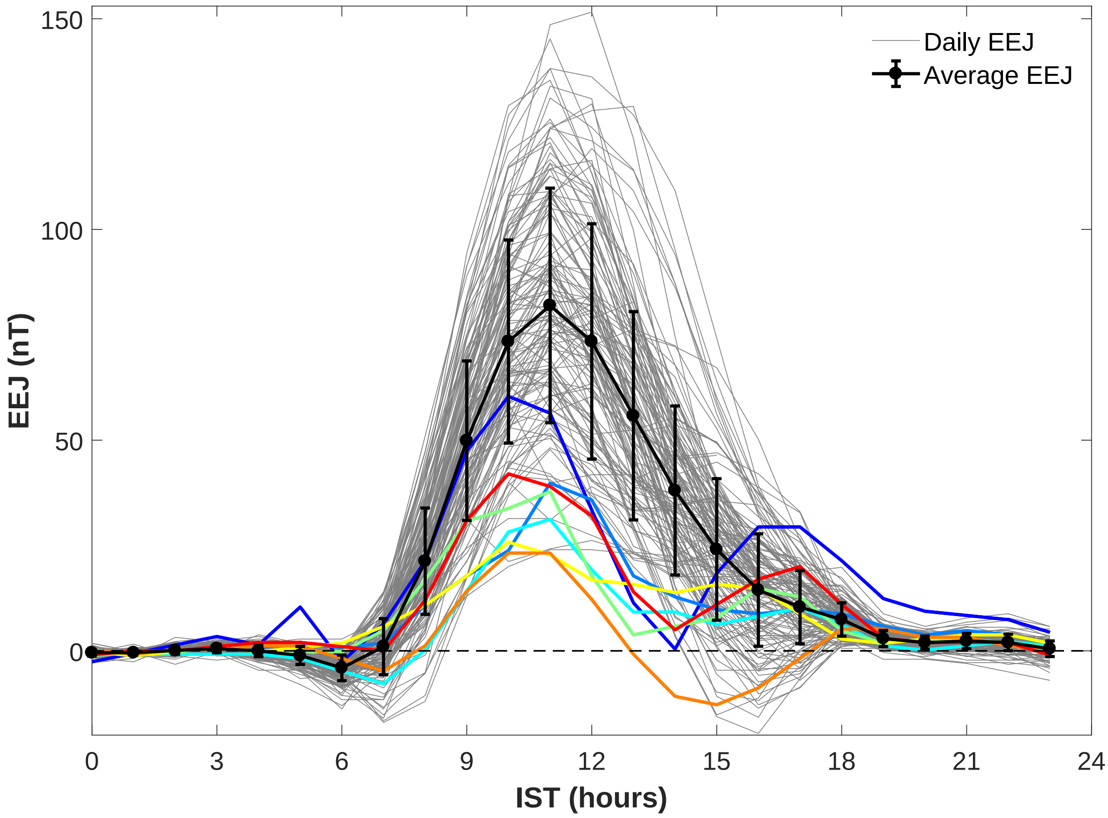

Figure 5.7: Temporal variations of EEJ on 147 geomagnetically quiet days (gray and multi-colour) during September-October months under high solar epoch and it's average variation (black) with standard deviation (1σ values with vertical bars). The multi-coloured lines depict the EEJ variations on days in which EEJ values are continuously below 1σ variations during afternoon hours.

Earlier theoretical [*Forbes and Lindzen*, 1976; *Hanuise et al.*, 1983; *Marriott et al.*, 1979; *Stening*, 1989b] and experimental works [*Gurubaran*, 2002; *Sridharan et al.*, 2002; *Bhattacharyya and Okpala*, 2015] acknowledged the contribution of semi-diurnal tides in altering the electric fields primarily generated by the diurnal tides over the equatorial region. Although the influence of semi-diurnal tides is more prominent during solar minima [*Chakrabarty et al.*, 2014; *Pandey et al.*, 2018], Figure 5.7 suggests that the influence of sem-diurnal tides during solar maxima cannot be ruled out on occasions. In fact, in Chapter 4, it is shown that the high occurrence of CEJ events over India during afternoon hours in June solstice under low solar epoch are due to westward Sq electric field and argued that it is due to the influence of semi-diurnal tides. It is evident from Figure 5.7 that the quiet time CEJ events during equinox in solar maximum period occur mostly between 1500 IST and 1800 IST. However, the maximum reductions in EEJ on events 1 - 3 occurred during 1100 - 1400 IST (see Figure 4). Therefore, it is suggested that the large reductions in electric fields on events 1 - 3 are probably due to combined effects of DDEF and semi-diurnal tides. In absence of observations of winds during events 1 - 3, this aspect could not be verified at present. Future, investigations are needed to confirm this proposition.

5.5 Summary

Based on 16 years of EEJ data over India, three cases of unusually large disturbance dynamo events over equatorial latitudes are identified. It is found that the prominent cases of unusually large disturbance dynamo electric field events mostly occurred during equinox and high solar activity period. Based on the reduction in EEJ strength, it is estimated that the westward electric field perturbations for these cases lie in the range of 0.7 ± 0.2 - 1.2 ± 0.3 mVm^{-1} during daytime. These electric field perturbations during daytime are significantly larger than the existing disturbance dynamo model estimates reported so far [e.g., *Fejer et al.*, 2008b; *Huang and Chen*, 2008] and are comparable to nighttime disturbance dynamo effects. It is suggested that detailed modeling investigation that takes into account the role of semi-diurnal tidal influence on equatorial ionosphere is needed to quantify the role of disturbance dynamo on equatorial ionosphere during daytime.

Chapter 6

Estimation of nighttime E-region current density over dip-equator

Excerpt

In previous chapters, the observations of equatorial electrojet are obtained from the magnetic field measured by ground-based magnetometers after subtracting the average nighttime values. This is with the assumption that during nighttime the ionospheric current over low-latitudes is negligibly small. However, existence of such current and its possible strength is one of the unresolved issues in ionospheric physics and geomagnetism. A detailed investigation is carried out to estimate the same over Indian longitudes using rocket borne in-situ measurements of E-region electron density and zonal current density from Thumba (8.5°, 76.9°E), empirical plasma drift model [*Fejer et al.*, 2008a] and equatorial electrojet model developed by *Anandarao* [1976]. This investigation reveals that the nighttime E-region current densities vary from ∼0.3 to ∼0.7 $\mu\mathrm{Am}^{-2}$ during pre-midnight to early morning hours under geomagnetically quiet conditions. The nighttime current densities over the dip equator are estimated using three different methods involving theoretical model and measurements (discussed in methodology section). The values obtained are found to be consistent with one another within the uncertainty limits. Altitude structures in the E-region current densities are also noticed which are shown to be associated with those in the electron densities. The horizontal component of the magnetic field induced by these nighttime ionospheric currents is estimated to vary between ∼2 and ∼6 nT during geomagnetically quiet periods. This investigation confirms the existence of nighttime ionospheric current and opens up a possibility of estimating base line value for geomagnetic field fluctuations as observed by ground-based magnetometer.

6.1 Introduction

The strengths and variations of EEJ currents during daytime had been derived in detail using rocket borne magnetometer measurements over Indian [e.g. *Sastry*, 1970; *Sampath and Sastry*, 1979, and references cited therein], Peruvian [e.g. *Davis et al.*, 1967; *Shuman*, 1970] and Brazilian [e.g. *Pfaff et al.*, 1997, and references cited therein] longitudes. Systematic observations of the electrojet current strengths during daytime were obtained by ground-based magnetometers [e.g. *Rastogi and Iyer*, 1976]. Satellite borne measurements of these current densities during daytime [*Jadhav et al.*, 2002; *Lühr et al.*, 2004, etc.] are also available. However, the existence (or the lack of it) of the possible ionospheric current during nighttime and its characteristics over low-equatorial latitudes are not well understood. This is because of the fact that during nighttime, the ionospheric E-region plasma density decreases drastically. As a consequence, the midnight values of Sq current are generally taken as the base line for the overhead equivalent ionospheric current system. However, based on theoretical calculations, *Takeda and Araki* [1985] concluded that the ionospheric Sq currents flow westward in the nighttime during high solar activity period and their contribution to the geomagnetic Sq field is about 1/10 of the maximum Sq variation. On the other hand, the nocturnal currents are shown to be weak during low solar activity period and below the detection limit. In addition, *Campbell* [1973] and *Mayaud* [1976] found that the geomagnetic variations during nighttime are not negligible on many occasions. *Campbell* [1979] suggested that the ground geomagnetic variations during nighttime may be present even during apparently quiet conditions. *Matsushita and Maeda* [1965] used the daily mean as the base level to be representative of the zero Sq current and showed the presence of significant nighttime ionospheric current. On the other hand, if the nighttime Sq level is taken as the base value, as in *Matsushita* [1968], it would imply zero ionospheric current during nighttime. Therefore, determination of the base geomagnetic level is important to determine the nighttime E-region current over low-equatorial latitudes.

Based on only a single rocket flight, *Davis et al.* [1967] inferred small westward current in E-region (corresponding to magnetic variation of about 6 nT on the rocket borne magnetometer) during midnight hours around 100 km altitude over the Peruvian dip equatorial sector. This inference was derived using the data obtained from the ascent and descent phases of the rocket flight. After a few days, under similar geomagnetic conditions, *Shuman* [1970] did not detect any significant current over the same place and around the same local time during the descent phase of the rocket, although the resolution of the magnetic measurements was slightly better (5 nT). It is to be noted here that the magnetometer measurements are not expected to alter significantly depending on the ascent and descent phases of the rocket as current integrated over large area is measured. Thus, considering that rocket wake does not modify the magnetometer measurements, the results of *Shuman* [1970] is in contradiction with the results of *Davis et al.* [1967]. Over the Indian dip equatorial sector (Thumba), in situ measurements of zonal current density at three different times (pre-noon, post-noon and pre midnight) on 29 August 1968 were reported by *Sastry* [1970]. Figure 6.1 depicts the altitude profiles of zonal current densities obtained from sounding rocket experiments conducted at 1108 IST, 1415 IST and 2300 IST. Around noon hours, the strength of current density was ~9.4 μAm^{-2}. Whereas, at night the magnetic field strengths were observed to be within the measurement uncertainties (~4 nT) and the nighttime currents were concluded [*Sastry*, 1970] to be absent. *Onwumechili* [1992a] compiled the available in situ measurements of ionospheric current density over the globe and the nighttime current over the dip equatorial region was suggested to be absent.

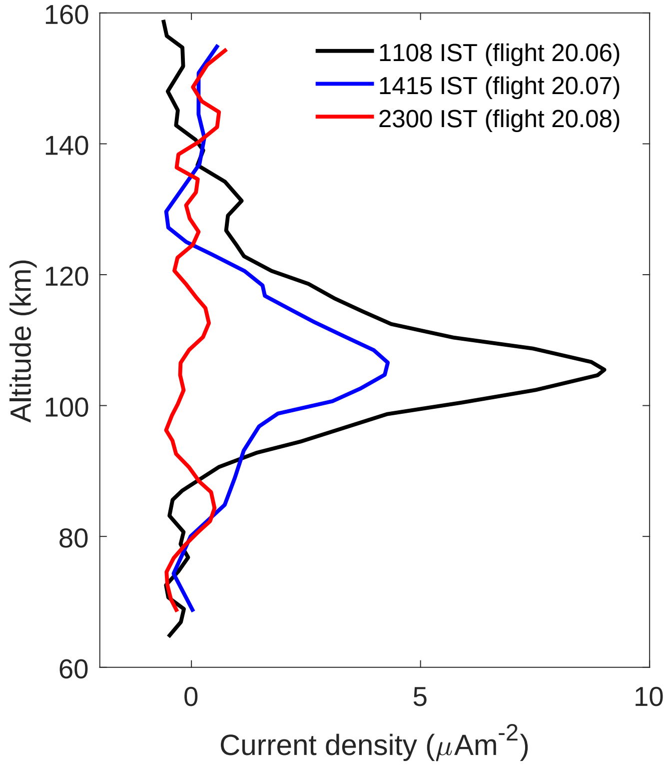

Figure 6.1: Altitude profiles of zonal current densities measured using sounding rocket flight experiments conducted at 1108 IST, 1415 IST and 2300 IST on 29 August 1968 [after *Sastry*, 1970].

The above observations pose an uncertainty on the magnitude of the current that can be expected to flow through the equatorial E-region during nighttime. Further, as suggested by *Haerendel and Eccles* [1992] and *Eccles et al.* [2015], the generation of pre-reversal enhancement (PRE) of the equatorial F-region zonal electric field will depend crucially on the closure of the F-region dynamo current through the E-region in the low and equatorial latitudes. Therefore, determination of nighttime E-region current is essential to understand the underlying processes that couple E and F regions over low-equatorial latitudes during nighttime. There was an attempt by *Stening and Winch* [1987] to estimate the ionospheric current using the in situ measurements of electron density, obtained over Thumba [*Prakash et al.*, 1970], and with a fixed zonal Sq electric field of -0.3 mVm^{-1}.

Figure 6.2 depicts the nighttime current density estimated by *Stening and Winch* [1987]. The maximum magnitude of current density was found to be up to 0.28 μAm^{-2} around 102 km. Thus, based on current density estimate on this

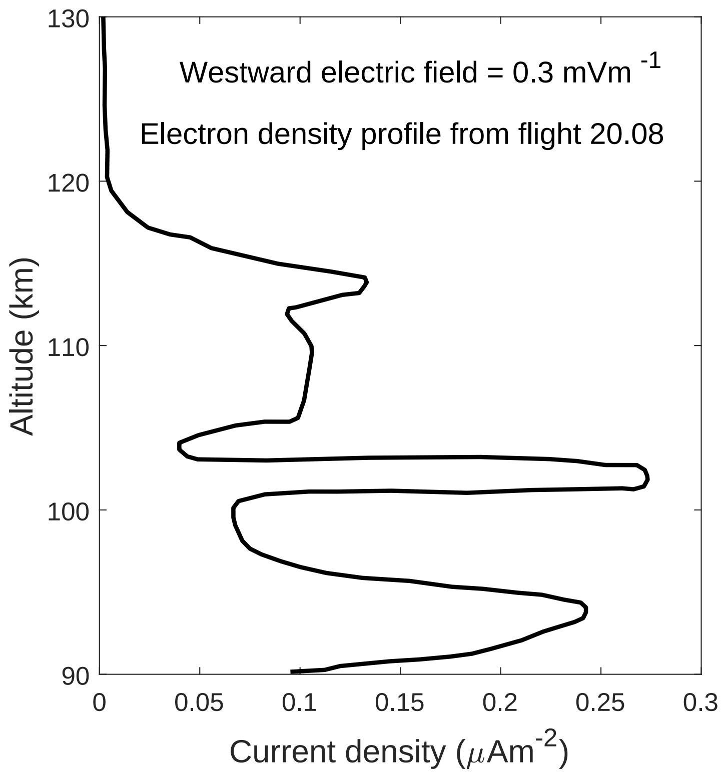

Figure 6.2: An altitude profile of nighttime current density estimated by *Stening and Winch* [1987].

occasion, *Stening and Winch* [1987] concluded the flow of a finite ionospheric current during nighttime. Further, *Rastogi et al.* [1996] reported that the nocturnal variation of horizontal geomagnetic field over Huancayo showed remarkable similarity with corresponding variation of ionospheric electric field determined by Doppler radar. This indicates a finite nighttime ionospheric current which can be inferred by ground-based magnetometer. However, it is difficult to separate ionospheric and magnetospheric components from these magnetometer measurements in spite of the resolution being 0.1 nT in the present digital magnetometer systems as their effects are comparable on ground during nighttime. It is not clear whether the ground-based magnetometer measurements during nighttime, even in magnetically quiet times, are free from the contributions from magnetosphere. During geomagnetically disturbed period, many authors [e.g. *Matsushita*, 1971; *Onwumechili and Ezema*, 1977; *Chakrabarty et al.*, 2005] had indicated the non-ionospheric (magnetospheric) origin of the currents responsible for the magnetic fluctuations observed at the ground. Therefore, a comprehensive understanding on the magnitude of the nighttime E-region current and its variation with time is missing till date although the nighttime horizontal component of the magnetic field measured by the magnetometers is being used as base or reference value for determining the daytime electric fields [*Rastogi and Patil*, 1986]. These variations in the reference value during magnetically disturbed period make matters worse with regard to the determination of the daytime electric fields is concerned.

Given the above background, it is imperative that knowledge about the changes in nocturnal ionospheric current during geomagnetically quiet time is essential to comprehensively understand the equatorial electrodynamics. In this context, the present investigation is important as it provides estimation of the equatorial E-region current at a few local nighttimes by different methods using experimental data and modeling investigations.

6.2 Details of observations and other inputs

In the present investigation, electron densities and plasma wave information obtained from six rocket flights containing Langmuir probe system with high frequency response [*Prakash and Subbaraya*, 1967; *Subbaraya et al.*, 1983, 1985] conducted over Thumba, during 1967 to 1975, are utilized as inputs. In addition, in situ measurements of zonal current density [*Sastry*, 1970; *Sampath and Sastry*, 1979] using magnetometer on board two rocket flights over Thumba are used. Throughout this work, time corresponds to local time (LT) which, for Thumba (76.9°E) is about 22 min behind the Indian Standard Time, IST (time corresponding to 82.5°E).

It is important to note here that simultaneous measurements of electron and current densities were obtained on 29 August 1968 at 1353 LT [*Subbaraya et al.*, 1972] and 3 March 1973 at 1158 LT [*Sampath and Sastry*, 1979]. The red and black coloured curves in Figures 6.3a and 6.3c depict measured current and electron densities. The zonal plasma drifts, calculated using these simultaneous measurements, are depicted in Figures 6.3b and 6.3d. These zonal drifts are used to calculate the value of R ($= \sigma_H/\sigma_P$) which is subsequently utilized to estimate the nighttime current densities (method discussed in section 6.3.1). Note that these two rocket flight experiments belong to high (yearly averaged F10.7 index in year 1968 is ∼150 sfu) and low (yearly averaged F10.7 index 1973 is ∼90 sfu) solar activity periods. Since R is independent of electron densities (to be discussed later), average values of R are utilized to compute the altitude profiles of nighttime current densities. The validity of using these R values to the nighttime is discussed in section 6.3.1.

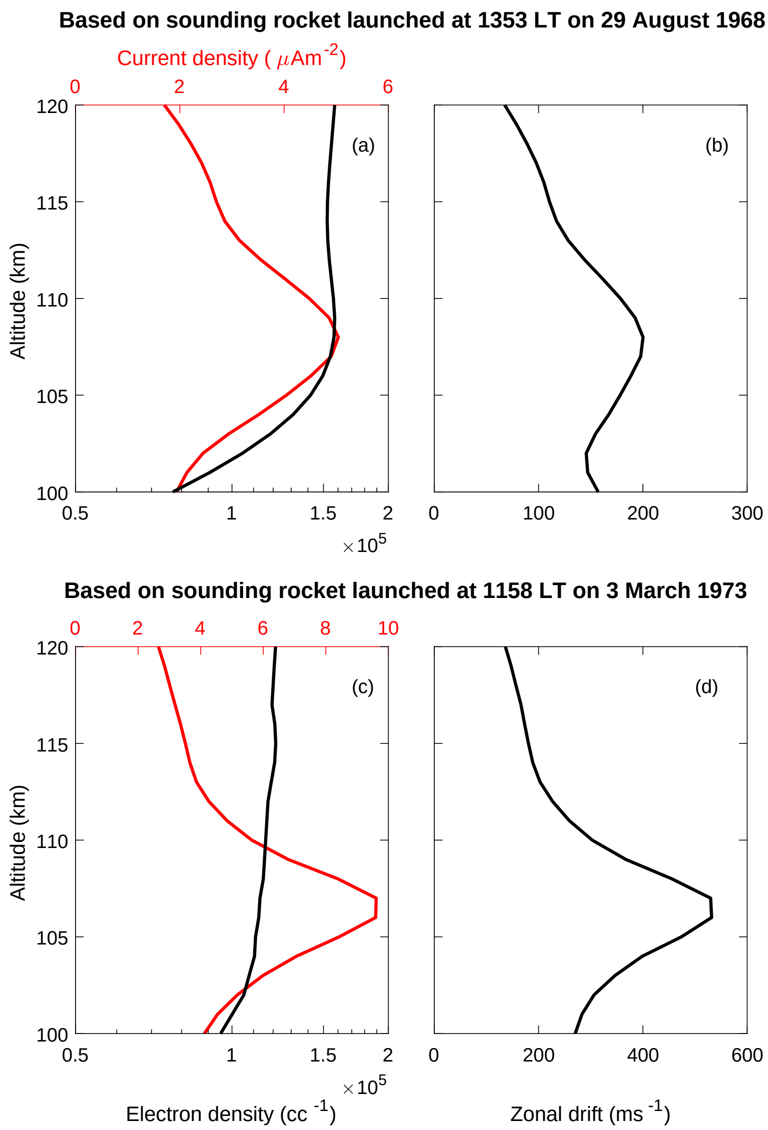

Figure 6.3: Altitude profiles of current and electron density simultaneously measured at 1353 LT and 1158 LT [from *Subbaraya et al.*, 1972; *Sampath and Sastry*, 1979]. Zonal plasma drifts obtained based on these measurements.

The observed presence of Two-stream waves in the electron density measurements [e.g. *Farley*, 2009] is also used to give the physical estimate of minimum strength of nighttime current density that must be present over the altitude range wherein Two-stream waves were detected. The generation of Two-stream wave is shown [*Sekar et al.*, 2013] to be possible only when the dip angle (I)$<$ 1.5°. The present investigation makes use of the electron density observations from Thumba during 1967 to 1975 wherein the dip angle was between $-1.0°$ and $-1.1°$ and thus consistent with the conclusion of *Sekar et al.* [2013]. Further, as the objective of the present investigation is to find out the nighttime E-region current density that is a realistic representative of the nighttime base value during quiet time, the electron density profiles before 2100 LT are avoided to minimize the contributions from PRE. The other important input parameters are as follows.

i The altitude profiles of neutral density and temperature are taken from NRLMSISE-00 [*Picone et al.*, 2002] model.

ii The geomagnetic field in altitude-latitude plane is adopted from International Geomagnetic Reference Field (IGRF)-12 model [*Thébault et al.*, 2015].

iii The vertical drifts corresponding to quiet time Sq electric fields over the dip equator are taken from F-region vertical plasma drift model of *Fejer et al.* [2008a]. The model values are preferred compared to climatology obtained using the measurements of F-layer movements as the observations were unable to explain the presence of Two-stream waves observed in the night (for details see Chapter 3).

6.3 Methods to estimate nighttime current density

Three different approaches have been adopted to estimate the nighttime current density in the dip-equatorial E-region. These methods are described in ensuing subsections and results obtained from these methods are compared in section 6.5.

6.3.1 Method-1: Based on the ratio R deduced from observations

In order to estimate the altitude profiles of nighttime current density, the altitude profiles of electron density and plasma drifts in the zonal direction are needed. A few measurements of electron density over Indian sector during nighttime are available in literature [*Subbaraya et al.*, 1983, 1985; *Gupta*, 1986, 1990]. However, measurement of background plasma drift in zonal direction is difficult and such observations are not available over Indian longitudes. Therefore, a methodology is evolved based on a few assumptions and a coordinate system in which x, y and z directions are along zonal (positive eastward), meridional (positive northward) and vertical (positive upward) directions respectively. The assumptions are as follows,

i. The zonal solar quiet time $(E_{Sq})_x$ field does not vary much within the altitude region of 100 - 120 km.

ii. The ratio R ($= \sigma_H/\sigma_P$ where σ_H and σ_P are Hall and Pedersen conductivities) remains the same during day and night in all solar epochs.

In the Chapter 3, it is shown that the *Fejer et al.* [2008a] model drifts represent the vertical drifts over the Indian sector well barring early morning hours. Therefore, estimates of nighttime current density are obtained based on above assumptions and the $(E_{Sq})_x$ values corresponding to *Fejer et al.* [2008a] empirical model drifts.

To verify the validity of second assumption, the ratio of the conductivities (R) is estimated using neutral number density and temperature from the NRLMSISE-00 model, geomagnetic field values from IGRF-12 model and measured altitude profiles of electron density. Figure 6.4a depicts the altitude profiles of R during day and nighttimes in solar maximum and minimum conditions. The ratio R is essentially independent of electron density variations. The variations of neutral density during day-night and at different solar epochs are not significant enough to affect R. It is also verified that the R value does not change much even if one uses other neutral density models [e.g., *Jacchia*, 1971] instead of NRLMSISE-00 model. Hence the assumption (ii) is valid for the present purpose of estimation of nighttime current.

Figure 6.4a reveals that the peak R value is close to 30 around 100 *km*. This is similar to the earlier calculation of *Anandarao et al.* [1977], which also reveals that these values of R are nearly same around peak E-region even if one considers the field line integrated values of conductivities. However, the peak height determined by these theoretical calculations is well known [*Forbes*, 1981] to be lower by about 5 km than the height determined from measurements. This R is also shown to be equivalent to the ratio of electric fields in vertical (E_z) and zonal (E_x) directions [*Anandarao et al.*, 1977; *Sekar et al.*, 2013] as follows,

$$R = \frac{E_z}{E_x} = \frac{V_x}{V_z} \tag{6.1}$$

where V_x and V_z are the plasma drifts in zonal and vertical directions respectively.

Therefore, to deduce the altitude profile of R by means of experimental observations, simultaneous measurements of electron ($N_{e,day}$) and current densities ($J_{x,day}$) are used. These values correspond to daytime in high and low solar activity periods. In addition, the vertical plasma drift (V_z) corresponding to the local time of rocket flights have been taken from *Fejer et al.* [2008a] model.

$$R = \frac{V_x}{V_z} = \frac{1}{|\mathbf{e}|}\left(\frac{J_{x,day}}{N_{e,day}}\right)\frac{1}{V_z} \tag{6.2}$$

where **e** is the charge of electron.

Figure 6.4b depicts the altitude profiles of R and its errors in high and low solar activity periods based on the equation (6.2). It is to be noted here that R values below 100 km are not shown as the current density measurements in that altitude region are below the sensitivity limit of the rocket borne magnetometer. From Figure 6.4b, it is clear that the deduced R values remain the same (within the error limits) for both solar epochs. By taking clue from the theoretical calculation on the invariance of R values during day and night in all solar epochs, the average value (R_{avg}) (shown in Figure 6.4c) along with measured nighttime electron density ($N_{e,night}$) and vertical plasma drift ($V_{z,night}$) from *Fejer et al.*

[2008a] model at the time of rocket flight experiment are used to estimate nighttime current density. The following expression is used to calculate the nighttime current density ($J_{x,night}$),

$$J_{x,night} = |\mathbf{e}|\ N_{e,night}\ R_{avg}\ V_{z,night} \tag{6.3}$$

The observed $N_{e,night}$ values and the empirical plasma drift model values of V_z corresponding to that local time are used.

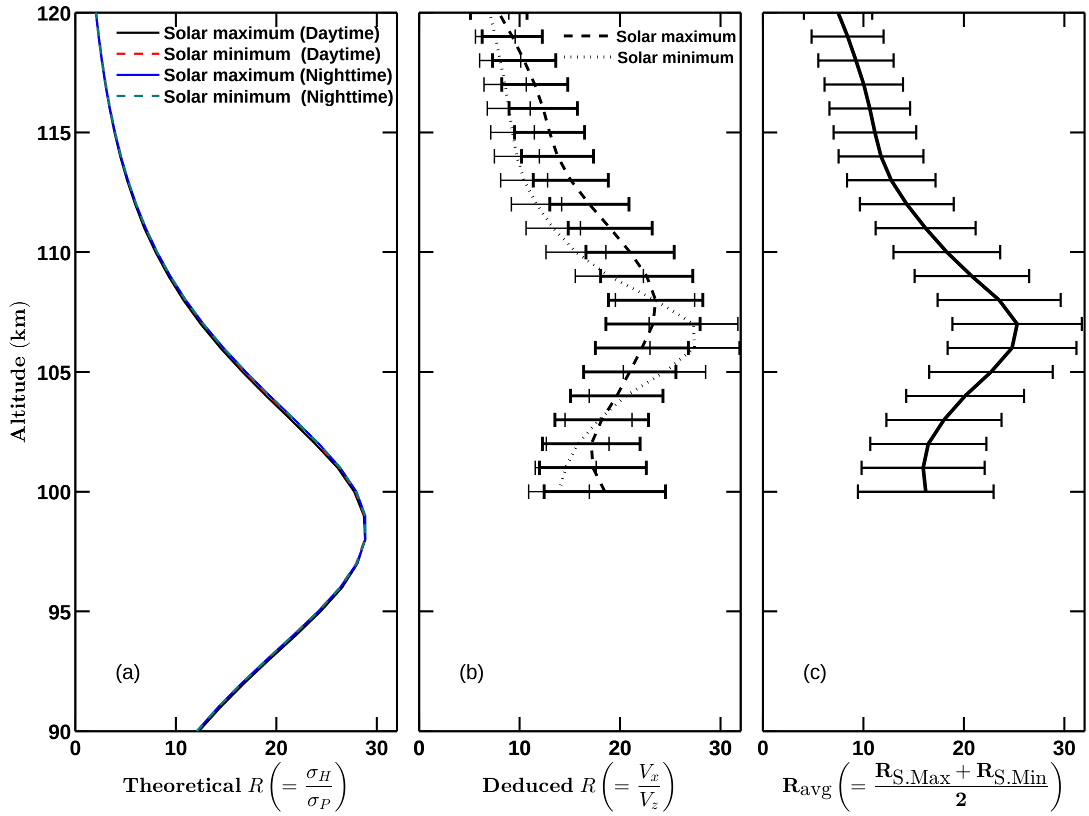

Figure 6.4: Altitude profiles of ratio R obtained based on (a) Hall to Pedersen conductivities during day and night at different solar epoch, (b) equation (6.2), using simultaneous measurements of current and electron density during daytime at high (dotted) and low (dashed) solar activity conditions and vertical drifts from *Fejer et al.* [2008a] model corresponding to the time of rocket flights, (c) The altitude profile of the average values of R shown in Figure 6.4b.

6.3.2 Method-2: Based on the observation of Two-stream waves

As mentioned earlier, the dip equatorial E-region ionosphere is characterized by the generation of Two-stream waves. These plasma waves are essentially generated when electrons stream through the background ions with velocity exceeding ion-acoustic speed [*Farley*, 2009]. The electron densities measured over Thumba at different local times on several nights show [*Prakash et al.*, 1970; *Gupta*, 1986] the presence of Two-stream plasma wave. The threshold plasma drift in the zonal direction needed to trigger the Two-stream waves is given [*Sudan et al.*, 1973] by,

$$V_{x,min} = (1+\chi)c_s \tag{6.4}$$

where c_s is the ion acoustic velocity (330 m/s) of the medium and χ is given by,

$$\chi = \frac{\nu_e \nu_i}{\Omega_e \Omega_i} \tag{6.5}$$

where ν and Ω represent neutral collision and gyro frequencies respectively and subscripts e and i are used for electron and ions respectively.

The $V_{x,min}$ values along with the corresponding electron densities are used to have the physical estimate of minimum strength of current density ($J_{x,night,min}$) that must be present over the altitude range where presence of Two-stream waves was observed using following expression.

$$J_{x,night,min} = |\mathbf{e}|\ N_{e,night}\ (1+\chi)c_s \tag{6.6}$$

The observed $N_{e,night}$ values are used from those rocket flights that detected Two-stream waves.

6.3.3 Method-3: Based on the equatorial electrojet model

The details of a equatorial electrojet developed earlier by *Anandarao* [1976] are provided in the Chapter 2. This model is used, without invoking the wind effects, to calculate the nighttime current density in the zonal direction with the inputs of previously mentioned electron density profiles and E-region Sq electric field values. Based on the earlier works [*Richmond*, 1973; *Anandarao*, 1976; *Anandarao and Raghavarao*, 1987; *Raghavarao and Anandarao*, 1987] during daytime, the contributions of horizontal winds and shears in them to the zonal current densities over the dip equator are not found to be significant and are well within the estimation uncertainty. In the absence of systematic measurements of vertical winds in the E-region during nighttime, the contribution of vertical wind to the current density estimates could not be determined.

The inputs to the model are altitude profile of electron densities and $(E_{Sq})_x$ value at a particular time for which the model calculation is made. Further, the same electron density profile is used at all the latitudes. These inputs are taken from the in situ measurements of electron densities during nighttime [*Subbaraya et al.*, 1983, 1985; *Gupta*, 1986, 1990] and the empirical model of plasma drift [*Fejer et al.*, 2008a] over the dip equator corresponding to Indian longitude. In addition to these, NRLMSISE-00 model of neutral density and temperature along with IGRF-12 model of geomagnetic field are used for the evaluation of ionospheric conductivities.

Based on sensitivity studies performed in Chapter 2, it is found that the maximum uncertainties in the nighttime zonal current density (J_x) and vertical polarization electric field (E_z) over the dip-equator are less than 21% and 14% respectively.

6.4 Estimation of induced magnetic field

The magnetic fields induced at ground by ionospheric currents are computed based on the method described Chapter 2 (equation 2.16). The uncertainty in the computed magnetic field is less than 22% (see section 2.1.4 of Chapter 2).

6.5 Results and discussion

As mentioned in section 6.3.1, Figure 6.4 shows that R does not change significantly with respect to day and nighttime conditions and solar epochs. This aspect is used subsequently to derive the nighttime E-region current over the Indian sector.

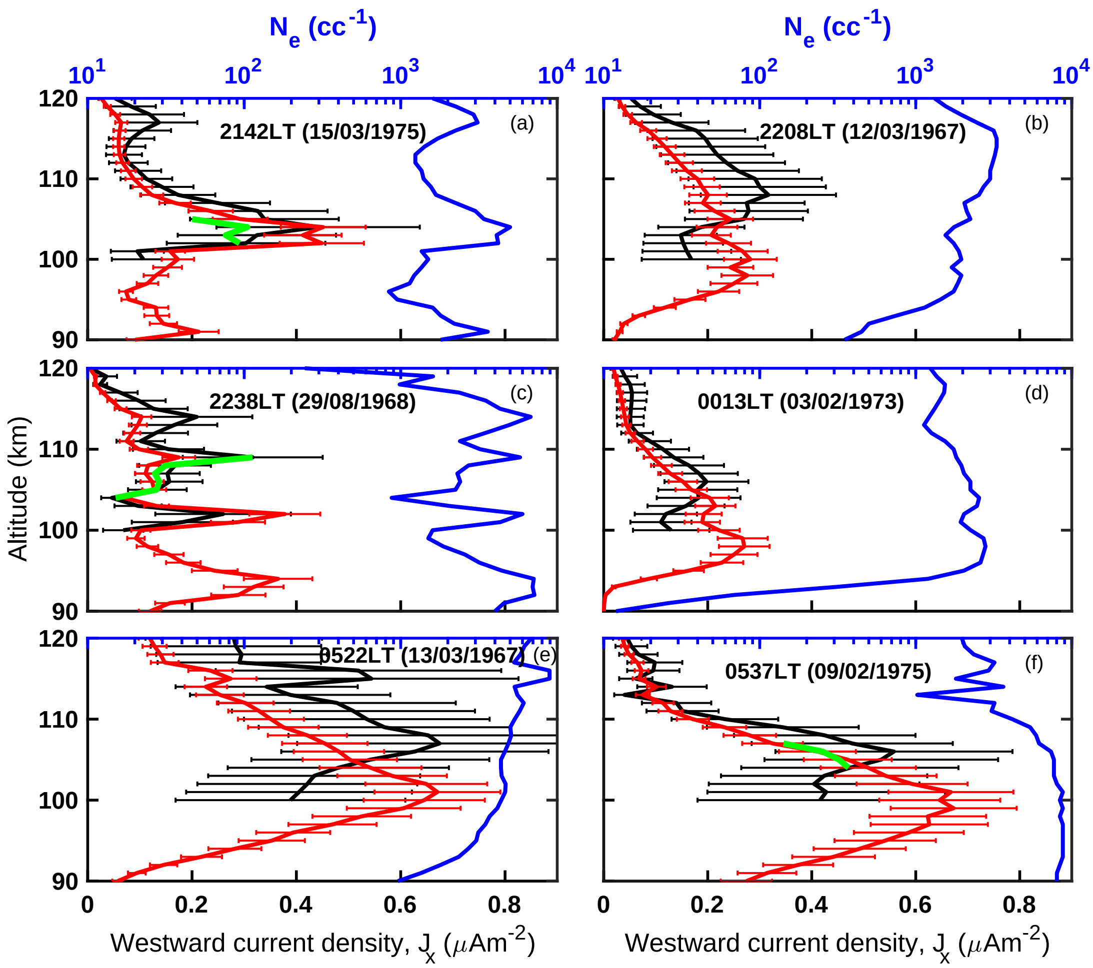

Figure 6.5: Altitude profiles of estimated nighttime current densities (black) using method 1 and equation (6.3), the measured electron density profiles (blue curves) and R_{avg} values (see Figure 6.4c). The altitude profiles of nighttime current densities over the dip equator (red colours) using the electrojet model of *Anandarao* [1976]. The minimum current density (green) obtained using method 2 and equation (6.6) over the altitude wherein presence of Two-stream waves was observed. Subplots (a, b, c and d) correspond to the profiles at various local times when the nighttime electron density measurements over Thumba during magnetically quiet conditions were available.

Figure 6.5 depicts the altitude profiles of westward current densities during nighttime for geomagnetically quiet conditions estimated using the deduced R_{avg} values (black) using equation (6.3), and electrojet model (red) described in Chapter 2, over the dip-equator. The corresponding electron densities measured over Thumba at different local times on a few nights are overlaid on this figure (blue coloured curves). In addition, minimum current densities ($J_{x,night,min}$) estimated using equation (6.6) are also plotted in Figure 6.5 (green coloured curves) over the altitude range wherever the Two-stream plasma waves were observed. The nighttime current density ranges from ~0.3 μAm^{-2} near midnight to ~0.7 μAm^{-2} during early morning hours. The electrojet model estimated current densities match well (within the uncertainty limits) with the deduced current density above altitude region of 100 km.

The present investigation of the estimation of nighttime current density is based on the in-situ electron density measurements conducted at different solar epochs and seasons. Thus, it is rather difficult to bring out the local time variation of nighttime current density as the electron density (N_e) and Sq electric fields (E_{Sq}) vary with these geophysical conditions. Nevertheless, comparison of these current densities in the subplots of Figure 6.5 advances our understanding in the following ways,

1. The peak altitudes (see black curves of subplots 6.5b and 6.5d - f) of the current density deduced using method 1 lie closer to the altitude of 107 km corresponding to the peak value of R whenever the altitude profiles of electron density are devoid of large structures between 100 km and 110 km. Thus, the values of R_{avg} remains nearly constant. Therefore, the peak values of current density ($J_{x,max}$) are found to vary, from one case to another, linearly with the variations of N_e and V_z at the peak altitude. The values given in Table 6.1 (obtained using method 1) are found to be consistent with this inference. For example, by comparing cases 2 and 5 in Table 6.1, the change in J_x is found to be almost doubled when N_e is nearly doubled without considerable change in V_z.

Case No.	Time and date	Altitude of peak J_x h_p (km)	N_e (cc^{-1}) at h_p	R_{avg} at h_p	Downward V_z (ms^{-1})	Westward $J_{x,max}$ (μAm^{-2})
1	2142 on 15/03/1975	104	5000	20.1	27.4	0.44
2	2208 on 12/03/1967	108	2540	23.5	33.1	0.32
3	2238 on 29/08/1968	109	5790	20.8	16.4	0.32
4	0013 on 03/02/1973	106	2240	24.8	22.2	0.20
5	0522 on 13/03/1967	107	4880	25.3	34.1	0.67
6	0537 on 09/02/1975	106	7356	24.8	19.1	0.56

Table 6.1: The derived values of westward peak current density ($J_{x,max}$) using method 1, altitude (h_p) of $J_{x,max}$, measured electron density (N_e) at h_p, deduced R_{avg} at h_p and downward vertical drift (V_z) based on empirical model corresponding to the six rocket flights under consideration.

2. In the absence of altitudinal structures, the altitude gradients in J_x profiles (above and/or below $J_{x,max}$) obtained using the methods 1 and 3 are found to be larger whenever the J_x values are more (subplots 6.5e and 6.5f) compared to corresponding gradients whenever the J_x values are small (subplots 6.5b and 6.5d). This is consistent with the work of *Onwumechili* [1992b] where the strength and thickness of electrojet current density based on daytime measurements over the dip-equator were shown to be inversely proportional. However, it must be noted here that the multiple layers in current density (subplots 6.5a and 6.5c) are often observed during nighttime and determination of the thickness of the peak current layer is not unambiguous.

3. In the presence of large structures in N_e profile between 100 km and 110 km (subplots 6.5a and 6.5c), the current density maximizes at the altitude wherever electron densities and R_{avg} values are optimum. Thus, the peak current density need not lie around 107 km (refer cases 1 and 3 of Table 6.1).

4. In the presence of multiple layers in current density profile whenever the electron density is structured (subplots 6.5a and 6.5c), the altitude of peak current density can be identified using method 2, as the Two-stream waves observed by rocket borne measurements usually appear in the vicinity of the peak current.

5. The peak altitudes determined by method 3 are lower than those obtained by the other methods whenever the electron densities are devoid of large structures. However, the altitude profiles of the current densities obtained from all the three methods go nearly hand-in-hand with one another whenever the altitude structures in N_e are present.

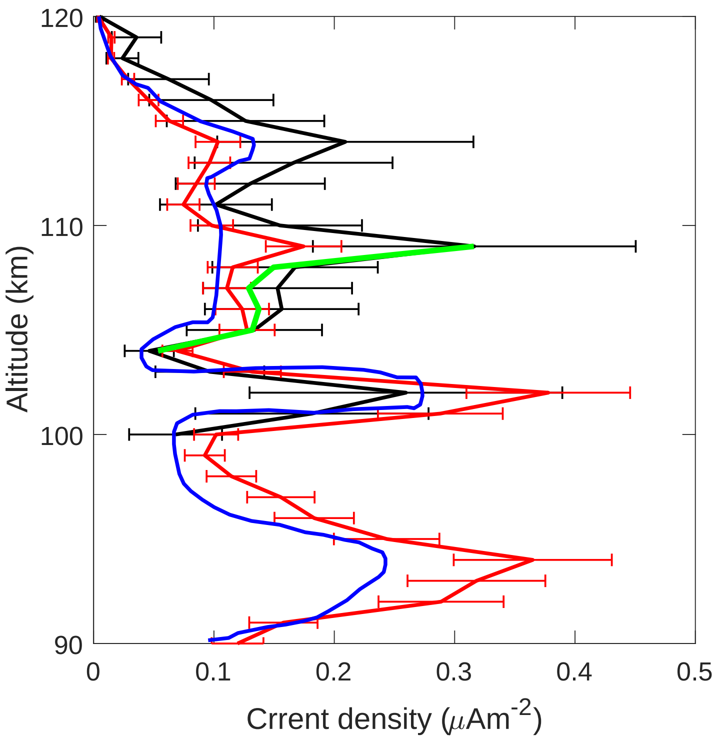

Figure 6.6: Altitude profile of current density obtained corresponding to 2238 LT based on Methods-1 (black), 2 (green) and 3 (red), and that estimated by *Stening and Winch* [1987] in blue.

The blue coloured curve in Figure 6.6 depicts the altitude profile of current density estimated by *Stening and Winch* [1987]. This estimation was based on westward electric field of 0.3 mVm^{-1} and electron density profile [*Prakash et al.*, 1970] obtained using rocket flight experiment conducted at 2238 LT on 29 August 1968 from Thumba. In the present investigation, the estimates of westward current density based on this electron density profile are estimated using three methods (see Figure 6.5c). The values obtained using these three methods are overlaid in Figure 6.6. It is to be noted that, around the electrojet altitudes (~105 km) the nighttime current density estimated by *Stening and Winch* [1987] are smaller than those obtained in the present investigation. Those estimates are significantly smaller than the minimum westward current density obtained based on Two-stream waves criteria (green coloured curve). This is probably because of smaller value of zonal electric field used by *Stening and Winch* [1987] to compute the nighttime current density. The electric field assumed by *Stening and Winch* [1987] is insufficient to generate Two-stream waves. However, the observation revealed the presence of Two-stream wave on this night.

In addition to the altitudinal structure in the current densities, the electrojet model provides latitudinal extents also. As mentioned earlier the altitude profiles of electron densities and the $(E_{Sq})_x$ from plasma drift model are given as inputs to the electrojet model. Figure 6.7 represents the contour plots of westward current densities over the magnetic latitude-altitude plane. The colourbar in Figure 6.7 corresponds to the strength of current densities. As the sensitivity study revealed that maximum progressive uncertainty in the current density obtained by combining the individual uncertainties of all input parameters is less than 21%, the difference between successive contours in each subplot is kept at 30% of the corresponding peak current density values over the dip equator.

Islands of current density contours are seen in subplots 6.7a and 6.7c. These distinct islands are missing in subplot 6.7e and 6.7f. They are more conspicuous only when the input electron densities have altitudinal structures. As a result, the altitude of peak current densities is not well defined. However, when the input electron densities have less structures the peak current altitude is well defined and island structures (in the altitude-latitude plane) disappear (subplots 6.7d - f). Hence, the effect of electron density structures in nighttime electrojet current needs further attention.

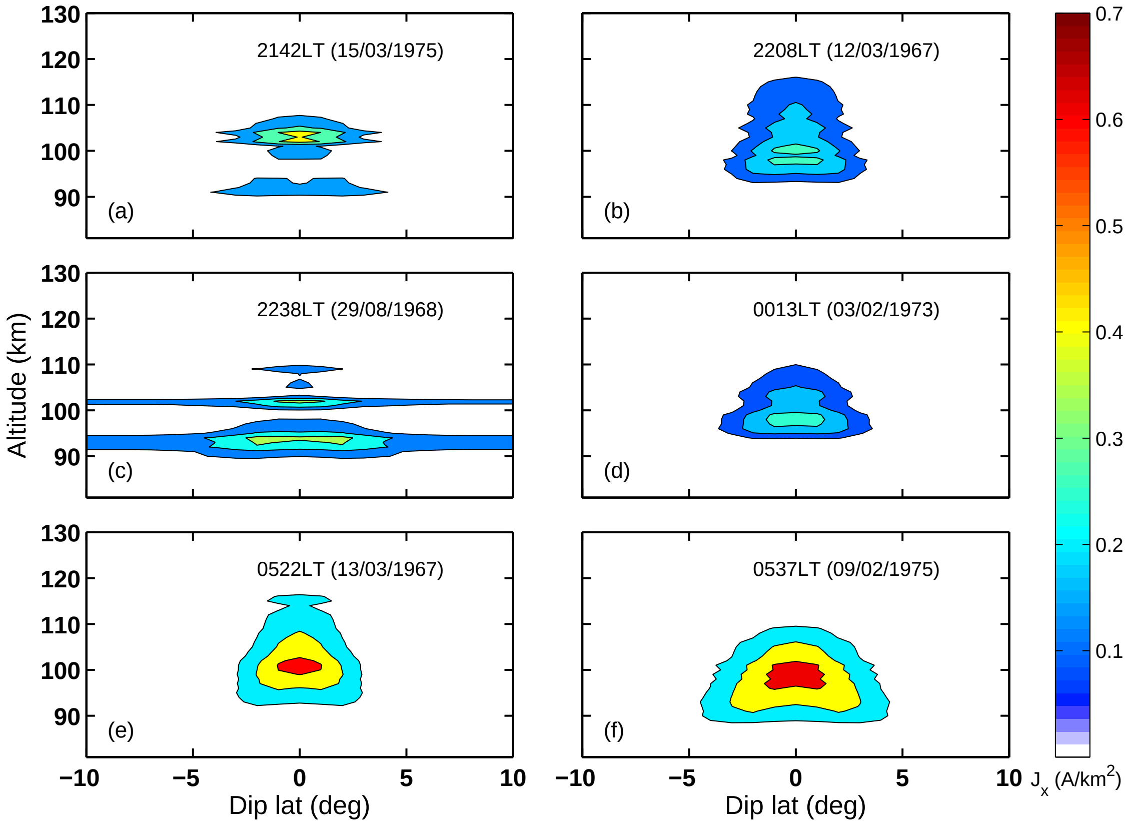

Figure 6.7: Contours of iso-current density in zonal direction over magnetic latitude-altitude region obtained using electrojet model of *Anandarao* [1976] and measured electron density profiles (blue) over the dip equator. In this model calculation, zonal Sq electric field is chosen from the empirical model of plasma drift [*Fejer et al.*, 2008a] over Indian longitude. The colourbar represent strength current density (A/km^2). Current density contours in each subplot are plotted with steps of 30% of peak values over the dip equator. Subplots (a, b, c and d) correspond to iso-current contours corresponding to electron density measurement at different local times on a few nights.

In order to examine this effect, the altitude structures in electron densities measured at 2238 LT on 29 August, 1968 are gradually smoothed by Savitzky-Golay method [*Savitzky and Golay*, 1964] in the altitude range of 90 to 120 km. These electron density profiles along with a single value of $(E_{Sq})_x$ are used as input to the electrojet model and the corresponding current density profiles are obtained. Figure 6.8 depicts the resulting iso-current density contours along with the input electron density values. Without smoothing the electron density profile, the island structures and larger latitudinal extent are observed (see Figure 6.8a) in current density contours. Allowing more than 10 km structures between 90 and 120 km, the gaps between the islands have reduced and the latitudinal extent of the second island around 100 km has considerably reduced (see Figure 6.8b). On further smoothing of the electron density, the reduction in the latitudinal extent of current density and disappearance of island structures are noticed in Figure 6.8c. Therefore, the valley and peak in the altitude profile of electron density in region of 90 to 120 km appears to decide the gap between the islands and latitudinal extent of contours representing current density.

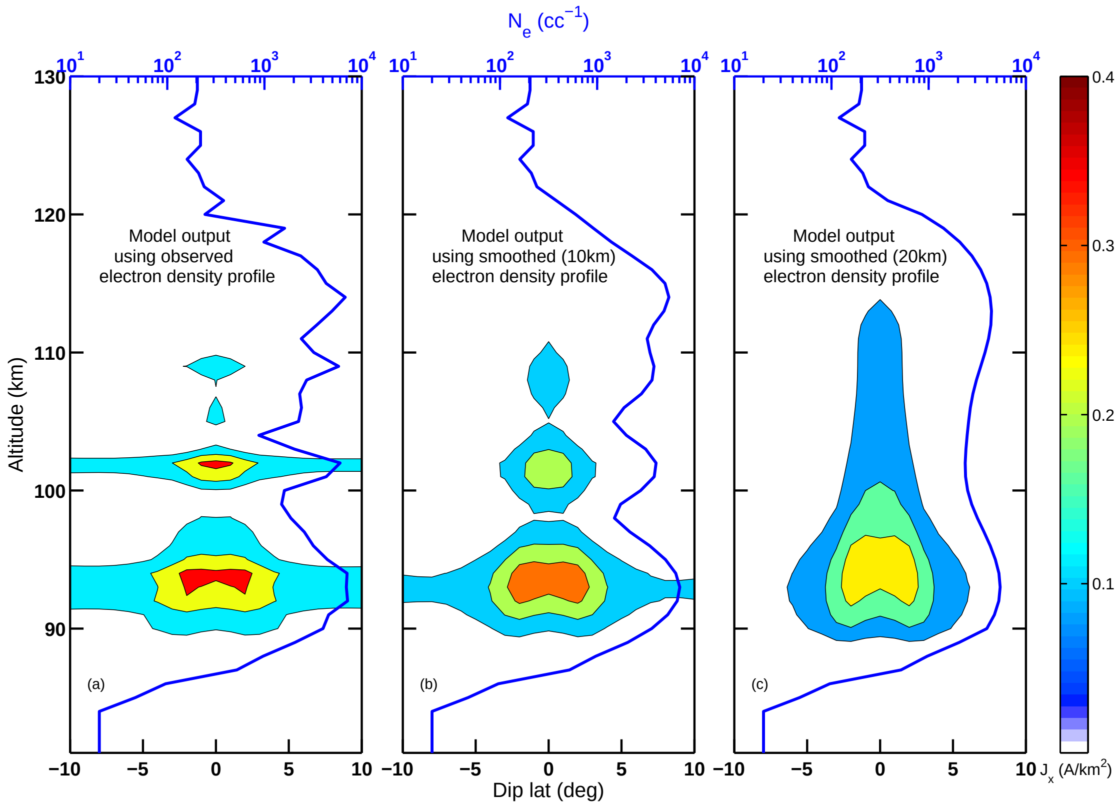

Figure 6.8: (a) High resolution plots of iso-current density contours given in subplot 6.6c. The input electron density profile (blue) is also overlaid. (b) and (c) Iso-current density profiles after progressively smoothing the electron density profile shown in subplot a) and using them as the input for current density calculation. The corresponding input electron density profiles are also shown in each subplot. Current density contours in each subplot are plotted with steps of 30% of the peak current values over the dip equator. Note: Colourbar scales are adjusted to bring out the features in current density contours.

Based on the current density estimates by the electrojet model, the horizontal component (H) of the magnetic field induced at ground are calculated (based on method described in section 2.1.2 of Chapter 2) for all the cases depicted in Figure 6.7. These calculated magnetic fields with uncertainties (marked in orange colour within red circles) are shown along with the hourly variations in the electrojet strength (represented by black line), derived on the basis of magnetic field measurements, in Figure 6.9. The strength of horizontal component of magnetic field induced at ground by these equatorial currents are estimated based on the magnetic field measurements over dip-equatorial station Trivandrum (TRD) and off-equatorial station Alibag (ABG) (for details see section 2.5 of Chapter 2). The hourly values of observed magnetic field induced by the electrojet current on these days are depicted with black coloured curves.

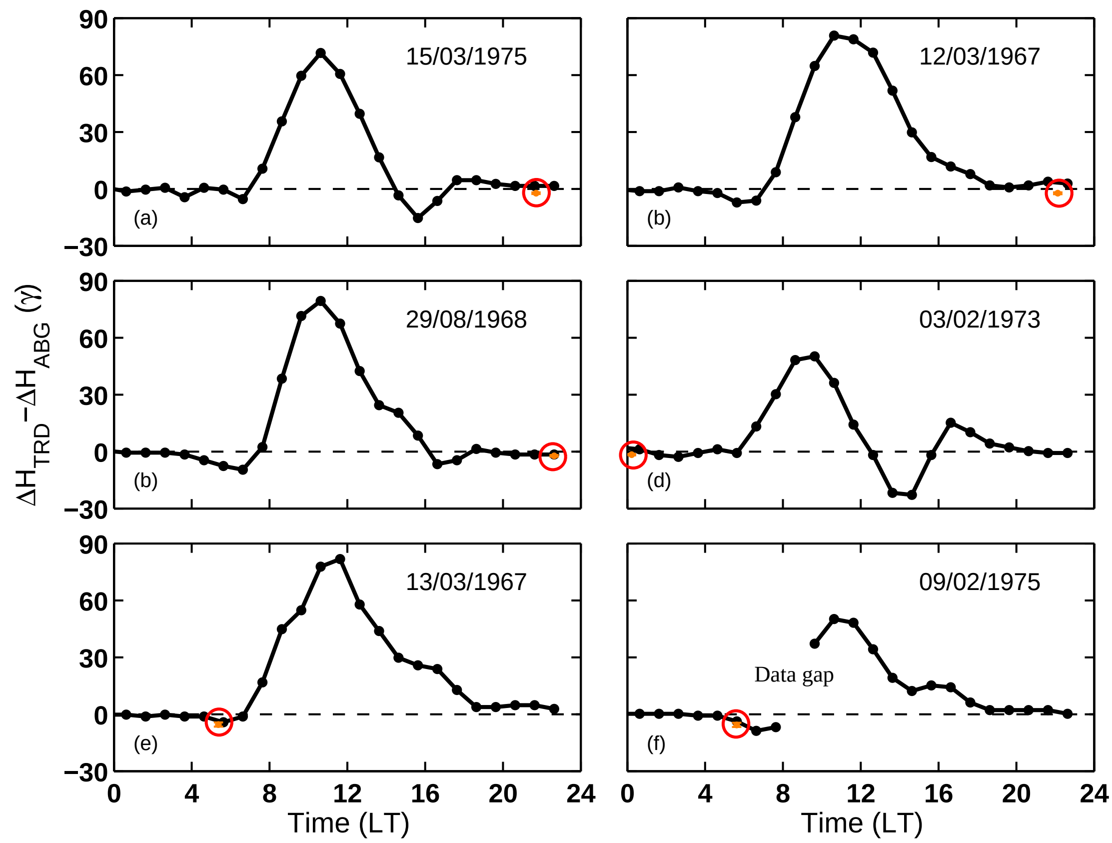

Figure 6.9: Ground-based magnetometer measured hourly variation electrojet strength over Thumba ($\Delta H_{TRD} - \Delta H_{ABG}$ in black). Orange dots correspond to the calculated horizontal component of magnetic field induced over ground by the nighttime current densities shown in figure 6.7.

It is well known [*Raghavarao et al.*, 1984] that during nighttime there is a valley in the altitude profile of the electron density centered around 125 - 130 km. In order to investigate the effect of this valley region on the polarization field in vertical direction (E_z), an exercise is carried out using the electrojet model with varying depth of the valley. For this investigation, the electron density measurement obtained at 2238 LT on 29 August, 1968 is first smoothed and then used as input to the electrojet model with varying depth in the valley region. Figure 6.10 depicts the resulting contours of polarization field in vertical direction (E_z), wherein 20% difference of the peak values are maintained by different contours. However, there is no appreciable change in current densities around 105 km (not shown). It is found that E_z increases around 125 km when there is a deep valley while it is progressively decreasing as depth of the valley region decreases. Further, the minimum strength of polarization electric field in vertical direction required for the generation of Two-stream waves is about 13.8 mVm^{-1} ($E_z = V_{x,min} \times B$) at 105 km.

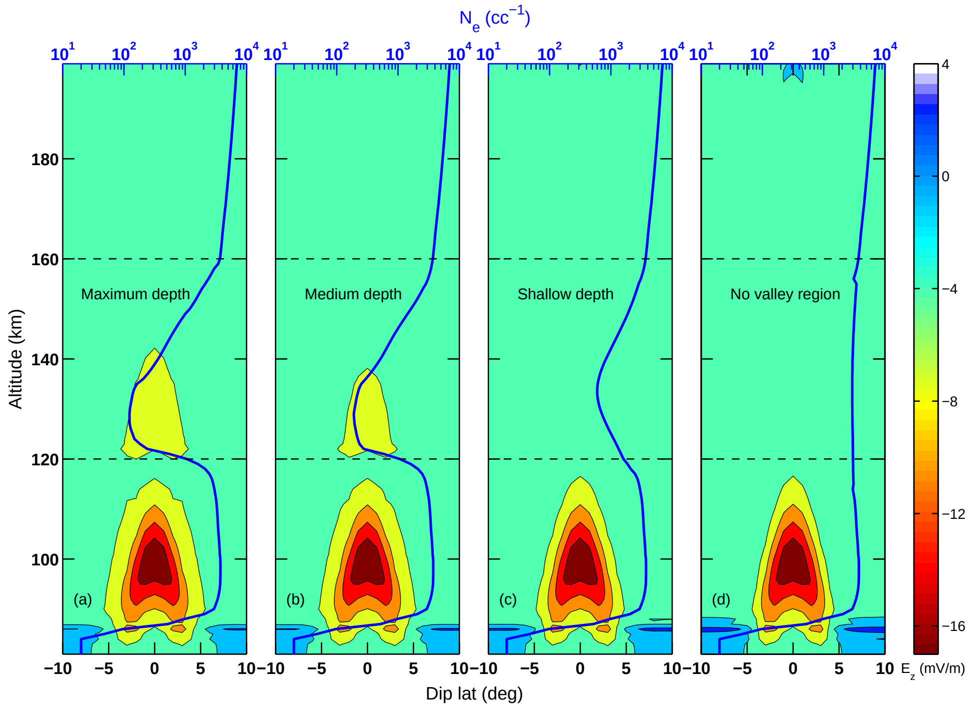

Figure 6.10: Effects of the depth of the valley region on the polarization electric field in vertical direction (E_z in mVm^{-1}) for (a) maximum, (b) medium, (c) shallow depth and (d) no valley region. Electric field contours in each subplot are plotted with steps of 20% of peak values over the dip equator.

The electrojet model calculated E_z values, near the altitude region wherein the presence of Two-stream waves was observed during measurements, (as provided in Table 6.2) are found to be consistent with requirement for generation of Two-stream waves in those altitude region barring a case during morning hours. This is probably due to the fact that the *Fejer et al.* [2008a] model values deviate from the measurements during sunrise time in winter (as mentioned in section 6.3.1).

Time and date	$\mathbf{E_x}$ **($\mathbf{mVm^{-1}}$)**	$\mathbf{E_z}$ **($\mathbf{mVm^{-1}}$)**
2142 on 15/03/1975	−1.03	−18.7
2238 on 29/08/1968	−0.62	−19.1
0537 on 09/02/1975	−0.72	−13.4

Table 6.2: The values of polarization field in vertical direction (E_z in $\mathbf{mVm^{-1}}$) obtained using electrojet model closer to the altitude of observation of Two-stream waves and zonal Sq electric field used in the model calculations for the profiles of N_e used in this measurement wherein the presence of Two-stream waves was observed.

This investigation suggests that the nighttime base value of the horizontal component of magnetic field during geomagnetically quiet period over the Indian dip equatorial sector is well within 6 nT if one considers pre-midnight to early morning hours. However, during magnetically disturbed periods, the horizontal magnetic field may change during midnight hours in varying degrees owing to the alteration of ionospheric electric field or modulation of the magnetospheric current systems. Under such circumstances, it is important that these aspects are taken into account before any realistic estimation is made on the nighttime E-region current over the dip equatorial region.

6.6 Summary

The salient points that emerged from the present investigation are as follows,

1. The nighttime current density deduced from the available electron density measurements as well as an electrojet model reveals E-region current in the range of $\sim$0.3 - 0.7 μAm^{-2} during pre-midnight to early morning hours on geomagnetically quiet days.

2. The nocturnal E-region current density strength seems to decrease from the post-sunset hours to the midnight hours and then increase during early morning hours.

3. Altitude structures are seen in the nighttime E-region current density and are shown to be associated with the altitude structures in the electron density.

4. The trough and crest in the altitude structures of the electron density seem to decide the latitudinal extent and altitudinal stratification of the nighttime E-region current density.

5. The dip equatorial polarization field in vertical direction obtained from the electrojet model is shown to be sufficient to drive the observed Two-stream waves during nighttime in a limited altitude region around 105 km barring a case during early morning hours. The current density estimated using the Two-stream wave criterion is found to be well within the estimated currents.

6. The ground magnetometer observed magnetic field variations during quiet time are well within 6 nT and match fairly well with the calculated induced magnetic field deduced from the current density (obtained from electrojet model).

7. The well-known dip equatorial nighttime E-region valley in the electron density around 130 km is shown to increase the polarization field in vertical direction near this altitude depending upon the depth of the valley.

Chapter 7

Future scope

In the present thesis work, efforts are made to address a few scientific problems pertaining to low-latitude ionosphere electric fields under geomagnetically quiet and disturbed conditions. In addition, scientific understanding has been gained on some of the unresolved long standing problems on equatorial E-region currents. During these investigations, a few scientific problems have also emerged which need critical attention in the future. These problems are briefly discussed below.

Though longitudinal structures in ionospheric parameters have been reported earlier [e.g. *Sagawa et al.*, 2005; *Kil et al.*, 2007; *Alken and Maus*, 2010], the vertical drifts are averaged over 15° or 30° longitude bins to develop the global empirical models [*Scherliess and Fejer*, 1999; *Fejer et al.*, 2008a]. Therefore, at the times of large longitudinal gradients, these models may not efficiently represent the vertical drifts over a particular region. This is noticed for the Indian sector during early morning hours. At this local time, it is difficult to obtain the vertical drifts either by using F-layer movement owing to presence of plasma production processes or by using electrojet strengths owing their minuscule amplitudes. Therefore, further investigations are needed to bring out a clear picture of vertical drifts during early morning hours.

In general, the pre-reversal enhancement (PRE) is observed in vertical drifts around sunset hours. However, during June solstice in solar minimum, the PRE is found to be absent over some of the longitude sectors [*Scherliess and Fejer*, 1999; *Oyekola*, 2006], and even the reversed PRE like signatures are noticed over the Indian [*Subbarao and Krishna Murthy*, 1994] and African [*Oyekola et al.*, 2007] sectors. Simulations of suppressed PRE are available in literature [*Fesen et al.*, 2000; *Millward et al.*, 2001]. However, the modelling studies are required to understand the generation of reversed PRE.

In Chapter 4, it is shown that at least the quiet time CEJ events that occur during afternoon hours over Indian sector in June solstice under solar minimum are part of the Sq current system. In future, detailed investigations are needed to addresses this issue for CEJ events that occur during morning hours.

In general, the recovery phase a geomagnetic storm is not free from prompt penetration events. Therefore, it is challenging job to estimate the reductions in low latitude electric fields driven by the disturbance dynamo (DD) based on the observations. The changes in electric fields can be affected by enhanced or reduced tidal activities or contributions of higher order tides. These changes can act in tandem with DD or opposite to it, as noticed on some cases presented in Chapter 5. Therefore, the problem of estimating the DD perturbations becomes even more complex. Therefore, in order to estimate the DD perturbations, the detailed modelling investigations are needed to account for changes in electric field driven by variabilities in tidal activities.

As a follow up of the disturbance dynamo study on three extreme cases discussed in Chapter 5, the electric field perturbations on can be examined using ionosonde data from Trivandrum. This will throw light on the effects of disturbance dynamo on the equatorial ionosphere during evening and post-sunset hours.

Earlier investigations on dip-equatorial E-region current density during night time were sparse [*Davis et al.*, 1967; *Shuman*, 1970; *Sastry*, 1970; *Stening and Winch*, 1987]. Its estimates are obtained (see Chapter 6) by making use of the snapshot measurements of electron density profiles obtained on some geomagnetically quiet nights. Therefore, a detailed investigation is needed to estimate the dip-equatorial E-region current density throughout the night. In view of availability of the CHAMP satellite data, further investigations on nighttime current can be carried out to confirm the results obtained during this doctoral work.

Though the meridional and zonal winds do not affect the current calculations over the dip-equator, their contributions may not be negligible at off-equatorial latitudes. Attempts can be made to estimate these off-equatorial currents and the corresponding magnetic field can be compared with the ground based magnetometer measurements.

In future, investigations are required to understand the ionospheric electrodynamics during sunset/sunrise times, the effects due to longitudinal variations of ionospheric parameters and the nighttime electron density structures using modified models with appropriate observations.

Bibliography

Abdu, M. A. (2012), Equatorial spread F/plasma bubble irregularities under storm time disturbance electric fields, *Journal of Atmospheric and Solar-Terrestrial Physics*, *75-76*, 44–56, https://doi.org/10.1016/j.jastp.2011.04.024.

Abdu, M. A., Sobral, J. H. A., Richards, P., deGonzalez, M. M., Huang, Y. N., Reddy, B. M., Cheng, K., Szuszczewicz, E. P., and Batista, I. S. (1996), Zonal/meridional wind and disturbance dynamo electric field control of the low-latitude ionosphere based on the SUNDIAL/ATLAS 1 Campaign, *Journal of Geophysical Research: Space Physics*, *101*(A12), 26,729–26,740, https://doi.org/10.1029/96JA00321.

Abdu, M. A., Sastri, J. H., MacDougall, J., Batista, I. S., and Sobral, J. H. A. (1997), Equatorial disturbance dynamo electric field longitudinal structure and spread F: A case study from GUAR/EITS Campaigns, *Geophysical Research Letters*, *24*(13), 1707–1710, https://doi.org/10.1029/97GL01465.

Abdu, M. A., Batista, I. S., Takahashi, H., MacDougall, J., Sobral, J. H., Medeiros, A. F., and Trivedi, N. B. (2003), Magnetospheric disturbance induced equatorial plasma bubble development and dynamics: A case study in Brazilian sector, *Journal of Geophysical Research: Space Physics*, *108*(A12), https://doi.org/10.1029/2002JA009721.

Abdu, M. A., De Souza, J. R., Sobral, J. H. A., and Batista, I. S. (2006), Magnetic storm associated disturbance dynamo effects in the low and equatorial latitude ionosphere, *Recurrent magnetic storms: corotating solar wind Streams*, pp. 283–304, https://doi.org/10.1029/167GM22.

Aggarwal, M., Joshi, H. P., Iyer, K. N., Kwak, Y. S., Lee, J. J., Chandra, H., and Cho, K. S. (2012), Day-to-day variability of equatorial anomaly in GPS-TEC during low solar activity period, *Advances in Space Research*, *49*(12), 1709–1720, http://dx.doi.org/10.1016/j.asr.2012.03.005.

Akasofu, S., and Chapman, S. (1961), The ring current, geomagnetic disturbance, and the Van Allen radiation belts, *Journal of Geophysical Research*, *66*(5), 1321–1350, https://doi.org/10.1029/JZ066i005p01321.

Alken, P. (2009), A quiet time empirical model of equatorial vertical plasma drift in the Peruvian sector based on 150 km echoes, *Journal of Geophysical Research: Space Physics*, *114*(A2), https://doi.org/10.1029/2008JA013751.

Alken, P., and Maus, S. (2010), Electric fields in the equatorial ionosphere derived from CHAMP satellite magnetic field measurements, *Journal of Atmospheric and Solar-Terrestrial Physics*, *72*(4), 319–326, https://doi.org/10.1016/j.jastp.2009.02.006.

Amory-Mazaudier, C., Bolaji, O. S., and Doumbia, V. (2017), On the historical origins of the CEJ, DP2, and Ddyn current systems and their roles in the predictions of ionospheric responses to geomagnetic storms at equatorial latitudes, *Journal of Geophysical Research: Space Physics*, *122*(7), 7827–7833, https://doi.org/10.1002/2017JA024132.

Anandarao, B. G. (1976), Effects of gravity wave winds and wind shears on equatorial electrojet, *Geophysical Research Letters*, *3*(9), 545–548, http://dx.doi.org/10.1029/GL003i009p00545.

Anandarao, B. G. (1977), Studies on the dynamics of the equatorial ionosphere, Ph.D. thesis, Gujarat University.

Anandarao, B. G., and Raghavarao, R. (1987), Structural changes in the currents and fields of the equatorial electrojet due to zonal and meridional winds, *Journal of Geophysical Research*, *92*(A3), 2514–2526, http://dx.doi.org/10.1029/JA092iA03p02514.

Anandarao, B. G., Desai, J. N., Giles, M., Martelli, G., Raghavarao, R., and Rothwell, P. (1977), Electric field in the equatorial ionosphere, *Journal of Atmospheric and Terrestrial Physics*, *39*(8), 927–931, https://doi.org/10.1016/0021-9169(77)90174-X.

Anderson, D., Anghel, A., Chau, J., and Veliz, O. (2004), Daytime vertical E×B drift velocities inferred from ground-based magnetometer observations at low latitudes, *Space Weather*, *2*(11), http://dx.doi.org/10.1029/2004SW000095.

Anderson, D. N. (1973), A theoretical study of the ionospheric F region equatorial anomaly-I. Theory, *Planetary and Space Science*, *21*(3), 409–419, http://dx.doi.org/10.1016/0032-0633(73)90040-8.

Andriyas, T., and Andriyas, S. (2015), Relevance vector machines as a tool for forecasting geomagnetic storms during years 1996-2007, *Journal of Atmospheric and Solar-Terrestrial Physics*, *125-126*, 10–20, https://doi.org/10.1016/j.jastp.2015.02.005.

Appleton, E. V. (1946), Two Anomalies in the Ionosphere, *Nature*, *157*, 691, https://doi.org/10.1038/157691a0.

Baker, W. G., and Martyn, D. F. (1953), Electric currents in the ionosphere - The conductivity, *Philosophical Transactions of the Royal Society of London A*, *246*(913), 281–294, http://dx.doi.org/10.1098/rsta.1953.0016.

Balan, N., Jayachandran, B., Balachandran Nair, R., Namboothiri, S. P., Bailey, G. J., and Rao, P. B. (1992), HF Doppler observations of vector plasma drifts in the evening F-region at the magnetic equator, *Journal of Atmospheric and Terrestrial Physics*, *54*(1112), 1545–1554, http://dx.doi.org/10.1016/0021-9169(92)90162-E.

Balan, N., Souza, J., and Bailey, G. J. (2018), Recent developments in the understanding of equatorial ionization anomaly: A review, *Journal of Atmospheric and Solar-Terrestrial Physics*, *171*, 3–11, https://doi.org/10.1016/j.jastp.2017.06.020.

Balsley, B. B. (1964), Evidence of a stratified echoing region at 150 kilometers in the vicinity of the magnetic equator during daylight hours, *Journal of Geophysical Research*, *69*(9), 1925–1930, https://doi.org/10.1029/JZ069i009p01925.

Balsley, B. B. (1969), Some characteristics of non-two-stream irregularities in the equatorial electrojet, *Journal of Geophysical Research*, *74*(9), 2333–2347, https://doi.org/10.1029/JA074i009p02333.

Balsley, B. B., and Farley, D. T. (1971), Radar studies of the equatorial electrojet at three frequencies, *Journal of Geophysical Research*, *76*(34), 8341–8351, https://doi.org/10.1029/JA076i034p08341.

Bhardwaj, S. K., and Subba Rao, P. B. V. (2017), The afternoon counter-electrojet current system along the 75°E meridian during the IEEY, *Earth, Planets and Space*, *69*(1), 91, https://doi.org/10.1186/s40623-017-0675-6.

Bhargava, B. N., and Sastri, N. S. (1979), Some Characteristics of the occurrence of the afternoon counter-electrojet events in the India region, *Journal of geomagnetism and geoelectricity*, *31*(2), 97–101, http://dx.doi.org/10.5636/jgg.31.97.

Bhattacharyya, A., and Okpala, K. C. (2015), Principal components of quiet time temporal variability of equatorial and low-latitude geomagnetic fields, *Journal of Geophysical Research*, *120*(10), 8799–8809, http://dx.doi.org/10.1002/2015JA021673.

Bibl, K., and Reinisch, B. W. (1978), The universal digital ionosonde, *Radio Science*, *13*(3), 519–530, https://doi.org/10.1029/RS013i003p00519.

Bilitza, D. (1990), International reference ionosphere 1990, *NSSDC/WDC-A-R&S 90-22. National Space Science Data Center, Greenbelt.*

Bilitza, D., and Reinisch, B. W. (2008), International Reference Ionosphere 2007: Improvements and new parameters, *Advances in Space Research*, *42*(4), 599–609, https://doi.org/10.1016/j.asr.2007.07.048.

Bittencourt, J. A., and Abdu, M. A. (1981), A theoretical comparison between apparent and real vertical ionization drift velocities in the equatorial F region, *Journal of Geophysical Research*, *86*(A4), 2451–2454, http://dx.doi.org/10.1029/JA086iA04p02451.

Blanc, M., and Richmond, A. D. (1980), The ionospheric disturbance dynamo, *Journal of Geophysical Research*, *85*(A4), 1669–1686, http://dx.doi.org/10.1029/JA085iA04p01669.

Bowles, K. L. (1958), Observation of Vertical-Incidence Scatter from the Ionosphere at 41 Mc/sec, *Physical Review Letters*, *1*, 454–455, https://doi.org/10.1103/PhysRevLett.1.454.

Bowles, K. L., Cohen, R., Ochs, R., G., and Balsley, B. B. (1960), Radio echoes from field-aligned ionization above the magnetic equator and their resemblance to auroral echoes, *Journal of Geophysical Research*, *65*(6), 1853–1855, https://doi.org/10.1029/JZ065i006p01853.

Buneman, O. (1963), Excitation of Field Aligned Sound Waves by Electron Streams, *Physical Review Letters*, *10*, 285–287, https://doi.org/10.1103/PhysRevLett.10.285.

Butler, A. H., Sjoberg, J. P., Seidel, D. J., and Rosenlof, K. H. (2017), A sudden stratospheric warming compendium, *Earth System Science Data*, *9*(1), 63–76, https://doi.org/10.5194/essd-9-63-2017.

Cain, J. C., and Sweeney, R. E. (1973), The POGO data, *Journal of Atmospheric and Terrestrial Physics*, *35*(6), 1231–1247, http://dx.doi.org/10.1016/0021-9169(73)90021-4.

Campbell, W. H. (1973), The field levels near midnight at low and equatorial geomagnetic stations, *Journal of Atmospheric and Terrestrial Physics*, *35*, 1127–1146, http://dx.doi.org/10.1016/0021-9169(73)90010-X.

Campbell, W. H. (1979), Occurrence of AE and Dst geomagnetic index levels and the selection of the quietest days in a year, *Journal of Geophysical Research*, *84*(A3), 875–881, http://dx.doi.org/10.1029/JA084iA03p00875.

Chakrabarty, D., Sekar, R., Narayanan, R., Devasia, C. V., and Pathan, B. M. (2005), Evidence for the interplanetary electric field effect on the OI 630.0

nm airglow over low latitude, *Journal of Geophysical Research: Space Physics*, *110*(A11), https://doi.org/10.1029/2005JA011221.

Chakrabarty, D., Sekar, R., Sastri, J. H., and Ravindran, S. (2008), Distinctive effects of interplanetary electric field and substorm on nighttime equatorial F layer: A case study, *Geophysical Research Letters*, *35*(19), https://doi.org/10.1029/2008GL035415.

Chakrabarty, D., Sekar, R., Sastri, J. H., Pathan, B. M., Reeves, G. D., Yumoto, K., and Kikuchi, T. (2010), Evidence for OI 630.0 nm dayglow variations over low latitudes during onset of a substorm, *Journal of Geophysical Research: Space Physics*, *115*(A10), https://doi.org/10.1029/2010JA015643.

Chakrabarty, D., Fejer, B. G., Gurubaran, S., Pant, T. K., Abdu, M. A., and Sekar, R. (2014), On the pre-midnight ascent of F-layer in the June solstice during the deep solar minimum in 2008 over the Indian sector, *Journal of Atmospheric and Solar-Terrestrial Physics*, *121, Part B*, 177–187, http://dx.doi.org/10.1016/j.jastp.2014.01.002.

Chakrabarty, D., Rout, D., Sekar, R., Narayanan, R., Reeves, G. D., Pant, T. K., Veenadhari, B., and Shiokawa, K. (2015), Three different types of electric field disturbances affecting equatorial ionosphere during a long-duration prompt penetration event, *Journal of Geophysical Research: Space Physics*, *120*(6), 4993–5008, https://doi.org/10.1002/2014JA020759.

Chakrabarty, D., Hui, D., Rout, D., Sekar, R., Bhattacharyya, A., Reeves, G. D., and Ruohoniemi, J. M. (2017), Role of IMF By in the prompt electric field disturbances over equatorial ionosphere during a space weather event, *Journal of Geophysical Research: Space Physics*, *122*(2), 2574–2588, https://doi.org/10.1002/2016JA022781.

Chandra, H., Rastogi, R. G., Choudhary, R. K., and Sharma, S. (2016), Equatorial electrojet in the Indian region during the geomagnetic storm of 13 - 14 November 1998, *Journal of Earth System Science*, *125*(3), 669–675, https://doi.org/10.1007/s12040-016-0683-0.

Chapman, S. (1951), The equatorial electrojet as detected from the abnormal electric current distribution above Huancayo, Peru, and elsewhere, *Archiv für Meteorologie, Geophysik und Bioklimatologie, Serie A*, *4*(1), 368–390, https://doi.org/10.1007/BF02246814.

Chau, J. L., and Woodman, R. F. (2004), Daytime vertical and zonal velocities from 150-km echoes: Their relevance to F-region dynamics, *Geophysical Research Letters*, *31*(17), http://dx.doi.org/10.1029/2004GL020800.

Chau, J. L., Fejer, B. G., and Goncharenko, L. P. (2009), Quiet variability of equatorial E×B drifts during a sudden stratospheric warming event, *Geophysical Research Letters*, *36*(5), http://dx.doi.org/10.1029/2008GL036785.

Chau, J. L., Goncharenko, L. P., Fejer, B. G., and Liu, H.-L. (2012), Equatorial and low latitude ionospheric effects during sudden stratospheric warming events, *Space Science Reviews*, *168*(1), 385–417, https://doi.org/10.1007/s11214-011-9797-5.

Cohen, R., and Bowles, K. L. (1963), The association of plane-wave electron density irregularities with the equatorial electrojet, *Journal of Geophysical Research*, *68*(9), 2503–2525, http://dx.doi.org/10.1029/JZ068i009p02503.

Cohen, R., and Bowles, K. L. (1967), Secondary irregularities in the equatorial electrojet, *Journal of Geophysical Research*, *72*(3), 885–894, https://doi.org/10.1029/JZ072i003p00885.

Davis, T. N., and Sugiura, M. (1966), Auroral electrojet activity index AE and its universal time variations, *Journal of Geophysical Research*, *71*(3), 785–801, http://dx.doi.org/10.1029/JZ071i003p00785.

Davis, T. N., Burrows, K., and Stolarik, J. D. (1967), A latitude survey of the equatorial electrojet with rocket-borne magnetometers, *Journal of Geophysical Research*, *72*(7), 1845–1861, http://dx.doi.org/10.1029/JZ072i007p01845.

Deepa, V., Ramkumar, G., Antonita, M., Kumar, K. K., and Sasi, M. N. (2006), Vertical propagation characteristics and seasonal variability of tidal wind oscillations in the MLT region over Trivandrum (8.5°N, 77°E): First results from SKiYMET meteor radar, *Annales Geophysicae*, *24*(11), 2877–2889, https://www.ann-geophys.net/24/2877/2006/.

Eccles, J. V., St. Maurice, J. P., and Schunk, R. W. (2015), Mechanisms underlying the prereversal enhancement of the vertical plasma drift in the low-latitude ionosphere, *Journal of Geophysical Research*, *120*(6), 4950–4970, http://dx.doi.org/10.1002/2014JA020664.

Egedal, J. (1947), The magnetic diurnal variation of the horizontal force near the magnetic equator, *Terrestrial Magnetism and Atmospheric Electricity*, *52*(4), 449–451, http://dx.doi.org/10.1029/TE052i004p00449.

England, S. L., Maus, S., Immel, T. J., and Mende, S. B. (2006), Longitudinal variation of the E-region electric fields caused by atmospheric tides, *Geophysical Research Letters*, *33*(21), https://doi.org/10.1029/2006GL027465.

Farley, D. T. (1963), A plasma instability resulting in field-aligned irregularities in the ionosphere, *Journal of Geophysical Research*, *68*(22), 6083–6097, https://doi.org/10.1029/JZ068i022p06083.

Farley, D. T. (2009), The equatorial E-region and its plasma instabilities: a tutorial, *Annales Geophysicae*, *27*(4), 1509–1520, http://dx.doi.org/10.5194/angeo-27-1509-2009.

Fejer, B. G. (1981), The equatorial ionospheric electric fields. A review, *Journal of Atmospheric and Terrestrial Physics*, *43*(5), 377–386, https://doi.org/10.1016/0021-9169(81)90101-X.

Fejer, B. G., and Kelley, M. C. (1980), Ionospheric irregularities, *Reviews of Geophysics*, *18*(2), 401–454, http://dx.doi.org/10.1029/RG018i002p00401.

Fejer, B. G., and Scherliess, L. (1995), Time dependent response of equatorial ionospheric electric fields to magnetospheric disturbances, *Geophysical Research Letters*, *22*(7), 851–854, https://doi.org/10.1029/95GL00390.

Fejer, B. G., Paula, E. R., Gonzáez, S. A., and Woodman, R. F. (1991), Average vertical and zonal F region plasma drifts over Jicamarca, *Journal of Geophysical Research: Space Physics*, *96*(A8), 13,901–13,906, https://doi.org/10.1029/91JA01171.

Fejer, B. G., de Paula, E. R., Scherliess, L., and Batista, I. S. (1996), Incoherent scatter radar, ionosonde, and satellite measurements of equatorial F region vertical plasma drifts in the evening sector, *Geophysical Research Letters*, *23*(14), 1733–1736, http://dx.doi.org/10.1029/96GL01847.

Fejer, B. G., Jensen, J. W., and Su, S.-Y. (2008a), Quiet time equatorial F region vertical plasma drift model derived from ROCSAT-1 observations, *Journal of Geophysical Research*, *113*(A5), http://dx.doi.org/10.1029/2007JA012801.

Fejer, B. G., Jensen, J. W., and Su, S.-Y. (2008b), Seasonal and longitudinal dependence of equatorial disturbance vertical plasma drifts, *Geophysical Research Letters*, *35*(20), L20,106, http://dx.doi.org/10.1029/2008GL035584.

Fejer, B. G., Olson, M. E., Chau, J. L., Stolle, C., Lühr, H., Goncharenko, L. P., Yumoto, K., and Nagatsuma, T. (2010), Lunar-dependent equatorial ionospheric electrodynamic effects during sudden stratospheric warmings, *Journal of Geophysical Research*, *115*(A8), http://dx.doi.org/10.1029/2010JA015273.

Fejer, B. G., Hui, D., Chau, J. L., and Kudeki, E. (2014), Altitudinal dependence of evening equatorial F region vertical plasma drifts, *Journal of Geophysical Research: Space Physics*, *119*(7), 5877–5890, http://dx.doi.org/10.1002/2014JA019949.

Fejer, B. G., Blanc, M., and Richmond, A. D. (2017), Post-storm middle and low-latitude ionospheric electric fields effects, *Space Science Reviews*, *206*(1), 407–429, https://doi.org/10.1007/s11214-016-0320-x.

Fesen, C. G., Crowley, G., Roble, R. G., Richmond, A. D., and Fejer, B. G. (2000), Simulation of the pre-reversal enhancement in the low latitude vertical ion drifts, *Geophysical Research Letters*, *27*(13), 1851–1854, http://dx.doi.org/10.1029/2000GL000061.

Forbes, J. M. (1981), The equatorial electrojet, *Reviews of Geophysics*, *19*(3), 469–504, http://dx.doi.org/10.1029/RG019i003p00469.

Forbes, J. M., and Lindzen, R. S. (1976), Atmospheric solar tides and their electrodynamic effects-II. The equatorial electrojet, *Journal of Atmospheric and Terrestrial Physics*, *38*(9), 911–920, http://dx.doi.org/10.1016/0021-9169(76)90074-X.

Francey, R. J. (1970), Electron production in the ionospheric D region by cosmic X rays, *Journal of Geophysical Research*, *75*(25), 4849–4862, https://doi.org/10.1029/JA075i025p04849.

Fuller-Rowell, T. J., Millward, G. H., Richmond, A. D., and Codrescu, M. V. (2002), Storm-time changes in the upper atmosphere at low latitudes, *Journal of Atmospheric and Solar-Terrestrial Physics*, *64*(12), 1383–1391, https://doi.org/10.1016/S1364-6826(02)00101-3.

Gordon, W. E. (1958), Incoherent scattering of radio waves by free electrons with applications to space exploration by radar, *Proceedings of the IRE*, *46*(11), 1824–1829, http://dx.doi.org/10.1109/JRPROC.1958.286852.

Gouin, P. (1962), Reversal of the magnetic daily variation at Addis Ababa, *Nature*, *193*, 1145–1146, https://doi.org/10.1038/1931145a0.

Gouin, P., and Mayaud, P. N. (1967), A propos de l'existence possible d'un contre electrojet aux latitudes magnetiques equatoriales, *Ann. Geophys.*, *23*, 41–47.

Gupta, S. P. (1986), Formation of sporadic E layers at low magnetic latitudes, *Planetary and Space Science*, *34*(11), 1081–1085, http://dx.doi.org/10.1016/0032-0633(86)90019-X.

Gupta, S. P. (1990), Ionisation layers over the magnetic equator during meteor shower days, *Advances in Space Research*, *10*(10), 105–108, http://dx.doi.org/10.1016/0273-1177(90)90016-S.

Gupta, S. P. (1997), Features of E region irregularities at the magnetic equator and in its vicinity, *Advances in Space Research*, *20*(11), 2195–2198, http://dx.doi.org/10.1016/S0273-1177(97)00670-4.

Gupta, S. P. (2000), Two stream instability in E region over magnetic equator during morning hours, *Advances in Space Research*, *26*(8), 1257–1261, http://dx.doi.org/10.1016/S0273-1177(99)01212-0.

Gupta, S. P. (2001), Collected Works. Physical Research Laboratory, India.

Gupta, S. P., and Prakash, S. (1979), Experimental evidence of ion plasma oscillations in the apogee region of the Nike-Apache rocket, *Planetary and Space Science*, *27*(2), 145–150, http://dx.doi.org/10.1016/0032-0633(79)90044-8.

Gupta, S. P., Sekar, R., and Acharya, Y. B. (2004), In situ measurements of sub-meter plasma waves over low-latitude ionosphere during Leonid-99 meteor storm, *Annales Geophysicae*, *22*(6), 2033–2036, https://www.ann-geophys.net/22/2033/2004/.

Gurubaran, S. (2002), The equatorial counter electrojet: Part of a worldwide current system?, *Geophysical Research Letters*, *29*(9), http://dx.doi.org/10.1029/2001GL014519.

Gurubaran, S., Sathishkumar, S., and Veenadhari, B. (2016), On the role of atmospheric tides in the quiet-time variabilities of equatorial electrojet, *Journal of Indian Geophysical Union*, *Special Volume-2*, 87–98.

Haerendel, G., and Eccles, J. V. (1992), The role of the equatorial electrojet in the evening ionosphere, *Journal of Geophysical Research*, *97*(A2), 1181–1192, http://dx.doi.org/10.1029/91JA02227.

Haerendel, G., Lüst, R., and Rieger, E. (1967), Motion of artificial ion clouds in the upper atmosphere, *Planetary and Space Science*, *15*(1), 1–18, https://doi.org/10.1016/0032-0633(67)90062-1.

Hagan, M. E., and Forbes, J. M. (2002), Migrating and nonmigrating diurnal tides in the middle and upper atmosphere excited by tropospheric latent heat release, *Journal of Geophysical Research: Atmospheres*, *107*(D24), https://doi.org/10.1029/2001JD001236.

Hagan, M. E., Maute, A., Roble, R. G., Richmond, A. D., Immel, T. J., and England, S. L. (2007), Connections between deep tropical clouds and the Earth's ionosphere, *Geophysical Research Letters*, *34*(20), https://doi.org/10.1029/2007GL030142.

Hanson, W. B., and Heelis, R. A. (1975), Techniques for measuring bulk gas-motions from satellites, *Space Science Instrumentation*, *1*, 493–524.

Hanson, W. B., and Moffett, R. J. (1966), lonization transport effects in the equatorial F region, *Journal of Geophysical Research*, *71*(23), 5559–5572, http://dx.doi.org/10.1029/JZ071i023p05559.

Hanson, W. B., Cragin, B. L., and Dennis, A. (1986), The effect of vertical drift on the equatorial F-region stability, *Journal of Atmospheric and Terrestrial Physics*, *48*(3), 205–212, https://doi.org/10.1016/0021-9169(86)90095-4.

Hanuise, C., Mazaudier, C., Vila, P., Blanc, M., and Crochet, M. (1983), Global dynamo simulation of ionospheric currents and their connection with the equatorial electrojet and counter electrojet: A case study, *Journal of Geophysical Research*, *88*(A1), 253–270, http://dx.doi.org/10.1029/JA088iA01p00253.

Henderson, M. G., Reeves, G. D., Belian, R. D., and Murphree, J. S. (1996), Observations of magnetospheric substorms occurring with no apparent solar wind/IMF trigger, *Journal of Geophysical Research: Space Physics*, *101*(A5), 10,773–10,791, https://doi.org/10.1029/96JA00186.

Huang, C. M. (2013), Disturbance dynamo electric fields in response to geomagnetic storms occurring at different universal times, *Journal of Geophysical Research: Space Physics*, *118*(1), 496–501, http://dx.doi.org/10.1029/2012JA018118.

Huang, C. M., and Chen, M. Q. (2008), Formation of maximum electric potential at the geomagnetic equator by the disturbance dynamo, *Journal of Geophysical Research: Space Physics*, *113*(A3), http://dx.doi.org/10.1029/2007JA012843.

Huang, C.-S. (2012), Statistical analysis of dayside equatorial ionospheric electric fields and electrojet currents produced by magnetospheric substorms during sawtooth events, *Journal of Geophysical Research: Space Physics*, *117*(A2), https://doi.org/10.1029/2011JA017398.

Huang, C.-S., Foster, J. C., Goncharenko, L. P., Reeves, G. D., Chau, J. L., Yumoto, K., and Kitamura, K. (2004), Variations of low-latitude geomagnetic fields and Dst index caused by magnetospheric substorms, *Journal of Geophysical Research: Space Physics*, *109*(A5), https://doi.org/10.1029/2003JA010334.

Huang, C.-S., Foster, J. C., and Kelley, M. C. (2005), Long-duration penetration of the interplanetary electric field to the low-latitude ionosphere during the main phase of magnetic storms, *Journal of Geophysical Research: Space Physics*, *110*(A11), http://dx.doi.org/10.1029/2005JA011202.

Huba, J. D., and Joyce, G. (2007), Equatorial spread F modeling: Multiple bifurcated structures, secondary instabilities, large density bite-outs, and supersonic flows, *Geophysical Research Letters*, *34*(7), https://doi.org/10.1029/2006GL028519.

Huba, J. D., Lyon, J. G., and Hassam, A. B. (1987), Theory and simulation of the Rayleigh-Taylor instability in the limit of large Larmor radius, *Physical Review Letters*, *59*, 2971–2974, https://link.aps.org/doi/10.1103/PhysRevLett.59.2971.

Huba, J. D., Joyce, G., Sazykin, S., Wolf, R., and Spiro, R. (2005), Simulation study of penetration electric field effects on the low- to mid-latitude ionosphere, *Geophysical Research Letters*, *32*(23), https://doi.org/10.1029/2005GL024162.

Huba, J. D., Joyce, G., and Krall, J. (2008), Three-dimensional equatorial spread F modeling, *Geophysical Research Letters*, *35*(10), https://doi.org/10.1029/2008GL033509.

Hui, D., and Fejer, B. G. (2015), Daytime plasma drifts in the equatorial lower ionosphere, *Journal of Geophysical Research*, *120*(11), 9738–9747, http://dx.doi.org/10.1002/2015JA021838.

Hui, D., Chakrabarty, D., Sekar, R., Reeves, G. D., Yoshikawa, A., and Shiokawa, K. (2017), Contribution of storm time substorms to the prompt electric field disturbances in the equatorial ionosphere, *Journal of Geophysical Research: Space Physics*, *122*(5), 5568–5578, https://doi.org/10.1002/2016JA023754.

Hutton, R., and Oyinloye, J. O. (1970), The counter-electrojet in Nigeria, *Ann. Geophys.*, *26*, 921–926.

Immel, T. J., Sagawa, E., England, S. L., Henderson, S. B., Hagan, M. E., Mende, S. B., Frey, H. U., Swenson, C. M., and Paxton, L. J. (2006), Control of equatorial ionospheric morphology by atmospheric tides, *Geophysical Research Letters*, *33*(15), https://doi.org/10.1029/2006GL026161.

Iyer, K. N., Deshpande, M. R., and Rastogi, R. G. (1976), The equatorial anomaly in ionospheric total electron content and the equatorial electrojet current strength, *Proceedings of the Indian Academy of Sciences-Section A*, *84*(4), 129–138, https://doi.org/10.1007/BF03046803.

Jacchia, L. G. (1971), Revised Static Models of the Thermosphere and Exosphere with Empirical Temperature Profiles, *Smithsonian Astrophysical Observatory (SAO) Special Report*, *332*.

Jadhav, G., Rajaram, M., and Rajaram, R. (2002), A detailed study of equatorial electrojet phenomenon using Ørsted satellite observations, *Journal of Geophysical Research*, *107*(A8), 1175, http://dx.doi.org/10.1029/2001JA000183.

Janzhura, A., Troshichev, O., and Stauning, P. (2007), Unified PC indices: Relation to isolated magnetic substorms, *Journal of Geophysical Research: Space Physics*, *112*(A9), http://dx.doi.org/10.1029/2006JA012132.

Johnson, J. R., and Wing, S. (2014), External versus internal triggering of substorms: An information-theoretical approach, *Geophysical Research Letters*, *41*(16), 5748–5754, https://doi.org/10.1002/2014GL060928.

Kakad, B., Tiwari, D., and Pant, T. K. (2012), Study of post sunset vertical plasma drift at equatorial F-region using long-term (1990-2003) ionosonde measurements in Indian longitude, *Journal of Atmospheric and Solar-Terrestrial Physics*, *80*, 239–246, http://dx.doi.org/10.1016/j.jastp.2012.02.004.

Kelley, M. C. (2009), The Earth's Ionosphere: Electrodynamics and Plasma Physics, *Academic Press*.

Kelley, M. C., Makela, J. J., Chau, J. L., and Nicolls, M. J. (2003), Penetration of the solar wind electric field into the magnetosphere/ionosphere system, *Geophysical Research Letters*, *30*(4), https://doi.org/10.1029/2002GL016321.

Kikuchi, T., Lühr, H., Kitamura, T., Saka, O., and Schlegel, K. (1996), Direct penetration of the polar electric field to the equator during a DP 2 event as detected by the auroral and equatorial magnetometer chains and the EISCAT radar, *Journal of Geophysical Research: Space Physics*, *101*(A8), 17,161–17,173, http://dx.doi.org/10.1029/96JA01299.

Kikuchi, T., Hashimoto, K. K., Kitamura, T.-I., Tachihara, H., and Fejer, B. (2003), Equatorial counterelectrojets during substorms, *Journal of Geophysical Research*, *108*(A11), http://dx.doi.org/10.1029/2003JA009915.

Kil, H., Oh, S.-J., Kelley, M. C., Paxton, L. J., England, S. L., Talaat, E., Min, W., K., and Su, S.-Y. (2007), Longitudinal structure of the vertical E×B drift and ion density seen from ROCSAT-1, *Geophysical Research Letters*, *34*(14), https://doi.org/10.1029/2007GL030018.

Kil, H., Talaat, E. R., Oh, S.-J., Paxton, L. J., England, S. L., and Su, S.-Y. (2008), Wave structures of the plasma density and vertical E×B drift in low-latitude F region, *Journal of Geophysical Research: Space Physics*, *113*(A9), http://dx.doi.org/10.1029/2008JA013106.

Kil, H., Oh, J., S., Paxton, L. J., and Fang, W., T. (2009), High-resolution vertical E×B drift model derived from ROCSAT-1 data, *Journal of Geophysical Research: Space Physics*, *114* (A10), https://doi.org/10.1029/2009JA014324.

Kivelson, M. G., and Russell, C. (1995), *Introduction to space physics*, Cambridge university press.

Klimenko, M. V., Klimenko, V. V., and Karpachev, A. T. (2012), Formation mechanism of additional layers above regular F2 layer in the near-equatorial ionosphere during quiet period, *Journal of Atmospheric and Solar-Terrestrial Physics*, *90-91*, 179–185, http://dx.doi.org/10.1016/j.jastp.2012.02.011.

Kobea, A. T., Richmond, A. D., Emery, B. A., Peymirat, C., Lühr, H., Moretto, T., Hairston, M., and Amory-Mazaudier, C. (2000), Electrodynamic coupling of high and low latitudes: Observations on May 27, 1993, *Journal of Geophysical Research*, *105* (A10), 22,979–22,989, http://dx.doi.org/10.1029/2000JA000058.

Krishna Murthy, B. V., and Hari, S. S. (1996), Electric fields in the low latitude F-region, *Advances in Space Research*, *18* (6), 93–98, http://dx.doi.org/10.1016/0273-1177(95)00906-X.

Krishna Murthy, B. V., Hari, S. S., and Somayajulu, V. V. (1990), Nighttime equatorial thermospheric meridional winds from ionospheric h'F data, *Journal of Geophysical Research: Space Physics*, *95* (A4), 4307–4310, http://dx.doi.org/10.1029/JA095iA04p04307.

Krishna Murthy, B. V., Ravindran, S., Viswanathan, K. S., Subbarao, K. S. V., Patra, A. K., and Rao, P. B. (1998), Small-scale (∼3 m) E region irregularities at and off the magnetic equator, *Journal of Geophysical Research*, *103* (A9), 20,761–20,773, http://dx.doi.org/10.1029/98JA00928.

Kudeki, E., and Fawcett, C. D. (1993), High resolution observations of 150 km echoes at Jicamarca, *Geophysical Research Letters*, *20* (18), 1987–1990, http://dx.doi.org/10.1029/93GL01256.

Le, G., Slavin, J. A., and Strangeway, R. J. (2010), Space Technology 5 observations of the imbalance of regions 1 and 2 field-aligned currents and its implication to the cross-polar cap Pedersen currents, *Journal of Geophysical Research: Space Physics*, *115*(A7), https://doi.org/10.1029/2009JA014979.

Le Huy, M., and Amory-Mazaudier, C. (2005), Magnetic signature of the ionospheric disturbance dynamo at equatorial latitudes: "Ddyn", *Journal of Geophysical Research: Space Physics*, *110*(A10), http://dx.doi.org/10.1029/2004JA010578.

Lin, C. H., Wang, W., Hagan, M. E., Hsiao, C. C., Immel, T. J., Hsu, M. L., Liu, J. Y., Paxton, L. J., Fang, T. W., and Liu, C. H. (2007), Plausible effect of atmospheric tides on the equatorial ionosphere observed by the FORMOSAT-3/COSMIC: Three-dimensional electron density structures, *Geophysical Research Letters*, *34*(11), https://doi.org/10.1029/2007GL029265.

Liu, J.-M., Zhang, B.-C., Kamide, Y., Wu, Z.-S., Hu, Z.-J., and Yang, H.-G. (2011), Spontaneous and trigger-associated substorms compared: Electrodynamic parameters in the polar ionosphere, *Journal of Geophysical Research: Space Physics*, *116*(A1), https://doi.org/10.1029/2010JA015773.

Lühr, H., and Manoj, C. (2013), The complete spectrum of the equatorial electrojet related to solar tides: CHAMP observations, *Annales Geophysicae*, *31*(8), 1315–1331, https://doi.org/10.5194/angeo-31-1315-2013.

Lühr, H., Maus, S., and Rother, M. (2004), Noon-time equatorial electrojet: Its spatial features as determined by the CHAMP satellite, *Journal of Geophysical Research*, *109*(A1), http://dx.doi.org/10.1029/2002JA009656.

Lühr, H., Rother, M., Häusler, K., Alken, P., and Maus, S. (2008), The influence of nonmigrating tides on the longitudinal variation of the equatorial electrojet, *Journal of Geophysical Research: Space Physics*, *113*(A8), https://doi.org/10.1029/2008JA013064.

MacDougall, J. W., Grant, I. F., and Shen, X. (1995), The Canadian advanced digital ionosonde: design and results, *URSI INAG Ionospheric Station Inf. Bulletin, UAG-104*.

Madhav Haridas, M. K., Manju, G., and Pant, T. K. (2015), On the solar activity variations of nocturnal F region vertical drifts covering two solar cycles in the Indian longitude sector, *Journal of Geophysical Research*, *120*(2), 1445–1451, http://dx.doi.org/10.1002/2014JA020561.

Marcos, F., Bowman, B., and Sheehan, R. (2006), Accuracy of Earth's thermospheric neutral density models, in *AIAA/AAS Astrodynamics Specialist Conference and Exhibit*, p. 6167.

Marriott, R. T., Richmond, A. D., and Venkateswaran, S. V. (1979), The quiet-time equatorial electrojet and counter-electrojet, *Journal of geomagnetism and geoelectricity*, *31*(3), 311–340, doi:https://doi.org/10.5636/jgg.31.311.

Matsushita, S. (1968), Sq and L current systems in the ionosphere, *Geophysical Journal of the Royal Astronomical Society*, *15*(1-2), 109–125.

Matsushita, S. (1971), Interactions Between the Ionosphere and the Magnetosphere for Sq and L Variations, *Radio Science*, *6*(2), 279–294, http://dx.doi.org/10.1029/RS006i002p00279.

Matsushita, S., and Maeda, H. (1965), On the geomagnetic solar quiet daily variation field during the IGY, *Journal of Geophysical Research*, *70*(11), 2535–2558, http://dx.doi.org/10.1029/JZ070i011p02535.

Mayaud, P. N. (1976), Magnetospheric and night-time induced effects in the regular daily variation S_R, *Planetary and Space Science*, *24*, 1049–1057, http://dx.doi.org/10.1016/0032-0633(76)90123-9.

McPherron, R. L., Russell, C. T., and Aubry, M. P. (1973), Satellite studies of magnetospheric substorms on August 15, 1968: 9. Phenomenological model for substorms, *Journal of Geophysical Research*, *78*(16), 3131–3149, https://doi.org/10.1029/JA078i016p03131.

Millward, G. H., Mller-Wodarg, I. C. F., Aylward, A. D., Fuller-Rowell, T. J., Richmond, A. D., and Moffett, R. J. (2001), An investigation into the influence of tidal forcing on F region equatorial vertical ion drift using a global ionosphere-thermosphere model with coupled electrodynamics, *Journal of Geophysical Research*, *106*(A11), 24,733–24,744, http://dx.doi.org/10.1029/2000JA000342.

Mott-Smith, H. M., and Langmuir, I. (1926), The Theory of Collectors in Gaseous Discharges, *Physical Review*, *28*, 727–763, https://doi.org/10.1103/PhysRev.28.727.

Muralikrishna, P. (2006), Electron temperature variations in developing plasma bubbles rocket observations from Brazil, *Advances in Space Research*, *37*(5), 903–909, https://doi.org/10.1016/j.asr.2005.10.017.

Muralikrishna, P., Vieira, L. P., and Abdu, M. A. (2003), Electron density and electric field fluctuations associated with developing plasma bubbles, *Journal of Atmospheric and Solar-Terrestrial Physics*, *65*(14), 1315–1327, https://doi.org/10.1016/j.jastp.2003.08.010.

Nair, R. B., Jayachandran, B., Rao, P. B., and Balan, N. (1993), Seasonal, solar and magnetic activity effects on evening F region vertical plasma drifts, *Indian Journal of Radio & Space Physics*, *22*, 89–93, http://nopr.niscair.res.in/handle/123456789/35973.

Namba, S., and Maeda, K.-I. (1939), Radio wave propagation, *Corona, Tokyo*, p. 86.

Namboothiri, S. P., Balan, N., and Rao, P. B. (1989), Vertical plasma drifts in the F region at the magnetic equator, *Journal of Geophysical Research: Space Physics*, *94*(A9), 12,055–12,060, http://dx.doi.org/10.1029/JA094iA09p12055.

Nicolet, M., and Aikin, A. C. (1960), The formation of the D region of the ionosphere, *Journal of Geophysical Research*, *65*(5), 1469–1483, https://doi.org/10.1029/JZ065i005p01469.

Nishida, A. (1968), Geomagnetic Dp 2 fluctuations and associated magnetospheric phenomena, *Journal of Geophysical Research*, *73*(5), 1795–1803, https://doi.org/10.1029/JA073i005p01795.

Nopper, R. W., and Carovillano, R. L. (1978), Polar-equatorial coupling during magnetically active periods, *Geophysical Research Letters*, *5*(8), 699–702, https://doi.org/10.1029/GL005i008p00699.

Onwumechili, A., and Akasofu, S.-I. (1972), On the abnormal depression of Sq(H) under the equatorial electrojet in the afternoon, *Journal of geomagnetism and geoelectricity*, *24*(2), 161–173, http://dx.doi.org/10.5636/jgg.24.161.

Onwumechili, C. A. (1992a), A study of rocket measurements of ionospheric currents-I. General setting and night-time ionospheric currents, *Geophysical Journal International*, *108*(2), 633–640, http://dx.doi.org/10.1111/j.1365-246X.1992.tb04642.x.

Onwumechili, C. A. (1992b), A study of rocket measurements of ionospheric currents-III. Ionospheric currents at the magnetic dip equator, *Geophysical Journal International*, *108*(2), 647–659, http://dx.doi.org/10.1111/j.1365-246X.1992.tb04644.x.

Onwumechili, C. A., and Agu, C. E. (1981), Longitudinal variation of equatorial electrojet parameters derived from POGO satellite observations, *Planetary and Space Science*, *29*(6), 627–634, http://dx.doi.org/10.1016/0032-0633(81)90111-2.

Onwumechili, C. A., and Ezema, P. O. (1977), On the course of the geomagnetic daily variation in low latitudes, *Journal of Atmospheric and Terrestrial Physics*, *39*(9-10), 1079–1086, http://dx.doi.org/10.1016/0021-9169(77)90016-2.

Oppenheim, M. M., and Dimant, Y. S. (2016), Photoelectron-induced waves: A likely source of 150km radar echoes and enhanced electron modes, *Geophysical Research Letters*, *43*(8), 3637–3644, https://doi.org/10.1002/2016GL068179.

Oyekola, O. S. (2006), Comparison between nighttime ionosonde, incoherent scatter radar, AE-E satellite, and HF Doppler observations of F region vertical electrodynamic plasma drifts in the vicinity of the magnetic equator, *Journal of Geophysical Research*, *111*(A11), http://dx.doi.org/10.1029/2006JA011844.

Oyekola, O. S., Ojo, A., Akinrimisi, J., and dePaula, E. R. (2007), Seasonal and solar cycle variability in F-region vertical plasma drifts over Ouagadougou, *Journal of Geophysical Research*, *112*(A12), http://dx.doi.org/10.1029/2007JA012560.

Pai, G. L., and Sarabhai, V. A. (1964), Periodic fluctuations in the geomagnetic field during magnetic storms, *Planetary and Space Science*, *12*(9), 855–865, https://doi.org/10.1016/0032-0633(64)90045-5.

Pandey, K., Sekar, R., Anandarao, B. G., Gupta, S. P., and Chakrabarty, D. (2016), Estimation of nighttime dip-equatorial E-region current density using measurements and models, *Journal of Atmospheric and Solar-Terrestrial Physics*, *146*, 160–170, http://dx.doi.org/10.1016/j.jastp.2016.06.002.

Pandey, K., Sekar, R., Gupta, S. P., Chakrabarty, D., and Anandarao, B. G. (2017), Comparison of quiet time vertical plasma drifts with global empirical models over the indian sector: Some insights, *Journal of Atmospheric and Solar-Terrestrial Physics*, *157-158*, 42–54, http://dx.doi.org/10.1016/j.jastp.2017.03.012.

Pandey, K., Chakrabarty, D., and Sekar, R. (2018), Critical evaluation of the impact of disturbance dynamo on equatorial ionosphere during daytime, *Journal of Geophysical Research: Space Physics*, https://doi.org/10.1029/2018JA025686.

Pandey, K., Sekar, R., Anandarao, B. G., Gupta, S. P., and Chakrabarty, D. (2018), On the occurrence of afternoon counter electrojet over Indian longitudes during June solstice in solar minimum, *Journal of Geophysical Research: Space Physics*, *123*(3), 2204–2214, http://dx.doi.org/10.1002/2017JA024725.

Patil, A. R., Rao, D. R. K., and Rastogi, R. G. (1990a), Equatorial electrojet strengths in the Indian and American sectors Part I. During Low Solar Activity, *Journal of geomagnetism and geoelectricity*, *42*(7), 801–811, https://doi.org/10.5636/jgg.42.801.

Patil, A. R., Rao, D. R. K., and Rastogi, R. G. (1990b), Equatorial electrojet strengths in the Indian and American sectors Part II. During High Solar Activity, *Journal of geomagnetism and geoelectricity*, *42*(7), 813–823, https://doi.org/10.5636/jgg.42.813.

Patra, A. K., and Rao, N. V. (2006), Radar observations of daytime 150km echoes from outside the equatorial electrojet belt over Gadanki, *Geophysical Research Letters*, *33*(3), https://doi.org/10.1029/2005GL024564.

Patra, A. K., Sripathi, S., Rao, P. B., and Subbarao, K. S. V. (2005), Simultaneous VHF radar backscatter and ionosonde observations of low-latitude E region, *Annales Geophysicae*, *23*(3), 773–779, https://doi.org/10.5194/angeo-23-773-2005.

Patra, A. K., Chaitanya, P. P., Mizutani, N., Otsuka, Y., Yokoyama, T., and Yamamoto, M. (2012), A comparative study of equatorial daytime vertical E×B drift in the Indian and Indonesian sectors based on 150 km echoes, *Journal of Geophysical Research: Space Physics*, *117*(A11), https://doi.org/10.1029/2012JA018053.

Patra, A. K., Chaitanya, P. P., Otsuka, Y., Yokoyama, T., Yamamoto, M., Stoneback, R. A., and Heelis, R. A. (2014), Vertical E×B drifts from radar and C/NOFS observations in the Indian and Indonesian sectors: Consistency of observations and model, *Journal of Geophysical Research*, *119*(5), 3777–3788, http://dx.doi.org/10.1002/2013JA019732.

Patra, A. K., Chaitanya, P. P., St.-Maurice, J.-P., Otsuka, Y., Yokoyama, T., and Yamamoto, M. (2017), The solar flux dependence of ionospheric 150km radar echoes and implications, *Geophysical Research Letters*, *44*(22), 11,257–11,264, https://doi.org/10.1002/2017GL074678.

Pavan Chaitanya, P., Patra, A. K., and Rao, S. V. B. (2014), Quiet time short-period and day-to-day variations in E×B drift studied using 150 km radar echoes from Gadanki, *Journal of Geophysical Research: Space Physics*, *119*(4), 3053–3065, http://dx.doi.org/10.1002/2013JA019668.

Peymirat, C., Richmond, A. D., and Kobea, A. T. (2000), Electrodynamic coupling of high and low latitudes: Simulations of shielding/overshielding effects, *Journal of Geophysical Research: Space Physics*, *105*(A10), 22,991–23,003, http://dx.doi.org/10.1029/2000JA000057.

Pfaff, R. F., Sobral, J. H. A., Abdu, M. A., Swartz, W. E., LaBelle, J. W., Larsen, M. F., Goldberg, R. A., and Schmidlin, F. J. (1997), The Guará Campaign: A series of rocket-radar investigations of the Earth's upper atmosphere at the magnetic equator, *Geophysical Research Letters*, *24*(13), 1663–1666, http://dx.doi.org/10.1029/97GL01534.

Picone, J. M., Hedin, A. E., Drob, D. P., and Aikin, A. C. (2002), NRLMSISE-00 empirical model of the atmosphere: Statistical comparisons and scientific issues, *Journal of Geophysical Research*, *107*(A12), http://dx.doi.org/10.1029/2002JA009430.

Pingree, J. E., and Fejer, B. G. (1987), On the height variation of the equatorial F region vertical plasma drifts, *Journal of Geophysical Research*, *92*(A5), 4763–4766, http://dx.doi.org/10.1029/JA092iA05p04763.

Prabhakaran Nayar, S. R., and Sreehari, C. V. (2004), Investigation of height gradient in vertical plasma drift at equatorial ionosphere using multifrequency HF Doppler radar, *Journal of Geophysical Research*, *109*(A12), http://dx.doi.org/10.1029/2004JA010641.

Prakash, S., and Muralikrishna, P. (1976), The nature of electric field in E-region close to morning and evening reversals, *Geophysical Research Letters*, *3*(8), 445–447, http://dx.doi.org/10.1029/GL003i008p00445.

Prakash, S., and Pal, S. (1985), Electric fields and electron density irregularities in the equatorial electrojet, *Journal of Atmospheric and Terrestrial Physics*, *47*(8), 853–866, https://doi.org/10.1016/0021-9169(85)90060-1.

Prakash, S., and Subbaraya, B. H. (1967), Langmuir probe for the measurement of electron density and electron temperature in the ionosphere, *Review of Scientific Instruments*, *38*(8), 1132–1136, https://doi.org/10.1063/1.1721035.

Prakash, S., Gupta, S. P., and Subbaraya, B. H. (1969), Irregularities in the equatorial E region over Thumba, *Radio Science*, *4*(9), 791–796, http://dx.doi.org/10.1029/RS004i009p00791.

Prakash, S., Gupta, S. P., and Subbaraya, B. H. (1970), A study of the irregularities in the night time equatorial E-region using a Langmuir probe and plasma noise probe, *Planetary and Space Science*, *18*(9), 1307–1318, http://dx.doi.org/10.1016/0032-0633(70)90141-8.

Prakash, S., Gupta, S. P., Subbaraya, B. H., and Jain, C. L. (1971a), Electrostatic plasma instabilities in the equatorial electrojet, *Nature Physical Science*, *233*(38), 56–58, http://dx.doi.org/10.1038/physci233056a0.

Prakash, S., Gupta, S. P., and Subbaraya, B. H. (1971b), Cross field instability and ionization irregularities in the equatorial E region, *Nature Physical Science*, *230*, 170–171, http://dx.doi.org/10.1038/physci230170a0.

Prakash, S., Subbaraya, B. H., and Gupta, S. P. (1972), Rocket measurements of ionization irregularities in the equatorial ionosphere at Thumba & identification of plasma instabilities, *Indian Journal of Radio & Space Physics*, *01*(1), 72–80, http://nopr.niscair.res.in/handle/123456789/38055.

Prakash, S., Jain, C. L., Balsley, B. B., and Greenwald, R. A. (1974), Evidence of two types of electron density irregularities in the electrojet over Thumba, India, *Journal of Geophysical Research*, *79*(28), 4334–4336, http://dx.doi.org/10.1029/JA079i028p04334.

Prakash, S., Gupta, S. P., Sinha, H. S. S., and Rao, T. R. (1976), Ionization irregularities in the E region during counter electrojet, *Space Research XVI*, pp. 401–405.

Qian, C., Lei, J., and Wang, W. (2015), A simulation study on the impact of altitudinal dependent vertical plasma drift on the equatorial ionosphere in the evening, *Journal of Geophysical Research*, *120*(4), 2918–2925, http://dx.doi.org/10.1002/2014JA020626.

Rabiu, A. B., Folarin, O. O., Uozumi, T., Abdul Hamid, N. S., and Yoshikawa, A. (2017), Longitudinal variation of equatorial electrojet and the occurrence of its counter electrojet, *Annales Geophysicae*, *35*(3), 535–545, https://doi.org/10.5194/angeo-35-535-2017.

Raghavarao, R., and Anandarao, B. G. (1980), Vertical winds as a plausible cause for equatorial counter electrojet, *Geophysical Research Letters*, *7*(5), 357–360, http://dx.doi.org/10.1029/GL007i005p00357.

Raghavarao, R., and Anandarao, B. G. (1987), Equatorial electrojet and the Counter-Electrojet, *Indian Journal of Radio & Space Physics*, *16*, 54–75.

Raghavarao, R., Sharma, P., and Sivaraman, M. R. (1978), Correlation of ionization anomaly with the intensity of the electrojet, *Space Research*, *XVIII*, 277–280.

Raghavarao, R., Sridharan, R., and Suhasini, R. (1984), The importance of vertical ion currents on the nighttime ionization in the equatorial electrojet, *Journal of Geophysical Research*, *89*(A12), 11,033–11,037, https://doi.org/10.1029/JA089iA12p11033.

Raghavarao, R., Gupta, S. P., Sekar, R., Narayanan, R., Desai, J. N., Sridharan, R., Babu, V. V., and Sudhakar, V. (1987), In situ measurements of winds, electric fields and electron densities at the onset of equatorial spread-F, *Journal of Atmospheric and Terrestrial Physics*, *49*(5), 485–492, http://dx.doi.org/10.1016/0021-9169(87)90042-0.

Raghavarao, R., Sridharan, R., Sastri, J. H., Agashe, V. V., Rao, C. N., Rao, P. B., and Somayajulu, V. V. (1988), The Equatorial Ionosphere, World Ionosphere Thermosphere Study, *WITS Handbook*, *1*, 48–93.

Rajaram, G. (1977), Structure of the equatorial F-region, topside and bottomsidea review, *Journal of Atmospheric and Terrestrial Physics*, *39*(9), 1125–1144, https://doi.org/10.1016/0021-9169(77)90021-6.

Rama Rao, P. V. S., Gopi Krishna, S., Niranjan, K., and Prasad, D. S. V. V. D. (2006), Temporal and spatial variations in TEC using simultaneous measurements from the Indian GPS network of receivers during the low solar activity period of 2004-2005, *Annales Geophysicae*, *24*(12), 3279–3292, https://doi.org/10.5194/angeo-24-3279-2006.

Ramesh, K. B., and Sastri, J. H. (1995), Solar cycle and seasonal variations in F-region vertical drifts over Kodaikanal, India, *Annales Geophysicae*, *13*(6), 633–640, http://dx.doi.org/10.1007/s00585-995-0633-7.

Rastogi, R. G. (1974), Lunar effects in the counter electrojet near the magnetic equator, *Journal of Atmospheric and Terrestrial Physics*, *36*(1), 167–170, http://dx.doi.org/10.1016/0021-9169(74)90074-9.

Rastogi, R. G. (1975), On the criterion of geomagnetic field at the time of disappearance of equatorial Esq layer, *Indian Journal of Radio & Space Physics*, *04*(1), 1–5, http://nopr.niscair.res.in/handle/123456789/37649.

Rastogi, R. G., and Chandra, H. (2012), Response of equatorial ionosphere during the super geomagnetic storm of April 2000, *Indian Journal of Radio & Space Physics*, *41*, 524–535, http://nopr.niscair.res.in/handle/123456789/36904.

Rastogi, R. G., and Iyer, K. N. (1976), Quiet day variation of geomagnetic H-field at low latitudes, *Journal of Geomagnetism and Geoelectricity*, *28*(6), 461–479, http://dx.doi.org/10.5636/jgg.28.461.

Rastogi, R. G., and Patel, V. L. (1975), Effect of interplanetary magnetic field on ionosphere over the magnetic equator, *Proceedings of the Indian Academy Of Science*, *82*(A), 121–141.

Rastogi, R. G., and Patil, A. (1986), Complex structure of equatorial electrojet current, *Current Science*, *55*(9), 433–436.

Rastogi, R. G., Chandra, H., and James, M. E. (1996), Nocturnal variations of geomagnetic horizontal field at equatorial stations, *Geophysical Research Letters*, *23*(19), 2601–2604, http://dx.doi.org/10.1029/96GL02390.

Rastogi, R. G., Chandra, H., Janardhan, P., and Rahul, S. (2014), Equatorial and mid-latitude ionospheric currents over the Indian region based on 40 years of data at Trivandrum and Alibag, *Indian Journal of Radio & Space Physics*, *43*(4-5), 274–283, http://nopr.niscair.res.in/handle/123456789/30000.

Ravindran, S., and Krishna Murthy, B. V. (1997a), Occurrence of type I plasma waves in the equatorial electrojet during morning and evening hours, *Journal of Geophysical Research*, *102*(A5), 9761–9765, http://dx.doi.org/10.1029/96JA03742.

Ravindran, S., and Krishna Murthy, B. V. (1997b), Up-down asymmetry of type I plasma waves in the equatorial electrojet region, *Annales Geophysicae*, *15*(6), 774–778, http://dx.doi.org/10.1007/s00585-997-0774-y.

Reddy, C. A. (1989), The equatorial electrojet, *Pure and Applied Geophysics*, *131*(3), 485–508, https://doi.org/10.1007/BF00876841.

Reddy, C. A., Vikramkumar, B. T., and Viswanathan, K. S. (1987), Electric fields and currents in the equatorial electrojet deduced from VHF radar observations-I. A method of estimating electric fields, *Journal of Atmospheric and Terrestrial Physics*, *49*(2), 183–191, https://doi.org/10.1016/0021-9169(87)90053-5.

Reeves, G. D., Belian, R. D., and Fritz, T. A. (1991), Numerical tracing of energetic particle drifts in a model magnetosphere, *Journal of Geophysical Research: Space Physics*, *96*(A8), 13,997–14,008, https://doi.org/10.1029/91JA01161.

Reeves, G. D., Henderson, M. G., Skoug, R. M., F., T. M., Borovsky, J. E., Funtsen, H. O., C:Son Brandt, P., Mitchell, D. J., Jahn, J.-M., Pollock, C. J., McComas, D. J., and Mende, S. B. (2013), IMAGE, POLAR, and Geosynchronous Observations of Substorm and Ring Current Ion Injection, *American Geophysical Union*, pp. 91–101, https://doi.org/10.1029/142GM09.

Reinisch, B. W., Abdu, M., Batista, I., Sales, G. S., Khmyrov, G., Bullett, T. A., Chau, J., and Rios, V. (2004), Multistation digisonde observations of equatorial spread F in South America, *Annales Geophysicae*, *22*(9), 3145–3153, https://doi.org/10.5194/angeo-22-3145-2004.

Ren, Z., Wan, W., Xiong, J., and Liu, L. (2010), Simulated wave number 4 structure in equatorial F-region vertical plasma drifts, *Journal of Geophysical Research: Space Physics*, *115*, A05,301, https://doi.org/10.1029/2009JA014746.

Richmond, A. D. (1973), Equatorial electrojet-I. Development of a model including winds and instabilities, *Journal of Atmospheric and Terrestrial Physics*, *35*(6), 1083–1103, http://dx.doi.org/10.1016/0021-9169(73)90007-X.

Richmond, A. D., Peymirat, C., and Roble, R. G. (2003), Long-lasting disturbances in the equatorial ionospheric electric field simulated with a coupled magnetosphere-ionosphere-thermosphere model, *Journal of Geophysical Research: Space Physics*, *108*(A3), http://dx.doi.org/10.1029/2002JA009758.

Rishbeth, H. (1981), The F-region dynamo, *Journal of Atmospheric and Terrestrial Physics*, *43*(5), 387–392, https://doi.org/10.1016/0021-9169(81)90102-1.

Rishbeth, H., and Garriott, O. K. (1969), Introduction to ionospheric physics, *New York, Academic Press.*

Rodrigues, F. S., Nicolls, M. J., Milla, M. A., M., S. J., Varney, R. H., Strømme, A., Martinis, C., and Arratia, J. F. (2015), AMISR-14: Observations of equatorial spread F, *Geophysical Research Letters*, *42*(13), 5100–5108, https://doi.org/10.1002/2015GL064574.

Rout, D., Chakrabarty, D., Janardhan, P., Sekar, R., Maniya, V., and Pandey, K. (2017), Solar wind flow angle and geoeffectiveness of corotating interaction regions: First results, *Geophysical Research Letters*, *44*(10), 4532–4539, https://doi.org/10.1002/2017GL073038.

Rout, D., Chakrabarty, D., Sarkhel, S., Sekar, R., Fejer, B. G., Reeves, G. D., Kulkarni, A. S., Aponte, N., Sulzer, M. P., Mathews, J. D., Kerr, R. B., and Noto, J. (2018), The ionospheric impact of an ICME driven sheath region over Indian and American sectors in the absence of a typical geomagnetic storm, *Journal of Geophysical Research: Space Physics*, *123*, 4298–4308, https://doi.org/10.1029/2018JA025334.

Rush, C. M., and Richmond, A. D. (1973), The relationship between the structure of the equatorial anomaly and the strength of the equatorial electrojet, *Journal of Atmospheric and Terrestrial Physics*, *35*(6), 1171–1180, http://dx.doi.org/10.1016/0021-9169(73)90013-5.

Sagawa, E., Immel, T. J., Frey, H. U., and Mende, S. B. (2005), Longitudinal structure of the equatorial anomaly in the nighttime ionosphere observed by IMAGE/FUV, *Journal of Geophysical Research: Space Physics*, *110*, A11,302, https://doi.org/10.1029/2004JA010848.

Sampath, S., and Sastry, T. S. G. (1979), AC electric fields associated with the plasma instabilities in the equatorial electrojet-III, *Journal of Geomagnetism and Geoelectricity*, *31*(3), 391–400, http://doi.org/10.5636/jgg.31.391.

Sanatani, S. (1966), Electron density distribution in the ionosphere, Ph.D. thesis, Gujarat University.

Sastri, J. H. (1984), Duration of equatorial spread-F, *Annales Geophysicae*, *2*(3), 353–358.

Sastri, J. H. (1988), Equatorial electric-fields of ionospheric disturbance dynamo orgin, *Annales Geophysicae*, *6*(6), 635–642.

Sastri, J. H. (1990), Equatorial anomaly in F-region - A Review, *Indian Journal of Radio & Space Physics*, *19*(4), 225–240, http://nopr.niscair.res.in/handle/123456789/36285.

Sastri, J. H. (1996), Longitudinal dependence of equatorial F region vertical plasma drifts in the dusk sector, *Journal of Geophysical Research*, *101*(A2), 2445–2452, http://dx.doi.org/10.1029/95JA02759.

Sastri, J. H., Ramesh, K. B., Somayajulu, V. V., and Rao, J. V. S. V. (1991), Origin of short-period (30-300 s) Doppler frequency fluctuations of lower F region reflections in the equatorial electrojet region, *Radio Science*, *26*(6), 1403–1413, http://dx.doi.org/10.1029/91RS02021.

Sastri, J. H., Varma, V. K. M., and Prabhakaran Nayar, S. R. (1995), Height gradient of F region vertical drift in the evening equatorial ionosphere, *Geophysical Research Letters*, *22*(19), 2645–2648, http://dx.doi.org/10.1029/95GL02668.

Sastri, J. H., Lühr, H., Tachihara, H., Kitamura, T.-I., and Rao, J. V. S. V. (2000), Electric field fluctuations (25-35 min) in the midnight dip equatorial ionosphere, *Annales Geophysicae*, *18*(2), 252–256, https://doi.org/10.1007/s00585-000-0252-2.

Sastri, J. H., Kamide, Y., and Yumoto, K. (2003), Signatures for magnetospheric substorms in the geomagnetic field of dayside equatorial region: Origin of the ionospheric component, *Journal of Geophysical Research: Space Physics*, *108*(A10), https://doi.org/10.1029/2003JA009962.

Sastry, T. S. G. (1970), Diurnal changes in the parameters of the equatorial electrojet as observed by rocket-borne magnetometers, *Space Research X*, pp. 778–785.

Savitzky, A., and Golay, M. J. E. (1964), Smoothing and differentiation of data by simplified least squares procedures, *Analytical Chemistry*, *36*(8), 1627–1639, http://dx.doi.org/10.1021/ac60214a047.

Scherliess, L., and Fejer, B. G. (1997), Storm time dependence of equatorial disturbance dynamo zonal electric fields, *Journal of Geophysical Research: Space Physics*, *102*(A11), 24,037–24,046, http://dx.doi.org/10.1029/97JA02165.

Scherliess, L., and Fejer, B. G. (1999), Radar and satellite global equatorial F region vertical drift model, *Journal of Geophysical Research*, *104*(A4), 6829–6842, http://dx.doi.org/10.1029/1999JA900025.

Schoeberl, M. R. (1978), Stratospheric warmings: Observations and theory, *Reviews of Geophysics*, *16*(4), 521–538, http://dx.doi.org/10.1029/RG016i004p00521.

Sekar, R. (1990), Plasma instabilities and the dynamics of the equatorial F-region, Ph.D. thesis, Gujarat University.

Sekar, R., and Chakrabarty, D. (2008), Role of overshielding electric field on the development of pre-midnight plume event: Simulation results, *Journal of Atmospheric and Solar-Terrestrial Physics*, *70*(17), 2212–2221, https://doi.org/10.1016/j.jastp.2008.04.015.

Sekar, R., and Kelley, M. C. (1998), On the combined effects of vertical shear and zonal electric field patterns on nonlinear equatorial spread F evolution, *Journal of Geophysical Research: Space Physics*, *103*(A9), 20,735–20,747, https://doi.org/10.1029/98JA01561.

Sekar, R., and Raghavarao, R. (1987), Role of vertical winds on the Rayleigh-Taylor mode instabilities of the night-time equatorial ionosphere, *Journal of Atmospheric and Terrestrial Physics*, *49*(10), 981–985, https://doi.org/10.1016/0021-9169(87)90104-8.

Sekar, R., Chakrabarty, D., Narayanan, R., Sripathi, S., Patra, A. K., and Subbarao, K. S. V. (2004), Characterization of VHF radar observations associated with equatorial Spread F by narrow-band optical measurements, *Annales Geophysicae*, *22*(9), 3129–3136, https://doi.org/10.5194/angeo-22-3129-2004.

Sekar, R., Chakrabarty, D., and Pallamraju, D. (2012), Optical signature of shear in the zonal plasma flow along with a tilted structure associated with equatorial spread F during a space weather event, *Journal of Atmospheric and Solar-Terrestrial Physics*, *75-76*, 57–63, https://doi.org/10.1016/j.jastp.2011.05.009.

Sekar, R., Gupta, S. P., Acharya, Y. B., Chakrabarty, D., Pallamraju, D., Pathan, B. M., Tiwari, D., and Choudhary, R. K. (2013), Absence of streaming plasma waves around noontime over Thumba in recent times: Is it related to the movement of the dip equator?, *Journal of Atmospheric and Solar-Terrestrial Physics*, *103*, 8–15, http://dx.doi.org/10.1016/j.jastp.2013.02.005.

Sekar, R., Gupta, S. P., and Chakrabarty, D. (2014), On the altitude of initiation of the gradient drift waves at different longitude sectors in the vicinity of the dip equator, *Journal of Atmospheric and Solar-Terrestrial Physics*, *121*, 59–62, http://dx.doi.org/10.1016/j.jastp.2014.10.004.

Senior, C., and Blanc, M. (1984), On the control of magnetospheric convection by the spatial distribution of ionospheric conductivities, *Journal of Geophysical Research*, *89*(A1), 261–284, https://doi.org/10.1029/JA089iA01p00261.

Shuman, B. M. (1970), Rocket measurement of the equatorial electrojet, *Journal of Geophysical Research*, *75*(19), 3889–3901, http://dx.doi.org/10.1029/JA075i019p03889.

Simi, K. G., Thampi, S. V., Chakrabarty, D., Pathan, B. M., Prabhakaran Nayar, S. R., and Pant, T. K. (2012), Extreme changes in the equatorial electrojet under the influence of interplanetary electric field and the associated modification in the low-latitude F region plasma distribution, *Journal of Geophysical Research: Space Physics*, *117*(A3), http://dx.doi.org/10.1029/2011JA017328.

Singh, D., Gurubaran, S., and He, M. (2018), Evidence for the influence of DE3 tide on the occurrence of equatorial counter electrojet, *Geophysical Research Letters*, *45*, 21452150, http://dx.doi.org/10.1002/2018GL077076.

Smith, L. G. (1964), Langmuir probes for measurements in the ionosphere, *COSPAR Information Bull. No. 17, edited by K. Maeda*, pp. 37–81.

Somayajulu, V. V., Reddy, C. A., and Viswanathan, K. S. (1987), Penetration of magnetospheric convective electric field to the equatorial ionosphere during the substorm of March 22, 1979, *Geophysical Research Letters*, *14*(8), 876–879, https://doi.org/10.1029/GL014i008p00876.

Spencer, N. W., Brace, L. H., and Carignan, G. R. (1962), Electron temperature evidence for nonthermal equilibrium in the ionosphere, *Journal of Geophysical Research*, *67*(1), 157–175, https://doi.org/10.1029/JZ067i001p00157.

Spiro, R. W., Wolf, R. A., and Fejer, B. G. (1988), Penetrating of high-latitude-electric-field effects to low latitudes during SUNDIAL 1984, *Annales Geophysicae*, *6*, 39–49.

Sridharan, R., Pallam Raju, D., Somayajulu, V. V., Taori, A., Chakrabarty, D., and Raghavarao, R. (1999), Imprint of equatorial electrodynamical processes in the OI 630.0 nm dayglow, *Journal of Atmospheric and Solar-Terrestrial Physics*, *61*(15), 1143–1155, https://doi.org/10.1016/S1364-6826(99)00064-4.

Sridharan, S., Gurubaran, S., and Rajaram, R. (2002), Structural changes in the tidal components in mesospheric winds as observed by the MF radar during afternoon counter electrojet events, *Journal of Atmospheric and Solar-Terrestrial Physics*, *64*(12-14), 1455–1463, http://dx.doi.org/10.1016/S1364-6826(02)00109-8.

Sridharan, S., Sathishkumar, S., and Gurubaran, S. (2009), Variabilities of mesospheric tides and equatorial electrojet strength during major stratospheric warming events, *Annales Geophysicae*, *27*(11), 4125–4130, https://doi.org/10.5194/angeo-27-4125-2009.

Sripathi, S., Singh, R., Banola, S., Sreekumar, S., Emperumal, K., and Selvaraj, C. (2016), Characteristics of the equatorial plasma drifts as obtained by using Canadian Doppler ionosonde over southern tip of India, *Journal of Geophysical Research: Space Physics*, *121*(8), 8103–8120, https://doi.org/10.1002/2016JA023088.

Stening, R. J. (1977), Magnetic variations at other latitudes during reverse equatorial electrojet, *Journal of Atmospheric and Terrestrial Physics*, *39*(9), 1071–1077, http://dx.doi.org/10.1016/0021-9169(77)90015-0.

Stening, R. J. (1985), Modeling the equatorial electrojet, *Journal of Geophysical Research*, *90*(A2), 1705–1719, http://dx.doi.org/10.1029/JA090iA02p01705.

Stening, R. J. (1989a), A diurnal modulation of the lunar tide in the upper atmosphere, *Geophysical Research Letters*, *16*(4), 307–310, http://dx.doi.org/10.1029/GL016i004p00307.

Stening, R. J. (1989b), A calculation of ionospheric currents due to semidiurnal antisymmetric tides, *Journal of Geophysical Research*, *94*(A2), 1525–1531, http://dx.doi.org/10.1029/JA094iA02p01525.

Stening, R. J. (1992), The enigma of the counter equatorial electrojet and lunar tidal influences in the equatorial region, *Advances in Space Research*, *12*(6), 23–32, https://doi.org/10.1016/0273-1177(92)90036-W.

Stening, R. J., and Winch, D. E. (1987), Night-time geomagnetic variations at low latitudes, *Planetary and Space Science*, *35*(12), 1523–1539, http://dx.doi.org/10.1016/0032-0633(87)90078-X.

Stoneback, R. A., Heelis, R. A., Burrell, A. G., Coley, W. R., Fejer, B. G., and Pacheco, E. (2011), Observations of quiet time vertical ion drift in the equatorial ionosphere during the solar minimum period of 2009, *Journal of Geophysical Research*, *116*, A12,327, http://dx.doi.org/10.1029/2011JA016712.

Strobel, D. F., Young, T. R., Meier, R. R., Coffey, T. P., and Ali, A. W. (1974), The nighttime ionosphere: E region and lower F region, *Journal of Geophysical Research*, *79*(22), 3171–3178, https://doi.org/10.1029/JA079i022p03171.

Subbarao, K. S. V., and Krishna Murthy, B. V. (1994), Seasonal variations of equatorial spread-F, *Annales Geophysicae*, *12*(1), 33–39, https://doi.org/10.1007/s00585-994-0033-4.

Subbaraya, B. H., Muralikrishna, P., Sastry, T. S. G., and Prakash, S. (1972), A study of the structure of electrical conductivities and the electrostatic field within the equatorial electrojet, *Planetary and Space Science*, *20*(1), 47–52, http://dx.doi.org/10.1016/0032-0633(72)90139-0.

Subbaraya, B. H., Prakash, S., and Gupta, S. P. (1983), Electron densities in the equatorial lower ionosphere from the Langmuir probe experiments conducted at Thumba during 1966-1978, *Scientific report*, ISRO-PRL-SR-15-83.

Subbaraya, B. H., Prakash, S., and Gupta, S. P. (1985), Structure of the equatorial lower ionosphere from the Thumba Langmuir probe experiments, *Advances in Space Research*, *5*(7), 35–38, http://dx.doi.org/10.1016/0273-1177(85)90352-7.

Sudan, R. N., Akinrimisi, J., and Farley, D. T. (1973), Generation of small-scale irregularities in the equatorial electrojet, *Journal of Geophysical Research*, *78*(1), 240–248, http://dx.doi.org/10.1029/JA078i001p00240.

Sugiura, M., and Cain, J. C. (1966), A model equatorial electrojet, *Journal of Geophysical Research*, *71*(7), 1869–1877, http://dx.doi.org/10.1029/JZ071i007p01869.

Sugiura, M., and Poros, D. J. (1969), An improved model equatorial electrojet with a meridional current system, *Journal of Geophysical Research*, *74*(16), 4025–4034, http://dx.doi.org/10.1029/JA074i016p04025.

Takeda, M., and Araki, T. (1985), Electric conductivity of the ionosphere and nocturnal currents, *Journal of Atmospheric and Terrestrial Physics*, *47*(6), 601–609, http://dx.doi.org/10.1016/0021-9169(85)90043-1.

Tarpley, J. D. (1970), The ionospheric wind dynamo-II: Solar tides, *Planetary and Space Science*, *18*(7), 1091–1103, https://doi.org/10.1016/0032-0633(70)90110-8.

Thampi, S. V., Shreedevi, P. R., Choudhary, R. K., Pant, T. K., Chakrabarty, D., Sunda, S., Mukherjee, S., and Bhardwaj, A. (2016), Direct observational evidence for disturbance dynamo on the daytime low-latitude ionosphere: A case study based on the 28 June 2013 space weather event, *Journal of Geophysical Research: Space Physics*, *121*(10), 10,064–10,074, https://doi.org/10.1002/2016JA023037.

Thébault, E., et al. (2015), International Geomagnetic Reference Field: the 12th generation, *Earth, Planets and Space*, *67*(1), 1–19, http://dx.doi.org/10.1186/s40623-015-0228-9.

Tiwari, D., Patra, A. K., Viswanathan, K. S., Jyoti, N., Devasia, C. V., Subbarao, K. S. V., and Sridharan, R. (2003), Simultaneous radar observations of the electrojet plasma irregularities at 18 and 54.95 MHz over Trivandrum, India, *Journal of Geophysical Research*, *108*, 1368, http://dx.doi.org/10.1029/2002JA009698.

Untiedt, J. (1967), A model of the equatorial electrojet involving meridional currents, *Journal of Geophysical Research*, *72*(23), 5799–5810, http://dx.doi.org/10.1029/JZ072i023p05799.

Vasyliunas, V. M. (1970), Mathematical models of magnetospheric convection and its coupling to the ionosphere, in *Particles and Fields in the Magnetosphere*, pp. 60–71, https://doi.org/10.1007/978-94-010-3284-1_6.

Venkatesh, K., Fagundes, P. R., Prasad, D. S. V. V. D., Denardini, C. M., de Abreu, A. J., de Jesus, R., and Gende, M. (2015), Day-to-day variability of equatorial electrojet and its role on the day-to-day characteristics of the equatorial ionization anomaly over the Indian and Brazilian sectors, *Journal of Geophysical Research: Space Physics*, *120*(10), 9117–9131, http://dx.doi.org/10.1002/2015JA021307.

Vichare, G., and Rajaram, R. (2011), Global features of quiet time counterelectrojet observed by Ørsted, *Journal of Geophysical Research: Space Physics*, *116*, A04,306, http://dx.doi.org/10.1029/2009JA015244.

Vichare, G., Rawat, R., Jadhav, M., and Sinha, A. K. (2017), Seasonal variation of the Sq focus position during 2006-2010, *Advances in Space Research*, *59*(2), 542–556, http://dx.doi.org/10.1016/j.asr.2016.10.009.

Viswanathan, K. S., Vikramkumar, B. T., and Reddy, C. A. (1987), Electric fields and currents in the equatorial electrojet deduced from VHF radar observations-II. Characteristics of electric fields on quiet and disturbed days, *Journal of Atmospheric and Terrestrial Physics*, *49*(2), 193–200, https://doi.org/10.1016/0021-9169(87)90054-7.

Wei, Y., Hong, M., Wan , A., W.and Du, Lei, J., Zhao, B., Wang, W., Ren, Z., and Yue, X. (2008), Unusually long lasting multiple penetration of interplanetary electric field to equatorial ionosphere under oscillating imf bz, *Geophysical Research Letters*, *35*(2), L02,102, http://dx.doi.org/10.1029/2007GL032305.

Wolf, R. A. (1970), Effects of ionospheric conductivity on convective flow of plasma in the magnetosphere, *Journal of Geophysical Research*, *75*(25), 4677–4698, https://doi.org/10.1029/JA075i025p04677.

Wolf, R. A., Spiro, R. W., Sazykin, S., and Toffoletto, F. R. (2007), How the Earth's inner magnetosphere works: An evolving picture, *Journal of Atmospheric and Solar-Terrestrial Physics*, *69*(3), 288–302, https://doi.org/10.1016/j.jastp.2006.07.026.

Woodman, R. F. (1970), Vertical drift velocities and east-west electric fields at the magnetic equator, *Journal of Geophysical Research*, *75*(31), 6249–6259, http://dx.doi.org/10.1029/JA075i031p06249.

Woodman, R. F. (2009), Spread F - an old equatorial aeronomy problem finally resolved?, *Annales Geophysicae*, *27*(5), 1915–1934, https://doi.org/10.5194/angeo-27-1915-2009.

Woodman, R. F., and La Hoz, C. (1976), Radar observations of F region equatorial irregularities, *Journal of Geophysical Research*, *81*(31), 5447–5466, https://doi.org/10.1029/JA081i031p05447.

Yadav, S., Dabas, R. S., Rupesh, M. D., Upadhayaya, A. K., and Gwal, A. K. (2013), Temporal and spatial variation of equatorial ionization anomaly by using multistation ionosonde data for the 19th solar cycle over the Indian region, *Advances in Space Research*, *51*(7), 1253–1265, http://dx.doi.org/10.1016/j.asr.2012.11.009.

Yamazaki, Y., and Kosch, M. J. (2015), The equatorial electrojet during geomagnetic storms and substorms, *Journal of Geophysical Research: Space Physics*, *120*(3), 2276–2287, http://dx.doi.org/10.1002/2014JA020773.

Yamazaki, Y., and Maute, A. (2017), Sq and EEJ - A review on the daily variation of the geomagnetic field caused by ionospheric dynamo currents, *Space Science Reviews*, *206*(1), 299–405, https://doi.org/10.1007/s11214-016-0282-z.

Zaka, K. Z., Kobea, A. T., Assamoi, P., Obrou, O. K., Doumbia, V., Boka, K., Adohi, B. J.-P., and Mene, N. M. (2009), Latitudinal profile of the ionospheric disturbance dynamo magnetic signature: comparison with the DP2 magnetic disturbance, *Annales Geophysicae*, *27*(9), 3523–3536, https://doi.org/10.5194/angeo-27-3523-2009.

List of Publications

Publications included in the thesis

1. **Kuldeep Pandey**, R. Sekar, B. G. Anandarao, S. P. Gupta, and D. Chakrabarty (2016), Estimation of nighttime dip-equatorial E-region current density using measurements and models, *Journal of Atmospheric and Solar-Terrestrial Physics, 146*, 160 - 170.
   http://dx.doi.org/10.1016/j.jastp.2016.06.002

2. **Kuldeep Pandey**, R. Sekar, S. P. Gupta, D. Chakrabarty, B. G. Anandarao (2017), Comparison of quiet time vertical plasma drifts with global empirical models over the Indian sector: Some insights, *Journal of Atmospheric and Solar-Terrestrial Physics, 157 - 158*, 42 - 54.
   http://dx.doi.org/10.1016/j.jastp.2017.03.012

3. **Kuldeep Pandey**, R. Sekar, B. G. Anandarao, S. P. Gupta, and D. Chakrabarty (2018), On the occurrence of afternoon counter electrojet over Indian longitudes during June solstice in solar minimum, *Journal of Geophysical Research: Space Physics, 123(3)*, 2204 - 2214.
   http://dx.doi.org/10.1002/2017JA024725

4. **Kuldeep Pandey**, D. Chakrabarty and R. Sekar (2018), Critical evaluation of the impact of disturbance dynamo on equatorial ionosphere during daytime, *Journal of Geophysical Research: Space Physics, 123*.
   https://doi.org/10.1029/2018JA025686

Publications not included in the thesis

1. Rout, D., D. Chakrabarty, P. Janardhan, R. Sekar, V. Maniya, and **Kuldeep Pandey** (2017), Solar wind flow angle and geoeffectiveness of corotating interaction regions: First results, *Geophysical Research Letters, 44*, 45324539. http://dx.doi.org/10.1002/2017GL073038

2. Rout, D., **Kuldeep Pandey**, D. Chakrabarty, and R. Sekar, Significant electric field perturbations in low latitude ionosphere due to the passage of two consecutive ICMEs during 6 - 8 September 2017, *under revision in Journal of Geophysical Research: Space Physics.*

Presentations at International/National Conferences

1. **Kuldeep Pandey**, D. Chakrabarty, R. Sekar, "Effect of disturbance dynamo on equatorial ionosphere during daytime" presented in the 15th International Symposium on Equatorial Aeronomy (ISEA-15) held at Physical Research Laboratory, India during 22 - 26 October 2018 [*Poster presentation - Best Young Scientist Paper Award*].

2. **Kuldeep Pandey**, R. Sekar, B. G. Anandarao, S. P. Gupta, and D. Chakrabarty, "Afternoon counter electrojet over Indian longitudes during June solstice in solar minimum" presented in the 15th International Symposium on Equatorial Aeronomy (ISEA-15) held at Physical Research Laboratory, India during 22 - 26 October 2018 [*Oral presentation*].

3. **Kuldeep Pandey**, D. Chakrabarty, R. Sekar, "Significantly Large Impact of Disturbance Dynamo on Equatorial Ionosphere: Case Studies" presented in the 15th Annual Meeting of Asia Oceania Geosciences Society (AOGS) held at Hawaii, USA during 3 - 8 June 2018 [*Oral presentation*].

4. **Kuldeep Pandey**, R. Sekar, B. G. Anandarao, S. P. Gupta, and D. Chakrabarty, "On the Occurrence of Afternoon Counter Electrojet Over Indian Longitudes During June Solstice in Solar Minimum" presented in the 15th Annual Meeting of Asia Oceania Geosciences Society (AOGS) held at Hawaii, USA during 3 - 8 June 2018 [*Oral presentation*].

5. **Kuldeep Pandey**, R. Sekar, B. G. Anandarao, S. P. Gupta, D. Chakrabarty, "Estimation of nighttime current density and daytime zonal electric field over the dip-equatorial E-region" presented in the 3rd URSI-Regional Conference on Radio Science (URSI-RCRS-2017) held at National Atmospheric Research Laboratory, India during 1 - 4 March 2017 [*Poster presentation*].

6. **Kuldeep Pandey**, R. Sekar, B. G. Anandarao, S. P. Gupta, and D. Chakrabarty, "Estimation of nighttime equatorial E-region current densities using electrojet model" presented in the 19^{th} National Space Science Symposium (NSSS-2016) held at Vikram Sarabhai Space Centre, India during 9 - 12 February 2016 [*3^{rd} Prize in Students' Poster Presentation*].

7. **Kuldeep Pandey**, R. Sekar, B. G. Anandarao, S. P. Gupta, D. Chakrabarty, "Estimations of Nighttime Equatorial E-region Currents", presented in the 2^{nd} URSI-Regional Conference on Radio Science (URSI-RCRS-2015) held at Jawaharlal Nehru University, India during 16 - 19 November 2015 [*2^{nd} Prize in Students' Poster Presentation*].

International School Attended

Heliophysics Summer School (Year 12) held at High Altitude Observatory, Boulder, Colorado, USA during 24 - 31 July, 2018.

Publications attached with thesis

1. **Kuldeep Pandey**, R. Sekar, B. G. Anandarao, S. P. Gupta, and D. Chakrabarty (2016), Estimation of nighttime dip-equatorial E-region current density using measurements and models, *Journal of Atmospheric and Solar-Terrestrial Physics, 146*, 160 - 170.
http://dx.doi.org/10.1016/j.jastp.2016.06.002

2. **Kuldeep Pandey**, R. Sekar, S. P. Gupta, D. Chakrabarty, B. G. Anandarao (2017), Comparison of quiet time vertical plasma drifts with global empirical models over the Indian sector: Some insights, *Journal of Atmospheric and Solar-Terrestrial Physics, 157 - 158*, 42 - 54.
http://dx.doi.org/10.1016/j.jastp.2017.03.012

3. **Kuldeep Pandey**, R. Sekar, B. G. Anandarao, S. P. Gupta, and D. Chakrabarty (2018), On the occurrence of afternoon counter electrojet over Indian longitudes during June solstice in solar minimum, *Journal of Geophysical Research: Space Physics, 123(3)*, 2204 - 2214.
http://dx.doi.org/10.1002/2017JA024725

4. **Kuldeep Pandey**, D. Chakrabarty and R. Sekar (2018), Critical evaluation of the impact of disturbance dynamo on equatorial ionosphere during daytime, *Journal of Geophysical Research: Space Physics, 123*.
https://doi.org/10.1029/2018JA025686

Journal of Atmospheric and Solar-Terrestrial Physics 146 (2016) 160–170

Contents lists available at ScienceDirect

Journal of Atmospheric and Solar-Terrestrial Physics

journal homepage: www.elsevier.com/locate/jastp

Estimation of nighttime dip-equatorial E-region current density using measurements and models

Kuldeep Pandey [a,b], R. Sekar [a,*], B.G. Anandarao [a], S.P. Gupta [a], D. Chakrabarty [a]

[a] *Physical Research Laboratory, Navrangpura, Ahmedabad 380009, India*
[b] *Indian Institute of Technology-Gandhinagar, Ahmedabad 382424, India*

ARTICLE INFO

Article history:
Received 27 January 2016
Received in revised form
17 May 2016
Accepted 2 June 2016
Available online 7 June 2016

Keywords:
Equatorial ionosphere
Equatorial electrojet
Streaming plasma waves

ABSTRACT

The existence of the possible ionospheric current during nighttime over low-equatorial latitudes is one of the unresolved issues in ionospheric physics and geomagnetism. A detailed investigation is carried out to estimate the same over Indian longitudes using in situ measurements from Thumba (8.5°N, 76.9°E), empirical plasma drift model (Fejer et al., 2008) and equatorial electrojet model developed by Anandarao (1976). This investigation reveals that the nighttime E-region current densities vary from ~0.3 to ~0.7 A/km^2 during pre-midnight to early morning hours on geomagnetically quiet conditions. The nighttime current densities over the dip equator are estimated using three different methods (discussed in methodology section) and are found to be consistent with one another within the uncertainty limits. Altitude structures in the E-region current densities are also noticed which are shown to be associated with altitudinal structures in the electron densities. The horizontal component of the magnetic field induced by these nighttime ionospheric currents is estimated to vary between ~2 and ~6 nT during geomagnetically quiet periods. This investigation confirms the existence of nighttime ionospheric current and opens up a possibility of estimating base line value for geomagnetic field fluctuations as observed by ground-based magnetometer.

1. Introduction

It is well known that an intense current, commonly referred to as equatorial electrojet, flows in a narrow altitudinal band (peak around 105 km) over the dip equatorial regions. The strengths and variations of these currents during daytime had been derived in detail using rocket borne magnetometer measurements over Indian (e.g. Sastry, 1970; Sampath and Sastry, 1979 and references cited therein), Peruvian (e.g. Davis et al., 1967; Shuman, 1970) and Brazilian (e.g. Pfaff et al., 1997 and references cited therein) longitudes. Systematic observations of the electrojet current strengths during daytime were obtained by ground-based magnetometers (e.g. Rastogi and Iyer, 1976). Satellite borne measurements of these current densities during daytime (Jadhav et al., 2002; Lühr et al., 2004, etc.) are also available. However, the existence (or the lack of it) of the possible ionospheric current during nighttime and its characteristics over low-equatorial latitudes are not well understood. This is because of the fact that during nighttime, the ionospheric E-region plasma density goes down drastically. As a consequence, the midnight values of Sq current are generally taken as the base line for the overhead equivalent ionospheric current system. However, based on theoretical calculations, Takeda and Araki (1985) concluded that the ionospheric Sq currents flow westward in the nighttime during high solar activity period and their contribution to the geomagnetic Sq field is about 1/10 of the maximum Sq variation. On the other hand, the nocturnal currents are shown to be weak during low solar activity period and below the detection limit. In addition, Campbell (1973) and Mayaud (1976) found that the geomagnetic variations during nighttime are not negligible on many occasions. Campbell (1979) suggested that the ground geomagnetic variations during nighttime may be present even during apparently quiet conditions. Matsushita and Maeda (1965) used the daily mean as the base level to be representative of the zero Sq current and showed the presence of significant nighttime ionospheric current. On the other hand, if the nighttime Sq level is taken as the base value, as in Matsushita (1968), it would imply zero ionospheric current during nighttime. Therefore, determination of the base geomagnetic level is important to determine the nighttime E-region current over low-equatorial latitudes. Based on only a single rocket flight Davis et al. (1967) inferred small westward current in E-region (corresponding to magnetic variation of about 6 nT on the rocket borne magnetometer) during midnight hours around 100 km altitude over the Peruvian dip equatorial sector. This inference was derived

* Corresponding author.
E-mail address: rsekar@prl.res.in (R. Sekar).

http://dx.doi.org/10.1016/j.jastp.2016.06.002
1364-6826/

using the data obtained from the ascent and descent phases of the rocket flight. After a few days, under similar geomagnetic conditions, Shuman (1970) did not detect any significant current over the same place and around the same local time during the descent phase of the rocket, although the resolution of the magnetic measurements was slightly higher (5 nT). It is to be noted here that the magnetometer measurements are not expected to alter significantly depending on the ascent and descent phases of the rocket as current integrated over large area is measured. Thus, considering that rocket wake does not modify the magnetometer measurements, the results of Shuman (1970) are in contradiction with the results of Davis et al. (1967). Over the Indian dip equatorial sector (Thumba), Sastry (1970) measured about 9.4 A/km^2 peak current density during daytime but concluded the absence of such current (with uncertainty of 4 nT of magnetic measurements) during pre-midnight hours on the same day. Onwumechili (1992a) compiled the available in situ measurements of ionospheric current density over the globe and the nighttime current over the dip equatorial region was suggested to be absent.

The above observations pose an uncertainty on the magnitude of the current that can be expected to flow through the equatorial E-region during nighttime. Further, as suggested by Haerendel and Eccles (1992) and Eccles (2015), the generation of pre-reversal enhancement (PRE) of the equatorial F-region zonal electric field will depend crucially on the closure of the F-region dynamo current through the E-region in the low and equatorial latitudes. Therefore, determination of nighttime E-region current is essential to understand the underlying processes that couples E and F regions over low-equatorial latitudes during nighttime. There was an attempt by Stening and Winch (1987) to estimate the nighttime ionospheric current using the in situ measurements of electron density, obtained over Thumba (Prakash et al., 1970), and with a fixed zonal Sq electric field of -0.3 mV/m. They concluded that a finite ionospheric current flows during nighttime. Further, Rastogi et al. (1996) reported that the nocturnal variation of horizontal geomagnetic field over Huancayo showed remarkable similarity with corresponding variation of ionospheric electric field determined by Doppler radar. This indicates a finite nighttime ionospheric current which can be inferred by ground-based magnetometer. However, it is difficult to separate ionospheric and magnetospheric components from these magnetometer measurements in spite of the resolution being 0.1 nT in the present digital magnetometer systems as their effects are comparable on ground during nighttime. It is not clear whether the ground-based magnetometer measurements during nighttime, even during magnetically quiet times, are free from the contributions from magnetosphere. During geomagnetically disturbed period, many authors (e.g. Matsushita, 1971; Onwumechili and Ezema, 1977; Chakrabarty et al., 2005) had indicated the non-ionospheric (magnetospheric) origin of the currents responsible for the magnetic fluctuations observed at the ground. Therefore, a comprehensive understanding on the magnitude of the nighttime E-region current and its variation with time is missing till date although the nighttime horizontal component of the magnetic field measured by the magnetometers is being used as base or reference value for determining the daytime electric fields (Rastogi and Patil, 1986). These variations in the reference value during magnetically disturbed period make matter worse as far as the determination of the daytime electric fields is concerned. Given the above background, it is imperative that knowledge about the changes in nocturnal ionospheric current during geomagnetically quiet time is essential to comprehensively understand the equatorial electrodynamics. In this context, the present investigation is important as it provides estimation of the equatorial E-region current at a few local nighttimes by different methods using experimental data and modeling investigations.

2. Details of observations and other inputs

In the present investigation, electron densities and plasma wave information obtained from six rocket flights containing Langmuir probe system with high frequency response (Prakash and Subbaraya, 1967; Subbaraya et al., 1983, 1985) conducted over Thumba, during 1967–1975, are utilized as inputs. In addition, in situ measurements of zonal current density (Sastry, 1970; Sampath and Sastry, 1979) using magnetometer on board two rocket flights over Thumba are used. Throughout this work, time corresponds to local time (*LT*) which for Thumba (76.9°E) is about 22 min behind the Indian Standard Time, *IST* (time corresponding to 82.5°E). It is important to note here that simultaneous measurements of electron and current densities obtained on 29 *August*, 1968 at 1354 *LT* (Subbaraya et al., 1972) and 3 *March*, 1973 at 1159 *LT* (Sampath and Sastry, 1979) are used to calculate the R values ($R = \sigma_H/\sigma_P$, ratio of Hall (σ_H) to Pedersen (σ_P) conductivities). These flights correspond to high (yearly averaged sunspot number in 1968 was 150) and low (yearly averaged sunspot number in 1973 was 54) solar activity periods. This R value is used to deduce the altitude profile of nighttime current densities over the dip equator. The validity of the extrapolation of R value to the nighttime is discussed in Section 3.1. Further, the observed presence of streaming waves (plasma waves generated due to the streaming of electrons in the dip equatorial E-region with velocity exceeding ion-acoustic speed) in the electron density measurements (e.g. Farley, 2009) is also used to give the physical estimate of minimum strength of nighttime current density that must be present over the altitude range wherein streaming waves were detected. The generation of streaming wave is shown (Sekar et al., 2013) to be possible over Thumba only when the dip angle $(I) < 1.5°$. The present investigation makes use of the electron density observations from Thumba during 1967–1975 wherein the dip angle was between $-1.0°$ and $-1.1°$ and thus consistent with the conclusion of Sekar et al. (2013). Further, as the objective of the present investigation is to find out the nighttime E-region current density that is a realistic representative of the nighttime base value during quiet time, the electron density profiles before 2100 *LT* are avoided to minimize the contributions from PRE. The other important input parameters are as follows:

(i) The altitude profiles of neutral density and temperature are taken from Jacchia-71 (Jacchia, 1971) model which is built-in electrojet model used in this investigation.
(ii) The geomagnetic field in altitude-latitude plane is adopted from International Geomagnetic Reference Field (IGRF)-11 model (Finlay et al., 2010).
(iii) The vertical drifts corresponding to quiet time Sq electric fields over the dip equator are taken from F-region vertical plasma drift model of Fejer et al. (2008).

It is to be noted here that the accuracy of the electron density measurements is 5% (Subbaraya et al., 1983), the resolution of drift measurements is 10% (Fejer et al., 2008) and the standard deviation of neutral parameters is 8% (Marcos, 1990). These numbers determine the maximum uncertainty in the estimated nighttime current values.

3. Methods to estimate nighttime current density

Three different approaches have been adopted to estimate the nighttime current density in the equatorial E-region. These are described and compared in the subsequent sections.

3.1. Method-1: based on the ratio R deduced from observations

In order to estimate the altitude profiles of nighttime current density, the altitude profiles of electron density and plasma drifts in the zonal direction are needed. A few measurements of electron density during nighttime are available in the literature (Subbaraya et al., 1983, 1985; Gupta, 1986, 1990). However, measurement of background plasma drift in the zonal direction is difficult and systematic observations are not available over Indian longitudes. Therefore, a methodology is evolved based on a few assumptions and a coordinate system in which *x*, *y* and *z* directions are along zonal (positive eastward), meridional (positive northward) and vertical (positive upward) directions respectively. The assumptions are as follows:

1. In the present investigation, the electric fields corresponding to the F-region plasma drifts are taken to represent the E-region Sq electric field (E_{Sq}) as the low latitude E-region dynamo electric fields get mapped to the equatorial F-region. This assumption can lead to an uncertainty in drift of ~2 m/s considering the altitude of satellite (around 600 km), latitude ($\pm 5°$) binning of plasma drift measurements, geometry of magnetic field and typical altitudinal gradient (Pingree and Fejer, 1987) of plasma drifts (about 0.005 m s^{-1} km^{-1}) during nighttime over another dip equatorial station Jicamarca.
2. The zonal solar quiet time $(E_{Sq})_x$ field does not vary much within the altitude region of 100–120 km.
3. The ratio R $(= \sigma_H/\sigma_P)$ remains the same during day and night in all solar epochs.

Based on these assumptions, the empirical model (Fejer et al., 2008) of F-region vertical plasma drift corresponding to $(E_{Sq})_x$ over Indian longitude sector is utilized. This model is compared with vertical plasma drifts estimated using measurements by various techniques. This comparison revealed that the model values and polarities of the plasma drifts match well (within the experimental uncertainties) with the inferred drifts from individual case studies except on a few occasions. This aspect is not directly relevant for the present work and will be addressed in a separate communication. To verify the validity of third assumption, the ratio of the conductivities (R) is estimated using neutral number density and temperature from the Jacchia-71 model (Jacchia, 1971), geomagnetic field values from IGRF-11 model and measured altitude profiles of electron density. Fig. 1a depicts the altitude profiles of R during day and night times in solar maximum and minimum conditions. The ratio R is essentially independent of electron density variations. The variations of neutral density during day-night and at different solar epochs are not significant enough to affect R. It is also verified that the R value does not change much even if one uses other neutral density models (e.g. NRLMSISE-00)

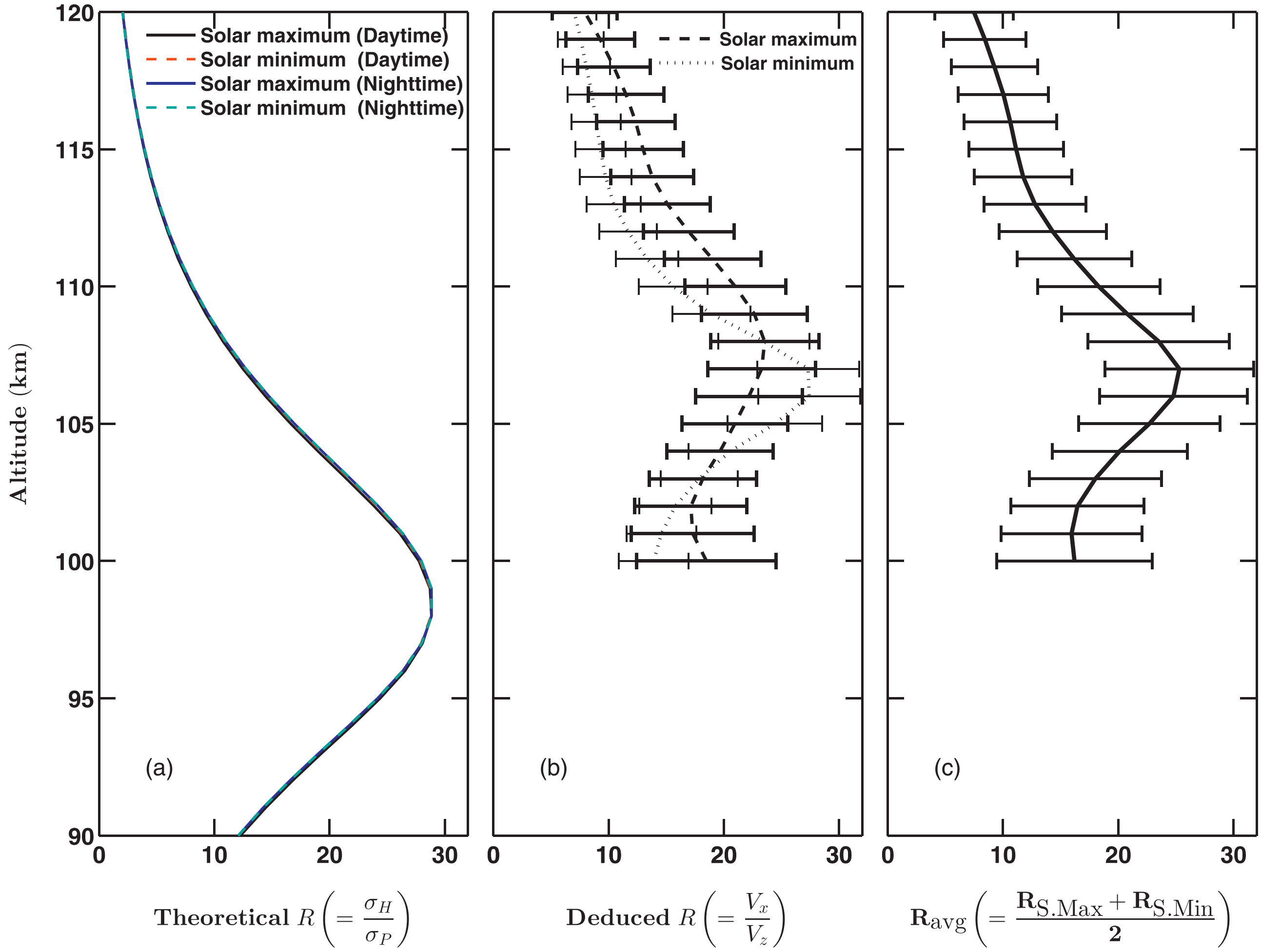

Fig. 1. (a) Altitude profiles of ratio (R) of the Hall to Pedersen conductivities during day and night at different solar epoch estimated using Jacchia-71 model values of neutral density and temperature along with geomagnetic fields from IGRF-11 model. (b) Deduced altitude profiles of R values, based on Eq. (2), using simultaneous measurements of current and electron densities during daytime at high (dotted) and low (dashed) solar activity conditions. In this estimation the plasma drift in vertical direction (corresponding to Sq electric field) at the time of measurement is obtained from the empirical model of Fejer et al. (2008). (c) The altitude profile of the average values of R shown in (b). (For interpretation of the references to color in this figure, the reader is referred to the web version of this paper.)

instead of Jacchia-71 model. Hence the assumption (3) is valid for the present purpose of estimation of nighttime current.

Fig. 1a reveals that the peak R value is close to 30 around 100 km. This is similar to the earlier calculation of Anandarao et al. (1977), which also reveals that these values of R are nearly same around peak E-region even if one considers the field line integrated values of conductivities. However, the peak height determined by these theoretical calculations is well known (Forbes, 1981) to be lower than the height determined from measurements by more than 5 km. This R is also shown to be equivalent to the ratio of electric fields in vertical (E_z) and zonal (E_x) directions (Anandarao et al., 1977; Sekar et al., 2013) as follows:

$$R = \frac{E_z}{E_x} = \frac{V_x}{V_z} \tag{1}$$

where V_x and V_z are the plasma drifts in zonal and vertical directions respectively. Therefore, to deduce the altitude profile of R by means of experimental observations, simultaneous measurements of electron $(N_{e,day})$ and current densities $(J_{x,day})$ are used. These values correspond to daytime in high and low solar activity periods. In addition, the vertical plasma drift (V_z) corresponding to the local time of rocket flights have been taken from Fejer et al. (2008) model:

$$R = \frac{V_x}{V_z} = \frac{1}{|\mathbf{e}|}\left(\frac{J_{x,day}}{N_{e,day}}\right)\frac{1}{V_z} \tag{2}$$

where $\mathbf{e}$ is the charge of electron. Fig. 1b depicts the altitude profiles of R and its errors in high and low solar activity periods based on Eq. (2). It is to be noted here that R values below 100 km are not shown as the current density measurements in that altitude region are below the sensitivity limit of the rocket borne magnetometer. From Fig. 1b, it is clear that the deduced R values remain the same (within the error limits) for both solar epochs. By taking clue from the theoretical calculation on the invariance of R values during day and night in all solar epochs, the average value (R_{avg}) (shown in Fig. 1c) along with measured nighttime electron density $(N_{e,night})$ and vertical plasma drift $(V_{z,night})$ from Fejer et al. (2008) model at the time of rocket flight experiment is used to estimate nighttime current density. The following expression is used to calculate the nighttime current density $(J_{x,night})$:

$$J_{x,night} = |\mathbf{e}| N_{e,night} R_{avg} V_{z,night} \tag{3}$$

The observed $N_{e,night}$ values and the empirical plasma drift model values of V_z corresponding to that local time are used.

3.2. Method-2: based on the observation of streaming waves

As mentioned earlier, the dip equatorial E-region ionosphere is characterized by the generation of streaming waves. These plasma waves are essentially generated when electrons stream through the background ions with velocity exceeding ion-acoustic speed (Farley, 2009). The electron densities measured over Thumba at different local times on several nights show (Prakash et al., 1970; Gupta, 1986) the presence of streaming plasma wave. The threshold plasma drift in the zonal direction needed to trigger the streaming waves is given (Sudan et al., 1973) by,

$$V_{x,min} = (1 + \chi)c_s \tag{4}$$

where c_s is the ion-acoustic speed (330 m/s) of the medium and χ is given by,

$$\chi = \frac{\nu_e \nu_i}{\Omega_e \Omega_i} \tag{5}$$

where ν and Ω represent neutral collision and gyro frequencies respectively and subscripts e and i are used for electron and ions respectively. The $V_{x,min}$ values along with the corresponding electron densities are used to have the physical estimate of minimum strength of current density $(J_{x,night,min})$ that must be present over the altitude range where the presence of streaming waves was observed using the following expression:

$$J_{x,night,min} = |\mathbf{e}| N_{e,night}(1 + \chi)c_s \tag{6}$$

The observed $N_{e,night}$ values are used from those rocket flights that detected streaming waves.

3.3. Method-3: based on the equatorial electrojet model

A physics based model for equatorial electrojet was developed earlier by Anandarao (1976) and important results on the effect of winds during daytime electrojet current system (Anandarao, 1976, 1977; Anandarao and Raghavarao, 1987; Raghavarao and Anandarao, 1987, etc.) obtained using this model are available in the literatures. In the present study this model is used, without invoking the wind effects, to calculate the nighttime current density in the zonal direction with the inputs of previously mentioned electron density profiles and E-region Sq electric field values. Based on the earlier works (Richmond, 1973; Anandarao, 1976; Anandarao and Raghavarao, 1987; Raghavarao and Anandarao, 1987) during daytime, the contributions of horizontal winds and shears in them to the zonal current densities over the dip equator are not found to be significant and are well within the estimation uncertainty. In the absence of systematic measurements of vertical winds in the E-region during nighttime, the contribution of vertical wind to the current density estimates could not be determined.

In this model, the ionospheric current density ($\mathbf{J}$) is expressed in terms of Ohm's law and the current conservation equation ($\nabla \cdot \mathbf{J} = 0$ which implies $\mathbf{J} = \nabla \times \mathbf{A}$, where $\mathbf{A}$ is the vector potential) is solved along with Maxwell's equation for electrostatic condition in geocentric co-ordinate system (r, θ, ϕ) where r is the radial distance from the center of the earth, θ is the magnetic co-latitude and ϕ is the longitude. A current function ψ is defined as $\psi = -r \sin\theta A_\phi$ where A_ϕ is the component of vector potential $\mathbf{A}$ in ϕ direction. The following second order elliptic partial differential equation is derived by solving the electrodynamic equations:

$$f_1\frac{\partial^2\psi}{\partial r^2} + 2f_2\frac{\partial^2\psi}{\partial r\partial\theta} + f_3\frac{\partial^2\psi}{\partial\theta^2} + f_4\frac{\partial\psi}{\partial r} + f_5\frac{\partial\psi}{\partial\theta} + f_6 = 0 \tag{7}$$

The coefficients f_1–f_6 are functions of ionospheric conductivities and the zonal electric fields (Sugiura and Poros, 1969; Anandarao, 1977; Anandarao and Raghavarao, 1987; Raghavarao and Anandarao, 1987). Eq. (7) is numerically solved in the region encompassing 80–200 km altitude and magnetic co-latitude between 75° and 105° with the boundary conditions $\psi = 0$ at all the boundaries (i.e. $\psi_{at\ 80\ km, 200\ km, -75°, 105°} = 0$). In deriving Eq. (7), variations in all physical parameters along the longitudinal direction are neglected. Thus this equation is numerically solved in two dimensions along the vertical and latitudinal directions. The grid sizes of $\Delta r = 1$ km and $\Delta\theta = 0.25°$ are employed for the present investigation. Further details of this model can be found in Anandarao and Raghavarao (1987) and Raghavarao and Anandarao (1987). The inputs to the model are altitude profile of electron densities and $(E_{Sq})_x$ value at the particular time for which the model calculation is made. Further, the same electron density profile is used at all the latitudes. These inputs are taken from the in situ measurements of electron densities during nighttime (Subbaraya et al., 1983, 1985; Gupta, 1986, 1990) and the empirical model of plasma drift (Fejer et al., 2008) over the dip equator corresponding to Indian longitude. In addition to these, Jachhia-71 model of neutral density and temperature along with IGRF-11 model of geomagnetic field are used for the evaluation of ionospheric conductivities. The equations for vertical polarization electric field (E_r) and current density in the zonal direction, without wind effects, can be written (Sugiura and Poros, 1969; Raghavarao and Anandarao, 1987) as follows:

$$E_r = \frac{\sigma_H}{\sigma_P} E_\phi \cos I + J_r\left(\frac{\cos^2 I}{\sigma_P} + \frac{\sin^2 I}{\sigma_0}\right) - J_\theta\left(\frac{1}{\sigma_0} - \frac{1}{\sigma_P}\right)\sin I \cos I \tag{8}$$

$$J_\phi = \sigma_H\left(E_r \cos I - E_\theta \sin I\right) + \sigma_P E_\phi \tag{9}$$

where σ_0 is the direct conductivity; E_r, E_θ and E_ϕ are electric fields along r, θ and ϕ directions respectively; J_r, J_θ and J_ϕ are current densities along r, θ and ϕ directions respectively. Over the dip equator, the radial (r) and azimuthal (ϕ) directions used in this section are same as vertically up (z) and zonal (x) directions used in the previous subsections. A sensitivity study of the model is performed by considering previously mentioned maximum uncertainties in the electron density, electric field, neutral density and temperature individually and the changes in peak current density over the dip equator are noted. The changes in current densities are found to be linear with changes in electron density and electric field. However, the changes with the neutral parameters yield a nonlinear response with maximum deviation less than 3%. Combining the errors in the inputs and variations in neutral parameters, the maximum uncertainties in current density (J_x) and polarization electric field (E_z) over the dip equator are found to be less than 20% and 12% respectively.

4. Estimation of induced magnetic field

In order to estimate the magnetic field induced at ground by ionospheric current, a method described by Anandarao (1977) is adopted. In this method, the magnetic field potential (V) induced by an infinitely long line of current is defined based on Biot–Savart's law as

$$V = \frac{\mu_0 C}{2\pi} \tan^{-1}\left(\frac{\cos\theta}{(r/a) - \sin\theta}\right) \tag{10}$$

where μ_0 and C are the permeability of free space and line current (in Amperes) respectively. The line current C is obtained from current density J_x using $C = \int_r \int_\theta J_x \, dr \, d\theta$. The symbols a and r denote the earth's radius and distance of the line of current from the center of earth respectively. Further, the horizontal (northward) component of magnetic field (H) induced due to ionospheric current is given by,

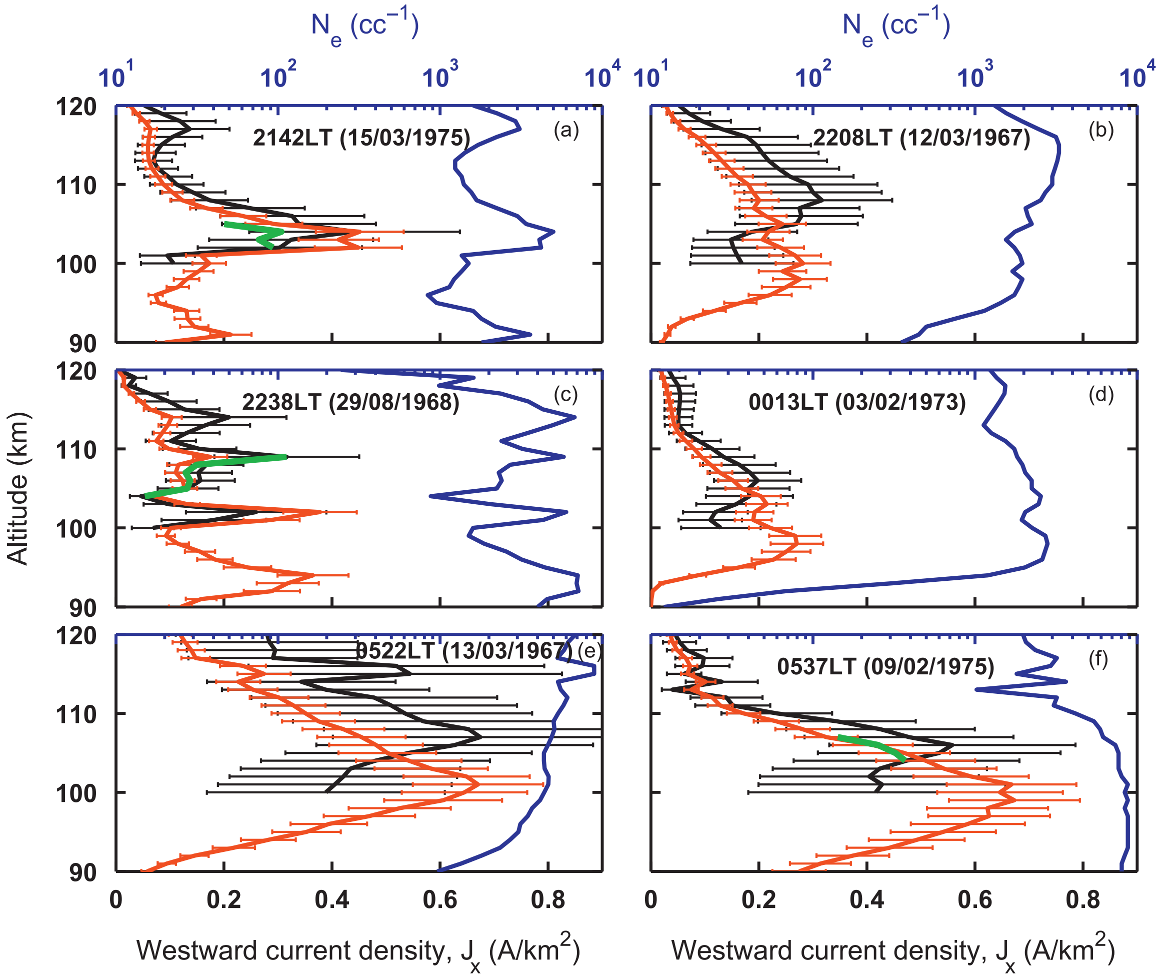

Fig. 2. Altitude profiles of estimated nighttime current densities (black) using method 1 and Eq. (3), the measured electron density profiles (blue curves) and R_{avg} values (see Fig. 1(c)). The altitude profiles of nighttime current densities over the dip equator (red colors) using the electrojet model of Anandarao (1976). The minimum current density (green) obtained using method 2 and Eq. (6) over the altitude wherein the presence of streaming waves was observed. Subplots (a–d) correspond to the profiles at various local times when the nighttime electron density measurements over Thumba during magnetically quiet conditions were available. (For interpretation of the references to color in this figure caption, the reader is referred to the web version of this paper.)

Table 1
The derived values of westward peak current density ($J_{x,max}$) using method 1, altitude (h_p) of $J_{x,max}$, measured electron density (N_e) at h_p, deduced R_{avg} at h_p and downward vertical drift (V_z) based on empirical model corresponding to the six rocket flights under consideration.

Case no.	Time and date	Altitude, h_p (km) of $J_{x,max}$	N_e (cc^{-1}) at h_p	R_{avg} at h_p	Downward V_z (m/s)	Westward $J_{x,max}$ (A/km^2)
1	2142 on 15/03/1975	104	5000	20.1	27.4	0.44
2	2208 on 12/03/1967	108	2540	23.5	33.1	0.32
3	2238 on 29/08/1968	109	5790	20.8	16.4	0.32
4	0013 on 03/02/1973	106	2240	24.8	22.2	0.20
5	0522 on 13/03/1967	107	4880	25.3	34.1	0.67
6	0537 on 09/02/1975	106	7356	24.8	19.1	0.56

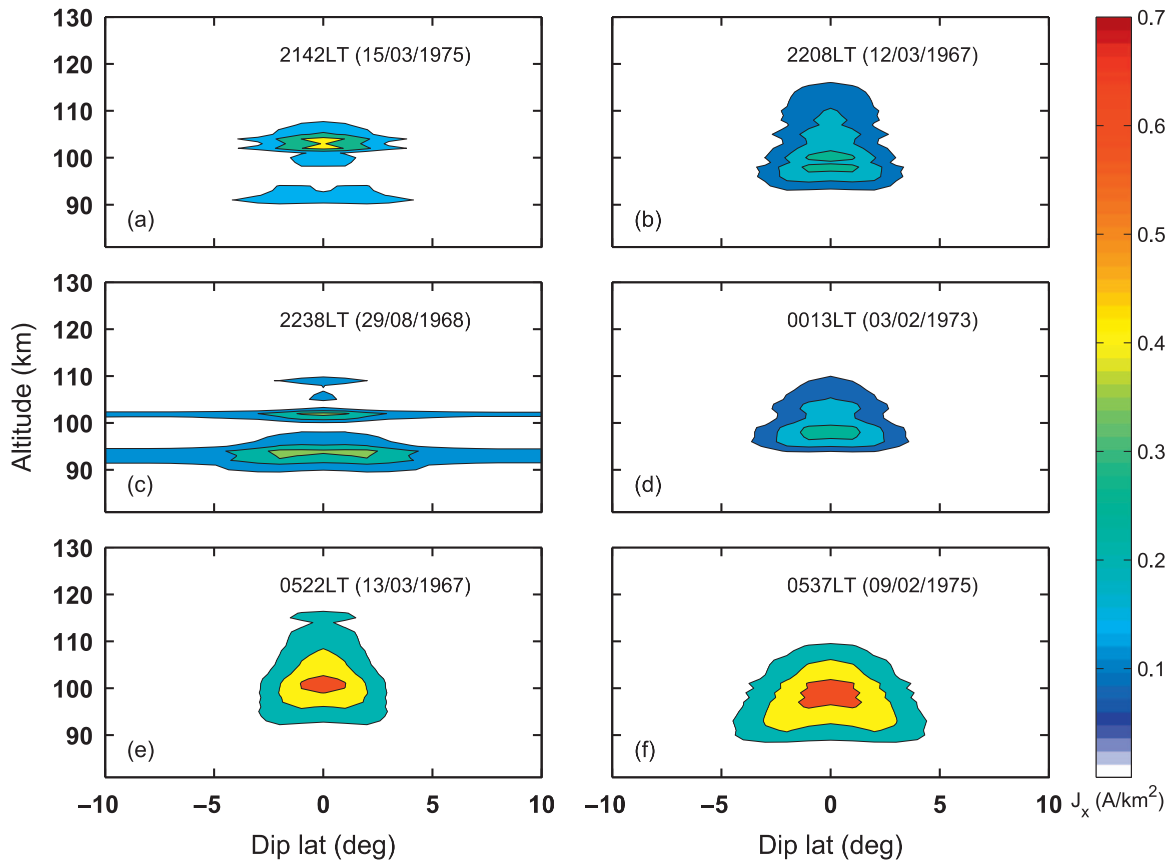

Fig. 3. Contours of iso-current density in zonal direction over magnetic latitude-altitude region obtained using electrojet model of Anandarao (1976). In this model calculation the electron densities are taken from in situ rocket measurements and zonal Sq electric field is chosen from the empirical model of plasma drift (Fejer et al., 2008) over Indian longitude. The color-bar represent strength current density (A/km^2). Current density contours in each subplot are plotted with steps of 30% of peak values over the dip equator. Subplots (a–d) correspond to iso-current contours corresponding to electron density measurement at different local times on a few nights. (For interpretation of the references to color in this figure the reader is referred to the web version of this paper.)

$$H = -\frac{1}{r}\frac{\partial V}{\partial \theta} = \frac{\mu_0 C}{2\pi r}\frac{(r/a)\sin\theta - 1}{(r/a)^2 + 1 - 2(r/a)\sin\theta} \quad (11)$$

The numerical simulation plane is divided into 1°(in θ) × 4 km (in r) blocks and induced H is calculated. H of each blocks are added up to get the net induced values at ground. The maximum uncertainty in H is found to be less than 20%.

5. Results and discussion

As mentioned in Section 3.1, Fig. 1 shows that R does not change significantly with respect to day and night time conditions and solar epochs. This aspect is used subsequently to derive the nighttime E-region current over the Indian sector. Fig. 2 depicts the altitude profiles of westward current densities during nighttime for geomagnetically quiet conditions estimated using the deduced R_{avg} values (black) using Eq. (3), and electrojet model (red) using Eq. (9), over the dip equator. The corresponding electron densities measured over Thumba at different local times on a few nights are overlaid on this figure (blue). In addition, minimum current densities ($J_{x,night,min}$) estimated using Eq. (6) are also plotted in Fig. 2 (with green color) over the altitude range wherever the streaming plasma waves were observed. The nighttime current density ranges from ~0.3 A/km^2 near midnight to ~0.7A/km^2 during early morning hours. The electrojet model estimated current densities match well (within the uncertainty limits) with the deduced current density above altitude region of 100 km.

The present investigation of the estimation of nighttime current density is based on the in situ electron density measurements conducted at different solar epochs and seasons. Thus, it is rather difficult to bring out the local time variation of nighttime current density as the electron density (N_e) and Sq electric fields (E_{Sq}) vary with these geophysical conditions. Nevertheless, comparison of

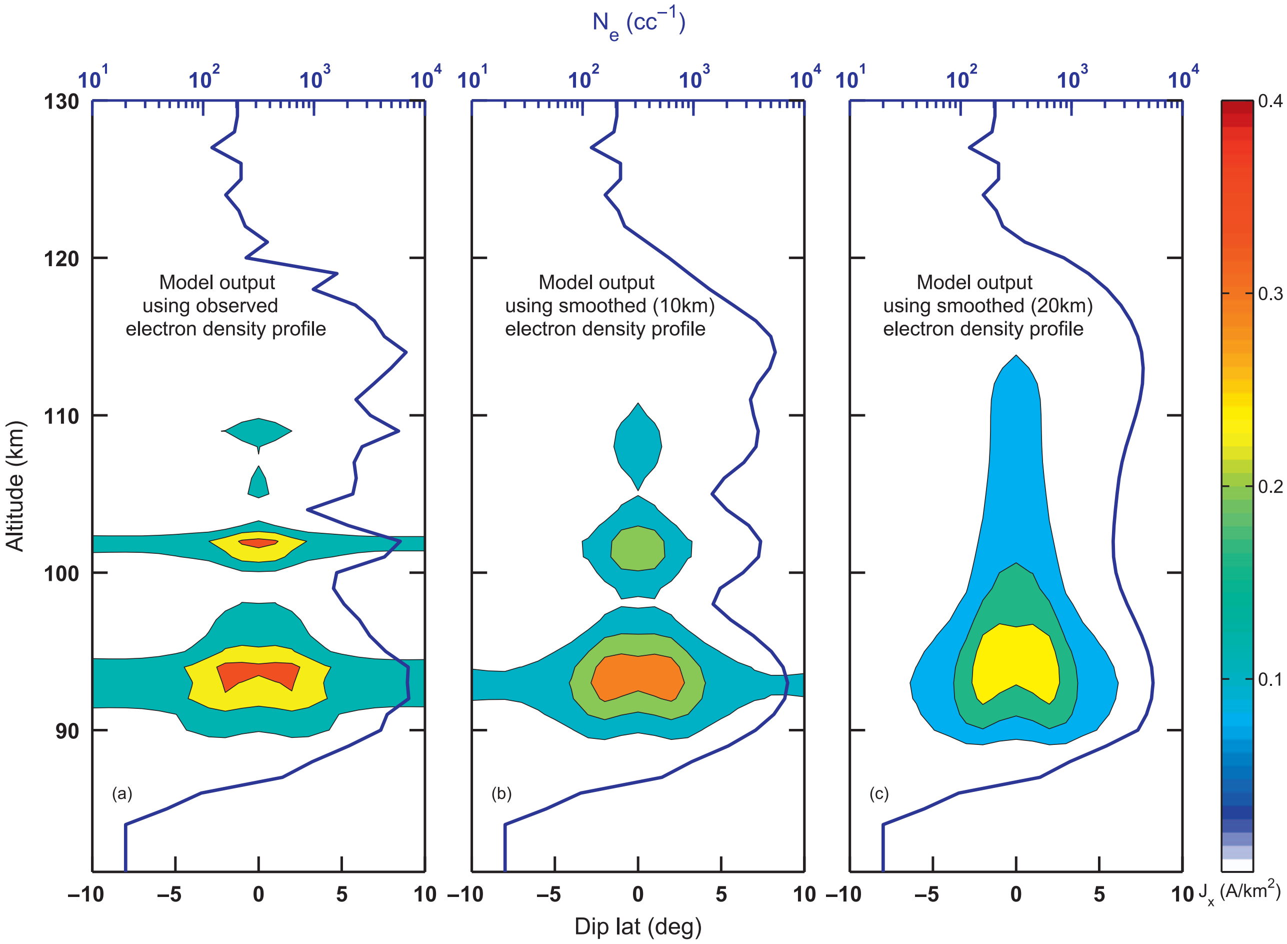

Fig. 4. (a) High resolution plots of iso-current density contours given in subplot 3(c). The input electron density profile (blue) is also overlaid. (b) and (c) Iso-current density profiles obtained after progressively smoothing the electron density profile shown in subplot (a) and using them as the input for current density calculation. The corresponding input electron density profiles are also shown in each subplot. Current density contours in each subplot are plotted with steps of 30% of the peak current values over the dip equator. *Note*: Color-bar scales are adjusted to bring out the features in current density contours. (For interpretation of the references to color in this figure caption, the reader is referred to the web version of this paper.)

these current densities in the subplots of Fig. 2 gives rise to the following points:

1. The peak altitudes (see black curves of subplots 2b, d, e and f) of the current density deduced using method 1 lie closer to the altitude of 107 km corresponding to the peak value of R whenever the altitude profiles of electron density are devoid of large structures between 100 km and 110 km. Thus, the values of R_{avg} at the altitude of peak current density remain nearly constant. Therefore, the peak values of current density ($J_{x,max}$) are found to vary, from one case to another, linearly with the variations of N_e and V_z at the peak altitude. The values given in Table 1 (obtained using method 1) are found to be consistent with this inference. For example, by comparing cases 2 and 5 in Table 1, the change in J_x is found to be almost doubled when N_e is nearly doubled without considerable change in V_z.
2. In the presence of large structures in N_e profile between 100 km and 110 km (subplots 2a and c), the current density maximizes at the altitude wherever electron densities and R_{avg} values are optimum. Thus, the peak current density need not lie around 107 km (refer cases 1 and 3 of Table 1).
3. In the absence of altitudinal structures, the altitude gradients in J_x profiles (above and/ or below $J_{x,max}$) obtained using the methods 1 and 3 are found to be larger whenever the J_x values are more (subplots 2e and f) compared to corresponding gradients whenever the J_x values are small (subplots 2b and d). This is consistent with the work of Onwumechili (1992b) where the strength and thickness of electrojet current density based on daytime measurements over the dip-equator were shown to be inversely proportional. However, it must be noted here that multiple layers in current density (subplots 2a and c) are often observed during nighttime and determination of the thickness of the peak current layer is not unambiguous.
4. In the presence of multiple layers in current density profile whenever the electron density is structured (subplots 2a and c), the altitude of peak current density can be identified using method 2, as the streaming waves observed by rocket borne measurements usually appear in the vicinity of the peak current.
5. The peak altitudes determined by method 3 are lower than those obtained by the other methods whenever the electron densities are devoid of large structures. However, the altitude profiles of the current densities obtained from all the three methods go nearly hand-in-hand with one another whenever the altitude structures in N_e are present.

In addition to the altitudinal structure in the current densities, the electrojet model provides latitudinal extents also. As mentioned earlier the altitude profiles of electron densities and the $(E_{Sq})_x$ from plasma drift model are given as inputs to the electrojet model. Fig. 3 represents the contour plots of westward current densities over the magnetic latitude-altitude plane. The color-bar in Fig. 3 corresponds to the strength of current densities. As the

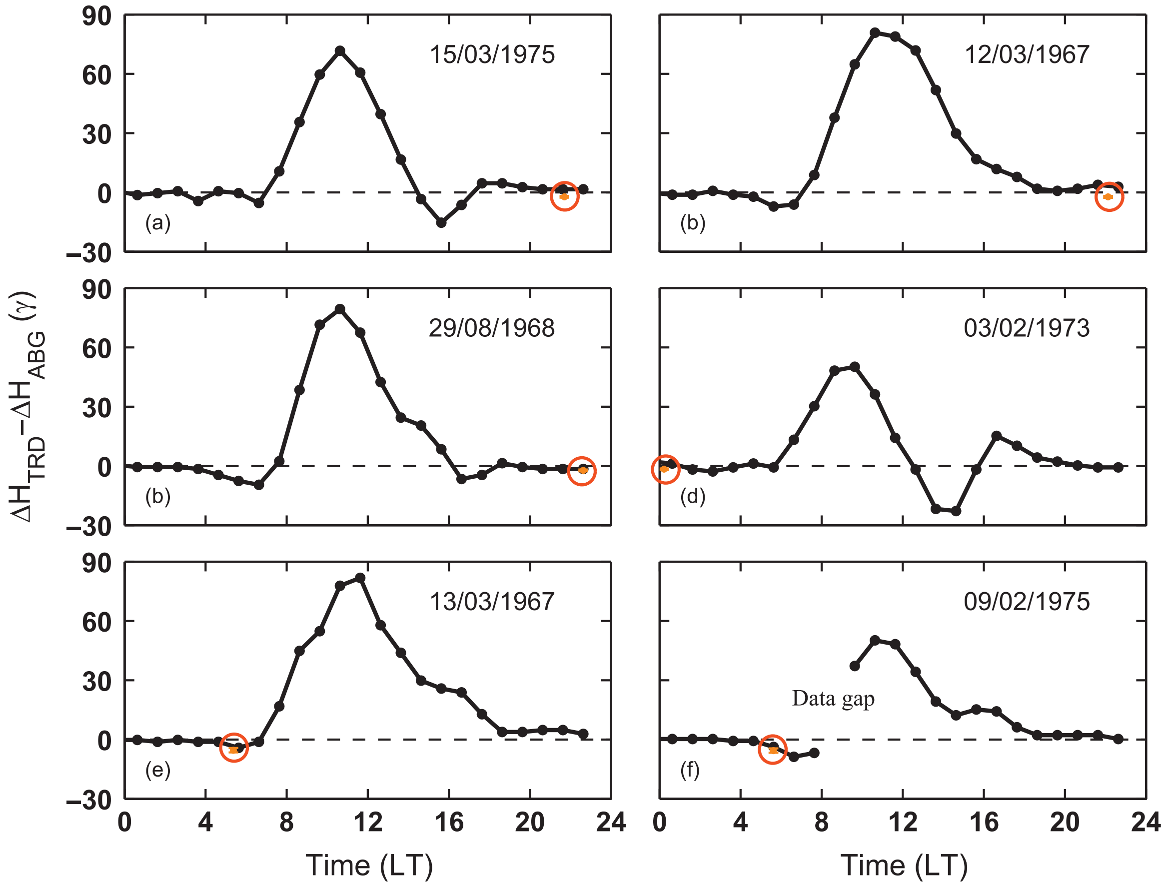

Fig. 5. Ground-based magnetometer measured hourly variation of electrojet strength over Thumba (ΔH_{TRD} – ΔH_{ABG} in black). Orange dots correspond to the calculated horizontal component of magnetic field induced at ground by the nighttime current densities shown in Fig. 3 using Eq. (11). (For interpretation of the references to color in this figure caption, the reader is referred to the web version of this paper.)

sensitivity study revealed that maximum progressive uncertainty in the current density obtained by combining the individual uncertainties of all input parameters is less than 20%, the difference between successive contours in each subplot is kept at 30% of the corresponding peak current density values over the dip equator.

Islands of current density contours are seen in subplots 3a and c. These distinct islands are missing in subplot 3b. They are more conspicuous only when the input electron densities have altitudinal structures. As a result, the altitude of peak current densities is not well defined. However, when the input electron densities have less structures the peak current altitude is well defined and island structures (in the altitude–latitude plane) disappear (subplots 3d–f). Hence, the effect of electron density structures in nighttime electrojet current needs further attention. In order to examine this effect, the altitude structures in electron densities measured at 2238 *LT* on 29 *August*, 1968 are gradually smoothed by Savitzky–Golay method (Savitzky and Golay, 1964) in the altitude range of 90–120 km. These electron density profiles along with a single value of $(E_{Sq})_x$ are used as input to the electrojet model and the corresponding current density profiles are obtained. Fig. 4a–c depicts the resulting iso-current density contours along with the input electron density values. Without smoothing the electron density profile, the island structures and larger latitudinal extent are observed (see Fig. 4a) in current density contours. Allowing more than 10 km structures between 90 and 120 km, the gaps between the islands have reduced and the latitudinal extent of the second island around 100 km has considerably reduced (see Fig. 4b). On further smoothing of the electron density, the reduction in the latitudinal extent of current density and disappearance of island structures are noticed in Fig. 4c. Therefore, the valley and peak in the altitude profile of electron density in region of 90–120 km appears to decide the gap between the islands and latitudinal extent of contours representing current density.

Based on the current density estimates by the electrojet model, the horizontal component (H) of the magnetic field induced at ground is calculated using Eq. (11) for all the cases depicted in Fig. 3. These calculated magnetic fields with uncertainties (marked in orange within red circles) are shown along with the hourly variations in the electrojet strength (represented by black line), derived on the basis of magnetic field measurements, in Fig. 5. It is known that strength of equatorial electrojet can be estimated based on the magnetic field measurements over a dip equatorial and an off-equatorial stations. Over the Indian sector, this can be done using magnetic measurements from Thumba and Alibag (18.6°N, 72.9°E, Dip angle 23.5°), a dip equatorial and off-equatorial stations respectively. It is known (e.g. Rastogi and Patil, 1986) that ΔH_{TRD} – ΔH_{ABG} represents strength of equatorial electrojet where ΔH is calculated by subtracting nighttime base value from the instantaneous H value (where ΔH_{TRD} and ΔH_{ABG} represent the ΔH values over Thumba and Alibag respectively). The nighttime base value is calculated by taking average of the five hourly values starting from 2300 h to 0300 h. The H values calculated from the nighttime currents obtained from the electrojet model are found to be consistent with the magnetic measurements.

It is well known that during nighttime there is a valley in the altitude profile of the electron density centered around 125–130 km. In order to investigate the effect of this valley region on the polarization field in the vertical direction (E_z), an exercise is carried out using the electrojet model with varying depth of the valley. For this investigation, the electron density measurement obtained at 2238 *LT*

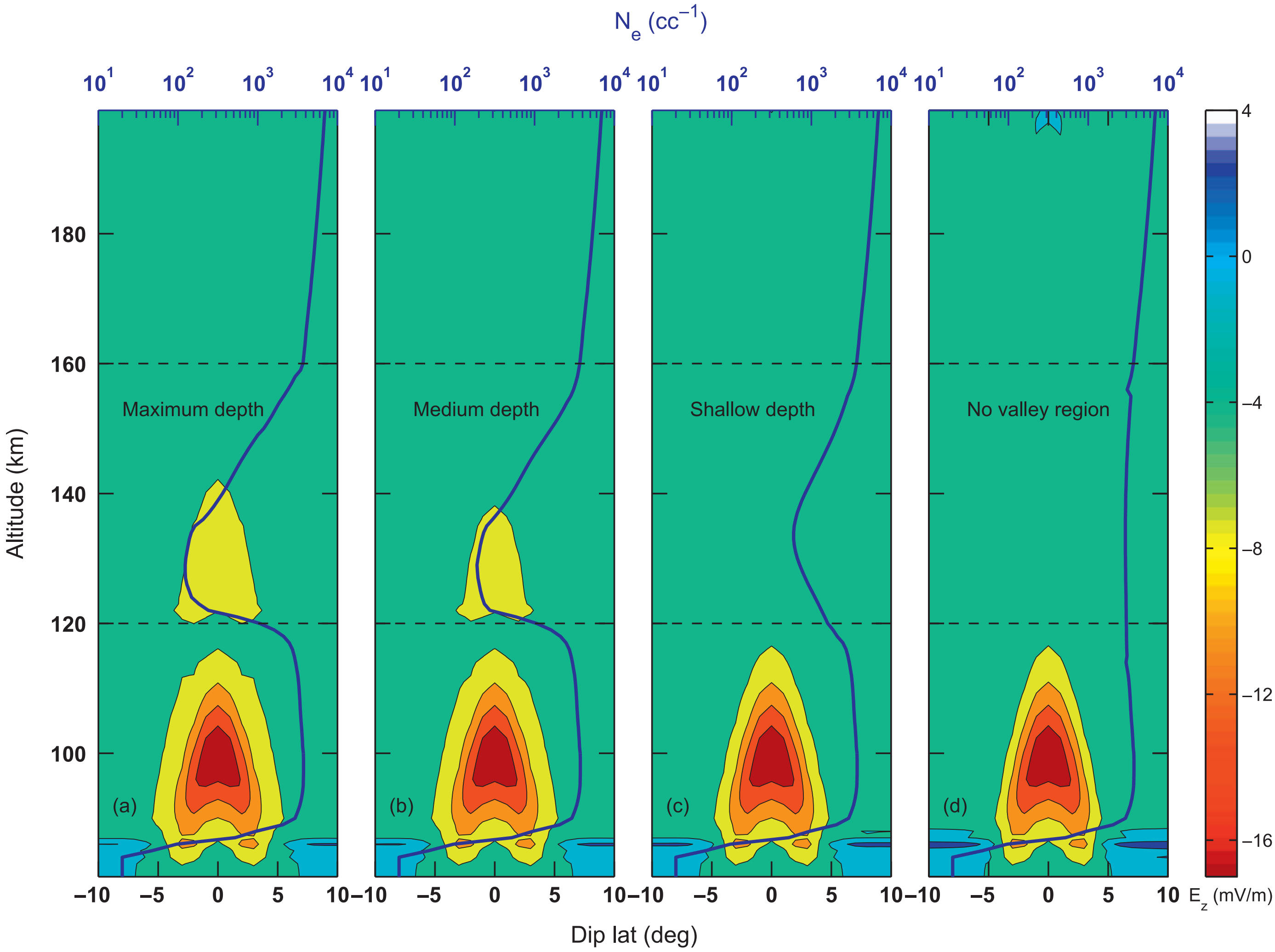

Fig. 6. Effects of the depth of the valley region on the polarization electric field in vertical direction (E_z in mV/m) for (a) maximum, (b) medium, (c) shallow depth and (d) no valley region. Iso-electric field contours in each subplot are plotted with steps of 20% of peak values over the dip equator. (For interpretation of the references to color in this figure, the reader is referred to the web version of this paper.)

Table 2
The values of polarization electric field in vertical direction (E_z in mV/m) obtained using electrojet model closer to the altitude of observation of streaming waves and zonal Sq electric field used in the model calculations.

Time and date	E_x (mV/m)	E_z (mV/m)
2142 on 15/03/1975	−1.03	−18.7
2238 on 29/08/1968	−0.62	−19.1
0537 on 09/02/1975	−0.72	−13.4

on 29 *August*, 1968 is first smoothed and then used as input to the electrojet model with varying depth of the valley region. Fig. 6 depicts the resulting contours of polarization field in the vertical direction (E_z), wherein 20% difference of the peak values are maintained by successive contours. However, there is no appreciable change in current densities around 105 km (not shown). It is found that E_z increases around 125 km when there is a deep valley while it progressively decreases as depth of the valley region reduces. Further, the minimum strength of polarization electric field in the vertical direction required for the generation of streaming waves is about 13.8 mV/m ($E_z = V_{x,min} \times B$) at 105 km. The electrojet model calculated E_z values, near the altitude region wherein the presence of streaming waves was observed during measurements (as provided in Table 2), are found to be consistent with requirement for generation of streaming waves in those altitude region barring a case during morning hours. This is probably due to the fact that the Fejer et al. (2008) model values deviate from the measurements on a few occasions (as mentioned in Section 3.1).

This investigation suggests that the nighttime base value of the horizontal component of magnetic field during geomagnetically quiet period over the Indian dip equatorial sector is well within 6 nT if one considers pre-midnight to early morning hours. However, during magnetically disturbed periods, the horizontal magnetic field may change during midnight hours in varying degrees owing to the alteration of ionospheric electric field or modulation of the magnetospheric current systems. Under such circumstances, it is important that these aspects are taken into account before any realistic estimation is made on the nighttime E-region current over the dip equatorial region. This is beyond the scope of the present work and will be attempted in future.

6. Summary

The salient points that emerged from the present investigation are as follows:

1. The nighttime current density deduced using method 1 and the available electron density measurements as well as with an

electrojet model reveals E-region current in the range of ~ 0.3–0.7 A/km^2 during pre-midnight to early morning hours on geomagnetically quiet days.
2. The nocturnal E-region current density strength seems to decrease from the post-sunset hours to the midnight hours and then increase during early morning hours.
3. Altitude structures are seen in the nighttime E-region current density and are shown to be associated with the altitude structures in the electron density.
4. The trough and crest in the altitude structures of the electron density seem to decide the latitudinal extent and altitudinal stratification of the nighttime E-region current density.
5. The dip equatorial polarization electric field in the vertical direction obtained from the electrojet model is shown to be sufficient to drive the observed streaming waves during nighttime in a limited altitude region around 105 km baring a case during early morning hours. The current density estimated using the streaming wave criterion is found to be well within the estimated currents.
6. The ground magnetometer observed magnetic field variations during quiet time are well within 6 nT and match fairly well with the calculated induced magnetic field deduced from the current density (obtained from electrojet model).
7. The well-known dip equatorial nighttime E-region valley in the electron density around 130 km is shown to increase the polarization electric field in the vertical direction near this altitude depending upon the depth of the valley.

Acknowledgments

We dedicate this work to the fond memory of Prof. R. Raghavarao whose sustained interest in the equatorial electrojet has been highly inspirational. One of the coauthors, B.G. Anandarao, fondly recalls the discussions that he had with Drs. Koneru S. Rao and Suhasini Rao on the numerical techniques used for the electrojet model. The hourly values of magnetic field measurements are courtesy of Indian Institute of Geomagnetism, Mumbai and obtained from the Word Data Center for Geomagnetism, Kyoto. All the rocket flight experiments mentioned in the paper were supported by the Indian Space Research Organization. This work is supported by the Department of Space, Government of India.

References

Anandarao, B.G., 1976. Effects of gravity wave winds and wind shears on equatorial electrojet. Geophys. Res. Lett. 3 (9), 545–548. http://dx.doi.org/10.1029/GL003i009p00545.
Anandarao, B.G., 1977. Studies on the dynamics of the equatorial ionosphere (Ph.D. thesis), Gujarat University.
Anandarao, B.G., Desai, J.N., Giles, M., Martelli, G., Raghavarao, R., Rothwell, P., 1977. Electric field in the equatorial ionosphere. J. Atmos. Terr. Phys. 39, 927–931.
Anandarao, B.G., Raghavarao, R., 1987. Structural changes in the currents and fields of the equatorial electrojet due to zonal and meridional winds. J. Geophys. Res. 92 (A3), 2514–2526. http://dx.doi.org/10.1029/JA092iA03p02514.
Campbell, W.H., 1973. The field levels near midnight at low and equatorial geomagnetic stations. J. Atmos. Terr. Phys. 35, 1127–1146. http://dx.doi.org/10.1016/0021-9169(73)90010-X.
Campbell, W.H., 1979. Occurrence of AE and Dst geomagnetic index levels and the selection of the quietest days in a year. J. Geophys. Res. 84 (A3), 875–881. http://dx.doi.org/10.1029/JA084iA03p00875.
Chakrabarty, D., Sekar, R., Narayanan, R., Devasia, C.V., Pathan, B.M., 2005. Evidence for the interplanetary electric field effect on the OI 630.0 nm airglow over low latitude. J. Geophys. Res. 110 (A11), 301. http://dx.doi.org/10.1029/2005JA011221.
Davis, T.N., Burrows, K., Stolarik, J.D., 1967. A latitude survey of the equatorial electrojet with rocket-borne magnetometers. J. Geophys. Res. 72 (7), 1845–1861. http://dx.doi.org/10.1029/JZ072i007p01845.
Eccles St., J.V., Maurice, J.P., Schunk, R.W., 2015. Mechanisms underlying the prereversal enhancement of the vertical plasma drift in the low-latitude ionosphere. J. Geophys. Res. 120 (6), 4950–4970. http://dx.doi.org/10.1002/2014JA020664.
Farley, D.T., 2009. The equatorial E-region and its plasma instabilities: a tutorial. Ann. Geophys. 27 (4), 1509–1520. http://dx.doi.org/10.5194/angeo-27-1509-2009.
Fejer, B.G., Jensen, J.W., Su, S.Y., 2008. Quiet time equatorial F region vertical plasma drift model derived from ROCSAT-1 observations. J. Geophys. Res. 113 (A5), 304. http://dx.doi.org/10.1029/2007JA012801.
Finlay, C.C., et al., 2010. International geomagnetic reference field: the eleventh generation. Geophys. J. Int. 183 (3), 1216–1230. http://dx.doi.org/10.1111/j.1365-246X.2010.04804.x.
Forbes, J.M., 1981. The equatorial electrojet. Rev. Geophys. 19 (3), 469–504. http://dx.doi.org/10.1029/RG019i003p00469.
Gupta, S.P., 1986. Formation of sporadic E layers at low magnetic latitudes. Planet. Space Sci. 34 (11), 1081–1085.
Gupta, S.P., 1990. Ionisation layers over the magnetic equator during meteor shower days. Adv. Space Res. 10 (10), 105–108. http://dx.doi.org/10.1016/0273-1177(90)90016-S.
Haerendel, G., Eccles, J.V., 1992. The role of the equatorial electrojet in the evening ionosphere. J. Geophys. Res. 97 (A2), 1181–1192. http://dx.doi.org/10.1029/91JA02227.
Jacchia, L.G., 1971. Revised Static Models of the Thermosphere and Exosphere with Empirical Temperature Profiles, Smithsonian Astrophysical Observatory (SAO) Special Report 332.
Jadhav, G., Rajaram, M., Rajaram, R., 2002. A detailed study of equatorial electrojet phenomenon using Ørsted satellite observations. J. Geophys. Res. 107 (A8), 1175. http://dx.doi.org/10.1029/2001JA000183.
Lühr, H., Maus, S., Rother, M., 2004. Noon-time equatorial electrojet: its spatial features as determined by the CHAMP satellite. J. Geophys. Res. 109 (A1), 306. http://dx.doi.org/10.1029/2002JA009656.
Marcos, F.A., 1990. Accuracy of atmospheric drag models at low satellite altitudes. Adv. Space Res. 10 (3), 417–422. http://dx.doi.org/10.1016/0273-1177(90)90381-9.
Matsushita, S., 1968. Sq and L current systems in the ionosphere. Geophys. J. R. Astron. Soc. 15 (1–2), 109–125.
Matsushita, S., 1971. Interactions between the ionosphere and the magnetosphere for Sq and L variations. Radio Sci. 6 (2), 279–294. http://dx.doi.org/10.1029/RS006i002p00279.
Matsushita, S., Maeda, H., 1965. On the geomagnetic solar quiet daily variation field during the IGY. J. Geophys. Res. 70 (11), 2535–2558. http://dx.doi.org/10.1029/JZ070i011p02535.
Mayaud, P.N., 1976. Magnetospheric and night-time induced effects in the regular daily variation S_R. Planet. Space Sci. 24, 1049–1057. http://dx.doi.org/10.1016/0032-0633(76)90123-9.
Onwumechili, C.A., 1992a. A study of rocket measurements of ionospheric currents —I. General setting and night-time ionospheric currents. Geophys. J. Int. 108 (2), 633–640. http://dx.doi.org/10.1111/j.1365-246X.1992.tb04642.x.
Onwumechili, C.A., 1992b. A study of rocket measurements of ionospheric currents —III. Ionospheric currents at the magnetic dip equator. Geophys. J. Int. 108 (2), 647–659. http://dx.doi.org/10.1111/j.1365-246X.1992.tb04644.x.
Onwumechili, C.A., Ezema, P.O., 1977. On the course of the geomagnetic daily variation in low latitudes. J. Atmos. Terr. Phys. 39 (9–10), 1079–1086. http://dx.doi.org/10.1016/0021-9169(77)90016-2.
Pfaff, R.F., Sobral, J.H.A., Abdu, M.A., Swartz, W.E., LaBelle, J.W., Larsen, M.F., Goldberg, R.A., Schmidlin, F.J., 1997. The Guará Campaign: a series of rocket-radar investigations of the Earth's upper atmosphere at the magnetic equator. Geophys. Res. Lett. 24 (13), 1663–1666. http://dx.doi.org/10.1029/97GL01534.
Pingree, J.E., Fejer, B.G., 1987. On the height variation of the equatorial F region vertical plasma drifts. J. Geophys. Res. 92 (A5), 4763–4766. http://dx.doi.org/10.1029/JA092iA05p04763.
Prakash, S., Gupta, S.P., Subbaraya, B.H., 1970. A study of the irregularities in the night time equatorial E-region using a Langmuir probe and plasma noise probe. Planet. Space Sci. 18 (9), 1307–1318. http://dx.doi.org/10.1016/0032-0633(70)90141-8.
Prakash, S., Subbaraya, B.H., 1967. Langmuir probe for the measurement of electron density and electron temperature in the ionosphere. Rev. Sci. Instrum. 38 (8), 1132–1136. http://dx.doi.org/10.1063/1.1721035.
Raghavarao, R., Anandarao, B.G., 1987. Equatorial electrojet and the Counter-Electrojet. Indian J. Radio Space Phys. 16, 54–75.
Rastogi, R.G., Chandra, H., James, M.E., 1996. Nocturnal variations of geomagnetic horizontal field at equatorial stations. Geophys. Res. Lett. 23 (19), 2601–2604. http://dx.doi.org/10.1029/96GL02390.
Rastogi, R.G., Iyer, K.N., 1976. Quiet day variation of geomagnetic H-field at low latitudes. J. Geomagn. Geoelectr. 28 (6), 461–479. http://dx.doi.org/10.5636/jgg.28.461.
Rastogi, R.G., Patil, A., 1986. Complex structure of equatorial electrojet current. Curr. Sci. 55 (9), 433–436.
Richmond, A.D., 1973. Equatorial electrojet—I. Development of a model including winds and instabilities. J. Atmos. Terr. Phys. 35 (6), 1083–1103. http://dx.doi.org/10.1016/0021-9169(73)90007-X.
Sampath, S., Sastry, T.S.G., 1979. AC electric fields associated with the plasma instabilities in the equatorial electrojet-III. J. Geomagn. Geoelectr. 31 (3), 391–400. http://dx.doi.org/10.5636/jgg.31.391.
Sastry, T.S.G., 1970. Diurnal changes in the parameters of the equatorial electrojet as observed by rocket-borne magnetometers. Space Res. X, 778–785.

Savitzky, A., Golay, M.J.E., 1964. Smoothing and differentiation of data by simplified least squares procedures. Anal. Chem. 36 (8), 1627–1639. http://dx.doi.org/10.1021/ac60214a047.

Sekar, R., Gupta, S.P., Acharya, Y.B., Chakrabarty, D., Pallamraju, D., Pathan, B.M., Tiwari, D., Choudhary, R.K., 2013. Absence of streaming plasma waves around noontime over Thumba in recent times: is it related to the movement of the dip equator?. J. Atmos. Sol.-Terr. Phys. 103, 8–15. http://dx.doi.org/10.1016/j.jastp.2013.02.005.

Shuman, B.M., 1970. Rocket measurement of the equatorial electrojet. J. Geophys. Res. 75 (19), 3889–3901. http://dx.doi.org/10.1029/JA075i019p03889.

Stening, R.J., Winch, D.E., 1987. Night-time geomagnetic variations at low latitudes. Planet. Space Sci. 35 (12), 1523–1539. http://dx.doi.org/10.1016/0032-0633(87)90078-X.

Subbaraya, B.H., Muralikrishna, P., Sastry, T.S.G., Prakash, S., 1972. A study of the structure of electrical conductivities and the electrostatic field within the equatorial electrojet. Planet. Space Sci. 20 (1), 47–52. http://dx.doi.org/10.1016/0032-0633(72)90139-0.

Subbaraya, B.H., Prakash, S., Gupta, S.P., 1983. Electron Densities in the Equatorial Lower Ionosphere from the Langmuir Probe Experiments Conducted at Thumba During 1966–1978. Scientific Report, ISRO-PRL-SR-15-83.

Subbaraya, B.H., Prakash, S., Gupta, S.P., 1985. Structure of the equatorial lower ionosphere from the Thumba Langmuir probe experiments. Adv. Space Res. 5 (7), 35–38. http://dx.doi.org/10.1016/0273-1177(85)90352-7.

Sudan, R.N., Akinrimisi, J., Farley, D.T., 1973. Generation of small-scale irregularities in the equatorial electrojet. J. Geophys. Res. 78 (1), 240–248. http://dx.doi.org/10.1029/JA078i001p00240.

Sugiura, M., Poros, D.J., 1969. An improved model equatorial electrojet with a meridional current system. J. Geophys. Res. 74 (16), 4025–4034. http://dx.doi.org/10.1029/JA074i016p04025.

Takeda, M., Araki, T., 1985. Electric conductivity of the ionosphere and nocturnal currents. J. Atmos. Terr. Phys. 47 (6), 601–609. http://dx.doi.org/10.1016/0021-9169(85)90043-1.

Journal of Atmospheric and Solar–Terrestrial Physics 157–158 (2017) 42–54

Contents lists available at ScienceDirect

Journal of Atmospheric and Solar–Terrestrial Physics

journal homepage: www.elsevier.com/locate/jastp

Comparison of quiet time vertical plasma drifts with global empirical models over the Indian sector: Some insights

Kuldeep Pandey[a,b], R. Sekar[a,*], S.P. Gupta[a], D. Chakrabarty[a], B.G. Anandarao[a]

[a] *Physical Research Laboratory, Navrangpura, Ahmedabad 380009, India*
[b] *Indian Institute of Technology-Gandhinagar, Ahmedabad 382424, India*

A R T I C L E I N F O

Keywords:
Equatorial electrojet
Vertical plasma drifts
Streaming and gradient drift plasma waves

A B S T R A C T

The threshold vertical plasma drifts and their polarities are inferred from E-region irregularities reported earlier using different experiments conducted from India during geomagnetically quiet time. In addition, the hourly variations of magnetometer data sets are used in conjunction with an equatorial electrojet model (Anandarao, 1976) to deduce the vertical drifts around noon time (10:00–140:00 *LT*). These results are then compared with the vertical drifts presented by empirical models (Scherliess and Fejer, 1999; Fejer et al., 2008a) corresponding to the 60°*E* longitude sector. In general, the vertical drifts presented by empirical models are consistent with those inferred from snapshot measurements of E-region irregularities at different local times of the day except around sunrise hours. Further, the vertical drifts presented by Fejer et al. (2008a) model match fairly well with seasonally averaged vertical drifts deduced (within 1σ variation) using magnetometer data. A time difference is noticed between occurrence of pre-reversal enhancement in vertical drifts over India reported earlier using different techniques and Scherliess and Fejer (1999) model. Probable reason for the time difference is discussed. The occurrence characteristic of afternoon equatorial counter electrojet in June solstice during low solar epoch is consistent with the drifts obtained from empirical models. The seasonally averaged vertical drifts during nighttime reported earlier using ionosonde/HF radar experiments are not consistent with the presence of streaming plasma waves on a few occasions. Further, nocturnal vertical drifts are systematically under-estimated and probable reason for this is discussed.

1. Introduction

It is well known that the solar quiet (*Sq*) time electric field (E) is generated in the E-region of ionosphere by dynamo action. *Sq* electric fields over low latitude regions are mapped to the dip-equatorial F-region where they cause electrodynamic drifts of the plasma, $\mathbf{V} = \frac{\mathbf{E}\times\mathbf{B}}{B^2}$, B being the strength of the geomagnetic field. Therefore, the E-region zonal electric field (E_x) is treated as driving agency for the vertical drift (V_z) in the F-region. The vertical drifts are known (Fejer, 1981) to be upward during daytime and downward in nocturnal hours under geomagnetically quiet periods. The diurnal variations of vertical drifts in different seasons over the Peruvian sector had been presented (e.g., Woodman, 1970) in the past using highly accurate (better than 2 ms^{-1}) measurements of V_z obtained with Incoherent Scatter Radar (ISR) at Jicamarca.

The low latitude ionosphere is characterized by several large scale plasma processes, like equatorial electrojet, plasma irregularities (streaming and gradient drift waves) associated with it, plasma fountain, plasma bubbles, etc. The generation and evolution of all these processes depend on the strength and/or polarity of *Sq* electric field. Hence, in order to address the low latitude ionospheric processes in a comprehensive manner, it is important to know the variations in *Sq* electric field in different seasons and solar cycles. In absence of ISR over the Indian sector, the vertical drifts or zonal electric fields had been traditionally deduced (refer Section 2) based on ionosonde, phase path sounder, HF Doppler radar and magnetometer measurements. Considering the fact that each of these techniques come with its own limitations and uncertainties (discussed later), it is important to evaluate the consistency of the vertical drifts derived from different techniques with those obtained from global empirical models already available. This will help not only to understand the merits and demerits of individual techniques in a better way but also to evaluate the applicability of global models of vertical drifts to accurately capture the ionospheric processes over the Indian sector.

As already stated, each technique used to derive the vertical drift comes with its own limitation(s). For example, in an ionosonde experiment the recorded movement of ionospheric F-layer along the vertical direction can be due to production by photo-ionization and/or

* Corresponding author.
E-mail address: rsekar@prl.res.in (R. Sekar).

http://dx.doi.org/10.1016/j.jastp.2017.03.012
Received 24 October 2016; Received in revised form 24 February 2017; Accepted 23 March 2017
Available online 28 March 2017
1364-6826/

loss by chemical recombination and/or by electrodynamic processes. The presence of all the three processes during daytime makes it difficult to compute the vertical drifts from the recorded layer movements. But, during nighttime, when plasma production is negligible in absence of solar ionizing radiation, the vertical drifts are deduced from the temporal movement of F-layer (apparent drift) after correcting for the layer movement due to chemical loss. Further, for layer movements above 300 km altitude the difference between electrodynamic and apparent vertical drifts arising due to recombination processes is shown (Bittencourt and Abdu, 1981; Krishna Murthy et al., 1990) to be negligible.

The measurements of V_z during twilight time and their nocturnal variations have been reported earlier (refer Section 2) using several experiments conducted from Trivandrum (TRD, $8.5°N$, $76.9°E$). In addition, the threshold value and polarity of vertical drift can be deduced from the presence/absence of E-region irregularities (streaming and gradient drift waves) reported earlier (refer Section 2) at different local times of the day using sounding rocket flight and VHF radar experiments over TRD.

A number of works reported in the past provided snap-shot as well as seasonally averaged vertical drifts. In the present work, an attempt is made to consolidate the measurements of vertical drifts made by a few techniques from the Indian dip-equatorial stations and compare them with the drifts presented by global empirical models of Scherliess and Fejer (1999) and Fejer et al. (2008a) (henceforth Scherliess-99 and Fejer-08), to investigate their consistencies over the Indian sector. Further, considering the fact that in empirical models the vertical drifts have been averaged over at least $\pm 5°$ dip-latitude, the vertical drifts presented earlier using ionosonde and HF radar techniques over Kodaikanal (KDK, $10.3°N$, $77.5°E$), whose dip-latitude is less than $1.5°$, are also used for this comparison. In addition, the vertical drifts around noon hours are deduced using seasonally averaged hourly variation of magnetometer data in conjunction with an equatorial electrojet model (Anandarao, 1976) and used for this comparison.

2. Details of the dataset

In the present investigation, the average F-region vertical drifts measured during nighttime from ionosonde (Sastri, 1984; Subbarao and Krishna Murthy, 1994; Krishna Murthy and Hari, 1996; Madhav Haridas et al., 2015), phase path sounder (Ramesh and Sastri, 1995; Sastri, 1996) and HF Doppler radar (Nair et al., 1993) experiments are used. Further, the electric fields deduced from E-region irregularities during day and night are also utilized. As the equatorial vertical drifts are sensitive to geomagnetic conditions (Fejer et al., 2008b), the present work pertains to only the quiet time conditions with Ap < 30 and/or Kp ≤ 3. The available observational data sets span over five decades (1957–2008) involving solar flux variations during several solar cycles. The solar flux levels of $F_{10.7} < 130$ *sfu* and $F_{10.7} > 160$ *sfu* are respectively considered to represent the low and high solar epochs similar to those considered by the empirical models.

The observations with different time axes are converted into a single time format corresponding to the local time (*LT*) at TRD (longitude $76.9°E$). The observations are classified into three seasons, namely, December solstice (November–December–January–February), equinox (March-April, September-October) and June solstice (May–June–July–August) similar to the seasonal classifications followed in Scherliess-99 and Fejer-08.

The ionosonde observations of F layer movement reported by Subbarao and Krishna Murthy (1994) are converted into vertical plasma drift after correcting for chemical recombination effects based on their work. Further, apparent drifts reported by Sastri (1984) using ionosonde observations over KDK during 1957–1959 can be treated as electrodynamic drifts since the layer heights are well above 300 km during solar maximum.

The vertical drifts have been reported using phase path sounder over KDK (Ramesh and Sastri, 1995; Sastri, 1996) and Doppler radar over TRD (Nair et al., 1993) operated at 4 MHz and 5.5 MHz respectively. As the altitudes of reflecting layers, corresponding to these high operative frequencies, were considered to be well above 300 km during pre-midnight hours, no explicit corrections for the recombination losses were made in those results.

The presence of streaming and gradient drift waves was reported using back scatter radars operated from TRD in HF (18 MHz) (Tiwari et al., 2003) and VHF (54.95 MHz) (Prakash and Muralikrishna, 1976) frequencies. The limiting values of plasma drifts using threshold condition of streaming waves (refer Section 3) and their polarities from Doppler shift are deduced. The plasma drifts deduced from the E-region structures (e.g., Reddy et al., 1987; Viswanathan et al., 1987) are not considered in the present work, as the calibration factors to convert them to ambient plasma drifts are not available.

The in-situ measurements (e.g., Prakash et al., 1971; Gupta, 2000) of electron density profiles and structures in them had been obtained using high frequency Langmuir probes (Prakash and Subbaraya, 1967; Subbaraya et al., 1983, 1985) on board rocket flight experiments. Those were conducted over TRD at different local times of the day covering different seasons under high and low solar epochs. The generation processes of electron density structures depend on the ambient electric fields. As mentioned earlier, the limiting plasma drifts are deduced from the presence of streaming waves. In addition, the observed gradient in the altitude profile of electron densities and the presence/absence of gradient drift waves are used to deduce the polarity of vertical electric field from which the direction of zonal electric field is inferred, as these two components are related over the dip-equator.

The vertical drifts deduced from the observations of E-region structures, mentioned above, under high and low solar epochs are summarized in Tables 1 and 2 respectively. The Tables provide limiting values of vertical drift for the presence of streaming waves ($> +12\ \mathrm{ms}^{-1}$ during daytime, $< -12\ \mathrm{ms}^{-1}$ during nighttime) while the inverse conditions are taken for their absence. Further, for the time interval when streaming waves have been detected on some days and found absent on some other days the vertical drift are indicated with $\sim \pm 12\ \mathrm{ms}^{-1}$. The observations of streaming waves spanned from 1967 to 1999 when the dip angle over TRD was between $-0.9°$ and $+1.2°$ (IGRF-12, Thébault, 2015). Hence, the existence of streaming waves is consistent with the conclusion of Sekar et al. (2013).

Barium vapour cloud release experiments provide in-situ measurements of plasma drifts associated with ambient electric field. The vertical drifts around twilight time measured with these experiments over TRD (e.g., Anandarao et al., 1977) and Sriharikota (SHK, $13.7°N$, $80.2°E$, a station close to the dip-equator) (e.g., Sekar, 1990) are used in the present work.

In the present work, a methodology (see Appendix) is adopted to derive the quiet time vertical drifts during 10:00–14:00 *LT* using magnetometer datasets. The parameter $\Delta H_{equator} - \Delta H_{off-equator}$ (where H is the horizontal component of geomagnetic field and ΔH is calculated by subtracting nighttime base value from the instantaneous H values), derived using ground based magnetometer data, is conventionally (Rastogi and Patel, 1975) used as a proxy for the strength of equatorial electrojet. Assuming that the variations in ionospheric conductivities are not significant during 10:00–14:00 *LT*, variations in $\Delta H_{equator} - \Delta H_{off-equator}$ during this period can be treated as variations in the zonal electric fields.

Finally, the empirical models Scherliess-99 and Fejer-08 provide the dip-equatorial vertical plasma drifts at different local times and seasons during geomagnetically quiet periods. In order to compare with the vertical drifts derived based on measurements by different techniques mentioned earlier, the model drifts corresponding to $60°E$ longitude which is closest to Indian-dip equator are reproduced from Figure 8 of Scherliess-99 and Figure 7 of Fejer-08.

3. Results

Fig. 1 depicts the diurnal variations of vertical drift (black colored solid curves) presented by Scherliess-99 model for high solar epoch. Subplots 1(a), 1(b) and 1(c) show the vertical drifts in December solstice (November–December–January–February), equinox (March–April, September–October) and June solstice (May–June–July–August) respectively.

In subplot 1(a), the blue and green colored (solid, dash and dash-dot) curves portray the average nocturnal variations of V_z obtained using ionosonde/radar experiments from TRD and KDK respectively. The blue colored dash curve represents V_z computed using the average nocturnal variations of $h'F$ presented by Subbarao and Krishna Murthy (1994); and blue colored dash-dot curve portrays the average V_z variation during nighttime presented by Madhav Haridas et al. (2015). The green colored dashed and solid curves depict the average vertical drifts during dusk-midnight hours presented by Sastri (1984) and Ramesh and Sastri (1995) respectively. The 1σ variation in vertical drift at prereversal enhancement (PRE) time, as provided by Ramesh and Sastri (1995), is reproduced with green colored solid vertical bar on the top right corner of subplot 1(a) as well as in subplots 1(b-c). It must be noted that 1σ variation will be provided subsequently in this work wherever it is available in the literature under consideration here.

The twilight time in-situ measurements of vertical drifts reported by Anandarao et al. (1977) and Sekar (1990) are shown with magenta colored dots at the particular LT of the experiments. The average nocturnal variation of vertical drifts corresponding to the zonal electric fields presented by Krishna Murthy and Hari (1996) is shown with the dark magenta colored solid curve. In addition, average variation of vertical drift around noon hours deduced from magnetometer records is portrayed with the maroon colored solid curve. The standard deviation (σ) of these deduced vertical drifts, estimated based on the variations in $\Delta H_{TRD} - \Delta H_{ABG}$ (see Appendix), is shown as vertical bars on the curve.

The vertical arrows (at the bottom of subplot) are drawn at the particular LT corresponding to the sounding rocket experiments, listed in Tables 1 and 2, in which the streaming waves have been observed. Similarly, the solid horizontal lines (at the bottom of subplot) are drawn for the particular time interval during which the streaming waves have been observed using VHF radar experiments, listed in Tables 1 and 2. The presence or absence of streaming waves is respectively portrayed with teal or red colors. It is to be noted that teal and red colored horizontal lines are simultaneously used for certain durations when presence of streaming waves were detected on some days and found absent on some other days.

In subplots 1(b) and 1(c) the same notations which have been used in subplot 1(a) are followed to present the vertical drifts corresponding to equinox and June solstice respectively. An additional green colored dotted curve in subplot 1(c) depicts the vertical drift presented by Sastri (1996). The 1σ variation in vertical drifts at PRE time, as provided by Sastri (1996), is reproduced with green colored dotted vertical bar on top right corner in subplot 1(c).

Fig. 2 depicts the diurnal variations of vertical drift (black solid curves) presented by Scherliess-99 model corresponding to different seasons under low solar epoch. The values of V_z obtained using experiments conducted from TRD, KDK, SHK and magnetometer records are overlaid in respective subplots with same notations as in Fig. 1. Note that, if the ionosonde/radar derived average nocturnal vertical drifts are not available from the same works that are used to construct Fig. 1, the respective color codes and pattern of the curves are not utilized in Fig. 2 to maintain uniformity and avoid ambiguity. The additional blue colored solid curves in Fig. 2 portray the average nocturnal V_z variations presented by Nair et al. (1993). The nighttime averaged 1σ variation in vertical drifts, as provided by Nair et al. (1993), is reproduced with blue colored solid vertical bars in respective subplots of Fig. 2.

Figs. 3 and 4 depict the diurnal variations of vertical drifts (black curves) presented by Fejer-08 model corresponding to different seasons under high and low solar epochs respectively. The vertical drifts obtained using experiments conducted over TRD, KDK, SHK and magnetometer records under high and low solar epochs are overlaid in Figs. 3 and 4 with same notations and color codes as in Figs. 1 and 2 respectively.

The gray colored horizontally shaded region in each subplot marks the range of vertical drift values in which presence of streaming waves can be expected. The reasoning for this demarcation is as follows. The generation of streaming waves is known (Farley, 2009) to get triggered whenever magnitude of zonal drift (V_x) of electrons exceeds the ion-acoustic speed of the medium, which is about 370 ms^{-1} at ~105 km altitude over the Indian sector. The plasma drifts along the zonal (V_x) and vertical (V_z) directions are known (Anandarao et al., 1977; Sekar et al., 2013) to be connected, over the dip-equator, by a relation $V_x=RV_z$, where R is equal to the ratio of Hall to Pedersen conductivities. Recently, R is shown (Pandey et al., 2016) to remain nearly same, irrespective of local time of the day and solar epoch, with it's value about 30 at ~105 km altitude. Hence, whenever the streaming waves are present the magnitude of vertical drift must be greater than 12 ms^{-1}. The above inference of limiting plasma drift of $\sim \pm 12\ ms^{-1}$ gets the support from the occurrence of streaming waves on some days and absence on some other days (see subplots 1b, 2a-2c, 3b, 4a-4c). It is expected that the vertical drifts would lie within or outside this gray colored shaded region whenever the streaming waves are present (teal colored vertical arrows/horizontal lines) or absent (red colored vertical arrows/horizontal lines) respectively.

As stated earlier, Tables 1 and 2 summarize the results from sounding rocket flights (e.g. Prakash et al., 1969, 1970, 1974; Prakash and Pal, 1985; Gupta and Prakash, 1979; Gupta, 1986, 1997) and VHF/HF radar (e.g. Sastri et al., 1991; Ravindran and Krishna Murthy, 1997a, 1997b; Krishna Murthy et al., 1998) experiments. The necessary vertical drift for the observed presence ($> +12\ ms^{-1}$ or $< -12\ ms^{-1}$), absence ($\leq +12\ ms^{-1}$ or $\geq -12\ ms^{-1}$) or some days present and some days absent ($\sim \pm 12\ ms^{-1}$) of streaming waves is also provided in the respective entries of Tables 1 and 2. In addition, the vertical drifts obtained from Scherliess-99 and Fejer-08 models at respective LT, season and solar epoch corresponding to the rocket flights are also given in Tables 1 and 2. Further, the vertical drifts obtained from both the empirical models corresponding to the starting time of the respective VHF radar experiments are also provided in Tables. Note that, if the magnitude of vertical drift obtained from empirical model deviates from the criterion of deduced $|V_z|$ given above, the value is highlighted with red color. Further, if direction of this vertical drift differs from that deduced from observation, the cell is highlighted with gray color. This notation is not followed for cases wherein deduced $|V_z| \sim 12\ ms^{-1}$.

On comparing the vertical drifts given in Tables 1 and 2 it is observed that in general, vertical drifts presented by both the empirical models are consistent with the criterion for presence or absence of streaming waves, though some deviations are also observed. The amplitudes of vertical drifts obtained from Scherliess-99 and Fejer-08 models are found to deviate from the deduced threshold values of $|V_z|$ on six and five occasions respectively (see the red colored entries in Tables 1 and 2). The deviations in V_z with respect to Fejer-08 model drifts are within the uncertainly limits of measurements (about 10%) for Fejer-08 model, barring two durations 13:38–14:38 LT in December solstice under high solar epoch and 09:23–10:23 LT in June solstice under low solar epoch. However, in case of Scherliess-99 model, except an occasion during 14:08–14:38 LT in equinox under high solar epoch, all the deviations in V_z are beyond the uncertainty limits of measurements (relative precision of about 2 ms^{-1}). Even in the cases when streaming waves are present on some days and absent on some other days (implying amplitude of vertical drifts closer to 12 ms^{-1}), the Fejer-08

Table 1
Comparison of vertical plasma drifts in high solar epoch deduced from experimental observations (rocket/radar) with global empirical model (Scherliess-99 and Fejer-08) drifts. Positive and negative values indicate upward and downward drift respectively. The red colored entries denote the instances when the magnitudes of the model drifts are different from the threshold drifts deduced from E-region irregularity observations whereas the gray boxes identify the instances when the polarity of the model drifts are not in accordance with the inferred polarities.

Season	Experiment	Date	Time/Duration	Vertical drift (ms^{-1})			Literature
				Deduced	Scherliess-99	Fejer-08	
December solstice	Rocket	21-12-1978	02:08	< -12	-21.2	-24.4	Gupta (2000)
		21-12-1978	05:53	< -12	-09.5	-15.8	Gupta (2000)
		12-02-1981	10:35	$> +12$	$+17.4$	$+24.0$	Prakash and Pal (1985)
		02-02-1968	18:34	$> +12$	$+26.8$	$+30.5$	Prakash et al. (1969); Gupta and Prakash (1979)
	Radar	03-02-1999	07:08–09:38	$\leq +12$	$+03.3$	$+05.4$	Tiwari et al. (2003)
		03-02-1999	10:08–13:08	$> +12$	$+16.3$	$+23.2$	Tiwari et al. (2003)
		03-02-1999	13:38–14:38	$\leq +12$	$+14.3$	$+17.1$	Tiwari et al. (2003)
Equinox	Rocket	28-04-1980	05:58	$> +12$	-18.3	-23.1	Gupta (2000)
		12-03-1967	18:35	$> +12$	$+32.9$	$+41.5$	Gupta (2001)
	Radar	19-03-1991	04:43–05:13	< -12	-24.8	-41.5	Ravindran and Krishna Murthy (1997a)
		15-03-1991	06:18–06:38	≥ -12	-06.5	-13.0	Ravindran and Krishna Murthy (1997a)
		15-03-1991	07:48–08:13	$\leq +12$	$+07.2$	$+02.7$	Ravindran and Krishna Murthy (1997a)
		20-03-1979, 15-03-1991, 17-03-1991	07:53–09:08	$\sim +12$	$+12.3$	$+08.0$	Viswanathan et al. (1987); Ravindran and Krishna Murthy (1997a)
		20-03-1979, 21-03-1979, 21-09-1979	10:08–13:38	$> +12$	$+23.8$	$+27.0$	Viswanathan et al. (1987); Ravindran and Krishna Murthy (1997b)
		20-03-1979, 21-03-1979	13:38–14:08	$\sim +12$	$+15.3$	$+12.0$	Viswanathan et al. (1987)
		21-03-1979	14:08–14:38	$\leq +12$	$+12.8$	$+12.0$	Viswanathan et al. (1987)
		15-03-1979, 21-03-1979	14:38–16:48	$\sim +12$	$+10.8$	$+11.4$	Viswanathan et al. (1987); Ravindran and Krishna Murthy (1997a)
		15-03-1979, 16-03-1979, 21-03-1979	16:48–17:38	$\leq +12$	$+07.7$	$+10.2$	Viswanathan et al. (1987); Ravindran and Krishna Murthy (1997a)
		15-03-1979, 16-03-1979	17:38–18:23	$> +12$	$+15.6$	$+21.5$	Ravindran and Krishna Murthy (1997a)
June solstice	Rocket	13-08-1982	07:02	$\leq +12$	$+01.6$	-02.9	Gupta (2001)
		12-08-1982	07:18	$\leq +12$	$+05.1$	-02.0	Gupta (2001)
		29-08-1968	13:53	$\leq +12$	$+06.5$	$+08.7$	Gupta (2001)
		29-08-1968	22:38	< -12	-16.6	-16.2	Prakash et al. (1970); Gupta and Prakash (1979)

model drifts seem to be more consistent with deduced vertical drifts than Scherliess-99 model drifts. This is clearly visible during 08:00–10:00 *LT* and 13:00–16:00 *LT*. Hence, Fejer-08 model is found to represent the vertical drifts over the Indian sector better compared to Scherliess-99 model. However, it is observed that both the empirical models fail to capture the polarity of vertical drift during early morning hours (around 06:00 *LT*), see gray colored cells in Tables 1 and 2, though in June solstice the Scherliess-99 model seems to predict better compared to Fejer-08 model. The probable reasons for deviations in amplitude and polarity of the vertical drifts presented by empirical models from the deduced V_z on a few occasions are discussed in Section 4.

Around noon hours (10:00–14:00 *LT*), the average variations of vertical drifts deduced from magnetometer records match (within 1σ variation) with the corresponding variations presented by both Scherliess-99 and Fejer-08 models in equinox and June solstice under high solar epoch, see maroon and black colored solid curves in Figs. 1 and 3. However, the vertical drift deduced in these seasons during low solar epoch match (within 1σ variation) with the corresponding variations presented by Fejer-08 model better compared to Scherliess-99 model, see Figs. 2 and 4. In December solstice (when 1σ variations are largest) the deduced values of V_z match (within 1σ variation) with the corresponding variations presented by both the empirical models irrespective of solar epoch. In general, the average values of deduced V_z match fairly well with both the empirical models during high solar epoch while these values match well with Fejer-08 model during low solar epoch. This is probably due to better longitudinal resolution used in Fejer-08 model (refer Section 4). Further, the values of V_z deduced from magnetometer data are observed to capture the presence or absence of streaming waves. Interestingly, the deduced vertical drifts are $\sim$12 ms^{-1} during the time intervals wherein streaming waves were detected on some days and found absent on some other days.

During nighttime, the average values of V_z obtained using ionosonde/radar experiments are not sufficient for the generation of streaming waves in low solar epoch (see Figs. 2 and 4) on a few occasions. In high solar epoch, the pre-midnight vertical drifts in both the solstices are (in general) sufficient for the presence of streaming waves (see subplots 1a, 3a and 1c, 3c), though during post-midnight hours the vertical drifts are sufficient for the presence of streaming waves on some occasions only (see subplots 3a and 3c). However, during equinox in high solar epoch some of the average vertical drifts are sufficient to capture the presence of streaming waves. Further, it is observed that the ionosonde/radar deduced vertical drifts are always smaller than those presented by empirical models in different seasons (e.g., see subplots 3a, 3b and 3c) and solar flux levels (e.g., see subplots 3a and 4a). In general, the differences are about 10 ms^{-1} or greater with the maximum deviation occurring in equinoctial months (e.g., notice the difference in V_z of middle panel compared to top or bottom panel in any figure). It is to be noted that considering typical height resolution of 3 km (Patra et al., 2005) and the temporal resolution of 15 min in ionosonde experiments (Sastri, 1984; Krishna Murthy and Hari, 1996; Madhav Haridas et al., 2015), the typical uncertainty in vertical drift is $\sim$5 ms^{-1}. The uncertainty in the vertical drifts deduced using HF phase path sounder or Doppler radars is less than 1 ms^{-1} (Prabhakaran Nayar and Sreehari, 2004). Therefore, the observed differences between the measured vertical drifts (derived using ionosonde/Phase path sounder/Doppler radar) and the model drifts are larger than the typical uncertainties of the measurements involved. The probable reasons for significant difference are discussed in Section 4. In addition, it is observed that during nighttime Scherliess-99 model values of V_z are smaller compared to Fejer-08 model. The probable reasons for this are also discussed in Section 4.

During PRE hours, the peak amplitude of V_z is known to vary day-to-day (Balan et al., 1992) and also dependent on the solar flux level

Table 2
Same as Table (1) but corresponds to low solar epoch.

Season	Experiment	Date	Time/ Duration	Vertical drift (ms^{-1}) Deduced	Scherliess-99	Fejer-08	Literature
December solstice	Rocket	09-02-1975	05:37	< -12	-13.1	-18.8	Gupta (1986)
		28-01-1971	10:18	$> +12$	$+18.2$	$+18.9$	Prakash et al. (1971)
		19-02-1975	10:43	$> +12$	$+18.4$	$+19.1$	Gupta (1997)
		28-01-1971	10:48	$> +12$	$+18.4$	$+19.3$	Prakash et al. (1971)
	Radar	18-01-1974	05:38–06:08	< -12	-13.0	-24.6	Prakash and Muralikrishna (1976)
		18-01-1974, 23-11-1983	06:58–08:08	$\leq +12$	$+03.7$	$+03.6$	Prakash and Muralikrishna (1976); Viswanathan et al. (1987)
		23-11-1983, 25-11-1983, 05-01-1993	08:08–10:08	$\sim +12$	$+10.4$	$+10.9$	Viswanathan et al. (1987); Ravindran and Krishna Murthy (1997b)
		23-11-1983, 25-11-1983, 26-11-1983, 05-01-1993	10:08–12:38	$> +12$	$+17.9$	$+18.5$	Viswanathan et al. (1987); Ravindran and Krishna Murthy (1997b)

(continued on next page)

Table 2 *(continued)*

December solstice	Radar	23-11-1983 to 26-11-1983, 05-01-1993	12:38–15:38	$\sim +12$	+15.6	+14.7	Viswanathan et al. (1987); Ravindran and Krishna Murthy (1997b)
December solstice	Radar	23-11-1983, 26-11-1983	15:38–17:23	$\leq +12$	+06.5	+04.8	Viswanathan et al. (1987)
December solstice	Radar	06-12-1973	19:38–20:38	$\leq +12$	−03.6	−01.3	Prakash and Muralikrishna (1976)
Equinox	Rocket	03-03-1973	11:58	$> +12$	+21.2	+19.5	Gupta (2001)
Equinox	Rocket	07-04-1972	12:08	$> +12$	+20.6	+17.9	Gupta and Prakash (1979)
Equinox	Rocket	13-10-1972	12:38	$\leq +12$	+18.6	+13.6	Gupta (2001)
Equinox	Rocket	15-03-1975	21:42	< -12	−16.9	−27.5	Gupta (1997)
Equinox	Radar	06-09-1994	03:53–05:38	< -12	−13.7	−30.0	Krishna Murthy et al. (1998)
Equinox	Radar	10-03-1972, 05-09-1994	06:38–08:38	$\leq +12$	−08.9	−06.0	Prakash et al. (1974); Krishna Murthy et al. (1998)
Equinox	Radar	10-03-1972, 12-10-1983	08:38–09:38	$\sim +12$	+16.5	+15.9	Prakash et al. (1974); Sastri et al. (1991)
Equinox	Radar	10-03-1972, 12-10-1983, 05-09-1994	09:38–13:08	$> +12$	+20.8	+26.7	Prakash et al. (1974); Viswanathan et al. (1987); Krishna Murthy et al. (1998)
Equinox	Radar	10-10-1983, 12-10-1983, 05-09-1994	13:08–14:38	$\sim +12$	+16.6	+09.7	Viswanathan et al. (1987); Krishna Murthy et al. (1998)
Equinox	Radar	10-03-1972, 11-10-1983, 12-10-1983, 05-09-1994	14:38–17:53	$\leq +12$	+10.4	+06.3	Prakash et al. (1974); Viswanathan et al. (1987); Krishna Murthy et al. (1998)
June solstice	Rocket	12-08-1972	07:23	$\leq +12$	+02.8	−04.9	Gupta and Prakash (1979)
June solstice	Radar	20-06-1983, 24-06-1983	07:53–08:53	$\leq +12$	+09.6	−01.1	Viswanathan et al. (1987)
June solstice	Radar	21-06-1983, 24-06-1983	08:53–09:23	$\sim +12$	+20.0	+09.6	Viswanathan et al. (1987)
June solstice	Radar	23-06-1983, 24-06-1983	09:23–10:23	$\leq +12$	+23.1	+14.8	Viswanathan et al. (1987)
June solstice	Radar	20-06-1983 to 23-06-1983	11:23–13:23	$\sim +12$	+21.4	+16.3	Viswanathan et al. (1987)
June solstice	Radar	20-06-1983, 23-06-1983	13:23–13:53	$\leq +12$	+07.5	+06.8	Viswanathan et al. (1987)

(Ramesh and Sastri, 1995; Sastri, 1996). However, the time of PRE over the Indian sector have been shown (Namboothiri et al., 1989; Nair et al., 1993) to be same within a solar epoch and hence the occurrence times of PRE are compared. Incidentally, it is found that the vertical drifts presented using ionosonde/radar experiments maximize around the time of Barium vapour cloud experiments (the solid blue, green and magenta colored curves in subplots 3(a), 3(b) and 4(a) peak around the time of magenta colored solid circles). It is also to be noted that the

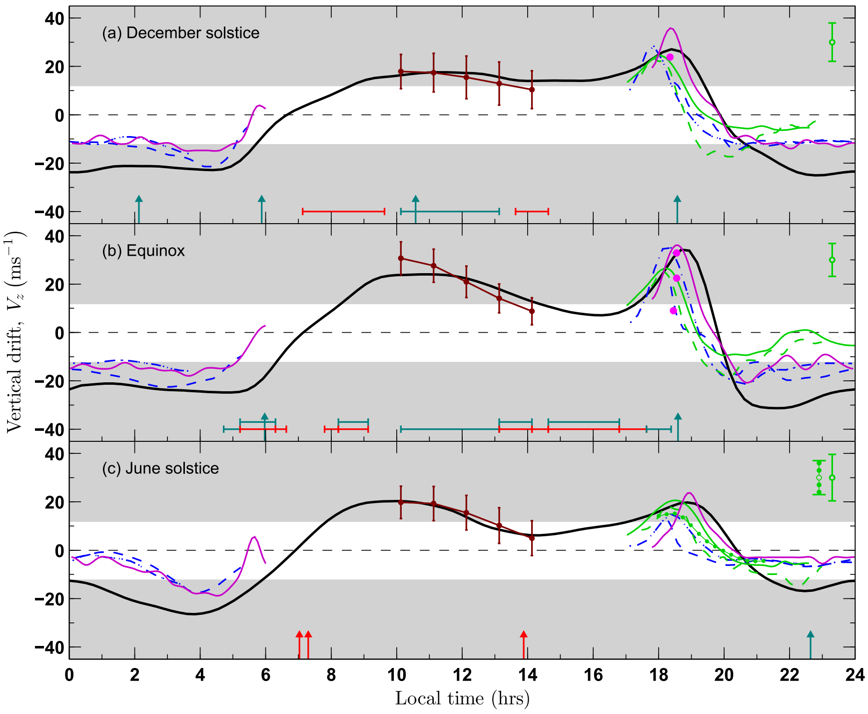

Fig. 1. Vertical drift variations during high solar epoch over the Indian sector provided by Scherliess and Fejer (1999) model (black) and experiments conducted from TRD and KDK (blue, dark magenta and green colored curves respectively) along with the 1σ variation in them (wherever available) with the same notation shown on the top right corner. Vertical drifts measured using vapour release experiments are shown with magenta colored dots and those deduced from magnetometer records is shown with maroon colored curves. The presence or absence of streaming waves observed using sounding rocket flights (vertical arrows) and VHF Doppler radars (horizontal lines) are portrayed with teal or red colors respectively. The durations when streaming waves were detected on some days and found absent on some other days are depicted with simultaneous horizontal lines in teal and red colors. (See text for more details). (For interpretation of the references to color in this figure legend, the reader is referred to the web version of this article.)

time of PRE observed in V_z presented by Scherliess-99 model is later in *LT* compared to these times (e.g., see Fig. 1). A probable reason for this difference in time is discussed in Section 4.

4. Discussion

As mentioned in Section 3, Fejer-08 model is found to be more consistent with the reported presence or absence of streaming waves than Scherliess-99 model. Further, the vertical drift provided by Fejer-08 model also seem to represent the measured drifts better during low

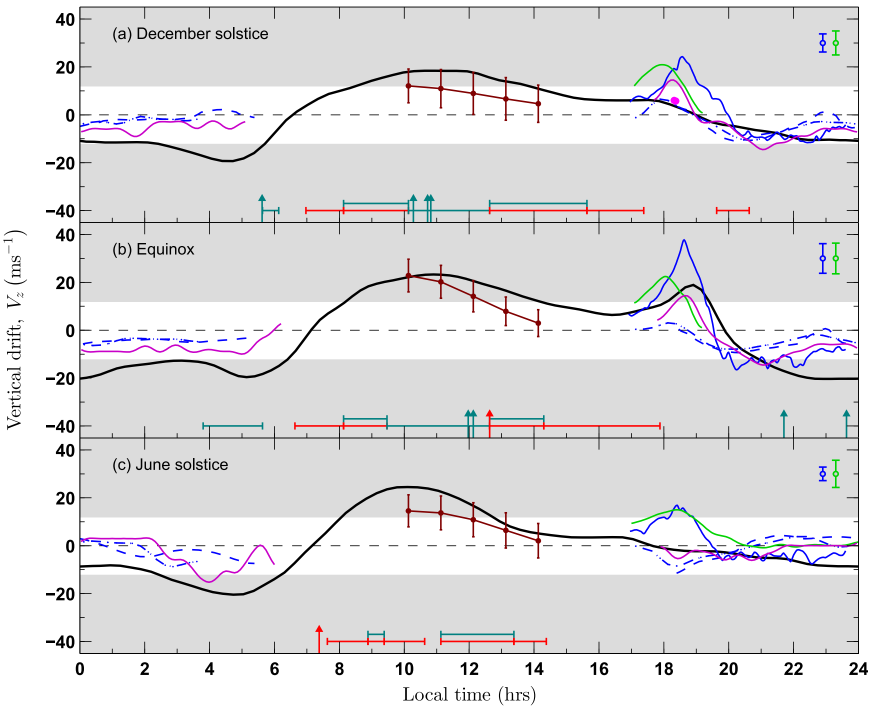

Fig. 2. Same as Fig. Fig. 1 but corresponds to low solar epoch. (For interpretation of the references to color in this figure, the reader is referred to the web version of this article.)

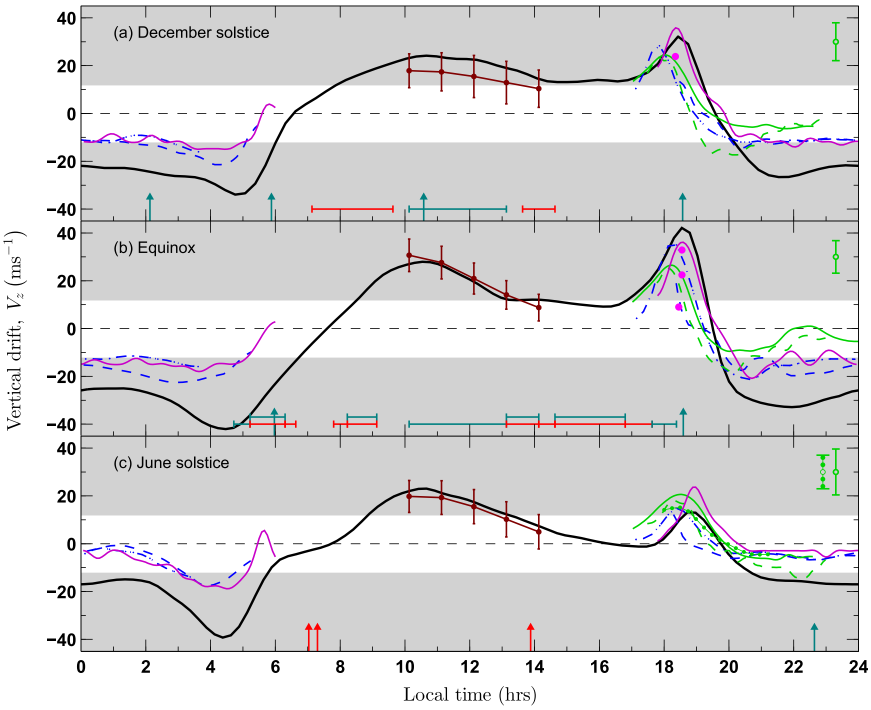

Fig. 3. Same as Fig. 1 but comparison is with the Fejer et al. (2008a) model drifts. (For interpretation of the references to color in this figure, the reader is referred to the web version of this article.)

solar epoch as far as the PRE and daytime deduced drifts are concerned. To investigate the probable reasons for Fejer-08 model being more consistent than Scherliess-99 model, the data sets and methodology used to develop these empirical models are looked into.

It is to be noted that empirical models were developed based on the in-situ observations of plasma drifts at the altitude of satellite. The techniques employed to measure the plasma drifts are entirely different from the experimental techniques adopted to get these observations over the Indian sector. In Scherliess-99 model, the input for vertical drifts were obtained from Ion Drift Meter (IDM, on board AE-E satellite) measurements over $\pm 7.5°$ dip-latitude ranges around the globe during 1977–1979 and Jicamarca ISR measurements from 1968

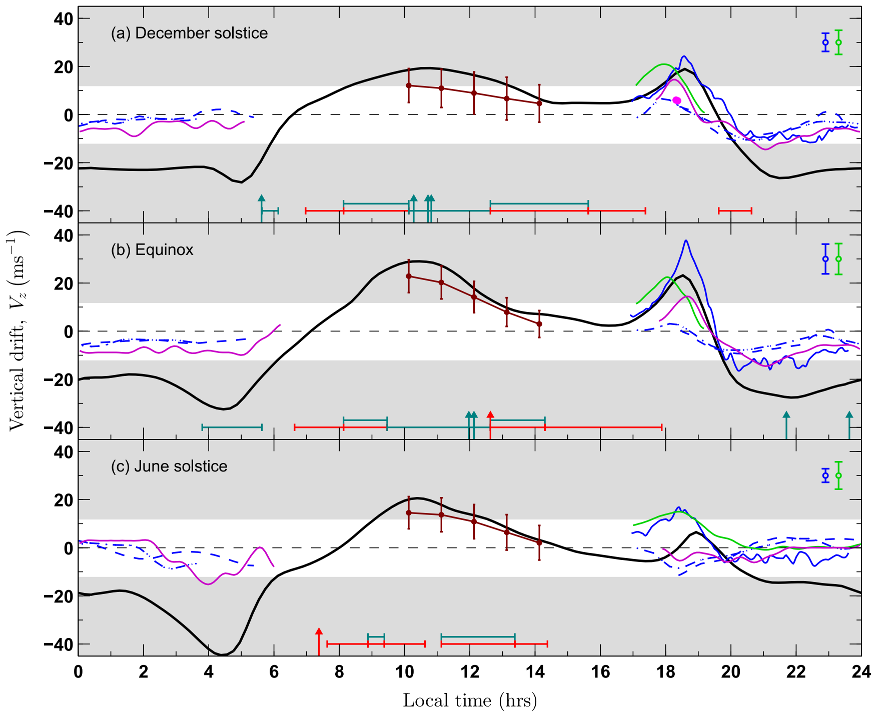

Fig. 4. Same as Fig. 2 but comparison is with the Fejer et al. (2008a) model drifts. (For interpretation of the references to color in this figure, the reader is referred to the web version of this article.)

to 1992. On the other hand, in Fejer-08 model the input for vertical drifts were obtained from Ionospheric Plasma and Electrodynamics Probe Instrument (IPEI, on board ROCSAT-1 satellite) measured vertical drifts over $\pm 5°$ dip-latitude ranges around the globe from 1999 to 2004. These vertical drifts were binned over 60° and 30° longitudes in Scherliess-99 and Fejer-08 models respectively. Further, different methodologies were adopted to develop both the empirical models. In Scherliess-99 model, the V_z values around the globe were constrained with different statistical weights to make electric field curl-free ($\oint \mathbf{E} \cdot d\mathbf{l} = 0$). However, in Fejer-08 model, the vertical drifts were not constrained to satisfy for irrotational electric field, though, this condition was used to estimate the accuracy of this model. As mentioned in Scherliess and Fejer (1999), satellite measurements of V_z during nighttime (that have more uncertainty compared to daytime) were given less statistical weight compared to daytime measurements and whenever the highly accurate daytime vertical drifts were available from Jicamarca ISR, those data sets were given even higher statistical weight (about 75%). Under this scenario, the V_z values provided by Scherliess-99 model over the Indian sector, which is nearly at antipodal point of the Peruvian sector, could become uncertain.

The occurrence of afternoon equatorial counter electrojet (CEJ) had been shown (Rastogi et al., 2014) to be highest during June solstice under low solar epoch. Interestingly, the Fejer-08 model drift values reveal downward drifts in the afternoon hours which is consistent with the observations of Rastogi et al. (2014). The presence of downward drift in June solstice during solar minimum years also gets credence from the works of Gurubaran (2002) and Bhattacharyya and Okpala (2015). It was shown that equatorial CEJ under similar conditions was due to additional contribution from global current system that gets superimposed on the *Sq* current system. Further, the small afternoon upward drifts in this season given by Scherliess-99 model are also favorable for the generation of CEJ with a little help from additional external agency. Therefore, both the models support the morphological feature of occurrence of CEJ during this season. As far as the high solar epoch is concerned, negligible vertical plasma drift obtained from Fejer-08 model in the afternoon hours during the June solstice is consistent with the occurrence characteristic of partial CEJ at this local time reported by Rastogi et al. (2014). This feature is not efficiently captured by Scherliess-99 model. In view of these outcomes, in the forthcoming discussion on vertical drifts during different times of the day, barring evening hours, V_z presented by experimental observations are compared with Fejer-08 model only. During PRE time a discussion based on both the models is presented.

4.1. Vertical drifts in morning hours

The vertical drifts presented using ionosonde/radar experiments are insufficient for the generation of streaming waves observed around 06:00 *LT*. Their presence is supported by Fejer-08 model, although the polarity of vertical drifts presented by this model is not consistent with the respective observation on a few occasions during 06:00–08:00 *LT*, as mentioned in Section 3. To investigate the probable reasons for this inconsistency with the empirical model, the diurnal variations of V_z over the dip-equatorial longitudes presented in Fig. 4 of Fejer-08 become important. It is observed from their work that, though the vertical drifts are small during 06:00–08:00 *LT* around the Indian sector, they show variation in polarity with longitude even for a particular *LT*. Therefore, the longitudinal averaging of V_z used in Fejer-08 model (given above) could result in loss of polarity information. Therefore, it is rather difficult to bring out the clear picture of V_z during morning hours.

4.2. Vertical drifts during daytime

In general, the daytime vertical drifts presented by Fejer-08 model and those deduced using magnetometer data sets around noon hours (10:00–14:00 *LT*) match within 1σ variation. In general, the magnetometer deduced V_z capture the presence or absence of streaming waves, suggesting that the magnetometer data can be effectively used to gauge the vertical drift/zonal electric field variations from 10:00 *LT* to 14:00 *LT*.

4.3. Vertical drifts in evening hours

It is noticed that the time of occurrence of PRE, as predicted by Scherliess-99 model, is slightly later than the corresponding times observed by most of the ionosonde/HF radar experiments during high solar epoch. In this regard, Fejer-08 model is closer with Indian observations. This may be partly due to the better longitudinal resolution of the Fejer-08 model in comparison with the Scherliess-99 model. More importantly, the Indian stations are east of $60°E$ longitude and the model drifts have been presented corresponding to $60°E$ with finite longitudinal averaging. As the local sunset will occur over the Indian sector earlier than that over $60°E$, the model drifts can occur at a later time than what Indian observations suggest. During low solar epoch, the PRE feature itself is more conspicuous in Fejer-08 model (particularly during solstices) than in Scherliess-99 model and the Indian observations are reasonably consistent with the Fejer-08 model outputs in all the seasons except in June solstice as far as the time of occurrence of PRE is concerned.

It is interesting to note here that in June solstice under low solar epoch, PRE was found to be present (e.g., Ramesh and Sastri, 1995) on some occasions, absent (e.g., Scherliess-99) on other occasions and reverse PRE (e.g., Subbarao and Krishna Murthy, 1994; Chakrabarty et al., 2014) was also observed. Therefore, the occurrence of PRE in June solstice under low solar epoch is ambiguous. The suppression of PRE in June solstice under low solar epoch was also reported over Peruvian (Scherliess and Fejer, 1999) and African (Oyekola, 2006) sectors. Further, the occurrence of reverse PRE is also noticed in the vertical drifts over African sector that was presented in Fig. 1(a) of Oyekola et al. (2007) corresponding to June solstice in low solar epoch. In general, the occurrence of reverse PRE is found in June solstice when solar flux level is low. The modeling studies of reverse PRE are not found, though simulation results for suppressed PRE are available (Fesen et al., 2000; Millward et al., 2001). The observed variability on the occurrence of PRE during June solstice in low solar epoch needs to be investigated in detail to arrive at a bigger picture. There are differences, of course, between the magnitude of V_z during PRE time given by Indian observations and the model values on some occasions. It is known that the peak values of V_z during PRE hours depend on solar flux level (Fejer et al., 1996; Sastri, 1996; Madhav Haridas et al., 2015) and change on a day-to-day basis (Woodman, 1970; Balan et al., 1992). In absence of significant recombination effect (as the layer height is generally more than 300 km) during PRE time and unlikely occurrence of equatorial spread-F before PRE, ionosonde/HF radar measurements can be used to infer V_z on a day-to-day basis.

4.4. Vertical drifts during nighttime

The vertical drifts presented by Fejer-08 model capture the observed presence/absence of streaming waves during nighttime. However, the vertical drifts presented using ionosonde/HF radar experiments are not sufficient, on most of the occasions, to capture the observed presence of streaming waves and differ from vertical drifts presented by Fejer-08 model by 10 ms^{-1} or more in general. The sources of these deviations could be improper correction of βH, gradients in vertical drifts, instrumental bias and/or inaccurate determination of height of plasma layer, etc. To delineate the probable causes of these large differences the contributions that can arise from these factors are looked into.

As the vertical drifts (used in the present work) are, in general, obtained only for the duration when altitude of plasma layers remains above 300 km, the contribution due to chemical recombination would be negligible (Bittencourt and Abdu, 1981). Even otherwise, it is shown (Kakad et al., 2012; Subbarao and Krishna Murthy, 1994) that contribution due to recombination process can be about 2 ms^{-1} or 4 ms^{-1} corresponding to the movement of plasma layer above or below 300 km respectively.

The altitude variation of vertical drifts over the Indian sector around PRE hours have been reported earlier (Raghavarao et al., 1987; Sastri et al., 1995; Prabhakaran Nayar and Sreehari, 2004). However, the altitude gradient in vertical drifts during nighttime over the Indian sector are not known. Therefore, a typical (Pingree and Fejer, 1987) altitude gradient in the vertical drift over the dip-equatorial station (Jicamarca) is taken as a representative value. The altitude averaged gradient in nocturnal V_z was shown by Pingree and Fejer (1987) to be around 0.005 ms^{-1} km^{-1} (averaged nighttime value). As the altitudes probed by the ionosonde/radar experiments (bottom side of F-layer, i.e. around 300 km) and the ROCSAT-1 satellite (used in Fejer-08 model) are separated by about 300 km, V_z values could differ by about 2 ms^{-1}. Further, if the altitude gradient in vertical drifts are assumed to follow the opposite pattern above and below F-layer peak as observed by Fejer et al. (2014) and simulated by models (Klimenko et al., 2012; Qian et al., 2015), the difference in V_z would be even less than 2 ms^{-1}.

Finally, the accuracy of vertical drifts deduced using ionosonde/radar experiments depends (to the first order) on how accurately the altitude of plasma layer is determined. This is particularly difficult during equatorial spread-F (ESF) events. Therefore, to investigate a possible relationship, if any, between the percentage occurrence of ESF (Subbarao and Krishna Murthy, 1994) over TRD and difference between V_z, obtained using ionosonde/radars experiments and Fejer-08 model, the two parameters are looked together. In general, the differences in V_z are found to follow the percentage of occurrence of ESF. For e.g., under high solar epoch, the occurrence of ESF was higher (Subbarao and Krishna Murthy, 1994) during pre-midnight than post mid-night hours in all the seasons; and the corresponding differences in vertical drifts are observed to follow the similar pattern (see Fig. 3). Under low solar epoch, the ESF occurrence in June solstice was higher (Subbarao and Krishna Murthy, 1994) during post-midnight than pre-midnight hours; and corresponding differences in vertical drifts are observed to follow this pattern (see subplot 4b). Further, under high solar epoch the occurrence of ESF during pre-midnight hours was maximum in equinox; and the differences in vertical drifts are also maximum during pre-midnight hours in equinox (see subplot 3b). Under low solar epoch, the occurrence of ESF during post-midnight was maximum in June solstice; and the difference in vertical drifts during post-midnight is also maximum in June solstice (see subplot 4c).

From the above discussion, it appears that the seasonal V_z presented using ionosonde/radar experiments might have suffered from an uncertainty arising out of the inaccurate determination of ionospheric height parameter in the presence of ESF events. It is important to note that the plasma irregularities associated with ESF move upward and thus can result in systematic underestimation of the downward drifts, which is seen in Figs. 1–4. Therefore, presence of ESF is probably the most important reason for the underestimation of ionosonde/HF radar derived vertical drifts. Further, with appropriate (without ESF traces) choice of ionograms and proper correction for recombination loss, the ionosonde/HF radar experiments can be used to deduce the vertical drifts during nighttime. Another interesting feature in vertical drifts during June solstice under low solar epoch was reported by Chakrabarty et al. (2014). They had shown that the vertical drifts increase and become upward during midnight hours, which is not observed in vertical drifts presented by the empirical models but confirmed by C/NOFS observations.

5. Summary

The vertical plasma drifts obtained or deduced with several techniques over the Indian sector are compared with those presented by the global empirical models (Scherliess and Fejer, 1999; Fejer et al., 2008a). The salient points that have emerged from this study are as follows:

1. In general, the vertical drifts presented by Fejer et al. (2008a) model represent vertical drifts over the Indian sector better than Scherliess and Fejer (1999) model and other average nocturnal vertical drifts deduced using ionosonde/radar experiments.
2. The empirical models fail to capture the direction of vertical drifts in morning hours (around 06:00 LT). This is probably due to longitudinal averaging that results in loss of polarity information.
3. The vertical drifts (corresponding to zonal electric fields) deduced around noon hours (10:00–14:00 LT) from magnetometer records match with vertical drifts presented by Fejer et al. (2008a) model and capture the presence/absence of streaming waves in general.
4. For distinctive drift features like PRE, the time difference between occurrence of PRE reported by the empirical models and the ground-based observations is found on some occasions and this can be due to the different longitudinal averaging schemes used in the models.
5. The seasonally averaged nocturnal vertical drifts deduced using ionosonde/HF radar experiments are not sufficient, on most of the occasions, to capture the observed presence of streaming waves. The deviations of vertical drifts obtained using ionosonde/HF radar experiments from the Fejer et al. (2008a) model drift values closely follow the percentage occurrence of ESF indicating inaccuracy in the determination of vertical drifts based on ionospheric height variations in the presence of ESF.
6. Both the empirical models Scherliess and Fejer (1999) and Fejer et al. (2008a) support the occurrence characteristic of afternoon equatorial CEJ in June solstice under low solar epoch.

Acknowledgments

The hourly values of magnetic field measurements are courtesy of Indian Institute of Geomagnetism, Mumbai and obtained from the World Data Center for Geomagnetism, Kyoto (http://wdc.kugi.kyoto-u.ac.jp/). The Kp, Ap and Dst values are obtained from the Word data center for Geomagnetism, Kyoto. The solar flux values (at 10.7 cm) are obtained from Laboratory for Atmospheric and Space Physics (http://lasp.colorado.edu/lisird/tss/noaa_radio_flux.html). All the rocket flight experiments conducted from Thumba Equatorial Rocket Launching Station (TERLS) or Sriharikota High Altitude Range (SHAR) have been supported by the Indian Space Research Organization and the data are obtained from published results (provided in Tables 1 and 2). The vertical drifts reported using empirical model, ionosonde, HF phase path sounder, HF Doppler radar and VHF backscatter radar are obtained from the published results (given in Section 2). This work is supported by the Department of Space, Government of India.

Appendix A

A model was developed by Anandarao (1976) to obtain the ionospheric current density and details of the model can be obtained from the earlier works of Anandarao and Raghavarao (1987) and Raghavarao and Anandarao (1987). The inputs required to the model are altitude profiles of electron density (N_e), neutral density, temperature and dip-equatorial zonal electric field. In addition, a methodology to obtain the horizontal component (H) of magnetic field induced at ground by the electrojet current along zonal direction was described by Anandarao (1977) using,

$$H_{induced} = \frac{\mu_0 C}{2\pi r}\frac{(r/a)\sin\theta - 1}{(r/a)^2 + 1 - 2(r/a)\sin\theta} \tag{1}$$

where C is line current obtained from zonal current density (J_ϕ or J_x), $C = \int_r \int_\theta J_x dr d\theta$. Here r and θ denote the distance and magnetic co-latitude of the line current respectively and a denotes the Earth's radius. Note that J_x values, integrated in the altitude and dip-latitude ranges of 80 to 130 km and $-5°$ to $+5°$ respectively, are used to derive $H_{induced}$. The $H_{induced}$ is taken as the representative of the H component of magnetic field induced at ground due to the equatorial electrojet.

In present work, the problem is reversed in pursuit of zonal electric field from the magnetometer observations. This is done by computing J_x with varying zonal electric field input to the electrojet model till the derived $H_{induced}$ value becomes equal to the observed $\Delta H_{equator} - \Delta H_{off-equator}$. Further, it is noticed that the N_e profiles, measured using sounding rocket flight experiments (Subbaraya et al., 1983; Gupta, 2001), over the equatorial electrojet region (90–110 km) did not reveal any significant temporal variation during 10:00–14:00 LT irrespective of solar epoch, though the absolute values of N_e are larger (about 40%) during solar maximum. Hence, the average N_e profile corresponding to the particular solar epoch and typical profiles of neutral parameters, as their effects on J_x are negligible (Pandey et al., 2016), are used in the electrojet model (Anandarao, 1976) to evaluate $H_{induced}$ for different zonal electric field values. The sensitivity studies (Pandey et al., 2016) were carried out by varying different parameters. This suggests ~5% uncertainty in the estimated zonal electric field.

The hourly magnetometer measurements from a dip-equatorial station Trivandrum (TRD, 8.5°N, 76.9°E, dip-lat. 1°S) and an off-equatorial station Alibag (ABG, 18.6°N, 72.9°E, dip-lat. 10°N) during 1985–1995 are used to obtain $\Delta H_{equator} - \Delta H_{off-equator}$ on geomagnetically quiet days (Kp $\leq$ 3 and Dst ≥ -20, on the selected day and also on the previous day). The observed values of $\Delta H_{TRD} - \Delta H_{ABG}$ on individual quiet days (gray) and their seasonally averaged (red) values along with 1σ variation during high (left panel) and low (right panel) solar epochs are depicted in Fig. 5. Based on these seasonally averaged values of $\Delta H_{TRD} - \Delta H_{ABG}$, the vertical drifts corresponding to zonal electric fields are obtained during 10:00–14:00 LT.

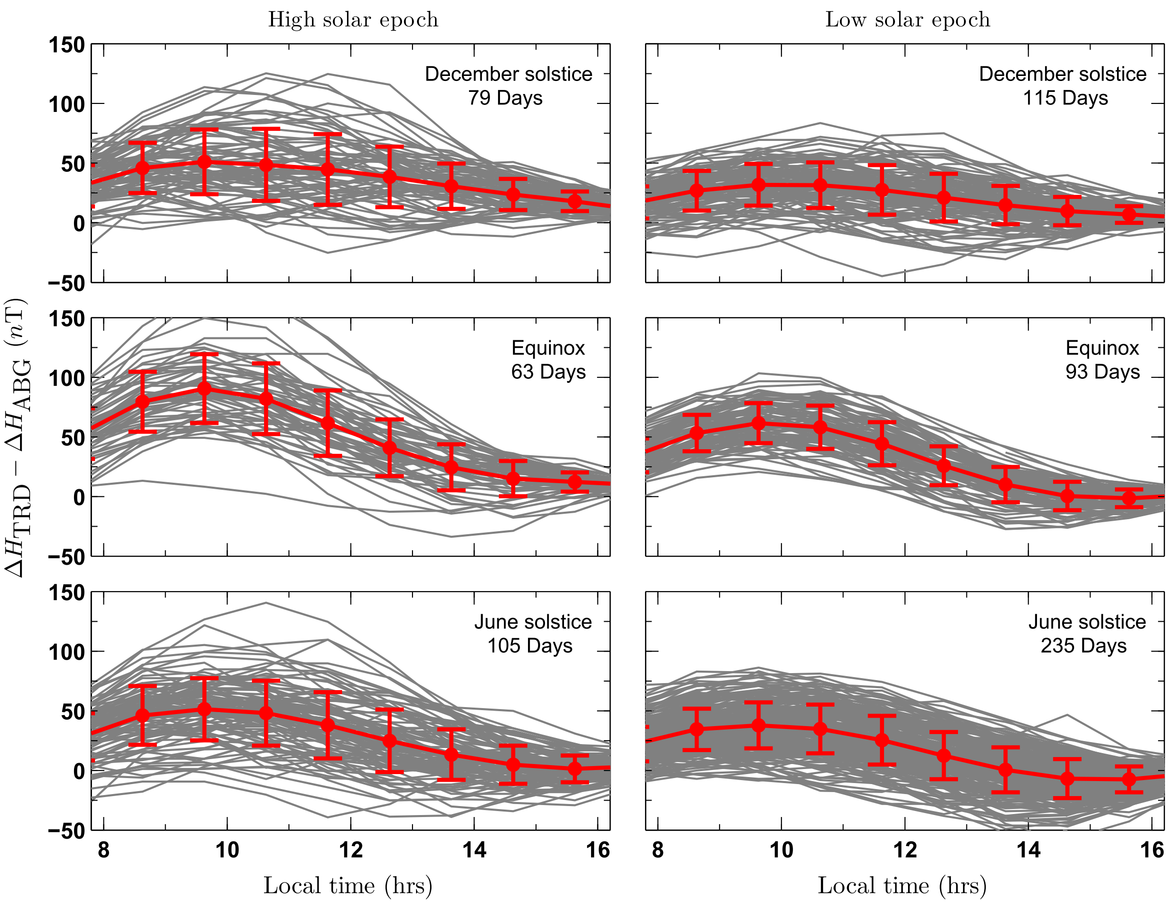

Fig. 5. Hourly variations of individual quiet days (gray colored lines) and seasonally averaged (red colored line) $\Delta H_{TRD} - \Delta H_{ABG}$ values along with 1σ variation during high (left panel) and low (right panel) solar epochs. The upper, middle and lower subplots represent variations in December solstice, equinox and June solstice respectively. The number of days used for seasonal average are also mentioned in each subplot. (The hourly values of magnetic field measurements are obtained from the World Data Center for Geomagnetism, Kyoto).

References

Anandarao, B.G., 1977. Studies on the Dynamics of the Equatorial Ionosphere. (Ph.D. thesis), Gujarat University.

Anandarao, B.G., 1976. Effects of gravity wave winds and wind shears on equatorial electrojet. Geophys. Res. Lett. 3 (9), 545–548, ⟨http://dx.doi.org/10.1029/GL003i009p00545⟩.

Anandarao, B.G., Raghavarao, R., 1987. Structural changes in the currents and fields of the equatorial electrojet due to zonal and meridional winds. J. Geophys. Res. 92 (A3), 2514–2526, ⟨http://dx.doi.org/10.1029/JA092iA03p02514⟩.

Anandarao, B.G., Desai, J.N., Giles, M., Martelli, G., Raghavarao, R., Rothwell, P., 1977. Electric field in the equatorial ionosphere. J. Atmos. Terr. Phys. 39, 927–931.

Balan, N., Jayachandran, B., Balachandran, R.Nair., Namboothiri, S.P., Bailey, G.J., Rao, P.B., 1992. HF Doppler observations of vector plasma drifts in the evening F-region at the magnetic equator. J. Atmos. Terr. Phys. 54 (1112), 1545–1554, ⟨http://dx.doi.org/10.1016/0021-9169(92)90162-E⟩..

Bhattacharyya, A., Okpala, K.C., 2015. Principal components of quiet time temporal variability of equatorial and low-latitude geomagnetic fields. J. Geophys. Res. 120 (10), 8799–8809, ⟨http://dx.doi.org/10.1002/2015JA021673⟩.

Bittencourt, J.A., Abdu, M.A., 1981. A theoretical comparison between apparent and real vertical ionization drift velocities in the equatorial F region. J. Geophys. Res. 86 (A4), 2451–2454, ⟨http://dx.doi.org/10.1029/JA086iA04p02451⟩.

Chakrabarty, D., Fejer, B.G., Gurubaran, S., Pant, T.K., Abdu, M.A., Sekar, R., 2014. On the pre-midnight ascent of F-layer in the June solstice during the deep solar minimum in 2008 over the Indian sector. J. Atmos. Sol. Terr. Phys. 121 (Part B), 177–187, ⟨http://dx.doi.org/10.1016/j.jastp.2014.01.002⟩.

Farley, D.T., 2009. The equatorial E-region and its plasma instabilities: a tutorial. Ann. Geophys. 27 (4), 1509–1520, ⟨http://dx.doi.org/10.5194/angeo-27-1509-2009⟩.

Fejer, B.G., 1981. The equatorial ionospheric electric fields. A Rev. J. Atmos. Terr. Phys. 43 (5), 377–386, ⟨http://www.sciencedirect.com/science/article/pii/002191698190101X⟩.

Fejer, B.G., Jensen, J.W., Su, S.Y., 2008a. Quiet time equatorial F region vertical plasma drift model derived from ROCSAT-1 observations. J. Geophys. Res. 113 (A5), 304, ⟨http://dx.doi.org/10.1029/2007JA012801⟩.

Fejer, B.G., Jensen, J.W., Su, S.Y., 2008b. Seasonal and longitudinal dependence of equatorial disturbance vertical plasma drifts. Geophys. Res. Lett. 35 (20), L20106, ⟨http://dx.doi.org/10.1029/2008GL035584⟩.

Fejer, B.G., Hui, D., Chau, J.L., Kudeki, E., 2014. Altitudinal dependence of evening equatorial F region vertical plasma drifts. J. Geophys. Res.: Space Physics 119 (7), 5877–5890, ⟨http://dx.doi.org/10.1002/2014JA019949⟩.

Fejer, B.G., de Paula, E.R., Scherliess, L., 1996. Incoherent scatter radar, ionosonde, and satellite measurements of equatorial F region vertical plasma drifts in the evening sector. Geophys. Res. Lett. 23 (14), 1733–1736, ⟨http://dx.doi.org/10.1029/96GL01847⟩.

Fesen, C.G., Crowley, G., Roble, R.G., Richmond, A.D., Fejer, B.G., 2000. Simulation of the pre-reversal enhancement in the low latitude vertical ion drifts. Geophys. Res. Lett. 27 (13), 1851–1854, ⟨http://dx.doi.org/10.1029/2000GL000061⟩.

Gupta, S.P., Prakash, S., 1979. Experimental evidence of ion plasma oscillations in the apogee region of the Nike-Apache rocket. Planet. Space Sci. 27 (2), 145–150, ⟨http://dx.doi.org/10.1016/0032-0633)(79)90044-8⟩..

Gupta, S.P., 1986. Formation of sporadic E layers at low magnetic latitudes. Planet. Space Sci. 34 (11), 1081–1085, ⟨http://dx.doi.org/10.1016/0032-0633)(86)90019-X⟩..

Gupta, S.P., 1997. Features of E region irregularities at the magnetic equator and in its vicinity. Adv. Space Res. 20 (11), 2195–2198, ⟨http://dx.doi.org/10.1016/S0273-1177)(97)00670-4⟩..

Gupta, S.P., 2000. Two stream instability in E region over magnetic equator during morning hours. Adv. Space Res. 26 (8), 1257–1261, ⟨http://dx.doi.org/10.1016/S0273-1177)(99)01212-0⟩.

Gupta, S.P., 2001. Collected Works. Physical Research Laboratory, India.

Gurubaran, S., 2002. The equatorial counter electrojet: part of a world-wide current system? Geophys. Res. Lett. 29 (9), 51-1–51-4, ⟨http://dx.doi.org/10.1029/2001GL014519⟩.

Kakad, B., Tiwari, D., Pant, T.K., 2012. Study of post sunset vertical plasma drift at equatorial F-region using long-term (1990–2003) ionosonde measurements in Indian longitude. J. Atmos. Sol. Terr. Phys. 80, 239–246, ⟨http://dx.doi.org/10.1016/j.jastp.2012.02.004⟩.

Klimenko, M.V., Klimenko, V.V., Karpachev, A.T., 2012. Formation mechanism of additional layers above regular F2 layer in the near-equatorial ionosphere during quiet period. J. Atmos. Sol. Terr. Phys. 9091, 179–185 http://dx.doi.org/10.1016/j.jastp.2012.02.011.

Krishna Murthy, B.V., Hari, S.S., 1996. Electric fields in the low latitude F-region. Adv. Space Res. 18 (6), 93–98 http://dx.doi.org/10.1016/0273-1177(95)00906-X.

Krishna Murthy, B.V., Hari, S.S., Somayajulu, V.V., 1990. Nighttime equatorial thermospheric meridional winds from ionospheric h′F data. J. Geophys. Res.: Space Phys. 95 (A4), 4307–4310 http://dx.doi.org/10.1029/JA095iA04p04307.

Krishna Murthy, B.V., Ravindran, S., Viswanathan, K.S., Subbarao, K.S.V., Patra, A.K., Rao, P.B., 1998. Small-scale (∼3 m) E region irregularities at and off the magnetic equator. J. Geophys. Res. 103 (A9), 20761–20773 http://dx.doi.org/10.1029/98JA00928.

Madhav Haridas, M.K., Manju, G., Pant, T.K., 2015. On the solar activity variations of nocturnal F region vertical drifts covering two solar cycles in the Indian longitude sector. J. Geophys. Res. 120 (2), 1445–1451 http://dx.doi.org/10.1002/2014JA020561.

Millward, G.H., Mller-Wodarg, I.C.F., Aylward, A.D., Fuller-Rowell, T.J., Richmond, A.D., Moffett, R.J., 2001. An investigation into the influence of tidal forcing on F region equatorial vertical ion drift using a global ionosphere-thermosphere model with coupled electrodynamics. J. Geophys. Res. 106 (A11), 24733–24744 http://dx.doi.org/10.1029/2000JA000342.

Nair, R.B., Jayachandran, B., Rao, P.B., Balan, N., 1993. Seasonal, solar and magnetic activity effects on evening F region vertical plasma drifts. Indian J. Radio Space Phys. 22, 89–93.

Namboothiri, S.P., Balan, N., Rao, P.B., 1989. Vertical plasma drifts in the F region at the magnetic equator. J. Geophys. Res.: Space Phys. 94 (A9), 12055–12060 http://dx.doi.org/10.1029/JA094iA09p12055.

Oyekola, O.S., 2006. Comparison between nighttime ionosonde, incoherent scatter radar, AE-E satellite, and HF Doppler observations of F region vertical electrodynamic plasma drifts in the vicinity of the magnetic equator. J. Geophys. Res. 111 (A11) http://dx.doi.org/10.1029/2006JA011844.

Oyekola, O.S., Ojo, A., Akinrimisi, J., dePaula, E.R., 2007. Seasonal and solar cycle variability in F-region vertical plasma drifts over Ouagadougou. J. Geophys. Res. 112 (A12)http://dx.doi.org/10.1029/2007JA012560.

Pandey, K., Sekar, R., Anandarao, B.G., Gupta, S.P., Chakrabarty, D., 2016. Estimation of nighttime dip-equatorial E-region current density using measurements and models. J. Atmos. Sol. Terr. Phys. 146, 160–170 http://dx.doi.org/10.1016/j.jastp.2016.06.002.

Patra, A.K., Sripathi, S., Rao, P.B., Subbarao, K.S.V., 2005. Simultaneous VHF radar backscatter and ionosonde observations of low-latitude E region. Ann. Geophys. 23 (3), 773–779, ⟨http://www.ann-geophys.net/23/773/2005/⟩.

Pingree, J.E., Fejer, B.G., 1987. On the height variation of the equatorial F region vertical plasma drifts. J. Geophys. Res. 92 (A5), 4763–4766 http://dx.doi.org/10.1029/JA092iA05p04763.

Prabhakaran Nayar, S.R., Sreehari, C.V., 2004. Investigation of height gradient in vertical plasma drift at equatorial ionosphere using multifrequency HF Doppler radar. J. Geophys. Res. 109 (A12)http://dx.doi.org/10.1029/2004JA010641.

Prakash, S., Subbaraya, B.H., 1967. Langmuir probe for the measurement of electron density and electron temperature in the ionosphere. Rev. Sci. Instrum. 38 (8), 1132–1136 http://dx.doi.org/10.1063/1.1721035.

Prakash, S., Muralikrishna, P., 1976. The nature of electric field in E-Region close to morning and evening reversals. Geophys. Res. Lett. 3 (8), 445–447 http://dx.doi.org/10.1029/GL003i008p00445.

Prakash, S., Pal, S., 1985. Electric fields and electron density irregularities in the equatorial electrojet. J. Atmos. Terr. Phys. 47 (8), 853–866, ⟨http://www.sciencedirect.com/science/article/pii/0021916985900601⟩.

Prakash, S., Gupta, S.P., Subbaraya, B.H., 1969. Irregularities in the equatorial E region over thumba. Radio Sci. 4 (9), 791–796 http://dx.doi.org/10.1029/RS004i009p00791.

Prakash, S., Gupta, S.P., Subbaraya, B.H., 1970. A study of the irregularities in the night time equatorial E-region using a Langmuir probe and plasma noise probe. Planet. Space Sci. 18 (9), 1307–1318 http://dx.doi.org/10.1016/0032-0633(70)90141-8.

Prakash, S., Gupta, S.P., Subbaraya, B.H., Jain, C.L., 1971. Electrostatic plasma instabilities in the equatorial electrojet. Nature 233 (38), 56–58 http://dx.doi.org/10.1038/physci233056a0.

Prakash, S., Jain, C.L., Balsley, B.B., Greenwald, R.A., 1974. Evidence of two types of electron density irregularities in the electrojet over Thumba, India. J. Geophys. Res. 79 (28), 4334–4336 http://dx.doi.org/10.1029/JA079i028p04334.

Qian, C., Lei, J., Wang, W., 2015. A simulation study on the impact of altitudinal dependent vertical plasma drift on the equatorial ionosphere in the evening. J. Geophys. Res. 120 (4), 2918–2925 http://dx.doi.org/10.1002/2014JA020626.

Raghavarao, R., Anandarao, B.G., 1987. Equatorial electrojet and the counter-electrojet. Indian J. Radio Space Phys. 16, 54–75 http://dx.doi.org/10.1016/0021-9169(87)90042-0.

Raghavarao, R., Gupta, S.P., Sekar, R., Narayanan, R., Desai, J.N., Sridharan, R., Babu, V.V., Sudhakar, V., 1987. In situ measurements of winds, electric fields and electron densities at the onset of equatorial spread-F. J. Atmos. Terr. Phys. 49 (5), 485–492 http://dx.doi.org/10.1016/0021-9169(87)90042-0.

Ramesh, K.B., Sastri, J.H., 1995. Solar cycle and seasonal variations in F-region vertical drifts over Kodaikanal. India Ann. Geophys. 13 (6), 633–640 http://dx.doi.org/10.1007/s00585-995-0633-7.

Rastogi, R.G., Patel, V.L., 1975. Effect of interplanetary magnetic field on ionosphere over the magnetic equator. Proc. Indian Acad. Sci. 82 (A), 121–141.

Rastogi, R.G., Chandra, H., Janardhan, P., Rahul, S., 2014. Equatorial and mid-latitude ionospheric currents over the Indian region based on 40 years of data at Trivandrum and Alibag. Indian J. Radio Space Phys. 43, 274–283.

Ravindran, S., Krishna Murthy, B.V., 1997a. Occurrence of type I plasma waves in the equatorial electrojet during morning and evening hours. J. Geophys. Res. 102 (A5), 9761–9765 http://dx.doi.org/10.1029/96JA03742.

Ravindran, S., Krishna Murthy, B.V., 1997b. Up-down asymmetry of type I plasma waves in the equatorial electrojet region. Ann. Geophys. 15 (6), 774–778. http://dx.doi.org/10.1007/s00585-997-0774-y.

Reddy, C.A., Vikramkumar, B.T., Viswanathan, K.S., 1987. Electric fields and currents in the equatorial electrojet deduced from VHF radar observations-I. A method of estimating electric fields. J. Atmos. Terr. Phys. 49 (2), 183–191, ⟨http://www.sciencedirect.com/science/article/pii/0021916987900535⟩.

Sastri, J.H., 1984. Duration of equatorial spread-F. Ann. Geophys. 2, 353–358.

Sastri, J.H., 1996. Longitudinal dependence of equatorial F region vertical plasma drifts in the dusk sector. J. Geophys. Res. 101 (A2), 2445–2452.

Sastri, J.H., Varma, V.K.M., Prabhakaran Nayar, S.R., 1995. Height gradient of F region vertical drift in the evening equatorial ionosphere. Geophys. Res. Lett. 22 (19), 2645–2648 http://dx.doi.org/10.1029/95GL02668.

Sastri, J.H., Ramesh, K.B., Somayajulu, V.V., Rao, J.V.S.V., 1991. Origin of short-period (30–300 s) Doppler frequency fluctuations of lower F region reflections in the equatorial electrojet region. Radio Sci. 26 (6), 1403–1413 http://dx.doi.org/10.1029/91RS02021.

Scherliess, L., Fejer, B.G., 1999. Radar and satellite global equatorial F region vertical drift model. J. Geophys. Res. 104 (A4), 6829–6842 http://dx.doi.org/10.1029/1999JA900025.

Sekar, R., Gupta, S.P., Acharya, Y.B., Chakrabarty, D., Pallamraju, D., Pathan, B.M., Tiwari, D., Choudhary, R.K., 2013. Absence of streaming plasma waves around noontime over Thumba in recent times: is it related to the movement of the dip equator? J. Atmos. Sol.-Terr. Phys. 103, 8–15 http://dx.doi.org/10.1016/j.jastp.2013.02.005.

Sekar, R., 1990. Plasma Instabilities and the Dynamics of the Equatorial F-region. (Ph.D. thesis), Gujarat University.

Subbarao, K.S.V., Krishna Murthy, B.V., 1994. Seasonal variations of equatorial spread-F. Ann. Geophys. 12 (1), 33–39.

Subbaraya, B.H., Prakash, S., Gupta, S.P., 1985. Structure of the equatorial lower ionosphere from the Thumba Langmuir probe experiments. Adv. Space Res. 5 (7), 35–38 http://dx.doi.org/10.1016/0273-1177(85)90352-7.

Subbaraya, B.H., Prakash, S., Gupta, S.P., 1983. Electron densities in the equatorial lower ionosphere from the Langmuir probe experiments conducted at Thumba during 1966–1978. Scientific Report, ISRO–PRL–SR–15–83.

Thébault, E., et al., 2015. International geomagnetic reference field: he 12th generation. Earth, Planets Space 67 (1), 1–19 http://dx.doi.org/10.1186/s40623-015-0228-9.

Tiwari, D., Patra, A.K., Viswanathan, K.S., Jyoti, N., Devasia, C.V., Subbarao, K.S.V., Sridharan, R., 2003. Simultaneous radar observations of the electrojet plasma irregularities at 18 and 54.95 MHz over Trivandrum, India. J. Geophys. Res. 108 (A10). http://dx.doi.org/10.1029/2002JA009698.

Viswanathan, K.S., Vikramkumar, B.T., Reddy, C.A., 1987. Electric fields and currents in the equatorial electrojet deduced from VHF radar observations-II. Characteristics of electric fields on quiet and disturbed days. J. Atmos. Terr. Phys. 49 (2), 193–200, ⟨http://www.sciencedirect.com/science/article/pii/0021916987900547⟩.

Woodman, R.F., 1970. Vertical drift velocities and east-west electric fields at the magnetic equator. J. Geophys. Res. 75 (31), 6249–6259 http://dx.doi.org/10.1029/JA075i031p06249.

Journal of Geophysical Research: Space Physics

RESEARCH ARTICLE
10.1002/2017JA024725

Key Points:
- Westward Sq electric field causes afternoon CEJ over India during June solstice in solar minimum
- The consequences of Fejer et al. (2008) empirical model drifts are brought out
- CEJ characteristics obtained from the electrojet model match well with observations

Correspondence to:
K. Pandey,
kuldeepak@prl.res.in

Citation:
Pandey, K., Sekar, R., Anandarao, B. G., Gupta, S. P., & Chakrabarty, D. (2018). On the occurrence of afternoon counter electrojet over Indian longitudes during June solstice in solar minimum. *Journal of Geophysical Research: Space Physics*, *123*. https://doi.org/10.1002/2017JA024725

Received 31 AUG 2017
Accepted 11 FEB 2018
Accepted article online 15 FEB 2018

On the Occurrence of Afternoon Counter Electrojet Over Indian Longitudes During June Solstice in Solar Minimum

Kuldeep Pandey[1,2], R. Sekar[1], B. G. Anandarao[1], S. P. Gupta[1], and D. Chakrabarty[1]

[1]Physical Research Laboratory, Ahmedabad, India, [2]Department of Physics, Indian Institute of Technology Gandhinagar, Gandhinagar, India

Abstract Studies made earlier using ground-based observations of geomagnetic field over the Indian longitudes revealed that the occurrence of equatorial counter electrojet (CEJ) events in afternoon hours is more frequent during June solstice (May-June-July-August) in solar minimum than in other periods. In general, the June solstice solar minimum CEJ events occur between 1500 local time (LT) and 1800 LT with peak strength of about −10 nT at around 1600 LT. In order to understand the frequent occurrence of these CEJ events, an investigation is carried out using an equatorial electrojet model (Anandarao, 1976, https://doi.org/10.1029/GL003i009p00545) and the empirical vertical drift model by Fejer et al. (2008, https://doi.org/10.1029/2007JA012801). The strength, duration, peak value, and the occurrence time of CEJ obtained using electrojet model match remarkably well with the corresponding observation of average geomagnetic field variations. The occurrence of CEJ is found to be due to solar quiet (Sq) electric field in the westward direction which is manifested as downward drift in Fejer et al. (2008, https://doi.org/10.1029/2007JA012801) model output during 1500–1800 LT. Further, the occurrence of afternoon reversal of Sq electric field in this season is shown to be consistent with earlier studies from Indian sector. Therefore, this investigation provides explicit evidence for the role of westward Sq electric field on the generation of afternoon CEJ during June solstice in solar minimum periods over the Indian sector indicating the global nature of these CEJ events.

1. Introduction

A strong eastward current is driven in the *E* region over the magnetic dip equator owing to the orthogonal orientation of the solar quiet (Sq) electric field and the horizontal component of geomagnetic field. This current flows within ±3° dip latitude at around 105 km and is well known as equatorial electrojet (EEJ). In order to characterize the EEJ, a large number of studies were extensively conducted using ground-based (Egedal, 1947; Rastogi & Patil, 1986; Venkatesh et al., 2015), rocket-borne (Davis et al., 1967; Sastry, 1970), and satellite-based magnetometers (Cain & Sweeney, 1973; Jadhav et al., 2002; Lühr et al., 2004; Onwumechili & Agu, 1981). Modeling efforts were also made to simulate different characteristics of EEJ (Anandarao, 1976; Forbes & Lindzen, 1976; Richmond, 1973; Stening, 1985; Sugiura & Poros, 1969). Excellent reviews on this topic are available in the literature (Forbes, 1981; Raghavarao & Anandarao, 1987; Reddy, 1989; Stening, 1992; Yamazaki & Maute, 2017). The electrojet region is also known to host different types of plasma irregularities as recorded comprehensively by earlier workers (Fejer & Kelley, 1980; Gupta, 2000; Kelley, 2009; Prakash et al., 1971). Further, the geomagnetic field variations due to electrojet current can be taken as a proxy for electric field variations (Rastogi & Patel, 1975) on a time scale shorter than the time scale associated with ionospheric conductivity variation. These electric fields during magnetically quiet times are referred to as solar quiet (Sq) electric field generated essentially by a dynamo action driven by tidal winds and hence associated with global current system. The dip equatorial vertical plasma drifts driven by Sq electric fields are measured directly using radar (e.g., Fejer, 1981; Woodman, 1970), Barium vapor cloud (e.g., Haerendel et al., 1967), and ion drift meter (e.g., Hanson & Heelis, 1975) techniques. A few methodologies were described in the literature (e.g., Anderson et al., 2004; Pandey et al., 2017) to derive the zonal Sq electric field from geomagnetic field observations.

In general, as mentioned earlier, the EEJ is eastward during daytime. On many occasions, however, the flow was observed to be westward during the afternoon periods (Gouin & Mayaud, 1967). This is generally referred to as the equatorial counter electrojet (CEJ). A number of studies (Bhargava & Sastri, 1979; Patil et al., 1990; Vichare & Rajaram, 2011; Rabiu et al., 2017) reported the occurrence of CEJ events around the globe, and their characteristics were established. Patil et al. (1990) showed that the afternoon CEJ events over the Indian sector occurred on a total of 110 days during the months of May-June-July-August (henceforth referred to as June solstice) in 1964–1965 which fall under solar minimum period. This gets credence from the work of Rastogi et al. (2014) wherein 40 years of ground-based geomagnetic field observations over Indian sector also brought out the maximum occurrence of afternoon CEJ during June solstice in low sunspot years.

Many mechanisms were proposed to explain the occurrence of CEJ events. Gouin and Mayaud (1967) suggested a possible scenario wherein there exist two counter streaming current systems at two different altitudes, and depending on their relative strengths, the EEJ or CEJ can be generated. However, the experimental support for this hypothesis in the form of a vertical profile of current density is not available in the literature. The effects of lunar phase variation on the occurrence of CEJ are extensively studied (Hutton & Oyinloye, 1970; Rastogi, 1974; Stening, 1989a). However, occurrence of afternoon CEJ on 25 days in a month of July during solar minimum over the Indian sector (see Rastogi et al., 2014, for details) cannot be accounted for by the lunar phase variation. Raghavarao and Anandarao (1980) showed that large vertical winds ($\sim$20 ms^{-1}) of gravity wave origin can generate CEJ. However, sustenance of such winds on daily basis lasting for $\sim$3 h could be difficult (Stening, 1992). Further, the effects of zonal wind and its vertical shears were shown to be mostly ineffective in altering the zonal current over the dip equator (Anandarao & Raghavarao, 1987; Richmond, 1973). It is also known that the polarity of the Sq electric field can be altered (e.g., Chau et al., 2009; Fejer et al., 2010) by the winds associated with the significant rise in temperature (known as sudden stratospheric warming or SSW) in the polar stratosphere in the winter hemisphere (Schoeberl, 1978) owing to disruption of polar vortex of westerly winds. This can lead to occurrence of CEJ during SSW events (Sridharan et al., 2009). However, the effects of SSW are pronounced in local winter (Schoeberl, 1978), and hence, frequent occurrence of CEJ in June solstice is not likely to be of SSW origin. Therefore, these mechanisms cannot successfully account for the characteristics of CEJ events in June solstice over the Indian sector. Though space weather events like disturbance dynamo (Blanc & Richmond, 1980), overshielding (Kobea et al., 2000), and substorm (Kikuchi et al., 2003) also produce CEJ, however, the present study is focused on the occurrence of CEJ during geomagnetically quiet conditions. The abnormal depressions in horizontal magnetic field over the dip equatorial stations, similar to the magnetic field signatures of CEJ events, were correlated with *foF*2 variation by Onwumechili and Akasofu (1972). Although those observations were in another season (December solstice) and may have a common driver, these authors did not explicitly discuss the possible role of Sq electric field. In addition, these authors (Onwumechili & Akasofu, 1972) did not remove off-equatorial magnetic field in their work, which was shown in later years (Rastogi, 1975) to be essential to ascertain CEJ events. In another investigation, the possibility of CEJ being part of global current system was discussed by Gurubaran (2002). However, in the investigation of Gurubaran (2002), the alteration of Sq electric fields was not explicitly discussed.

Taking into account of the facts that the Sq electric field pattern changes with season and the occurrence of CEJ events maximizes over the Indian sector during June solstice in solar minimum years, an investigation is carried out to establish the connection between polarity change in diurnal variation of Sq electric field and the occurrence of these CEJ events. This is done by computing the *E* region current densities and the corresponding horizontal magnetic field induced at ground using electrojet model by Anandarao (1976) (methodology described in section 2) providing inputs (described in section 2.1) corresponding to June Solstice in solar minimum years. Details of magnetic field observations used to compare with the magnetic field computed from model results are described in section 3. The results obtained are presented in section 4 and discussed in detail in section 5.

2. Methodology

A first principle model to compute the *E* region current densities was developed by Anandarao (1976) by solving generalized Ohm's law, current conservation equation along with curl-free electric field condition. These equations were reduced to a differential equation involving a current function and its derivatives in spherical polar coordinate system. This differential equation was solved numerically to compute the components of electric fields to obtain the zonal current density (J_ϕ) using the following equation.

$$J_\phi = \sigma_H \left(E_r \cos I - E_\theta \sin I\right) + \sigma_P E_\phi \quad (1)$$

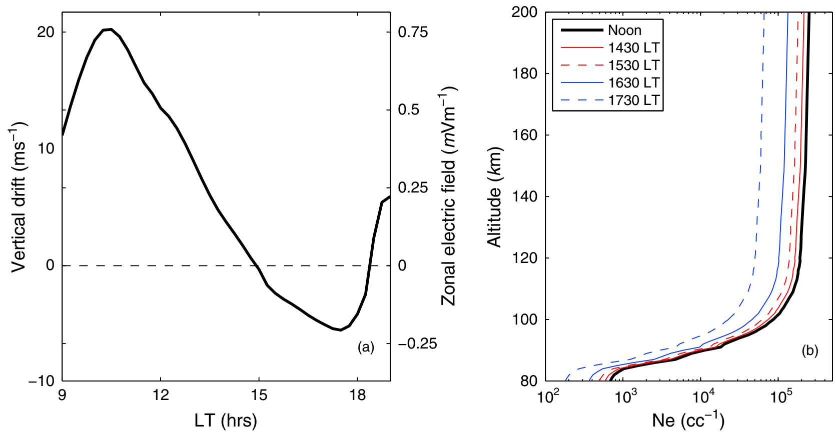

Figure 1. Inputs to the electrojet model (a) Vertical drifts (left Y axis) over 60°E longitude from Fejer et al. (2008) and the corresponding zonal electric field (right Y axis). (b) Altitude profiles of electron density (Ne) at different local times. The solid bold line represents the averaged electron density profile based on the measurements conducted from Trivandrum during 1000–1400 local time (LT) under low ($\langle F10.7 \rangle \leq 120$ sfu) solar activity periods. The other profiles are generated based on the solar zenith angle (χ) variation (see text for details).

where σ_H, σ_P, E_r, E_θ, E_ϕ, and I are conductivities in Hall and Pedersen directions; electric fields in radial, meridional, and zonal directions; and dip angle, respectively. The details of the model can be obtained from the earlier works of Anandarao and Raghavarao (1987) and Raghavarao and Anandarao (1987). In the present work, the average values of zonal current densities between 0930 local time (LT) and 1730 LT during June solstice in solar minimum years over the Indian sector are computed based on equation (1).

A method to evaluate the horizontal component of magnetic field induced (H_{ind}) at ground by this current system is described by Anandarao (1977) based on Biot-Savart's law.

$$H_{\text{ind}} = \frac{\mu_0 C}{2\pi r}\left[\frac{(r/a)\sin\theta - 1}{(r/a)^2 + 1 - 2(r/a)\sin\theta}\right], \tag{2}$$

where C represents the line current obtained by integrating the current density J_ϕ over the radial distance r and the magnetic colatitude θ in a geocentric coordinate system ($C = \int_r \int_\theta J_\phi \, \mathrm{d}r \, \mathrm{d}\theta$). The symbol "a" denotes the radius of Earth. Using the above equation, the average horizontal component of the induced magnetic field is computed for LT between 0930 and 1730 h during June solstice in solar minimum period over the Indian sector.

2.1. Inputs to the Electrojet Model

The inputs to the electrojet model are zonal Sq electric field, altitude profiles of E region electron density, neutral atmospheric density, and temperature, in addition to the three-dimensional geomagnetic field. The neutral atmospheric density and temperature are obtained from Naval Research Laboratory Mass Spectrometer Incoherent Scatter Extension-00 (NRLMSISE-00; Picone et al., 2002) model, and the geomagnetic field is taken from International Geomagnetic Reference Field-12th generation (IGRF-12; Thébault et al., 2015) model.

The systematic ground-based measurements of Sq electric field over India covering all local times and seasons are not available because of the absence of incoherent scatter radar in this sector. Based on in situ measurements of vertical drifts obtained using ion drift meters onboard AE-E and ROCSAT-1 satellites, Scherliess and Fejer (1999) and Fejer et al. (2008), respectively, developed global empirical models of vertical drifts. Recently, based on the scattered data that were available, Pandey et al. (2017) showed that the vertical drifts reported by Fejer et al. (2008) model corresponding to 60°E longitude (with ±15° longitude and ±5° dip latitude bin) represent the vertical drifts over the Indian sector fairly well at different local times of the day barring early morning hours. Therefore, the Sq electric fields at different local times are obtained based on climatological vertical drifts of Fejer et al. (2008) model. Figure 1a depicts these vertical drifts during June solstice in low solar flux conditions ($F10.7 \approx 130$ sfu). This is based on Figure 7 of Fejer et al. (2008) empirical model corresponding to 60°E longitude sector. The input zonal Sq electric field is then obtained by taking the cross product of vertical drift with and Earth's horizontal magnetic field (~37,400 nT) over Trivandrum (TRD).

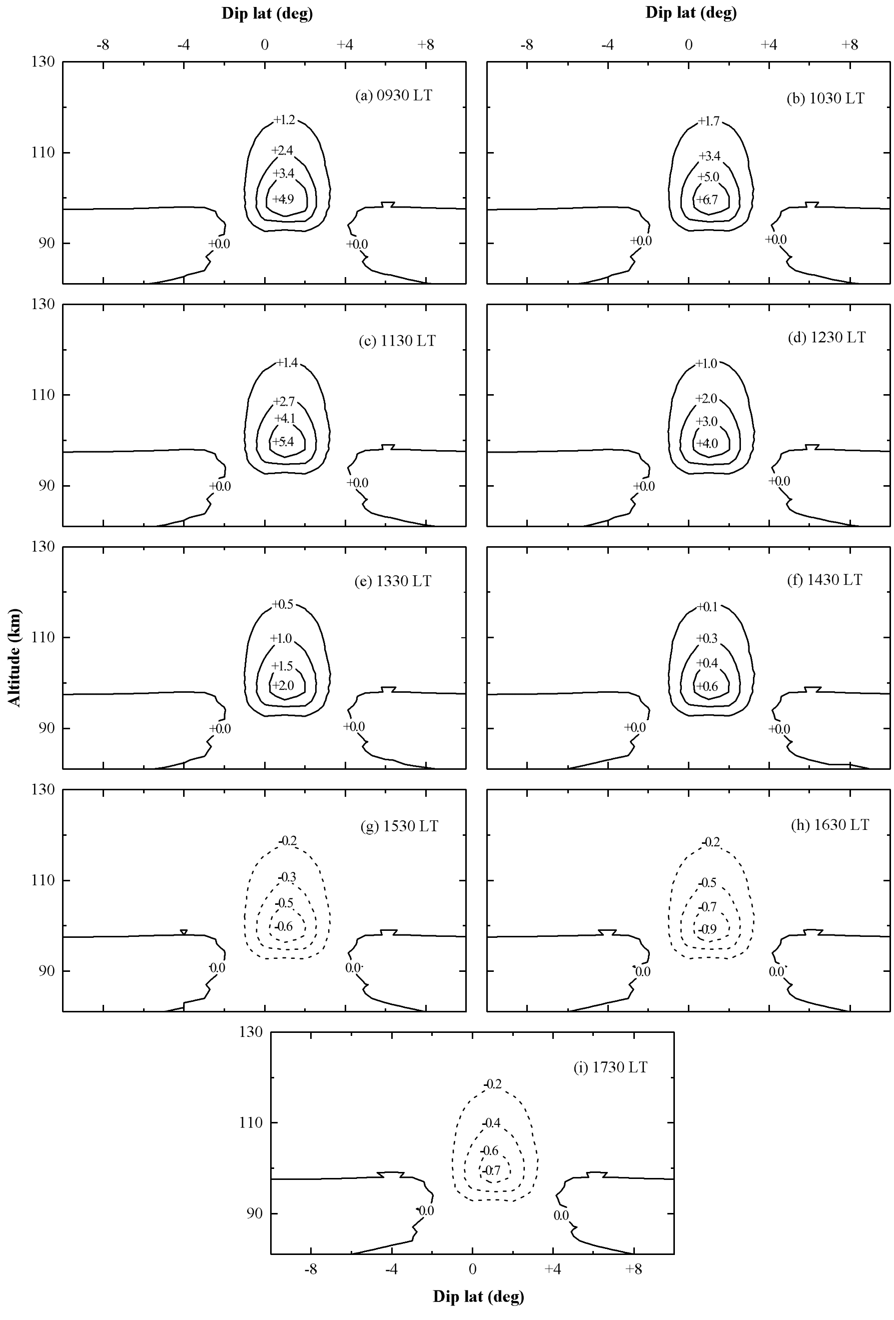

Figure 2. The contours of isocurrent densities (in μAm^{-2}) in the zonal direction, obtained from electrojet model in altitude dip latitude plane corresponding to inputs at different local times. Note that the solid and dashed whorls represent the positive (eastward) and negative (westward) values of current density, respectively. The current density values are shown on each contour with the maximum value marked at the center. LT = local time.

The input of *E* region electron densities to the model is based on the in situ measurements (Gupta, 2000; Subbaraya et al., 1983) that have been obtained using high-frequency Langmuir probe (Prakash & Subbaraya, 1967) onboard rocket experiments, conducted over TRD at different local times between 1968 and 1982. It is noticed that electron density profiles over the electrojet altitudes (90–110 km) do not reveal significant temporal variation during 1000–1400 LT for a given solar epoch. Therefore, electron density profiles measured between this time interval under low solar epoch ($\langle F10.7\rangle \leq 120$ sfu, where $\langle F10.7\rangle$ stands for annually averaged $F10.7$) are averaged and used as representative profile at noon (shown in Figure 1b). Since in situ

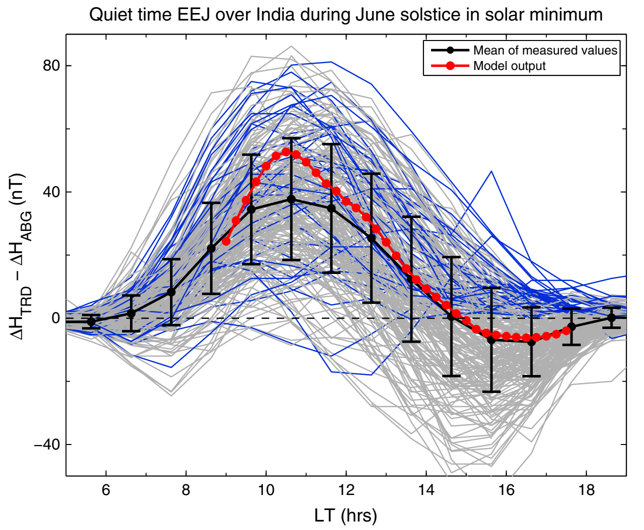

Figure 3. The hourly variations of equatorial electrojet (EEJ) strength deduced using magnetometer data corresponding to individual geomagnetic quiet days with normal (blue) and afternoon counter (gray) electrojet during June solstice in solar minimum years of solar cycle 22. It consists of 235 quiet days of observations whose mean values are depicted by black curve. The 1σ variation for each point is also indicated with vertical bars. The red curve corresponds to the magnetic field strength computed using EEJ model. LT = local time.

electron density profiles are not available at all local times, the empirical relationship between the electron density and solar zenith angle (χ) through $\cos^{1.31/2}(\chi)$ (IRI-90, Bilitza, 1990) is used along with the measured averaged noontime density profile to generate electron density profiles during 0930–1730 LT (see Figure 1b).

3. Details of Ground-Based Magnetic Field Observations Used for Comparison With Model Results

In order to compare the computed magnetic field (based on equation (2)) with the observations of electrojet strength, the ground-based magnetic field observations over India are utilized. The observations of horizontal component of geomagnetic field (H) from an equatorial (eq) and off-equatorial (off-eq) stations are conventionally used to extract the strength of EEJ (Rastogi & Patel, 1975). This is done by computing $\Delta H_{eq} - \Delta H_{off\text{-}eq}$ where ΔH is obtained by subtracting average values of H at nighttime from instantaneous H values. The geomagnetic field observations from an equatorial station TRD (8.5°N, 76.9°E, dip latitude 1°S) and off-equatorial station Alibag (ABG, 18.6°N, 72.9°E, dip latitude 10°N) are utilized to compute the strength of electrojet. The hourly variations of geomagnetic fields on quiet days ($Kp \leq 3$ and $DST \geq -20$, with similar conditions on previous day to avoid the effects of disturbance dynamo), are obtained from World Data Center Kyoto (http://wdc.kugi.kyoto-u.ac.jp/). For the present study, the differential horizontal geomagnetic field variations on 235 quiet days covering 6 years during June solstice months in solar minimum periods ($\langle F10.7 \rangle \leq 120$ sfu) are considered. These 235 days are spread over ascending (1985–1987) and descending (1993–1995) phases of solar cycle 22.

4. Results

The model-generated contours of isocurrent densities along the zonal direction in altitude dip latitude plane are depicted in Figure 2 at various local times. The strength of zonal current density (J_ϕ in units of μAm^{-2}) is also shown on each contour with the maximum value marked at the center. Based on the sensitivity studies carried out with various model inputs, the uncertainty in current density was found to be less than 18% (Pandey et al., 2016). The contours of current density plotted with solid and dashed lines correspond to the positive (eastward) and negative (westward) values of current density, respectively. It is to be noted that eastward electrojet peaks around 1030 LT. The flow of current becomes westward between 1430 LT and 1530 LT, and it remains so till 1730 LT. The peak of westward current density in general is found to be ~ -1 μAm^{-2} between 1530 LT and 1630 LT.

The horizontal components of magnetic field induced at ground by the electrojet currents are computed based on equation (2). The computation is carried out for every 15 min interval from 0930 LT and 1730 LT. Figure 3 depicts the computed variations of magnetic field (red curve with dots). The observed hourly variations of $\Delta H_{TRD} - \Delta H_{ABG}$ for 235 quiet days during June solstice in solar minimum periods are also shown in the figure as the blue and gray curves corresponding to normal EEJ and afternoon CEJ days, respectively. Out of these 235 quiet days of observations, CEJ occurred during 1500–1800 LT on 194 days. In order to generate a quiet time average variation of $\Delta H_{TRD} - \Delta H_{ABG}$, all the 235 quiet days (including both normal EEJ and afternoon CEJ days) are considered. This average curve is depicted in black with dots indicating hourly intervals. In addition, the 1σ variation for each point is indicated with vertical bars.

It is evident from Figure 3 that the model computed and mean of observed magnetic fields match well (within 1σ variation) between 0930 LT and 1730 LT. The peak magnetic field values corresponding to eastward electrojet occur ~1030 LT in both computed and observed values. On an average, CEJ events occur between 1500 LT and 1800 LT with peak (~ -10 nT) occurring around 1600 LT. In spite of using averaged inputs from different sets of data (see section 2), remarkable similarities are observed between the computed and mean observed values of magnetic field during CEJ hours (~1500–1730 LT). The time of commencement and the duration of CEJ obtained from the model computations closely follow the respective observations.

Further, the strength of peak CEJ and its time of occurrence obtained from model computations are almost the same as those from observations. The implications of these results are discussed in the following section.

5. Discussion

From Figures 1a and 2 it is clear that the reversal in electrojet takes place when the Sq electric field becomes westward. It is to be noted that the peak of the current density (see Figure 2) and the magnetic fields (see Figure 3) corresponding to normal electrojet are found to be at the same time (~1030 LT) when the zonal Sq electric field from empirical model (Fejer et al., 2008) maximizes (see Figure 1a). Incidentally, the local time corresponding to the monthly mean of Sq focii over the Indian sector during June solstice in solar minimum period was found to be around 1030 LT (Vichare et al., 2017). However, in afternoon hours, local time corresponding to the peak of CEJ current (~1630 LT) does not coincide with the time when westward Sq electric field maximizes (~1730 LT). This is due to considerable amount of decrease in electron density with χ variation after 1630 LT (see Figure 1b) that results in reduction of CEJ strength after ~1630 LT. Hence, the time of peak westward current is determined from the optimum values of zonal Sq electric field and electron density.

The average characteristics of CEJ events (strength, duration, peak value, and its time of occurrence) reported by earlier studies (Patil et al., 1990; Rastogi et al., 2014) pertain to different solar cycles and are similar to the observations presented in Figure 3. Further, the results obtained in the present work using electrojet model have exceptional similarities with these observations. However, on some occasions, the amplitude of CEJ is observed to be substantially larger than 1σ compared to averaged CEJ strength and commencement of some of CEJ events is at earlier local times (<1500 LT). These aspects are discussed later. It is clear from Figure 2 that depending on the polarity of the zonal Sq electric field being eastward or westward, the EEJ or CEJ appears. Thus, it is important to know the polarity of the zonal Sq electric field in afternoon hours. Fejer et al. (2008) model, employed in the present investigation, reveals westward Sq electric field during 1500–1800 LT in June solstice in solar minimum over Indian longitude. Considering the smaller values of westward Sq electric field after ~1500 LT and the uncertainties (less than 10% particularly during daytime) associated with the Fejer et al. (2008) model, additional clues for the westward Sq electric fields during afternoon hours in this season over the Indian region are gleaned from the earlier works and discussed in the ensuing subsection.

5.1. Earlier Observations That Indirectly Support Westward Sq Electric Field During Afternoon Hours

Various earlier measurements that indicate the westward Sq electric field in afternoon hours over the Indian sector during June solstice in solar minimum periods are described in the ensuing paragraphs.

The vertical Doppler drifts from the radar echoes due to the presence of plasma irregularities at 150 km region act as a proxy to zonal Sq electric field (Chau & Woodman, 2004; Kudeki & Fawcett, 1993). These measurements have been extensively used over the Peruvian sector (Hui & Fejer, 2015). Over the Indian sector, such measurements of the vertical drifts over Gadanki (13.5°N, 79.2°E, dip latitude 6.5°N) are reported by Pavan Chaitanya et al. (2014) and Patra et al. (2014). Patra et al. (2014) reported the vertical drifts for 4 days during July–August 2009 that indicate downward trend at ~1500 LT. As the radar observational time was limited to ~1500 LT, the westward Sq electric field could not be ascertained on most of the cases beyond this local time. However, on one occasion, simultaneous measurements of vertical drifts using in situ measurements by Communication/Navigation Outage Forecast System (C/NOFS) satellite and 150 km echo revealed westward electric field at ~1400 LT. On this CEJ day, continuous operation of radar revealed westward electric field till the end of the observation (~1530 LT). Some of the earlier reversals seen in Figure 3 can be accounted by westward electric field similar to this measurement. Further, Pavan Chaitanya et al. (2014) reported observations of 150 km echoes during 5 months in 2009 for a few consecutive days in each month. It is noticed from their observations that, on an average, the vertical drifts are close to 0 or negative ~1500 LT in June and July months and show decreasing trend around this time. Note that the decreasing trend in afternoon hours in months other than June solstice (e.g., December month) was not observed by both Pavan Chaitanya et al. (2014) and Patra et al. (2014). Thus, these case studies give credence to the presence of westward Sq electric fields in afternoon hours during June solstice in solar minimum period.

The polarity of Sq electric field can also be inferred from the measurements of *E* region electron density profiles and structures in them (Pandey et al., 2017). Recently, Pandey et al. (2017) have shown that the polarity of zonal Sq electric field and the limiting values of the drift deduced from such measurements match well with the empirical model of vertical drift (Fejer et al., 2008). Based on a rocket flight experiment conducted at 1554 LT on 17 August 1972 from TRD, Prakash et al. (1976) reported that the streaming waves were present on a CEJ day around 105–110 km and amplitudes of irregularities at altitudes below 100 km were found to be of the order of nongeophysical noise level (~0.5%) and thus considered by them as absence of irregularities. However, over the Indian region, the gradient drift waves are in general observed above 87 km in positive gradient region (Sekar et al., 2014), where electrojet current is negligible due to low value of *R* (ratio of Hall to Pedersen conductivities) (Pandey et al., 2016). Thus, the absence of gradient drift waves in the positive gradient region at very low altitudes (~90 km) indicates toward the westward Sq electric field on that day. Further, the presence of streaming waves above 105 km altitude indicates that the downward drift corresponding to zonal Sq electric field was more than the limiting value of 12 ms^{-1} (Pandey et al., 2017). Thus, the Sq electric field can be westward and with large amplitude on some occasions during afternoon in June solstice under solar minimum periods. This can account for large deviations (more than 1σ) in the amplitude of CEJ as observed on some occasions compared to the averaged CEJ strength depicted in Figure 3. Thus, the above set of observations provides another evidence for the presence of westward Sq electric field during daytime on a CEJ day.

The strength of Sq electric field can also be gauged from the morphology of the latitudinal location of the peak of ionization. The latitudinal distribution of ionization in low-latitude *F* region is controlled by plasma fountain effect. The equatorial plasma fountain is due to eastward Sq electric field pumping up the plasma from equatorial region vertically upward, which subsequently diffuses along the geomagnetic field with the modulation due to meridional wind to form a crest region over low latitudes (Hanson & Moffett, 1966). However, the location of the crest region of equatorial plasma fountain depends on the strength of zonal electric field (Anderson, 1973). The stronger eastward electric field shifts the crest of plasma fountain further away from the dip equator. Several works reported strong correlation between integrated EEJ strength and the development of plasma fountain (Aggarwal et al., 2012; Raghavarao et al., 1978; Rama Rao et al., 2006; Rush & Richmond, 1973). This correlation was also observed in total electron content (TEC) variations reported by earlier workers (e.g., Iyer et al., 1976), though seasonal dependence of TEC under different solar epochs is sparse (Rama Rao et al., 2006; Yadav et al., 2013). In one such work by Rama Rao et al. (2006), the monthly mean values of TEC at different latitudes over India are reported. The crest location of TEC during 2004, which is in the descending phase of solar cycle 23 ($\langle F10.7 \rangle \leq 110$ sfu), is found to be at ~12°N dip latitude. It can be noticed from Figure 7 of their work that the TEC values peaked for a short interval of time around noon and fall off sharply afterward during June–July compared to other months. The noontime peak in TEC indicates that zonal Sq electric field peaks around 1000–1030 LT as it takes about 2 h (Sanatani, 1966) to diffuse to the location of 12°N dip latitude. In addition, sharp decrease in TEC after noon indicates sharp decrease in zonal electric field. Further, the location of peak TEC was shown not to exceed beyond 6°N dip latitude during afternoon hours in June solstice, indicating that the zonal Sq electric field was relatively weak. Thus, the morphological variations of TEC over India indicate the decreasing trend of Sq electric field in the afternoon hours during June solstice in solar minimum periods. Since the latitudinal extent of EEJ is limited (±3°), the correlation between EEJ and plasma fountain obtained by these workers indicates the common role of Sq electric field in controlling both the phenomena.

An indirect inference of earlier (afternoon) reversal of Sq electric field can be obtained from the magnetic field observations at the focii of Sq current system. Based on geomagnetic field observations using chain of magnetometers during low solar activity ($\langle F10.7 \rangle < 90$ sfu) years 2006–2010, Vichare et al. (2017) reported that the local time corresponding to monthly mean of focii of Sq current system over the Indian sector during June solstice occurs earlier (~1030 LT) compared to other seasons. Interestingly, the time of maximum eastward electric field corresponding to vertical drifts over Indian sector reported by Fejer et al. (2008) model is also earlier (~1030 LT) in June solstice compared to other seasons. These observations are consistent with morphological variations of TEC observations discussed earlier. As the maximum of Sq current is observed earlier, it is expected that the descending phase of diurnal tide starts early during this season. Under these conditions, the contributions from components other than diurnal tides can govern the Sq current system and hence the zonal electric field depending upon the relative magnitudes and phases of diurnal and higher-order tidal components. These aspects can result in small or opposite polarity of zonal Sq electric field in afternoon hours during June solstice compared to other seasons.

A chain of magnetic field observations can also provide a clue to the polarity of the Sq electric field. Based on the principal component analysis of geomagnetic field variations measured using a chain of magnetometers over Indian region during June–July 1995, Gurubaran (2002) reported that the second harmonic plays a crucial role in the occurrence of CEJ in afternoon hours. The author (Gurubaran, 2002) also showed that on days of afternoon CEJ, a clockwise current system (located ~20 dip latitude in afternoon hours) owing to higher harmonics is superposed on the normal counterclockwise Sq current vortex (located ~30 dip latitude at noon) due to primary component. The author wondered whether CEJ is a part of global current system. Bhattacharyya and Okpala (2015) applied a similar analysis to quiet time geomagnetic field variations between 1999 and 2012 and reported that second and third harmonics contribute to the occurrence of CEJ events. In recent investigation, Bhardwaj and Subba Rao (2017) showed that the higher harmonics are associated with clockwise current system in afternoon. Therefore, the studies by Bhattacharyya and Okpala (2015) can also be taken to produce clockwise current cell in the afternoon. Thus, the results obtained from these systematic magnetic field variations measured using a chain of magnetometers over Indian region indicate toward formation of a counterclockwise current cell in morning and clockwise current cell during afternoon hours on CEJ days in addition to normal counterclockwise current cell. This can be taken as a support for eastward Sq electric field in morning hours and westward Sq electric field during afternoon hours at least during the periods of June solstice in solar minimum.

5.2. Possible Reason for Westward Sq Electric Field in Afternoon Hours

Section 5.1 provides alternate evidences for westward Sq electric field around 1500–1800 LT during June solstice in solar minimum periods that are consistent with the results of Fejer et al. (2008) for the Indian sector. Possible reason for this westward Sq electric field is discussed below.

Simultaneous long-term (1993-2011) observations of mesospheric winds by medium frequency (MF) radar at Tirunelveli (8.7°N, 77.8°E), a station close to the dip equator over India, and the strength of EEJ using geomagnetic field observations revealed that the second principal component acts as proxy for the occurrence of CEJ with enhanced tidal activities during solar minimum year when the occurrence of CEJ is more (Gurubaran et al., 2016). However, the role of relative strengths of diurnal and semidiurnal tides particularly during June solstice in solar minimum periods for the generation of CEJ is not clear from this work. Month-to-month variations of tidal amplitudes of mesospheric winds over TRD obtained using a meteor radar from June 2004 to May 2005 (descending phase of solar cycle 23, $\langle F10.7\rangle \leq 110$ sfu) are reported by Deepa et al. (2006). It is observed from Figures 9 to 14 of their work that the semidiurnal amplitudes are found to be larger than corresponding diurnal amplitude in meridional direction in the altitude region 94–98 km during the June solstice months. The phase difference between meridional diurnal and semidiurnal tides was found to be around 12 h in the altitude region 94–98 km in this solstice barring the month of June. Possible role of semidiurnal tides on equatorial quiet time vertical ion drifts measured by C/NOFS satellite was indicated by Stoneback et al. (2011) based on measurements over the Indian sector during deep solar minimum period (2008–2010) of solar cycle 23. Further, when semidiurnal tide is effective and contributes to the generation of afternoon CEJ, it is expected to cause eastward electric field influence around midnight hours. This aspect is confirmed by the premidnight ascent of *F* layer and upward ion drift observed by C/NOFS over the Indian sector during June solstice in deep solar minimum years 2008–2009 (Chakrabarty et al., 2014). These aspects are in support of role played by the semidiurnal tides during June solstice.

In theoretical studies (Forbes & Lindzen, 1976; Hanuise et al., 1983; Marriott et al., 1979) with assumptions of concentric geomagnetic and geographic equator and reduced amplitude of diurnal components, the features of CEJ are modeled by combination of symmetric semidiurnal tides. The observational support for the second assumption was provided by Sridharan et al. (2002) wherein a reduction in the diurnal tidal component and/or enhancement in semidiurnal amplitude was reported on afternoon CEJ days during June–July months in 1995 observed over Tirunelveli using MF radar and chain of magnetometers simultaneously. On the other hand, Stening (1989b) reproduced many features of CEJ by introducing antisymmetric semidiurnal tidal components. Numerical simulation of simultaneous Sq current and CEJ using different combinations of semidiurnal and diurnal tidal components is beyond the scope of this manuscript. However, based on earlier simulation works discussed above and the observational support on tidal winds from recent times, it appears that the semidiurnal tides play a crucial role in altering Sq electric field, which is shown by the present investigation to be essential to cause CEJ during June solstice in solar minimum periods over the Indian region.

Finally, the present investigation brings out the important consequence of the westward Sq electric fields that were obtained by Fejer et al. (2008) empirical model over Indian longitudes during June solstice in solar minimum in the generation of CEJ. Though the process appears to be obvious, the present work reproduces all the observed CEJ characteristics remarkably well. Further, if the Sq electric field is responsible for the generation of CEJ, the requirement (Stening, 1977) of a separate return current becomes superfluous. Therefore, the present investigation suggests that these CEJ events are part of a global current system. As the present work is not exhaustive covering all the seasons and solar epochs, the other suggested mechanisms discussed in section 1 are not precluded.

6. Summary

An investigation was carried out using an EEJ model and the inputs based on measurements and empirical model of vertical drift to understand frequent occurrence of CEJ events in afternoon hours over the Indian sector during June solstice in solar minimum period. The occurrence of CEJ is shown to be due to the westward Sq electric field between 1500 LT and 1800 LT. The empirical model-based westward Sq electric field is substantiated by various earlier observations from India. The magnetic field derived from the electrojet model is compared with the corresponding magnetic observations from India. The comparison revealed that the strength, duration, peak value, and the occurrence time of CEJ computed by the model match well with the observation, suggesting the explicit role of westward Sq electric field in the generation of these CEJ events. Therefore, the present investigation suggests that afternoon CEJ events over the Indian sector during June solstice in solar minimum periods are part of the global current system.

Acknowledgments
The hourly values of magnetic field measurements are courtesy of Indian Institute of Geomagnetism, Mumbai, and obtained from the World Data Center for Geomagnetism, Kyoto (http://wdc.kugi.kyoto-u.ac.jp/). The values of *Kp* and solar flux (at 10.7 cm) indices are obtained from the Word Data Center for Geomagnetism, Kyoto, and Laboratory for Atmospheric and Space Physics (http://lasp.colorado.edu/lisird/) respectively. This work is supported by the Department of Space, Government of India.

References

Aggarwal, M., Joshi, H. P., Iyer, K. N., Kwak, Y. S., Lee, J. J., Chandra, H., & Cho, K. S. (2012). Day-to-day variability of equatorial anomaly in GPS-TEC during low solar activity period. *Advances in Space Research*, *49*(12), 1709–1720. https://doi.org/10.1016/j.asr.2012.03.005

Anandarao, B. G. (1976). Effects of gravity wave winds and wind shears on equatorial electrojet. *Geophysical Research Letters*, *3*(9), 545–548. https://doi.org/10.1029/GL003i009p00545

Anandarao, B. G. (1977). Studies on the dynamics of the equatorial ionosphere (PhD thesis). Gujarat University.

Anandarao, B. G., & Raghavarao, R. (1987). Structural changes in the currents and fields of the equatorial electrojet due to zonal and meridional winds. *Journal of Geophysical Research*, *92*(A3), 2514–2526. https://doi.org/10.1029/JA092iA03p02514

Anderson, D., Anghel, A., Chau, J., & Veliz, O. (2004). Daytime vertical E × B drift velocities inferred from ground-based magnetometer observations at low latitudes. *Space Weather*, *2*, S11001. https://doi.org/10.1029/2004SW000095

Anderson, D. N. (1973). A theoretical study of the ionospheric *F* region equatorial anomaly—I. Theory. *Planetary and Space Science*, *21*(3), 409–419. https://doi.org/10.1016/0032-0633(73)90040-8

Bhardwaj, S. K., & Subba Rao, P. B. V. (2017). The afternoon counter-electrojet current system along the 75°E meridian during the IEEY. *Earth, Planets and Space*, *69*(1), 91. https://doi.org/10.1186/s40623-017-0675-6

Bhargava, B. N., & Sastri, N. S. (1979). Some characteristics of the occurrence of the afternoon counter-electrojet events in the India region. *Journal of Geomagnetism and Geoelectricity*, *31*(2), 97–101. https://doi.org/10.5636/jgg.31.97

Bhattacharyya, A., & Okpala, K. C. (2015). Principal components of quiet time temporal variability of equatorial and low-latitude geomagnetic fields. *Journal of Geophysical Research: Space Physics*, *120*, 8799–8809. https://doi.org/10.1002/2015JA021673

Bilitza, D. (Ed.) (1990). *International Reference Ionosphere 1990, NSSDC/WDC-A-R&S 90-22*. Greenbelt, MD: National Space Science Data Center.

Blanc, M., & Richmond, A. D. (1980). The ionospheric disturbance dynamo. *Journal of Geophysical Research*, *85*(A4), 1669–1686. https://doi.org/10.1029/JA085iA04p01669

Cain, J. C., & Sweeney, R. E. (1973). The POGO data. *Journal of Atmospheric and Terrestrial Physics*, *35*(6), 1231–1247. https://doi.org/10.1016/0021-9169(73)90021-4

Chakrabarty, D., Fejer, B. G., Gurubaran, S., Pant, T. K., Abdu, M. A., & Sekar, R. (2014). On the pre-midnight ascent of F-layer in the June solstice during the deep solar minimum in 2008 over the Indian sector. *Journal of Atmospheric and Solar-Terrestrial Physics*, *121*, 177–187. https://doi.org/10.1016/j.jastp.2014.01.002

Chau, J. L., & Woodman, R. F. (2004). Daytime vertical and zonal velocities from 150-km echoes: Their relevance to *F*-region dynamics. *Geophysical Research Letters*, *31*, L17801. https://doi.org/10.1029/2004GL020800

Chau, J. L., Fejer, B. G., & Goncharenko, L. P. (2009). Quiet variability of equatorial E × B drifts during a sudden stratospheric warming event. *Geophysical Research Letters*, *36*, L05101. https://doi.org/10.1029/2008GL036785

Davis, T. N., Burrows, K., & Stolarik, J. D. (1967). A latitude survey of the equatorial electrojet with rocket-borne magnetometers. *Journal of Geophysical Research*, *72*(7), 1845–1861. https://doi.org/10.1029/JZ072i007p01845

Deepa, V., Ramkumar, G., Antonita, M., Kumar, K. K., & Sasi, M. N. (2006). Vertical propagation characteristics and seasonal variability of tidal wind oscillations in the MLT region over Trivandrum (8.5°N, 77°E): First results from SKiYMET meteor radar. *Annales Geophysicae*, *24*, 2877–2889.

Egedal, J. (1947). The magnetic diurnal variation of the horizontal force near the magnetic equator. *Terrestrial Magnetism and Atmospheric Electricity*, *52*(4), 449–451. https://doi.org/10.1029/TE052i004p00449

Fejer, B. G. (1981). The equatorial ionospheric electric fields. A review. *Journal of Atmospheric and Terrestrial Physics*, *43*(5), 377–386.

Fejer, B. G., & Kelley, M. C. (1980). Ionospheric irregularities. *Reviews of Geophysics*, *18*(2), 401–454. https://doi.org/10.1029/RG018i002p00401

Fejer, B. G., Jensen, J. W., & Su, S. Y. (2008). Quiet time equatorial *F* region vertical plasma drift model derived from ROCSAT-1 observations. *Journal of Geophysical Research*, *113*, A05304. https://doi.org/10.1029/2007JA012801

Fejer, B. G., Olson, M. E., Chau, J. L., Stolle, C., Lühr, H., Goncharenko, L. P., et al. (2010). Lunar-dependent equatorial ionospheric electrodynamic effects during sudden stratospheric warmings. *Journal of Geophysical Research*, *115*, A00G03. https://doi.org/10.1029/2010JA015273

Forbes, J. M. (1981). The equatorial electrojet. *Reviews of Geophysics*, *19*(3), 469–504. https://doi.org/10.1029/RG019i003p00469

Forbes, J. M., & Lindzen, R. S. (1976). Atmospheric solar tides and their electrodynamic effects—II. The equatorial electrojet. *Journal of Atmospheric and Terrestrial Physics*, *38*(9), 911–920. https://doi.org/10.1016/0021-9169(76)90074-X

Gouin, P., & Mayaud, P. N. (1967). A propos de l'existence possible d'un "contre electrojet" aux latitudes magnetiques equatoriales. *Annales Geophysicae*, *23*, 41–47.

Gupta, S. P. (2000). Two stream instability in *E* region over magnetic equator during morning hours. *Advances in Space Research*, *26*(8), 1257–1261. https://doi.org/10.1016/S0273-1177(99)01212-0

Gurubaran, S. (2002). The equatorial counter electrojet: Part of a worldwide current system? *Geophysical Research Letters*, *29*(9), 1337. https://doi.org/10.1029/2001GL014519

Gurubaran, S., Sathishkumar, S., & Veenadhari, B. (2016). On the role of atmospheric tides in the quiet-time variabilities of equatorial electrojet. *Journal of Indian Geophysical Union*, *Special Volume-2*, 87–98.

Haerendel, G., Lüst, R., & Rieger, E. (1967). Motion of artificial ion clouds in the upper atmosphere. *Planetary and Space Science*, *15*(1), 1–18. https://doi.org/10.1016/0032-0633(67)90062-1

Hanson, W. B., & Heelis, R. A. (1975). Techniques for measuring bulk gas-motions from satellites. *Space Science Instrumentation*, *1*, 493–524.

Hanson, W. B., & Moffett, R. J. (1966). Ionization transport effects in the equatorial *F* region. *Journal of Geophysical Research*, *71*(23), 5559–5572. https://doi.org/10.1029/JZ071i023p05559

Hanuise, C., Mazaudier, C., Vila, P., Blanc, M., & Crochet, M. (1983). Global dynamo simulation of ionospheric currents and their connection with the equatorial electrojet and counter electrojet: A case study. *Journal of Geophysical Research*, *88*(A1), 253–270. https://doi.org/10.1029/JA088iA01p00253

Hui, D., & Fejer, B. G. (2015). Daytime plasma drifts in the equatorial lower ionosphere. *Journal of Geophysical Research: Space Physics*, *120*, 9738–9747. https://doi.org/10.1002/2015JA021838

Hutton, R., & Oyinloye, J. O. (1970). The counter-electrojet in Nigeria. *Annales Geophysicae*, *26*, 921–926.

Iyer, K. N., Deshpande, M. R., & Rastogi, R. G. (1976). The equatorial anomaly in ionospheric total electron content and the equatorial electrojet current strength. *Proceedings of the Indian Academy of Sciences - Section A*, *84*(4), 129–138. https://doi.org/10.1007/BF03046803

Jadhav, G., Rajaram, M., & Rajaram, R. (2002). A detailed study of equatorial electrojet phenomenon using Ørsted satellite observations. *Journal of Geophysical Research*, *107*(A8), 1175. https://doi.org/10.1029/2001JA000183

Kelley, M. C. (2009). *The Earth's ionosphere: Electrodynamics and plasma physics*. Burlington, MA: Academic Press.

Kikuchi, T., Hashimoto, K. K., Kitamura, T. I., Tachihara, H., & Fejer, B. (2003). Equatorial counterelectrojets during substorms. *Journal of Geophysical Research*, *108*(A11), 1406. https://doi.org/10.1029/2003JA009915

Kobea, A. T., Richmond, A. D., Emery, B. A., Peymirat, C., Lühr, H., Moretto, T., et al. (2000). Electrodynamic coupling of high and low latitudes: Observations on May 27, 1993. *Journal of Geophysical Research*, *105*(A10), 22,979–22,989. https://doi.org/10.1029/2000JA000058

Kudeki, E., & Fawcett, C. D. (1993). High resolution observations of 150 km echoes at Jicamarca. *Geophysical Research Letters*, *20*(18), 1987–1990. https://doi.org/10.1029/93GL01256

Lühr, H., Maus, S., & Rother, M. (2004). Noon-time equatorial electrojet: Its spatial features as determined by the CHAMP satellite. *Journal of Geophysical Research*, *109*, A01306. https://doi.org/10.1029/2002JA009656

Marriott, R. T., Richmond, A. D., & Venkateswaran, S. V. (1979). The quiet-time equatorial electrojet and counter-electrojet. *Journal of Geomagnetism and Geoelectricity*, *31*(3), 311–340. https://doi.org/10.5636/jgg.31.311

Onwumechili, A., & Akasofu, S. I. (1972). On the abnormal depression of Sq(H) under the equatorial electrojet in the afternoon. *Journal of Geomagnetism and Geoelectricity*, *24*(2), 161–173. https://doi.org/10.5636/jgg.24.161

Onwumechili, C. A., & Agu, C. E. (1981). Longitudinal variation of equatorial electrojet parameters derived from POGO satellite observations. *Planetary and Space Science*, *29*(6), 627–634. https://doi.org/10.1016/0032-0633(81)90111-2

Pandey, K., Sekar, R., Anandarao, B. G., Gupta, S. P., & Chakrabarty, D. (2016). Estimation of nighttime dip-equatorial E-region current density using measurements and models. *Journal of Atmospheric and Solar-Terrestrial Physics*, *146*, 160–170. https://doi.org/10.1016/j.jastp.2016.06.002

Pandey, K., Sekar, R., Gupta, S. P., Chakrabarty, D., & Anandarao, B. G. (2017). Comparison of quiet time vertical plasma drifts with global empirical models over the Indian sector: Some insights. *Journal of Atmospheric and Solar-Terrestrial Physics*, *157*, 42–54. https://doi.org/10.1016/j.jastp.2017.03.012

Patil, A. R., Rao, D. R. K., & Rastogi, R. G. (1990). Equatorial electrojet strengths in the Indian and American sectors. Part I. During low solar activity. *Journal of Geomagnetism and Geoelectricity*, *42*(7), 801–811.

Patra, A. K., Chaitanya, P. P., Otsuka, Y., Yokoyama, T., Yamamoto, M., Stoneback, R. A., & Heelis, R. A. (2014). Vertical E × B drifts from radar and C/NOFS observations in the Indian and Indonesian sectors: Consistency of observations and model. *Journal of Geophysical Research: Space Physics*, *119*, 3777–3788. https://doi.org/10.1002/2013JA019732

Pavan Chaitanya, P., Patra, A. K., & Rao, S. V. B. (2014). Quiet time short-period and day-to-day variations in E × B drift studied using 150 km radar echoes from Gadanki. *Journal of Geophysical Research: Space Physics*, *119*, 3053–3065. https://doi.org/10.1002/2013JA019668

Picone, J. M., Hedin, A. E., Drob, D. P., & Aikin, A. C. (2002). NRLMSISE-00 empirical model of the atmosphere: Statistical comparisons and scientific issues. *Journal of Geophysical Research*, *107*(A12), 1468. https://doi.org/10.1029/2002JA009430

Prakash, S., Gupta, S. P., Sinha, H. S. S., & Rao, T. R. (1976). Ionization irregularities in the *E* region during counter electrojet. *Space Research XVI*, *26*, 401–405.

Prakash, S., Gupta, S. P., Subbaraya, B. H., & Jain, C. L. (1971). Electrostatic plasma instabilities in the equatorial electrojet. *Nature*, *233*(38), 56–58. https://doi.org/10.1038/physci233056a0

Prakash, S., & Subbaraya, B. H. (1967). Langmuir probe for the measurement of electron density and electron temperature in the ionosphere. *Review of Scientific Instruments*, *38*(8), 1132–1136. https://doi.org/10.1063/1.1721035

Rabiu, A. B., Folarin, O. O., Uozumi, T., Abdul Hamid, N. S., & Yoshikawa, A. (2017). Longitudinal variation of equatorial electrojet and the occurrence of its counter electrojet. *Annales Geophysicae*, *35*(3), 535–545.

Raghavarao, R., & Anandarao, B. G. (1980). Vertical winds as a plausible cause for equatorial counter electrojet. *Geophysical Research Letters*, *7*(5), 357–360. https://doi.org/10.1029/GL007i005p00357

Raghavarao, R., & Anandarao, B. G. (1987). Equatorial electrojet and the counter-electrojet. *Indian Journal of Radio and Space Physics*, *16*, 54–75.

Raghavarao, R., Sharma, P., & Sivaraman, M. R. (1978). Correlation of ionization anomaly with the intensity of the electrojet. In *Space Research XVIII* (pp. 277–280). Oxford: Pergamon Press Ltd.

Rama Rao, P. V. S., Gopi Krishna, S., Niranjan, K., & Prasad, D. S. V. V. D. (2006). Temporal and spatial variations in TEC using simultaneous measurements from the Indian GPS network of receivers during the low solar activity period of 2004–2005. *Annales Geophysicae*, *24*(12), 3279–3292.

Rastogi, R. G. (1974). Lunar effects in the counter electrojet near the magnetic equator. *Journal of Atmospheric and Terrestrial Physics*, *36*(1), 167–170. https://doi.org/10.1016/0021-9169(74)90074-9
Rastogi, R. G. (1975). On the criterion of geomagnetic field at the time of disappearance of equatorial Esq layer. *Indian Journal of Radio & Space Physics*, *4*, 1–5.
Rastogi, R. G., Chandra, H., Janardhan, P., & Rahul, S. (2014). Equatorial and mid-latitude ionospheric currents over the Indian region based on 40 years of data at Trivandrum and Alibag. *Indian Journal of Radio & Space Physics*, *43*, 274–283.
Rastogi, R. G., & Patel, V. L. (1975). Effect of interplanetary magnetic field on ionosphere over the magnetic equator. *Proceedings of the Indian Academy Of Science*, *82*(A), 121–141.
Rastogi, R. G., & Patil, A. (1986). Complex structure of equatorial electrojet current. *Current Science*, *55*(9), 433–436.
Reddy, C. A. (1989). The equatorial electrojet. *Pure and Applied Geophysics*, *131*(3), 485–508. https://doi.org/10.1007/BF00876841
Richmond, A. D. (1973). Equatorial electrojet—I. Development of a model including winds and instabilities. *Journal of Atmospheric and Terrestrial Physics*, *35*(6), 1083–1103. https://doi.org/10.1016/0021-9169(73) 90007-X
Rush, C. M., & Richmond, A. D. (1973). The relationship between the structure of the equatorial anomaly and the strength of the equatorial electrojet. *Journal of Atmospheric and Terrestrial Physics*, *35*(6), 1171–1180. https://doi.org/10.1016/0021-9169(73)90013-5
Sanatani, S. (1966). Electron density distribution in the ionosphere (PhD thesis). Gujarat University.
Sastry, T. S. G. (1970). Diurnal changes in the parameters of the equatorial electrojet as observed by rocket-borne magnetometers. *Space Research*, *X*, 778–785.
Scherliess, L., & Fejer, B. G. (1999). Radar and satellite global equatorial *F* region vertical drift model. *Journal of Geophysical Research*, *104*(A4), 6829–6842. https://doi.org/10.1029/1999JA900025
Schoeberl, M. R. (1978). Stratospheric warmings: Observations and theory. *Reviews of Geophysics*, *16*, 521–538. https://doi.org/10.1029/RG016i004p00521
Sekar, R., Gupta, S. P., & Chakrabarty, D. (2014). On the altitude of initiation of the gradient drift waves at different longitude sectors in the vicinity of the dip equator. *Journal of Atmospheric and Solar-Terrestrial Physics*, *121*, 59–62. https://doi.org/10.1016/j.jastp.2014.10.004
Sridharan, S., Gurubaran, S., & Rajaram, R. (2002). Structural changes in the tidal components in mesospheric winds as observed by the MF radar during afternoon counter electrojet events. *Journal of Atmospheric and Solar-Terrestrial Physics*, *64*(12), 1455–1463. https://doi.org/10.1016/S1364-6826(02)00109-8
Sridharan, S., Sathishkumar, S., & Gurubaran, S. (2009). Variabilities of mesospheric tides and equatorial electrojet strength during major stratospheric warming events. *Annales Geophysicae*, *27*(11), 4125–4130. https://doi.org/10.5194/angeo-27-4125-2009
Stening, R. J. (1977). Magnetic variations at other latitudes during reverse equatorial electrojet. *Journal of Atmospheric and Terrestrial Physics*, *39*(9), 1071–1077. https://doi.org/10.1016/0021-9169(77)90015-0
Stening, R. J. (1985). Modeling the equatorial electrojet. *Journal of Geophysical Research*, *90*(A2), 1705–1719. https://doi.org/10.1029/JA090iA02p01705
Stening, R. J. (1989a). A diurnal modulation of the lunar tide in the upper atmosphere. *Geophysical Research Letters*, *16*(4), 307–310. https://doi.org/10.1029/GL016i004p00307
Stening, R. J. (1989b). A calculation of ionospheric currents due to semidiurnal antisymmetric tides. *Journal of Geophysical Research*, *94*(A2), 1525–1531. https://doi.org/10.1029/JA094iA02p01525
Stening, R. J. (1992). The enigma of the counter equatorial electrojet and lunar tidal influences in the equatorial region. *Advances in Space Research*, *12*(6), 23–32.
Stoneback, R. A., Heelis, R. A., Burrell, A. G., Coley, W. R., Fejer, B. G., & Pacheco, E. (2011). Observations of quiet time vertical ion drift in the equatorial ionosphere during the solar minimum period of 2009. *Journal of Geophysical Research*, *116*, A12327. https://doi.org/10.1029/2011JA016712
Subbaraya, B. H., Prakash, S., & Gupta, S. P. (1983). Electron densities in the equatorial lower ionosphere from the Langmuir probe experiments conducted at Thumba during 1966–1978 (Scientific Report). ISRO-PRL-SR-15-83.
Sugiura, M., & Poros, D. J. (1969). An improved model equatorial electrojet with a meridional current system. *Journal of Geophysical Research*, *74*(16), 4025–4034. https://doi.org/10.1029/JA074i016p04025
Thébault, E., Finlay, C. C., Beggan, C. D., Alken, P., Aubert, J., Barrois, O., et al. (2015). International Geomagnetic Reference Field: The 12th generation. *Earth, Planets and Space*, *67*(1), 1–19. https://doi.org/10.1186/s40623-015-0228-9
Venkatesh, K., Fagundes, P. R., Prasad, D. S. V. V. D., Denardini, C. M., de Abreu, A. J., de Jesus, R., & Gende, M. (2015). Day-to-day variability of equatorial electrojet and its role on the day-to-day characteristics of the equatorial ionization anomaly over the Indian and Brazilian sectors. *Journal of Geophysical Research: Space Physics*, *120*, 9117–9131. https://doi.org/10.1002/2015JA021307
Vichare, G., & Rajaram, R. (2011). Global features of quiet time counter electrojet observed by Ørsted. *Journal of Geophysical Research*, *116*, A04306. https://doi.org/10.1029/2009JA015244
Vichare, G., Rawat, R., Jadhav, M., & Sinha, A. K. (2017). Seasonal variation of the Sq focus position during 2006–2010. *Advances in Space Research*, *59*(2), 542–556. https://doi.org/10.1016/j.asr.2016.10.009
Yadav, S., Dabas, R. S., Rupesh, M. D., Upadhayaya, A. K., & Gwal, A. K. (2013). Temporal and spatial variation of equatorial ionization anomaly by using multistation ionosonde data for the 19th solar cycle over the Indian region. *Advances in Space Research*, *51*(7), 1253–1265. https://doi.org/10.1016/j.asr.2012.11.009
Yamazaki, Y., & Maute, A. (2017). Sq and EEJ—A review on the daily variation of the geomagnetic field caused by ionospheric dynamo currents. *Space Science Reviews*, *206*(1), 299–405. https://doi.org/10.1007/s11214-016-0282-z
Woodman, R. F. (1970). Vertical drift velocities and east-west electric fields at the magnetic equator. *Journal of Geophysical Research*, *75*(31), 6249–6259. https://doi.org/10.1029/JA075i031p06249

Journal of Geophysical Research: Space Physics

RESEARCH ARTICLE
10.1029/2018JA025686

Key Points:
- Large reduction in equatorial electrojet strength during daytime associated with disturbance dynamo
- Corresponding changes in electric field on some occasions are much larger than those reported earlier
- Additional influence of semidiurnal tides is proposed to account for the large reduction

Correspondence to:
K. Pandey,
kuldeepak@prl.res.in

Citation:
Pandey, K., Chakrabarty, D., & Sekar, R. (2018). Critical evaluation of the impact of disturbance dynamo on equatorial ionosphere during daytime. *Journal of Geophysical Research: Space Physics*, *123*. https://doi.org/10.1029/2018JA025686

Received 17 MAY 2018
Accepted 31 OCT 2018
Accepted article online 5 NOV 2018

Critical Evaluation of the Impact of Disturbance Dynamo on Equatorial Ionosphere During Daytime

Kuldeep Pandey[1,2], D. Chakrabarty[1], and R. Sekar[1]

[1]Physical Research Laboratory, Navrangpura, Ahmedabad, India, [2]Indian Institute of Technology Gandhinagar, Gandhinagar, India

Abstract Based on careful analysis of 16 years of hourly variations of the strength of equatorial electrojet (EEJ) derived using the ground-based magnetometers over the Indian sector, the role played by disturbance dynamo electric field disturbances on equatorial ionosphere is identified. It is found that most prominent cases of the effects of disturbance dynamo occurred during equinoctial months in high solar activity period. In three extreme cases, the reduction in EEJ strength from quiet time average values of the respective month is more than twice the standard deviations for at least 3 hr. Based on the methodology described in Pandey et al. (2017, https://doi.org/10.1016/j.jastp.2017.03.012), it is found that the westward electric field perturbations are as large as 0.7 ± 0.2 to 1.2 ± 0.3 mV/m around noon hours for these three cases. In contrast to the expectation of disturbance dynamo electric field perturbations over equatorial latitudes from the earlier models, these values during daytime are significantly larger and even caused reversals of EEJ on two occasions. A possible additional source to augment the reduction in the electric field is indicated.

1. Introduction

Ionospheric electric fields play crucial roles in the distribution of plasma and generation of plasma irregularities. The general characteristics of electric fields over low-latitude ionosphere under geomagnetically quiet conditions have been studied at different longitude sectors (Fejer, 1981; Pandey et al., 2017; Woodman, 1970) in the past and global empirical models (Fejer et al., 2008a; Scherliess & Fejer, 1999) have been constructed. During geomagnetically disturbed conditions, additional electric field perturbations modulate the ionospheric electric field. These electric field disturbances can occur instantaneously or after some delay. The instantaneous changes in electric field over middle and low latitudes are directly driven by prompt penetration (PP) or overshielding (OS) of interplanetary electric field owing to imbalance between Region 1 and Region 2 Field Aligned Currents (Kikuchi et al., 1996). In general, the lifetime of PP/OS electric field perturbations is less than an hour (Peymirat et al., 2000; Senior & Blanc, 1984). During disturbed geomagnetic conditions, the auroral electrojets (AEs) are intensified and causes Joule heating of the thermosphere. This sets off equatorward wind circulation (Mazaudier & Venkateswaran, 1990). At midlatitudes, due to Coriolis force, the equatorward flow turns westward which drives a part of ionized fluid. The westward movement of ionized plasma, in combination with downward component of Earth's magnetic field, produces an equatorward Pedersen current. The result is accumulation of positive charges toward the equator (and electrons toward poles). The poleward electric field, thus generated, gives rise to a large eastward Hall current and a poleward Pedersen current. This physical process is called the ionospheric disturbance dynamo (DD; Blanc & Richmond, 1980). The eastward current dominates roughly between 35° and 55° latitude and is interrupted at the dawn and dusk terminators owing to the strong conductivity gradients. The diverted currents close via two vortices that get formed poleward and equatorward of the strong eastward current flow region. The equatorward vortex resembles an *anti-Sq* current system (Le Huy & Amory-Mazaudier, 2005; Zaka et al., 2009), flowing essentially opposite to the quiet day currents and, therefore, driving westward electric field perturbations during daytime. The DD causes global scale magnetic disturbances (Fambitakoye et al., 1990) which have been characterized by latitudinal profile of D_{dyn} (Amory-Mazaudier et al., 2017; Le Huy & Amory-Mazaudier, 2005) that is defined as follows,

$$D_{dyn} = \Delta H - S_R - \text{SYMH}, \tag{1}$$

wherein ΔH, S_R, and SYMH are overall fluctuations in the horizontal geomagnetic field above various components of Earth's internal magnetic field magnetic field, magnetic field fluctuations due to quiet time ionospheric dynamo, and magnetic field induced by the ring current (and corrected for magnetic latitude), respectively. In this mathematical relationship, the contributions from the other ionospheric (DP2) and magnetospheric currents (e.g., Chapman-Ferraro and Tail currents) are assumed to be negligible during the recovery phase of the storm.

The effects of DD electric field (DDEF) are delayed in nature, but it can persist for several hours (Scherliess & Fejer, 1997). It is observed (Yamazaki & Kosch, 2015) that for an average storm with minimum Disturbance storm time (Dst) index ~ −95 nT, DDEF perturbations persist for approximately 24 hr during the recovery phase of the storm. The DDEF perturbations on low-latitude ionosphere have been extensively observed using both ground- (Fambitakoye et al., 1990; Fejer et al., 1983; Mazaudier & Venkateswaran, 1990; Sastri, 1988; Zaka et al., 2009) and space-based (Xiong et al., 2016; Zhang et al., 2017) experiments around the globe. Theoretical (e.g., Blanc & Richmond, 1980; C. M. Huang & Chen, 2008; Richmond et al., 2003; Spiro et al., 1988) and empirical (e.g., Fejer & Scherliess, 1995; Fejer et al., 2008b; Scherliess & Fejer, 1997) models have been developed to address the general characteristics of DDEF. A recent review paper by Fejer et al. (2017) provides an excellent overview of physics of the DD and its important characteristics. In theoretical models, DDEF perturbations over low latitudes are computed corresponding to step-like increase in the polar cap potential followed by sustenance for varying durations. Similarly, in the empirical models, the DDEF perturbations are obtained corresponding to different time delays after the step-like increase in AE followed by sustenance for varying durations. Based on Digisondes/ionosonde, an HF Doppler radar and magnetometers operated over Brazil and India, Abdu et al. (1997) showed that the DD drives opposite changes at the same UT on day and night sides. The eastward electric field of DD origin at night are shown (Abdu et al., 1996; Fejer & Scherliess, 1995) to maximize during postmidnight hour. It is also shown (e.g., Chandra et al., 2016; Rastogi & Chandra, 2012; Sastri, 1988) that the daytime DDEF may significantly reduce the strength of equatorial electrojet (EEJ). However, during the recovery phases of the geomagnetic storm, the effects due to possible OS (Simi et al., 2012) and/or substrom (Kikuchi et al., 2003) may also be present and need careful scrutiny. Based on these studies, a few important aspects regarding DDEF emerged out. First, the polarity of DDEF is opposite to that of the quiet time ionospheric electric field (Abdu et al., 1997). Second, DDEF is stronger in night than during daytime, and third, the magnitude of DDEF is less than 0.5 mV/m (C. M. Huang, 2013) during daytime. Further, it is important to rule out other processes for the estimation of effects due to DDEF alone.

During the recovery phase of a geomagnetic storm, PP/OS and substorm induced prompt electric field perturbations may coexist with DDEF perturbations. Hence, isolating the contribution of DDEF in the electric field perturbations over the equatorial ionosphere remains a challenging job till date. This is an important issue as it can introduce uncertainty in the derived amplitude of DDEF over equatorial latitudes. In order to circumvent this problem, the hourly averaged values of electric fields are generally considered for the development of empirical models of DD. This is based on the assumption that the transient electric field perturbations due to PP/OS electric fields are averaged out owing to their shorter lifetimes. Similar assumption is followed (Fathy et al., 2014; Nava et al., 2015) to separate the DDEF from PP/OS electric fields based on the wavelet analysis. However, on many occasions, the PP electric field perturbations are observed to persist for a much longer duration (C. S. Huang et al., 2005; Wei et al., 2008). Under such conditions, the estimation of DDEF can be uncertain significantly. Therefore, in order to estimate the contributions of DDEF over equatorial ionosphere, it is important to identify distinct cases of DD effects. In the present investigation, such cases are identified by utilizing the hourly variation of the EEJ strength over the Indian sector during 2000–2015. Based on the changes in EEJ, the minimum reductions in ionospheric electric fields during daytime are estimated. The estimates of DDEF based on magnetic field measurements are not available though attempts have been made (Le Huy & Amory-Mazaudier, 2005; Zaka et al., 2009) to deduce the geomagnetic field perturbations associated with DD. This is a step forward as it opens up possibilities to compare the DDEF with earlier estimates based on theoretical and empirical models (e.g., Blanc & Richmond, 1980; Fejer et al., 2008b; Fejer & Scherliess, 1995).

2. Data Set and Criteria for Selection of Events

In the present investigation, the hourly values of ring current index Dst are used to identify different phases of geomagnetic storm. The Dst index reaches minimum well before the occurrence of DD events and it remains in the recovery phase of the geomagnetic storm during the DD. Further, the 3-hourly Kp indices are utilized to categorize the geomagnetically quiet and disturbed days. The values of Dst and Kp indices are obtained from the World Data Center, Kyoto (http://wdc.kugi.kyoto-u.ac.jp/index.html).

The hourly values of north-south component of interplanetary magnetic field (IMF Bz), time shifted to the terrestrial bow shock nose, are obtained from NASA CDAWeb (https://cdaweb.sci.gsfc.nasa.gov). In addition, the hourly values of eastward (AU) and westward (AL) AE indices are also obtained from the NASA CDAWeb. IMF Bz > 0 (northward IMF Bz) on the event day is taken as marker for the absence of prompt perturbations driven by interplanetary electric field. Based on earlier study (Janzhura et al., 2007), AL > -400 nT (insignificant westward AE activity) on the event day is chosen to be a marker for the absence of magnetospheric substorm. As a consequence, it follows that prompt electric field perturbations can be considered to be absent if these criteria are fulfilled during the time periods when DDEFs are evaluated.

The hourly variations of the horizontal component (H) of geomagnetic field during 2000–2015 at Tirunelveli (TIR: 8.7°N, 77.8°E, Geom. Lat. 0.4°S) and Alibag (ABG: 18.6°N, 72.9°E, Geom. Lat. 9.9°N), obtained from Indian Institute of Geomagnetism, Mumbai (http://iigm.res.in/), are used to determine the strength of EEJ ($= \Delta H_{TIR} - \Delta H_{ABG}$) during this period following the methodology suggested by Rastogi and Patil (1986). The ΔH values of each station are obtained by subtracting the nighttime base value. The nighttime base values are calculated by averaging the hourly horizontal magnetic field values during 2300-0300 IST. IST is the Indian Standard Time which is 5.5 hr ahead of Universal time (IST = UT + 5.5 hr). The EEJ values on geomagnetically quiet days of each month are averaged to obtain the quiet time EEJ strength of the month along with the standard deviation (1σ). In choosing the quiet days, it is ascertained that Kp ≤ 3 not only on the reference quiet day but also on the previous day. This is to ascertain that the reference quiet days are truly *quiet*.

The events are selected based on three criteria: (1) the event occurred during the recovery phase of geomagnetic storm with Dst < -50 nT, (2) the event sustained for at least 3 hr with the reduction in EEJ strength on the event day being more than the standard deviations of the quiet time variations of the respective month, (3) throughout the event day (06–18 IST), IMF Bz > 0 and AL > -400 nT. On applying these stringent criteria on hourly EEJ variations during 2000–2015, three cases are identified in which the DD effects are found to be very significant (the reduction in EEJ strength is more than the 2σ level). These three events occurred on 03 September 2000, 18 September 2000, and 23 October 2003, and will be discussed in detail. The reduction in the EEJ strengths is between 1σ and 2σ levels for the other 10 cases, and EEJ variations are within 1σ level for 16 other cases.

The essence of aforementioned criteria are grossly (with a few small differences) similar to that used by Le Huy and Amory-Mazaudier (2005) to identify the cases of DD. In the present work, an additional condition of IMF Bz > 0 on the event day is imposed. In addition, the reference quiet level is constructed based on a number of quiet days, unlike a single quiet day used in earlier studies (Le Huy & Amory-Mazaudier, 2005; Zaka et al., 2009). Further, only those events are considered in which the EEJ reductions exceeding the 1σ variation persist for at least 3 hr. It is to be noted that, although both D_{dyn} and reduction in EEJ are driven by the DDEF perturbations, these are not identical parameters. D_{dyn} is obtained based on magnetic field measurements at a single station and removes the ring current contributions by subtracting SYMH, corrected for magnetic latitude. On the other hand, EEJ is deduced based on magnetic field data from dip-equatorial and off-equatorial stations with the assumption that the ring current contributions over both the stations remain the same. Therefore, in this work, terminologies like *reduction in EEJ* or *reversal in EEJ* are used when the effect of DDEF on EEJ is addressed, whereas the term D_{dyn} is used when the effect of DDEF on the H variation for a single station is addressed.

In order to study the effect of DDEF on plasma distribution, the global maps of Total Electron Content (TEC) on the event days are compared with the mean quiet time TEC maps for the respective months. These TEC values are obtained from NASA CDAWeb. Further, the solar EUV flux levels are also evaluated to examine the possible contribution of changes in EUV flux levels. The daily averaged values of solar EUV flux are obtained based on the Solar EUV Monitor (26–34 nm) on board SOHO satellite (https://dornsifecms.usc.edu/space-sciences-center/).

3. Method to Estimate Reduction in Zonal Electric Field

In order to estimate the reduction in zonal electric field corresponding to the reduction in EEJ strength driven by DDEF, the temporal changes in the EEJ strengths from the respective quiet time levels of the month are obtained. In order to remove the possible contributions of day-to-day variations from the reductions in EEJ strength, the lower envelope (-1σ level) of quiet time variations is taken as reference level. Mathematically, this can be represented as follows,

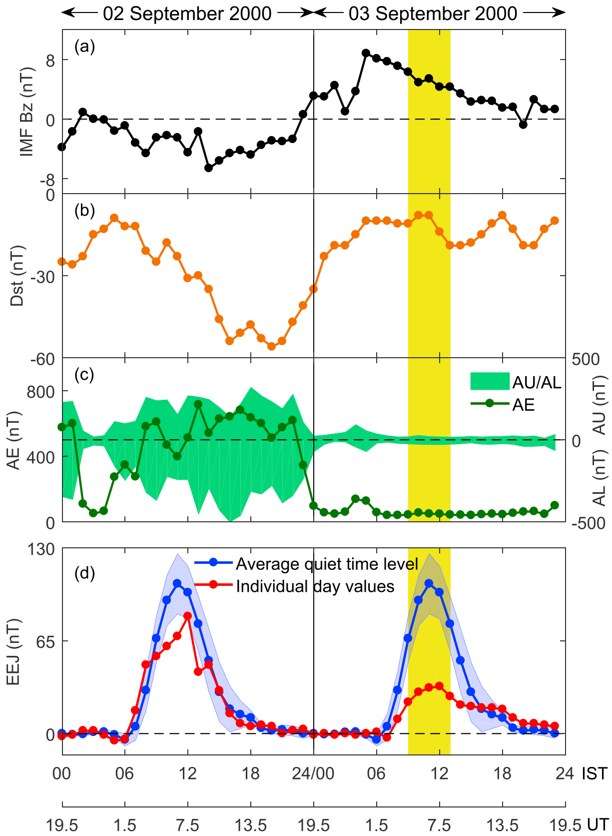

Figure 1. The geophysical conditions for event 1 (03 September 2000, on right) and a day prior to it (02 September 2000, on left). From the top to bottom are (a) the hourly values of north–south component of IMF Bz, (b) Dst index, (c) hourly variations of maximum AU and AL AE, and (d) hourly strength of EEJ along with average quiet time EEJ values of the month with standard deviations (blue-colored shaded area). The time interval during which reduction in EEJ on the event day is more than 2σ is marked with yellow rectangular box. IMF = interplanetary magnetic field; Dst = disturbance storm time; AE = Auroral Electrojet; EEJ = equatorial electrojet; AL = westward; AU = eastward; IST = Indian Standard Time.

$$\Delta EEJ(t) = EEJ_{Eventday}(t) - [EEJ_{Avg.quiet}(t) - 1\sigma(t)], \tag{2}$$

wherein the $EEJ_{Eventday}(t)$, $EEJ_{Avg.quiet}(t)$, and $1\sigma(t)$, respectively, represent the instantaneous EEJ value on the event day, the mean EEJ value of the quiet days of the month, and their standard deviation, all corresponding to time t.

Based on this $\Delta EEJ(t)$ and using the EEJ model of Anandarao (1976), the reductions in zonal electric field are estimated. The electrojet model computes the E-region current over the altitude (r) and colatitude (θ) ranges of 80–200 km and 75°–105°. The horizontal component (H_{ind}) of magnetic field induced at ground by the computed line current (C) is obtained based on Biot-Savart's law as follows,

$$H_{ind} = \frac{\mu_0 C}{2\pi r} \frac{(r/a)\sin\theta - 1}{(r/a)^2 + 1 - 2(r/a)\sin\theta}, \tag{3}$$

where a is radius of the Earth.

Pandey et al. (2017) developed an inverse method to estimate the ionospheric electric field using the electrojet model of Anandarao (1976). In this method, a reasonable input electric field ($E_{\phi 0}$) is assumed to compute the E-region current and magnetic field induced by it for a particular time, season, and solar epoch. The computed H_{ind} value is then compared with the value of EEJ strength deduced using magnetometer observations and the difference is minimized (to within 0.1 nT) by varying the input zonal electric field. The uncertainty in the estimated zonal electric field is less than 25%. This method has been successfully employed by

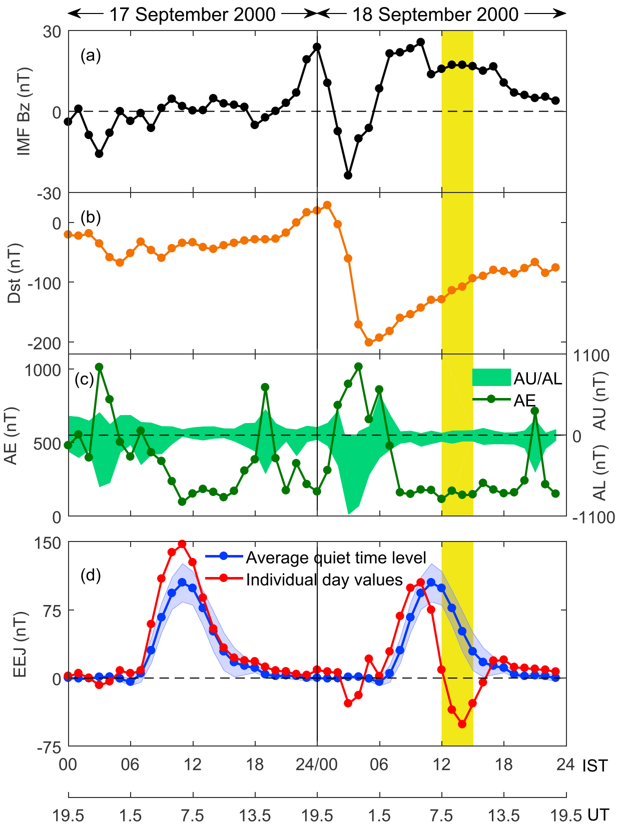

Figure 2. Same as Figure 1 but for event 2 (18 September 2000, right panel) and a day prior to it (17 September 2000, left panel). IMF = interplanetary magnetic field; Dst = disturbance storm time; AE = Auroral Electrojet; EEJ = equatorial electrojet; AL = westward; AU = eastward; IST = Indian Standard Time.

Pandey et al. (2017) to estimate the quiet time electric fields during different seasons and solar epochs over India and the values obtained were shown to match well with the empirical models of Scherliess and Fejer (1999) and Fejer et al. (2008a) over the Indian longitudes. In the present investigation, this method is used to estimate the minimum reduction in zonal electric field corresponding to ΔEEJ.

4. Results

As stated earlier, three events with significant variations in EEJ under the influence of DDEF are presented in this work. Henceforth, for convenience, the DD events on 03 September 2000, 18 September 2000, and 23 October 2003 are referred to as events 1, 2, 3, respectively. These events are described in sequence (Figures 1–3) in the following paragraphs. In these three figures, the hourly variations in IMF Bz, Dst, AE/AU/AL, and EEJ (on the day of event and on the previous day) are plotted sequentially from top to the bottom. The black, orange, and dark green-colored solid lines with dots are used to mark respective variations in IMF Bz, Dst, and AE indices. The AU and AL variations are marked by filled areas above and below the zero level, respectively, with the light green color. The quiet time average EEJ strength of the month and the 1σ variation for each point are shown with blue color shades in the bottom panel of Figures 1–3. Both UT and IST are given in all the figures.

4.1. Event 1 (03 September 2000)

The DD event on 03 September 2000 is depicted in Figure 1. It may be noted that IMF Bz turned southward in the early morning hours of the previous day (02 September 2000) and remained so until midnight. During this time, main phase of a geomagnetic storm is observed with Dst index intensifying up to ∼ −55 nT at 2100 IST which is followed by recovery phase of the geomagnetic storm. Further, the variations in AU and AL are ∼200 nT and ∼ −400 nT since morning till midnight. The EEJ strength on this day is mostly closer to the quiet time values (within 1σ variations) except for some time when the EEJ strength decreased below the 1σ level.

Event 1 occurred on the next day during the recovery phase of the geomagnetic storm. On this day (03 September), from dawn to dusk hours, IMF Bz is continuously northward, and activities in AEs are negligible (magnitude of AU/AL and AE is within 100 nT). However, significant reduction in EEJ strength is observed compared to the monthly average quiet time level. The peak value of EEJ remained closer to 35 nT which is almost one thirds of the quiet time peak EEJ level of 105 nT for this month. Interestingly, the reduction in EEJ strength from the quiet time level is even beyond the 2σ variations during 0900–1300 IST (highlighted with yellow-colored rectangular box in Figure 1).

4.2. Event 2 (18 September 2000)

Figure 2 depicts the variations of IMF Bz, Dst, AE/AU/AL, and EEJ during event 2 and on the previous day (17 September). In this case, IMF Bz turned southward during 0200–0500 IST on 17 September and remained closer to zero afterward. During 0200–0500 IST on 17 September, AE activity also got enhanced. The EEJ strength on this day exceeded the 1σ variation of the quiet time level during noon time.

On the event day (i.e., 18 September), IMF Bz turned significantly southward (∼ −25 nT) at 0300 IST. This is accompanied by the main phase of a strong geomagnetic storm as indicated by the Dst index that got enhanced up to ∼ −200 nT at 0500 IST. The variation of the Dst index after this time indicates the onset of the recovery phase. Importantly, the main phase of the geomagnetic storm was also accompanied with strong intensification of AE activity. During 0200–0600 IST, the strengths of AU and AL increased to about 550 and −1,100 nT. During 0600–1800 IST on the event day, IMF Bz was northward, and AL did not exceed ∼ −300 nT. However, the strength of EEJ decreased drastically during 1200–1500 IST (yellow-colored rectangular box in Figure 2) and went even below the 2σ variations of the quiet time level. As a consequence, the direction

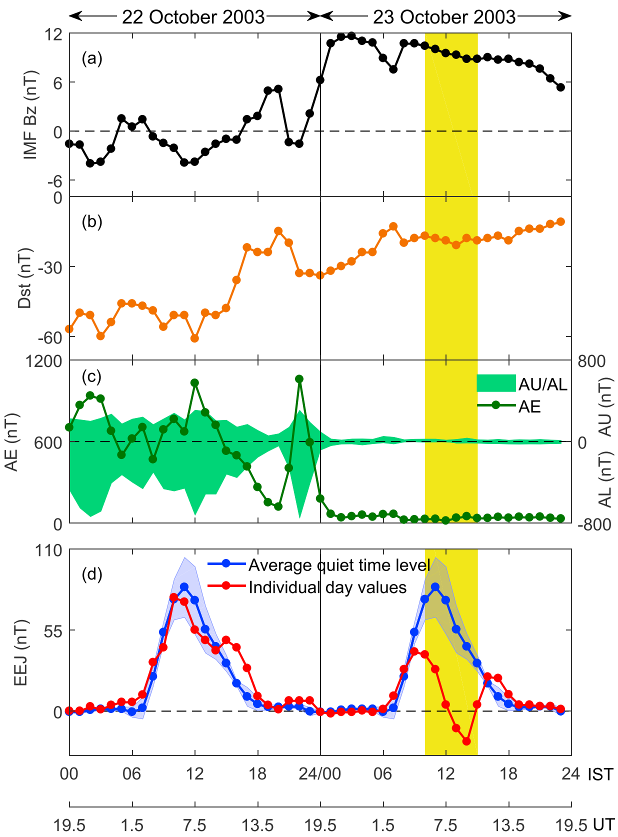

Figure 3. Same as Figure 1 but for event 3 (22 October 2003, right panel) and a day prior to it (23 October 2003, left panel). IMF = interplanetary magnetic field; Dst = disturbance storm time; AE = Auroral Electrojet; EEJ = equatorial electrojet; AL = westward; AU = eastward; IST = Indian Standard Time.

of electrojet current got reversed during 1300–1500 IST. The strength of reversed electrojet in this case was significantly strong and its peak value reached as high as ∼ −50 nT.

4.3. Event 3 (23 October 2003)

On the previous day (i.e., on 22 October 2003) of the event 3, IMF Bz was southward on a number of occasions and during those intervals, IMF Bz was ∼ −4 nT. In addition, AE activities were significant (AU ∼200 nT and AL ∼ −500 nT) throughout this day. A geomagnetic storm was already on as indicated by the Dst index and the recovery phase of this storm started after midday. The EEJ strength on this day is mostly closer to the quiet time level (within 1σ variation) except for some time during the afternoon hours.

The DD event (event 3) occurred on the next day (23 October) when IMF Bz was northward and the AE activities were minimal (AU/AL magnitudes below 100 nT). However, the EEJ strength decreased even below the 2σ variation from the quiet time level of the month during 1000–1500 IST (yellow-colored rectangular box in Figure 3) and similar to event 2, the reversal of electrojet took place during afternoon hours with its peak strength ∼ −20 nT.

The minimum reductions in EEJ on events 1–3 are obtained based on equation (2) which represents the change in EEJ strength from the lower envelope of quiet time variations (marked with blue-colored shade in Figures 1–3). The temporal changes in Δ*EEJ* on these events are depicted in panels (a)-(c) of Figure 4. The maximum strength of Δ*EEJ* on events 1–3 are about −52, −93, and −56 nT at 1100, 1300, and 1400 IST, respectively. It may be noted that as the quiet time reference variations changes with local time, the maximum Δ*EEJ* occur at slightly different local times compared to the time of minimum in actual EEJ variations depicted in Figures 1–3. Further, the EUV flux during events 1–3 remained at the same level (within 5%) as on the quiet days of the respective months. Therefore, these perturbations in EEJ are solely driven by the electric field and not due to changes in conductivity. The zonal electric fields corresponding to maximum strengths of Δ*EEJ* for events 1–3 are estimated based on method described in section 3. It is found that the perturbations in zonal electric fields for events 1, 2, and 3 are -0.7 ± 0.2, -1.2 ± 0.3, and -0.8 ± 0.2 mV/m, respectively.

As the dip-equatorial electric field plays an important role in the development of plasma fountain (Aggarwal et al., 2012; Raghavarao et al., 1978; Rama Rao et al., 2006; Rush & Richmond, 1973), the westward electric field perturbations obtained on events 1–3 are expected to suppress the F-region plasma fountain over low latitudes. In order to verify this aspect, the global TEC maps are generated corresponding to the time that is ∼2 hr after the maximum reduction in Δ*EEJ* for the events 1–3. This is to account for the time associated with plasma diffusion processes (Sanatani, 1966). For comparison with the event days, the mean quiet time TEC maps for the respective months are also generated for the same local time as that of the event day. Figure 5 depicts the global TEC maps on the event days (right panel) and mean quiet time level of the respective months (left panel). Locations of the dip-equator along with ±10° and ±20° dip-latitudes are drawn with the black-colored solid, dashed, and dotted curves, respectively. It can be noticed that the crests of the plasma fountain are well separated during quiet periods. However, on the event days, the crests are not well separated indicating the weakening of plasma fountain effect under the influence of westward DDEF.

4.4. Other Cases

The three cases presented so far pertain to the equinoctial months and high solar activity period. By relaxing the selection criterion in which reduction in EEJ is more than 2σ to a criterion in which reduction in EEJ is between 1σ and 2σ and keeping the rest of the criteria intact, 10 more cases are identified. These cases are tabulated in Table 1 in which the dates, time interval (IST) during which reduction in EEJ is between 1σ and 2σ, and the maximum zonal electric field corresponding to maximum strength of Δ*EEJ* are shown. It can be seen from Table 1 that out of 10 cases, 9 cases pertain to the high solar activity period and 6 cases pertain

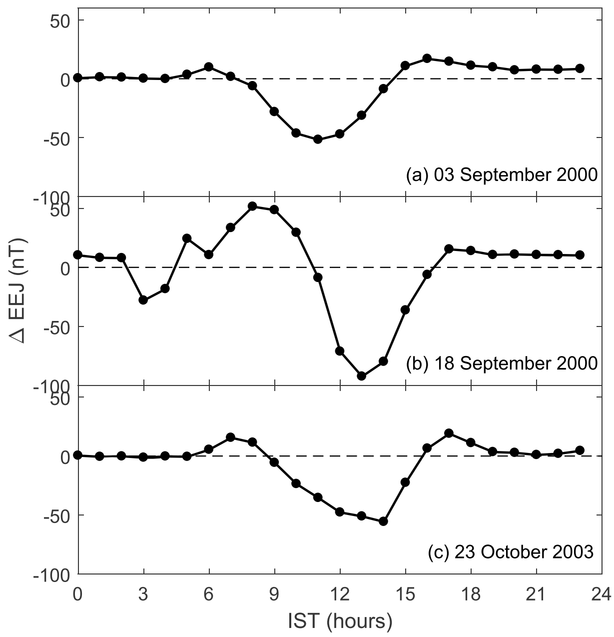

Figure 4. Temporal variation of change in equatorial electrojet EEJ, $\Delta EEJ(t) = EEJ_{Eventday}(t) - [EEJ_{Avg.quiet}(t) - 1\sigma(t)]$ for events 1, 2, and 3 are depicted in (a), (b), and (c), respectively. EEJ = equatorial electrojet; IST = Indian Standard Time.

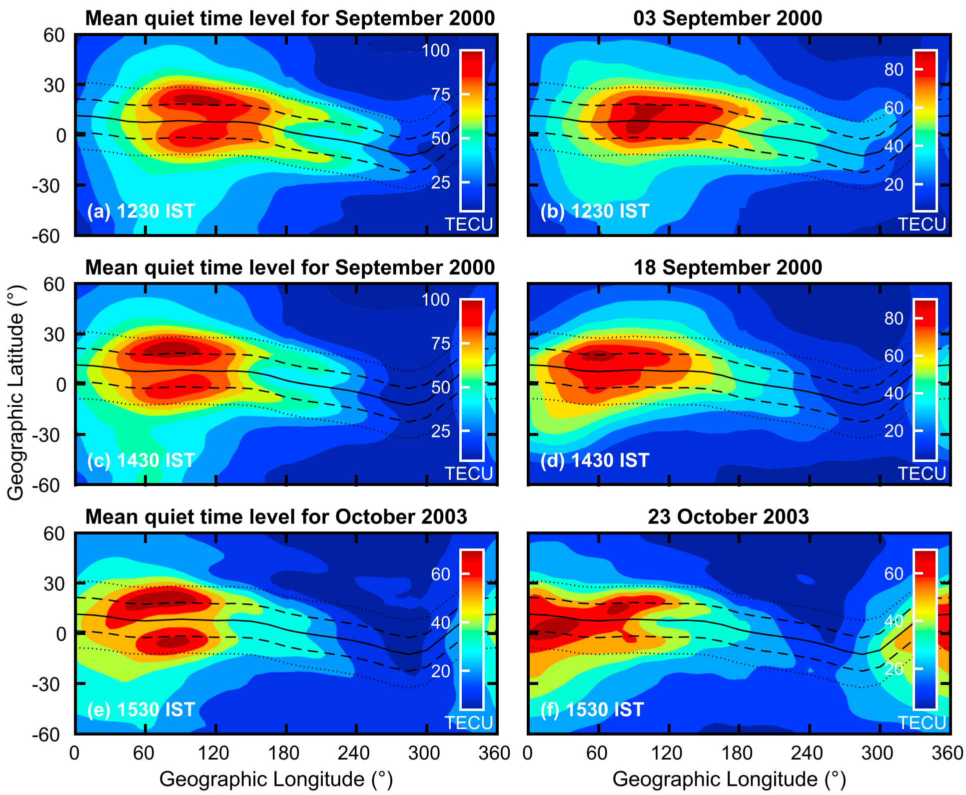

Figure 5. Global TEC maps on event days (right) and mean quiet time level for the respective months (left). The TEC maps corresponding the time that is about 2 hr after the maximum changes in ΔEEJ for events 1–3 are depicted from top to the bottom. Locations of the dip-equator along with ±10° and ±20° dip-latitudes are drawn with the black-colored solid, dashed, and dotted curves, respectively. The TEC values are in units of TECU, wherein 1 TECU = 10^{16} electrons per square meter. TEC = Total Electron Content; TECU = TEC unit; IST = Indian Standard Time.

Table 1
Details of the Events in Which Reduction in EEJ is Between 1σ and 2σ

Date	Time-interval (IST) during which reduction in EEJ is between 1σ and 2σ	Maximum change in zonal electric field (mV/m)
13 August 2000	10–12	−0.24
25 January 2001	13–16	−0.29
14 September 2001	09–13	−0.38
24 September 2001	13–15	−0.15
25 March 2002	10–12	−0.25
05 November 2003	14–16	−0.44
20 January 2005	12–15	−0.17
08 March 2012	11–15	−0.39
18 March 2013	11–13	−0.21
31 October 2013	11–14	−0.10

Note. The maximum change in electric field is estimated (with 25% uncertainty) corresponding to maximum strength of ΔEEJ. EEJ = equatorial electrojet.

to the equinoctial months. These cases are not discussed further as the focus of the present investigation is to address the significant (more than 2σ) reductions in EEJ strength under the influence of DD. By further relaxing the selection criterion for the EEJ variations to be within 1σ and keeping the rest of criteria intact, sixteen more cases are identified. As these changes may also be influenced by the quiet time tidal variabilities, it is not possible to unambiguously isolate the DD contributions in such cases. Therefore, these cases are not considered.

5. Discussion

Three examples are presented in this investigation revealing significant reduction in the strength of EEJ (occurrence of reversed electrojet in two cases) in the recovery phase of a geomagnetic storm without any prompt electric field perturbations. Subsequent to the disturbances in the AE at an earlier time, these reductions in EEJ occurred with varying time delays. This suggests the influence of westward electric field perturbations on the equatorial ionosphere due to DD. Westward electric field influences on the equatorial ionosphere during daytime can also arise due to OS condition (e.g., Simi et al., 2012) when IMF Bz suddenly turns northward after being stably southward for some time. This is not the case here. As there were minimal AE/AU/AL activities on all the three event days, the role of substorms (Kikuchi et al., 2003) in causing the reduction in EEJs can also be ruled out.

Recently, it is shown (Rout et al., 2018) that even in the absence of a typical geomagnetic disturbances (i.e., Dst > 0 and AL > -400 nT), significant changes can occur in EEJ and low-latitude electric fields. These perturbations are shown (Rout et al., 2018) to be driven by PP/OS electric fields due to the passage of the sheath region of Interplanetary Coronal Mass Ejection when the IMF Bz flip-flops between the positive and negative values in quick successions. In order to rule out this possibility, the IMF Bz values with 1 min temporal resolution are looked into. It is found that, during events 1–3, the IMF Bz values with even 1 min resolution are continuously northward (except being about −2 nT for 2 min at ~0930 IST for event 1). Therefore, the role of fast fluctuating IMF Bz to cause electric field changes over low latitudes in these cases can be ruled out.

It is known that the sudden stratospheric warming (SSW) events can drive perturbations in the ionospheric electric field (Chau et al., 2009; Fejer et al., 2010) and current (Bolaji et al., 2016; Sridharan et al., 2009). The list of major SSW events during 1958–2013 is provided by Butler et al. (2017). It is verified that neither events 1–3 nor those listed in Table 1 occurred during the period of SSW events. Therefore, the role of SSW in causing electric field changes in these cases can be ruled out.

In order to ascertain that reductions in EEJ during events 1–3 are caused by DD, the values of D_{dyn} are obtained for stations situated along the Indian geographic meridian (Geog. Lon. 80° ± 20°E). The values of D_{dyn} are obtained based on equation (1), given by Le Huy and Amory-Mazaudier (2005) and Amory-Mazaudier et al.

Table 2
List of Magnetometer Stations Utilized to Obtain the Latitudinal Variations in D_{dyn}

Sr no.	Station	Geog. Lat.	Geog. Lon. (°E)	Geom. Lat.
1	Novosibirsk	55.0°N	82.9	45.2°N
2	Alam Ata	43.3°N	76.9	33.9°N
3	Kashi	39.5°N	76.0	30.3°N
4	Golmud	36.4°N	94.9	26.0°N
5	Silchar	24.9°N	92.8	14.7°N
6	Ujjain	23.2°N	75.8	14.1°N
7	Nagpur	21.2°N	79.1	11.9°N
8	Alibag	18.6°N	72.9	9.9°N
9	Visakhapatnam	17.7°N	83.3	8.1°N
10	Pondicherry	11.9°N	79.9	2.6°N
11	Tirunelveli	8.7°N	77.8	0.4°S
12	Tuntungan	3.5°N	98.6	6.8°S
13	Martin De Vivies	37.8°S	77.6	46.4°S
14	Port Aux Francais	49.4°S	70.3	56.9°S
15	Mawson	67.6°S	62.9	73.1°S

(2017) except for the fact that in the present investigation, the construction of quiet time reference curve consists of a number of quiet days instead of a single quiet day. The stations used to derive D_{dyn} are listed in Table 2 with geographic coordinates and geomagnetic latitudes corresponding to the year 2000. The data for these stations are obtained from World Data Center, Kyoto, and Indian Institute of Geomagnetism, Mumbai. For event 3, the magnetometer records are not available for six of these stations (Alam Ata, Kashi, Golmud, Ujjain, Nagpur, Tuntungan). The variations in D_{dyn} for the events 1–3 with geomagnetic latitude are depicted in Figure 6 in blue, red, and black colors, respectively. These latitudinal profiles correspond to the times when magnitude of ΔEEJ is maximum (at 1100, 1300, and 1400 IST for events 1, 2, and 3, respectively) for each event. It is to be noted that the positive D_{dyn} corresponds to southward deviation in geomagnetic field compared to the quiet level. On all three events, the latitudinal variations are similar to those obtained by Zaka et al. (2009). The reductions in D_{dyn} are maximum over geomagnetic equator (Tirunelveli) and have opposite polarity compared to those for higher magnetic latitudes. This confirms the flow of an anti-Sq current system driven by the DD.

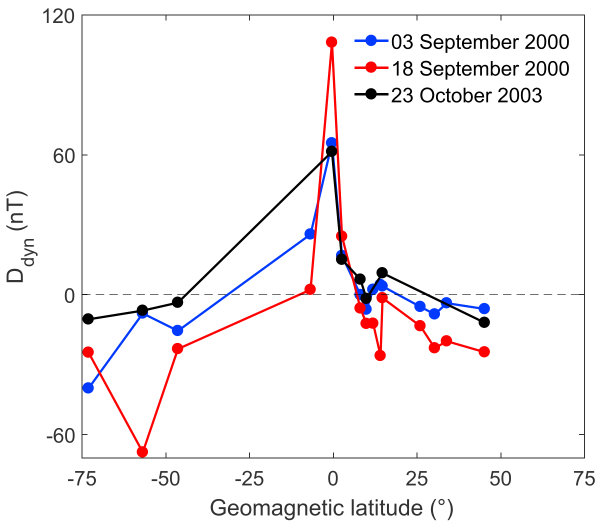

Figure 6. Latitudinal variations of D_{dyn} for events 1 (blue), 2 (red), and 3 (black). The values correspond to the time at which the strength of Δ*EEJ* is maximum for events 1 (1100 IST), 2 (1300 IST), and 3 (1400 IST).

In order to compare the estimates of electric fields with earlier modeling studies on DDEFs, it is worthwhile to discuss the results obtained by the earlier workers (e.g., Blanc & Richmond, 1980; Fejer et al., 2008b). Based on the empirical models of DD (Fejer et al., 2008b; Fejer & Scherliess, 1995; Scherliess & Fejer, 1997), the maximum perturbations in vertical drift were reported to be stronger during nighttime (~20 m/s) and weaker in daytime (~ −10 m/s). These values corresponds to electric field perturbations of ~0.5 mV/m during nighttime and ~ −0.25 mV/m in daytime. On the other hand, the investigations based on the theoretical models of DD (Blanc & Richmond, 1980; C. M. Huang, 2013; C. S. Huang et al., 2005; Richmond et al., 2003) revealed that the DDEF perturbations in daytime are below −0.5 mV/m. C. M. Huang and Chen (2008), based on numerical simulation, obtained the maximum DDEF perturbation to be within −0.5 mV/m during daytime over the geomagnetic equator. As discussed in earlier studies (e.g., Blanc & Richmond, 1980; Fuller-Rowell et al., 2002; C. S. Huang et al., 2005; Richmond et al., 2003), DDEF is generated by the westward and equatorward wind systems in both the hemispheres due to the Joule heating over the auroral regions subsequent to geomagnetic disturbances. The altered circulation patterns in each hemisphere generate an anti-Sq current system over the low-latitude region that positively charges

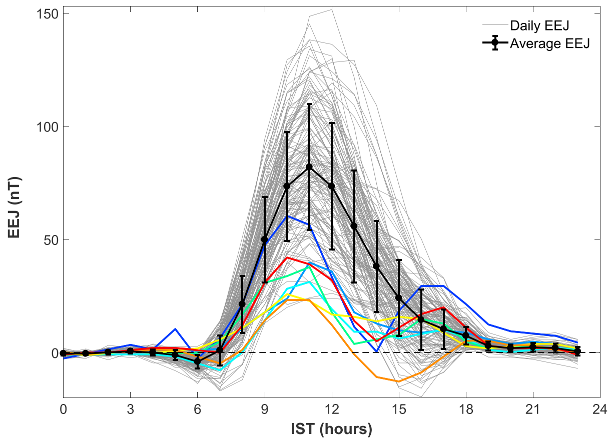

Figure 7. Temporal variations of EEJ on 147 geomagnetically quiet days (gray and multicolor) during September–October months under high solar epoch and its average variation (black) with standard deviation (1σ values with vertical bars). The multicolored lines depict the EEJ variations on days in which EEJ values are continuously below 1σ variations during afternoon hours. EEJ = equatorial electrojet; IST = Indian Standard Time.

the low-latitude ionosphere especially around the local midnight hours. Therefore, the DDEF effects are usually expected to be maximum during local midnight hours (Fuller-Rowell et al., 2002). During daytime, these positive charges that are built up due to the Pedersen and Hall currents associated with westward and equatorward circulation get mostly shorted out by large E-region conductivities (C. M. Huang, 2013). Further, as the disturbance winds over both the hemispheres will experience comparable drag forces during equinox, competing hemispherical effects will be minimum during equinoctial months. Hence, the DDEF effects are expected to be more in equinoctial months (C. M. Huang, 2013). During solstices, the DDEF effects may get reduced over the dip-equatorial region depending on the strength of the trans-hemispherical winds. Further, the DDEF generation is dependent on solar epoch, with higher magnitude during high solar epoch (Scherliess & Fejer, 1997). The impact of DD is expected to affect the equatorial ionosphere 6–15 hr after the onset of AE activity (Fejer & Scherliess, 1995; C. M. Huang & Chen, 2008).

In the present investigation, events 1–3 occurred in equinoctial months during high solar epoch. In addition to these events, 6 out of 10 events listed in Table 1 occurred in equinoctial months and 9 occurred in high solar epoch. Therefore, the present observations are consistent with the prevalent understanding as far as the season, solar epoch, and the polarity of DD perturbations are concerned. The magnitude of reduction in electric field for events listed in Table 1 are below 0.5 mV/m. However, for events 1–3, the magnitudes of reduction in electric field are 0.7 ± 0.2, 1.2 ± 0.3, and 0.8 ± 0.2 mV/m. Therefore, the values obtained on events 1–3 are unusually large compared to the earlier estimates of daytime DDEF based on theoretical and empirical models. This suggests toward a possible additional contribution for the reduction of electric field. In order to investigate this possibility, Figure 7 is presented. Figure 7 depicts hourly variations of the strength of EEJ on 147 geomagnetically quiet days during September–October months under solar maximum condition. Figure 7 does not contain events 1–3 and the cases presented in Table 1. In Figure 7, the EEJ variations on individual quiet days are depicted by gray and multicolored curves. The mean EEJ strength and 1σ variation are depicted by black-colored curve and vertical bars, respectively. The observations on most of the days follow the average quiet time pattern of generally rising from 0700 IST onward and reaching peak value of 80 ± 30 nT at 1100 IST before gradually falling to zero level around 1900 IST. However, on quite a few days, the EEJ values during afternoon hours are substantially reduced below 1σ variations and become closer to zero or negative. These are selectively marked with multicolored lines in Figure 7. It is important to note that the peak EEJ strength on these days are also less than the 1σ variations and occurred earlier in local time. This essentially indicates toward the influence of semidiurnal tides in generating the quiet time dynamo electric field. Under these circumstances, the quiet time reference curve may not be truly representative of the processes occurring on these days and this may bias the estimation of DDEF.

Earlier theoretical (Forbes & Lindzen, 1976; Hanuise et al., 1983; Marriott et al., 1979; Stening, 1989) and experimental works (Bhattacharyya & Okpala, 2015; Gurubaran, 2002; Sridharan et al., 2002) acknowledged the contribution of semidiurnal tides in altering the electric fields primarily generated by the diurnal tides over the equatorial region. Although the influence of semidiurnal tides is more prominent during solar minima (Chakrabarty et al., 2014; Pandey et al., 2018), Figure 7 suggests that the influence of semidiurnal tides during solar maxima cannot be ruled out on occasions. In fact, Pandey et al. (2018) showed that the high occurrence of CEJ events over India during afternoon hours in June solstice under low solar epoch are due to westward Sq electric field and argued that it is due to the influence of semidiurnal tides. It is evident from Figure 7 that the quiet time CEJ events during equinox in solar maximum period occur mostly between 1500 and 1800 IST. However, the maximum reductions in EEJ on events 1–3 occurred during 1100–1400 IST (see Figure 4). Therefore, it is suggested that the large reductions in electric fields on events 1–3 are probably due to combined effects of DDEF and semidiurnal tides. In absence of observations of winds during events 1–3, this aspect could not be verified at present. Future, investigations are needed to confirm this proposition.

6. Summary

Based on 16 years of EEJ data over India, three cases of unusually large DD events over equatorial latitudes are identified. It is found that the prominent cases of unusually large DDEF events mostly occurred during equinox and high solar activity period. Based on the reduction in EEJ strength, it is estimated that the westward electric field perturbations for these cases lie in the range of $0.7 \pm 0.2 - 1.2 \pm 0.3$ mV/m during daytime. These electric field perturbations during daytime are significantly larger than the existing DD model estimates reported so far (e.g., Fejer et al., 2008b; C. M. Huang & Chen, 2008) and are comparable to nighttime DD effects. It is suggested that detailed modeling investigation that takes into account the role of semidiurnal tidal influence on equatorial ionosphere is needed to quantify the role of DD on equatorial ionosphere during daytime.

Acknowledgments
The hourly values of geomagnetic field measured by the ground-based magnetometers are obtained from the Indian Institute of Geomagnetism, Mumbai (http://www.iigm.res.in/), and World Data Center (WDC), Kyoto (http://wdc.kugi.kyoto-u.ac.jp/index.html). The Dst and Kp indices are obtained from WDC, Kyoto. The hourly values of IMF Bz, AL, AU, and AE are obtained from NASA CDAWeb (https://cdaweb.sci.gsfc.nasa.gov). The global TEC values are obtained from NASA CDAWeb. The solar flux index at 10.7 cm is obtained from Laboratory for Atmospheric and Space Physics (http://lasp.colorado.edu). The EUV flux values are based on the Solar EUV Monitor on board SOHO satellite (https://dornsifecms.usc.edu/space-sciences-center/). This work is supported by Department of Space, Government of India.

References

Abdu, M. A., Sastri, J. H., MacDougall, J., Batista, I. S., & Sobral, J. H. A. (1997). Equatorial disturbance dynamo electric field longitudinal structure and spread F: A case study from GUAR/EITS Campaigns. *Geophysical Research Letters*, *24*(13), 1707–1710. https://doi.org/10.1029/97GL01465

Abdu, M. A., Sobral, J. H. A., Richards, P., deGonzalez, M. M., Huang, Y. N., Reddy, B. M., et al. (1996). Zonal/meridional wind and disturbance dynamo electric field control of the low-latitude ionosphere based on the SUNDIAL/ATLAS 1 Campaign. *Journal of Geophysical Research*, *101*(A12), 26,729–26,740. https://doi.org/10.1029/96JA00321

Aggarwal, M., Joshi, H. P., Iyer, K. N., Kwak, Y. S., Lee, J. J., Chandra, H., & Cho, K. S. (2012). Day-to-day variability of equatorial anomaly in GPS-TEC during low solar activity period. *Advances in Space Research*, *49*(12), 1709–1720. https://doi.org/10.1016/j.asr.2012.03.005

Amory-Mazaudier, C., Bolaji, O. S., & Doumbia, V. (2017). On the historical origins of the CEJ, DP2, and Ddyn current systems and their roles in the predictions of ionospheric responses to geomagnetic storms at equatorial latitudes. *Journal of Geophysical Research: Space Physics*, *122*, 7827–7833. https://doi.org/10.1002/2017JA024132

Anandarao, B. G. (1976). Effects of gravity wave winds and wind shears on equatorial electrojet. *Geophysical Research Letters*, *3*(9), 545–548. https://doi.org/10.1029/GL003i009p00545

Bhattacharyya, A., & Okpala, K. C. (2015). Principal components of quiet time temporal variability of equatorial and low-latitude geomagnetic fields. *Journal of Geophysical Research: Space Physics*, *120*, 8799–8809. https://doi.org/10.1002/2015JA021673

Blanc, M., & Richmond, A. D. (1980). The ionospheric disturbance dynamo. *Journal of Geophysical Research*, *85*(A4), 1669–1686. https://doi.org/10.1029/JA085iA04p01669

Bolaji, O. S., Oyeyemi, E. O., Owolabi, O. P., Yamazaki, Y., Rabiu, A. B., Okoh, D., et al. (2016). Solar quiet current response in the African sector due to a 2009 sudden stratospheric warming event. *Journal of Geophysical Research: Space Physics*, *121*, 8055–8065. https://doi.org/10.1002/2016JA022857

Butler, A. H., Sjoberg, J. P., Seidel, D. J., & Rosenlof, K. H. (2017). A sudden stratospheric warming compendium. *Earth System Science Data*, *9*(1), 63–76. https://doi.org/10.5194/essd-9-63-2017

Chakrabarty, D., Fejer, B. G., Gurubaran, S., Pant, T. K., Abdu, M. A., & Sekar, R. (2014). On the pre-midnight ascent of F-layer in the June solstice during the deep solar minimum in 2008 over the Indian sector. *Journal of Atmospheric and Solar-Terrestrial Physics*, *121*, 177–187. https://doi.org/10.1016/j.jastp.2014.01.002

Chandra, H., Rastogi, R. G., Choudhary, R. K., & Sharma, S. (2016). Equatorial electrojet in the Indian region during the geomagnetic storm of 13–14 November 1998. *Journal of Earth System Science*, *125*(3), 669–675. https://doi.org/10.1007/s12040-016-0683-0

Chau, J. L., Fejer, B. G., & Goncharenko, L. P. (2009). Quiet variability of equatorial E×B drifts during a sudden stratospheric warming event. *Geophysical Research Letters*, *36*, L05101. https://doi.org/10.1029/2008GL036785

Fambitakoye, O., Menvielle, M., & Mazaudier, C. (1990). Global disturbance of the transient magnetic field associated with thermospheric storm winds on March 23, 1979. *Journal of Geophysical Research*, *95*(A9), 15209–15218. https://doi.org/10.1029/JA095iA09p15209

Fathy, I., Amory-Mazaudier, C., Fathy, A., Mahrous, A. M., Yumoto, K., & Ghamry, E. (2014). Ionospheric disturbance dynamo associated to a coronal hole: Case study of 5–10 April 2010. *Journal of Geophysical Research: Space Physics*, *119*, 4120–4133. https://doi.org/10.1002/2013JA019510

Fejer, B. G. (1981). The equatorial ionospheric electric fields. A review. *Journal of Atmospheric and Terrestrial Physics*, *43*(5), 377–386. https://doi.org/10.1016/0021-9169(81)90101-X

Fejer, B. G., Blanc, M., & Richmond, A. D. (2017). Post-storm middle and low-Latitude ionospheric electric fields effects. *Space Science Reviews*, *206*(1), 407–429. https://doi.org/10.1007/s11214-016-0320-x

Fejer, B. G., Jensen, J. W., & Su, S. Y. (2008a). Quiet time equatorial F region vertical plasma drift model derived from ROCSAT-1 observations. *Journal of Geophysical Research*, *113*, A05304. https://doi.org/10.1029/2007JA012801

Fejer, B. G., Jensen, J. W., & Su, S. Y. (2008b). Seasonal and longitudinal dependence of equatorial disturbance vertical plasma drifts. *Geophysical Research Letters*, *35*, L20106. https://doi.org/10.1029/2008GL035584

Fejer, B. G., Larsen, M. F., & Farley, D. T. (1983). Equatorial disturbance dynamo electric fields. *Geophysical Research Letters*, *10*(7), 537–540. https://doi.org/10.1029/GL010i007p00537

Fejer, B. G., Olson, M. E., Chau, J. L., Stolle, C., Lühr, H., Goncharenko, L. P., et al. (2010). Lunar-dependent equatorial ionospheric electrodynamic effects during sudden stratospheric warmings. *Journal of Geophysical Research*, *115*, A00G03. https://doi.org/10.1029/2010JA015273

Fejer, B. G., & Scherliess, L. (1995). Time dependent response of equatorial ionospheric electric fields to magnetospheric disturbances. *Geophysical Research Letters*, *22*(7), 851–854. https://doi.org/10.1029/95GL00390

Forbes, J. M., & Lindzen, R. S. (1976). Atmospheric solar tides and their electrodynamic effects-II. The equatorial electrojet. *Journal of Atmospheric and Terrestrial Physics*, *38*(9), 911–920. https://doi.org/10.1016/0021-9169(76)90074-X

Fuller-Rowell, T. J., Millward, G. H., Richmond, A. D., & Codrescu, M. V. (2002). Storm-time changes in the upper atmosphere at low latitudes. *Journal of Atmospheric and Solar-Terrestrial Physics*, *64*(12), 1383–1391. https://doi.org/10.1016/S1364-6826(02)00101-3

Gurubaran, S. (2002). The equatorial counter electrojet: Part of a worldwide current system? *Geophysical Research Letters*, *29*(9), 1337. https://doi.org/10.1029/2001GL014519

Hanuise, C., Mazaudier, C., Vila, P., Blanc, M., & Crochet, M. (1983). Global dynamo simulation of ionospheric currents and their connection with the equatorial electrojet and counter electrojet: A case study. *Journal of Geophysical Research*, *88*(A1), 253–270. https://doi.org/10.1029/JA088iA01p00253